THE THERMAL DECOMPOSITION OF AMMONIUM METAVANADATE

by

Brian Victor Stewart B. Sc. (Hons)

A thesis submitted in partial fulfilment of the requirements for the degree of Doctor of Philosophy

Rhodes University
Grahamstown
September 1971

ACKNOWLEDGEMENTS

The author wishes to express his appreciation to:

Dr M. E. Brown, of Rhodes University, for his direction and keen interest in all aspects of the work and to thank him for valuable criticisms;

Professor L. Glasser, of Rhodes University for his valuable advice and discussions on the interpretation of the results and preparation of this thesis;

Dr V. Lovell, of the National Institute for Metallurgy, for the surface area determinations and Dr M. E. Brown for the Differential Enthalpic Analyses and electron micrographs;

Messrs J. Murray, G. Ranftelshofer and A. Sonemann, for technical assistance; and

Mrs I. Inggs and Mr G. Walters, for assistance in the preparation of this thesis.

The author also acknowledges financial assistance from the National Institute for Metallurgy.

C O N T E N T S

1.4 Previous Work/...

4. RESULTS/...

4.2.4. The Effect of/...

ABSTRACT

The isothermal, endothermic, stepwise decomposition of ammonium metavanadate (AMV) in inert (argon or nitrogen), oxidising (air or oxygen) and reducing (ammonia) atmospheres as well as under high vacuum (pressure $<$ 10 n bar) conditions has been investigated. The reverse reaction, the isothermal recombination of V_2O_5 with ammonia and water vapour has also been investigated.

The decomposition and recombination reactions were followed by continuously recording the mass loss of the sample with time using a Cahn R. G. Automatic Electrobalance. This enabled small samples ($\sim$ 10mg) to be used and consequently any self cooling of the sample during the decomposition was minimized. The intermediates and final products formed have been characterized by chemical analysis, X-ray powder diffraction studies, infrared spectroscopy and the mass loss involved in their formation. The changes in the physical properties of the samples during decomposition and recombination have been investigated by surface area measurements (using the BET method and krypton adsorption) and electron microscopy. Values for the enthalpy changes involved in the decomposition have been obtained by differential scanning calorimetry.

The stoichiometry of the isothermal decomposition of ammonium metavanadate, under the various conditions of surrounding atmosphere has been discussed. Except for the later stages of the decomposition in ammonia, the results correspond well to the gradual reduction of the ratio of "$(NH_4)_2O$" to "V_2O_5" units from the original 1:1 ratio in ammonium metavanadate to pure V_2O_5, with ammonia and water being evolved throughout the decomposition in the mole ratio of 2:1. The

The final product of the decomposition in vacuum, argon and air is V_2O_5 and in ammonia, below 360°, VO_2.

The kinetic parameters for each of the stages of the decomposition of AMV in each of the atmospheres studied have been determined. The mechanism of the first stage of the decomposition under the different conditions of surrounding atmosphere has been discussed from both the kinetic and the thermodynamic points of view. The absolute reaction rate theory has been applied to the decomposition in inert atmospheres enabling the formulae of the activated complexes formed during each stage to be calculated.

It has also been shown that the detailed atomic movements occurring during the first stage of the decomposition in ammonia can be predicted from a knowledge of the stoichiometry of the reaction and of the detailed crystal structures of the starting and product materials.

The kinetics and mechanism of the recombination of V_2O_5 with ammonia and water vapour to form AMV have also been discussed in detail.

1 INTRODUCTION

1.1 The Thermal Decomposition of Solids

The majority of solid thermal decomposition reactions which have been studied[1, 2] are of the type

$$A\,(s) \longrightarrow B\,(s) + C\,(g) \qquad 1.1$$

in which the reaction commences with the formation of the new phase B at specific points in the lattice of A. These points are lattice imperfections such as vacancies, interstitials, jogs in dislocations, Smekal cracks etc., as well as the surface of the crystal. The number of nuclei (initial decomposition centres) formed in any given time depends on both the number of these points and on the activation energy for nucleus formation. The nature of the nuclei is not always clearly defined but it is generally accepted that they are composed of previously formed solid reaction product; e. g. in the decomposition of barium azide[3] and silver oxalate[4] nuclei of metallic barium and silver, respectively are formed. Because of the differences in the molecular dimensions of the product and reactant phases, strain in the reactant lattice develops. Since smaller fragments of B will be more unstable than larger fragments, further reaction will tend to occur at the interface and the product phase thus spreads out from the nuclei. It is clear that once the nuclei overlap and solid A is depleted, the decomposition rate must decelerate.

The rate/time, pressure/time (pressure of the evolved gas C) or α/time (where α is the fraction of the compound decomposed) curves obtained in kinetic studies, can give some information on the process

of nucleation, the shape of the nuclei formed and their mode of growth. Basically these curves are sigmoidal and most of the forms encountered are merely variations of the sigmoidal type. (Fig. 1. 1). Curve (a) shows a symmetrical type where the point of inflexion and maximum rate occurs at $\alpha = 0.5$, but such behaviour is not typical and in general the value of α at the point of inflextion is not 0. 5. This is shown in (b) where the initial acceleratory period is of relatively short duration and the final decay period more pronounced. This type of curve is obtained for the thermal decomposition of lead styphnate[5] or mercuric oxalate[6]. In (c) the induction period is virtually absent and the maximum rate occurs at the beginning of the reaction; this is typical of cases where the nucleation process is very efficient and there is rapid coverage of the external surface with small nuclei e.g. lead azide[7]. With other substances (e. g. whole crystals of potassium azide[8] and of lithium aluminium hydride[9]) there is, in addition, a small evolution of gas at the beginning of the reaction (d). This initial evolution of gas appears to be a characteristic that is not directly related to the thermal decomposition process. It is caused most likely by the physical desorption of gases, water vapour, etc., from the crystalline surfaces or the accessible interior.

The importance of these curves is almost self-evident. For example an Arrhenius plot of a parameter such as the length of the induction period (the choice of which is consistent but arbitary) will be of significance in deciding just how easy nucleus formation is. On the other hand an Arrhenius plot of some parameter associated with the decay region will usually describe the activation energy for the pure growth process since at this point the influence of new nuclei is negligible. Mathematical analyses[1, 2] of the α /time curves can,

Figure 1.1

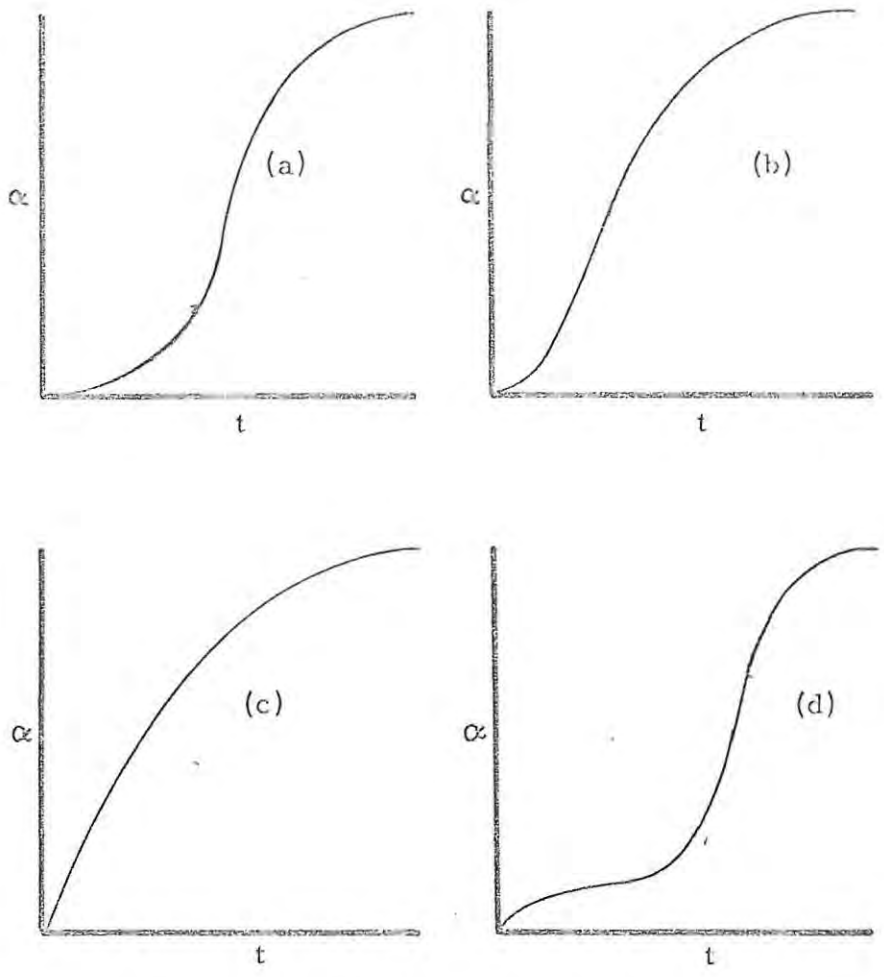

thus, supply information on the process of nucleation, the approximate shape of nuclei and the mechanism by which they grow in size as the reaction progresses through the solid. It must be stressed however that obedience to a particular kinetic equation is not proof that the mechanism on which the equation is based is actually occurring. All additional information possible, such as X-ray data, infrared spectra, visible and electron microscopy of the solid, etc., has to be taken into account. Growth may be from a fixed number of centres or from centres whose number is increasing as a function of time. The occurrence of branching chains of reaction can also be detected[18].

The two main sections of the α/time curve are the acceleratory and the deceleratory or decay section. These divisions are usually associated with the production of nuclei, their growth and the overlap of the nuclei followed by the shrinking of the product/reactant interface. Each of these will be dealt with separately below.

1.1.1 The Production of Nuclei

The laws of nucleation may be divided into those where nucleation only involves a single step or those where nucleation involves more than one step.

1.1.1.1 Nucleation Involving a Single Step

Nucleation may occur as a result of the decomposition of a single molecule or ion. If this applies to the case in question it can be shown[12] that nucleation occurs according to the exponential law.

$$dN/dt = kN_o \exp(-kt) \qquad 1.2$$

where N is the number of nuclei at time t, and N_o is the number of potential nucleus-forming sites. k is the probability factor for a single decomposing molecule to form a nucleus. Thus we find for k small (i. e. at the start of the reaction if the activation energy for nucleus formation is high) we can expand the exponential term in equation 1. 2 to obtain the approximate relationship.

$$N = kN_o t \qquad 1.3$$

or $$\frac{dN}{dt} = kN_o$$

i. e. the number of nuclei increases linearly with time. This has been found to occur in the initial stages of the dehydration of copper sulphate pentahydrate[10]. Similarly for k large, $N = N_o$ i. e. nucleation is instantaneous.

1. 1. 1. 2 Nucleation Involving more than One Event

When more than one event is necessary for nucleus formation we find that the exponent of t in equation (1. 3) is greater than unity. This can be accounted for in two ways.

Either a stable nucleus may result from a bimolecular process involving the combination of two active intermediates, each of which is formed at a constant rate, or several successive decompositions may be required to form a stable nucleus. Both of these hypotheses lead to the same power law[11].

$$dN/dt = kt^n \qquad 1.4$$

where k is a constant and n usually an integer.

The formation of a nucleus, however, does not necessarily mean that the nucleus will grow to a size where it will, in effect, represent appreciable decomposition of the solid. If the activation energy for nucleus growth is less than that required for nucleus formation, rapid growth of nuclei occurs at certain localised points on the crystal, resulting in the autocatalytic nature of curve (a) (Figure 1.1). However, if the activation energies of nucleus growth and nucleus formation are both of the same order, then a large number of small nuclei are formed as in curve (b). A reduction in, or the virtual removal of, the acceleratory region by grinding or crushing will yield a curve similar to curve (c). Curve (d) is simply a combination of (a) and (c) and represents two reaction processes one of which is initiated extremely rapidly.

1.1.2 The Acceleratory Region

In this region the growth of nuclei is the most important factor. No general mechanism covering all decompositions has, as yet, been obtained. A few generalisations have, however, been made. The most important of these general mechanisms for the acceleratory region are given below.

1.1.2.1 The Power Law

It can be shown[12] that the total volume, V(t), of all nuclei at time t, is given by:

$$V(t) = \int_0^t \sigma \left[\int_y^t G(x)\,dx \right]^{\lambda} \left[\frac{dN}{dt}\right]_{t=y} dy \qquad 1.5$$

where σ is a shape factor

$G(x)$ is a growth function

λ is the number of dimensions of the nucleus

N is the number of nuclei at time $t=y$

Now when $\frac{dN}{dt}$, or its appropriate form, as well as $G(x)$, is known, then $V(t)$ can easily be evaluated and hence the degree of decomposition is obtained.

Thus if power law nucleation and a linear growth rate are assumed then the degree of decomposition can be shown to be

$$\alpha = Ct^n \qquad 1.6$$

where C is a constant and n is usually an integer.

n = 2, corresponds to two dimensional growth e. g. Barium styphnate monohydrate[13]

n = 3, corresponds to the formation of a fixed number of nuclei which grow three-dimensionally; or linear growth of two-dimensional nuclei e. g. aged mercury fulminate[14]

n = 4, corresponds to the formation of compact, spherical nuclei which grow along a specific direction e. g. ammonium chromates[15]

1. 1. 2. 2 The Exponential Law

The decomposition of many substances (e. g. silver oxalate[16])

could not be explained by the above theory.

Garner and Hailes[17] derived the concept of linear branching chains of nuclei in order to explain these exceptions, and further postulated a constant branching coefficient, k', assuming that the rate of nucleation is constant.

The nett rate of nucleus production is then

$$\frac{dN}{dt} = kN + k'N \qquad 1.7$$

and it can be shown that in this case

$$\alpha = C'e^{k_2 t} \qquad 1.8$$

This concept of linear branching chains would however result in the crystal separating into isolated mosaic blocks which would then decompose slowly. Branching plate-like nuclei of constant width were then postulated and it can be shown that the same general exponential expression still applies in this case.

1. 1. 2. 3 The Prout-Tompkins Equation

In the above treatment, however, interference of chains during growth was neglected and Garner's linear branching chain theory, in the form in which it was originally presented, could not account for the deceleratory or decay region.

Prout and Tompkins[18] in their work on potassium permanganate evolved a mechanism to allow for this factor. In place of Garner's original equation it was proposed that the rate of nucleus formation dN/dt should be corrected by including a term for the probability of chain termination proportional to N, the number of nuclei at time t.

Thus

$$dN/dt = k_1 N_o + k_2 N - k_3 N \qquad 1.9$$

where k_2 is the probability of chain branching and k_3 is the probability of chain termination. When k_1, the nucleation constant, is large, the original sites N_o are soon exhausted and

$$dN/dt = (k_2 - k_3)N \qquad 1.10$$

This also holds when k_1 is small if it is assumed that the branching process predominates. If one considers strictly linear nuclei then at any instant

$$\frac{d\alpha}{dt} = k_4 N \qquad 1.11$$

These last two equations cannot be integrated until the functional dependance of α on k_3 and k_4 is introduced. Prout and Tompkins considered the case of a symmetrical sigmoid for which $\alpha_{\text{inflexion}} = \frac{1}{2}$. Now at $t = O$, $\alpha = O$ and $k_3 = O$ since interference is impossible at this stage. At $\alpha_{\text{inflexion}}$, dN/dt changes sign, thus at $\alpha_{\text{inflexion}} = \frac{1}{2}$, $k_2 = k_3$ where it is consistent to write $k_3 = k_2 \cdot \alpha / \alpha_{\text{inflexion}}$.

From these considerations the differential form of the Prout-Tompkins equation may be derived

$$\text{i.e.} \quad d\alpha/dt = k_2 \alpha(1 - \alpha) \qquad 1.12$$

and on integration we get

$$\log \frac{\alpha}{1 - \alpha} = k_2 t + C_2 \qquad 1.13$$

A modification of the Prout-Tompkins equation allowing for the inverse variation of the branching coefficient with time was introduced by Prout and Tompkins in order to describe the decomposition of silver permanganate[21]. This resulted in equation 1-14

$$\log \left(\frac{\alpha}{1 - \alpha} \right) = k_2' \log t + C_2' \qquad 1.14$$

Young[19] criticises equation 1.13 since it describes the kinetics of a reaction progressing via linear branching chains which can be terminated on reaching any part of the product phase, thus it suffers from the same crystallographic limitations as does the original equation of Garner. A more serious defect arises from the necessity in practice of two different rate constants for the acceleratory and deceleratory regions. These constants may even have different temperature coefficients, suggesting that $k_3 = k_2 \cdot \alpha / \alpha_{\text{inflexion}}$ is not a valid assumption.

These criticisms of Young's do not affect the concept of chain termination and it is in his opinion still valid to analyse the acceleratory regions of decompositions by the Prout-Tompkins equation, provided that it is recognized that branching is essentially a surface process which will be superceded once a complete envelope of product is formed. Young and Haynes[20] have also shown that a decomposition curve which can be analysed by the Prout-Tompkins equation during the decay period can frequently be better analysed by a contracting sphere expression (see later).

1.1.2.4 The Avrami-Erofeyev Equation

Quite apart from the special case of branching chains, an analysis of random nucleation leading to the experimental law must allow for the ingestion of potential nucleation sites. Avrami[22] and Erofeyev[23] working independently derived an equation which took this into account.

Avrami dealt with the nucleation process in a study of the kinetics of phase change. He used the terms "nuclei" (germ nuclei) and "grains" (growth nuclei), for centres below and above the critical size for steady growth respectively. The number of nuclei decreases in two ways with time. Some became activated for growth and others are ingested by growing grains. The type of grain interaction applicable to crystalline solids is the adherence of grains at common interfaces while continuing to grow normally elsewhere. Using this approach she derived a general equation for random nucleation followed by isotropic three-dimensional growth at a linear rate k_2.

$$-\log(1-\alpha) = \frac{6.S.Nok_2^3}{V_o k_1^3}\left[e^{-k_1 y} - 1 + k_1 t - \frac{(k_1 t)^2}{2!} + \frac{(k_1 t)^3}{3!} \right] \qquad 1.15$$

where S is a shape factor

V_o is the final volume of product obtained after decomposition

No is the number of nuclei randomly distributed/unit vol at time $t = 0$

k_1 is the rate of increase of No

At the start of the decomposition ($\alpha \ll 1$) we find that this equation reduces to the power law

i. e. $\alpha = Ct^n$ with $n = 2, 3, 4$ depending on the shape of the nuclei.

During the deceleratory or decay region, when t is large then the equation reduces to

$$\alpha = 1 - \exp\left[\frac{\sigma Nok_2^3}{Vo}\, t^3\right] \qquad 1.16$$

Erofeyev approached the problem in a different manner. He first derived a general kinetic equation:

$$\alpha = 1 - \exp\left(-\int_0^t p\,dt\right) \qquad 1.17$$

where p is the probability of the reaction of an individual molecule in an interval dt. This equation involves no assumptions regarding the properties of the reacting system. After differentiating he applied the general equation to the growth of reaction nuclei in solids. For three-dimensional growth, in general, the probability pdt is proportional to the total volume of the spherical layers traced, at the instant t, around the nuclear centres that have arisen at the instant t.

Thus, in general, depending on the shape of the nucleus

$$\alpha = 1 - \exp(-kt^n) \qquad 1.18$$

This is known as the Avrami-Erofeyev Equation.

Sharples[24] discusses the Avrami equation and its application to the crystallisation of polymers in some detail. He shows that the exponent n is in fact made up of two contributions: (i) the number of dimensions in which growth takes place, and (ii) the time dependence of the nucleation process.

TABLE 1.1

Values for the Avrami exponent, n, for various types of nucleation and growth (from Sharples[24])

n	Type of nucleation and growth
3 + 1 = 4	Spherulitic growth from sporadic nuclei ($n \propto t$)
3 + 0 = 3	Spherulitic growth from instantaneous nuclei
2 + 1 = 3	Disc-like growth from sporadic nuclei
2 + 0 = 2	Disc-like growth from instantaneous nuclei
1 + 1 = 2	Rod-like growth from sporadic nuclei
1 + 0 = 1	Rod-like growth from instantaneous nuclei

Much use has been made in the past of Avrami plots for determining mechanisms through application of the relationships in the table above.

Stringent tests are, however, necessary if it is to be established that a given set of crystallisation data conform accurately to an Avrami equation. Gent[25] has shown that the difference between two plots, one with n = 3 and the other with n = 4 is not very great so that considerable care is necessary if any weight is to be attached to the conclusion that the value of n determined for a given process is accurately known.

The essential requirements of the Avrami equation are; random nucleation, dependence of nucleation on the zeroth or first power of time, constant growth rate and unchanging density of the growing material. Sharples found on checking these requirements with polymer crystallisation that when $n < 4$, even if the result was an integer, no unambiguous conclusion could confidently be made.

1.1.3 The Deceleratory or Decay Region

In the decay region of the decomposition curve, overlap of nuclei results in a contracting interface. If this remains intact then the Avrami-Erofeyev equation may still hold. Because of the difference in molecular volume between product and reactant phases, the interface may collapse, leaving isolated blocks of material in which no nuclei are present. The same condition may arise from extensive growth of plate-like nuclei. In these isolated blocks, if each molecule has an equal probability of decomposing, the rate will be proportional to the amount of decomposed material.

i.e. $$d\alpha/dt = k(1 - \alpha)$$

$$\therefore \quad -\log(1 - \alpha) = kt \qquad 1.19$$

which is known as the UNIMOLECULAR DECAY LAW.

If the rate-determining factor in the decay becomes the number of remaining unreacted molecules then not all of the molecules will be favourably situated next to a product molecule and one obtains an equation which reduces to the Prout - Tompkins equation with a constant k' different to that applying over the acceleratory period.

The progression of the reactant/product interface may also become the rate-determining step. When the surface of a particle of material has become covered with product and the interface progresses inwards, the rate will obviously depend on the geometry of the particle and of the interface. Much work on this type of mechanism has been done by Bradley, Colvin, Hume[26] and others in the period 1928-1938. This type of treatment may thus lead to a contracting parallelopiped or a contracting sphere. If nucleation is confined to certain faces of the crystal only, then the mechanism may be a contracting rectangle or circle.

The most common of these is the contracting sphere and has been applied amongst others by Spencer and Topley[27], to silver carbonate (see later) and Gregg and Razouk[28] in their discussion of the decomposition of magnesium hydroxide. For the contracting sphere model, assuming spherical particles of initial radius a, the fraction decomposed at time t is

$$\alpha = \frac{\frac{4}{3}\pi a^3 - \frac{4}{3}\pi (a-kt)^3}{\frac{4}{3}\pi . a^3}$$

$$= 1 - \left(\frac{a - kt}{a}\right)^3$$

$$= 1 - (1 - k't)^3$$

$$\text{or} \quad 1 - (1 - \alpha)^{\frac{1}{3}} = k't \qquad 1.20$$

which is the usual form of the contracting sphere equation.

The nuclei, however, may not cover the surface and the rate of reaction can be governed by the spherical growth of single nuclei from points on the surface into the particle. Assuming a single nucleus per spherical particle it can be shown that the maximum rate would occur at $\alpha = 0.593$.

If nucleation is a random process and this is followed by rapid two-dimensional growth on the surface then this leads, as has been shown by Jacobs and Tompkins[29], to a linear function of log $(1-\alpha)$ plotted against t. Bradley, Colvin and Hume[26] have obtained good linear plots in accordance with this equation using data for the dehydration of calcium carbonate hexahydrate.

1.1.4 Diffusion Controlled Reactions

A comprehensive treatment of diffusion controlled reactions in general has been given by Harrison[30] and the mathematics of the diffusion equation has been discussed in detail by Crank[31]. It is, however, only necessary in the present instance to outline some of the aspects and equations of diffusion controlled reactions which have been applied to decomposition reactions.

The law of diffusion proposed by Fick in 1855 arose from the recognition that there is a close analogy, in terms of mathematical treatment, between diffusion and heat conduction. Fick's hypothesis was that the rate of transfer, F, of diffusing material across unit area of cross-section is proportional to the concentration gradient in the direction

of diffusion, viz.

$$F = - D \left(\partial c / \partial x \right) \qquad 1.21$$

The analagous equation for the rate of flow of heat is

$$H = - \lambda \left(\partial T / \partial x \right) \qquad 1.22$$

If equation 1.21 is converted into a partial differential equation for time dependant flow then,

$$\partial c / \partial t = D \nabla^2 C \qquad 1.23$$

Now if the concentration and temperature gradients are present simultaneously then D, T and t are all inter-related and it is necessary to apply the complete Laplacian operator to D as well as to C viz

$$\partial c / \partial t = \nabla^2 (DC) \qquad 1.24$$

This is the most general form of the differential equation for diffusion. Solutions of this equation are, of course, as numerous as the possible boundary conditions but in practice a few situations are very much more frequently encountered than others.

One of the more common methods of studying self-diffusion in solids is the exchange method where a solid sample is in contact with a well-stirred fluid (gas or liquid) and the labelled species diffuses either into or out of the solid. If the total amount of material which has diffused into or out of unit area of the solid by time t is M_t, which is proportional to α, then it can be shown that if the concentration of the diffusing material in the surrounding fluid is zero

$$M_t = \int_0^t D \left(\partial c / \partial x \right)_{x=0} dt$$

$$= 2 Co \left(Dt / \pi \right)^{\frac{1}{2}} \qquad 1.25$$

where Co is the initial concentration of diffusing material in the solid. This is one instance of the parabolic law which can also arise in a different way by considering the case of diffusion of some species across a growing layer of product. Here one must consider the product to form a layer on the surface of the material and the advance of the interface so formed to be controlled by the diffusion of some species through this layer.

A classical example of this is the formation of a film of oxide on the surface of a metal, and the diffusion of oxygen through this layer. If the thickness of this film at time t is X, the surface concentration of oxygen is Co and the volume of the oxide containing one mole of oxygen atoms is V_M, then by using a quasi stationary state treatment it can be shown[30] that

$$X = (2DCoV_M t)^{\frac{1}{2}} \qquad 1.26$$

which is the parabolic law for tarnish reactions. These were studied extensively by Wagner[32] in the 1930's.

In most practical circumstances the parabolic law is a very good approximation and the condition for its validity is

$$Co \ll (1/V_M) \qquad 1.27$$

If one considers the reaction of spherical particles in the above context one finds that three equations sometimes referred to[33, 34] as the Jander[35], Ginstling-Brounstein[36] and Dünwald-Wagner[37] equations are used. In references to these equations there is not always a clear indication of the nature of the approximations involved in them or of the fact that they do not all refer to the same situation. Harrison[30] does however clarify these points in his discussion.

The Dünwald-Wagner equation,

$$\alpha = 1 - (6/\pi^2) \sum_{n=1}^{\infty} \left(\frac{1}{n^2}\right) e^{-Dn^2\pi^2t^2/a^2} \qquad 1.28$$

where a is the radius of the spherical particles, is applicable to diffusion with constant D into or out of a system of spheres of uniform radius with constant surface concentration of the diffusing species. It is not appropriate to the situation of a sharp reaction interface advancing into the spherical particles but it is obeyed in certain cases of interdiffusion such as spinel formation[38] where the original interface gradually becomes blurred and finally disappears altogether.

The Jander and Ginstling-Brounstein equations are both attempts to treat, by the "quasi-stationary state" approach, the case of an advancing reaction interface considered in spherical geometry.

In Harrison's opinion the Jander equation is a very rough approximation to this situation and can only be applied for $\alpha \leq 0.15$ while the Ginstling-Brounstein equation is the proper analogue in spherical geometry of the parabolic law. The Ginstling-Brounstein equation is

$$1 - \tfrac{2}{3}\alpha - (1-\alpha)^{2/3} = 2DC\,V_M\,t/b^2 \qquad 1.29$$

where b is the initial radius of the sphere

C is the concentration of the diffusing species at all times

V_M is again the volume of immobile reaction product containing one mole of the diffusing species.

The validity of this equation depends on the constancy of D and the degree to which the system approaches spherical geometry. The linearity of a plot of the Ginstling-Brounstein function against t is shown by Harrison[39] and his co-workers not to be very sensitive to either of these conditions since linear Ginstling-Brounstein plots are obtained for the exothermic reaction of $SrCl_2$ with F_2 where there was a large

temperature gradient across the reacted material and the sample was a large crystal of rather irregular shape. He does however point out that the Ginstling-Brounstein plot expands the region occupied by the second half of the reaction ($\alpha > \frac{1}{2}$) greatly at the expense of the first half of the reaction. Also during the second half of the reaction, the interface is much more likely to have acquired a regular shape than at the start of the reaction and the temperature gradients would also have diminished with the diminishing rate of reaction.

1.1.5 General

It must be emphasized that conclusions from results merely expressing the extent of total reaction with time e. g. the amount of gas produced in a thermal decomposition study, or the change of an average macroscopic property such as density, must be, to some extent, speculative for both the mathematical relationship and the activation energies derived from the associated temperature coefficients often change with increasing extent of reaction. Moreover, the rate equations used in describing the results are often non-discriminatory and are found to be only approximately valid over part of the time period of the process. Indeed, the derivation of activation energies from the usual Arrhenius relation, based on an exponential dependence of some rate parameter on temperature, is often invalidated by the fact that equilibrium between activated and non-activated species in the rate determining process according to a Boltzmann distribution is not attained. Kinetic expressions derived from overall reaction velocities are thus insufficient to characterize the mechanism of the reaction with confidence.

1.2 The Importance of Crystal Structure in Controlling Solid-State Reactions

An important series of papers by Cohen and Schmidt[40] and their co-workers has stressed the thesis that, at least in certain types of solid-state reactions, reactivity is determined principally by the geometry of the reactant lattice; this is termed topochemical control or topotacticity. Although this has been applied in the main part to solid-state reactions of organic compounds (i. e. compounds of low symmetry) it will be shown that it can also be applied to those reactions of inorganic compounds where there are no major changes in the crystal structure or, more specifically, in the relative positions of atoms or groups of atoms, during the reaction. Perhaps one of the clearest examples of topochemical control is the photochemical dimerization of the transcinnamic acids.[41] Jacobs[42] agrees with Cohen and Schmidt and gives the thermal decomposition of calcite[43,44] as an example of a topotactic reaction. In the decomposition of calcite the decomposition nuclei are generally hexagonal in shape with their sides along the $\langle 110 \rangle$, $\langle 1\,1\,0 \rangle$ and $\langle 100 \rangle$ directions. This means that during growth the reactant-product interfaces lie on $\{1\,\bar{1}\,\ell\}$, $\{1\,1\,\ell\}$ and $\{100\}$ type planes. On these planes there are Ca^{2+} - Ca^{2+} distances in rhombohedral calcite which approximate closely the corresponding separations in cubic CaO. This implies strong topochemical influence during nucleus growth and suggests that anionic decomposition proceeds so as to allow the formation of product with a minimum of ionic displacement. The analogy with the work of Cohen and Schmidt on the photochemical dimerization of the transcinnamic acids, where again reaction proceeded with the minimum of molecular movement, is clearly very close.

Taylor et al[45] in their review of topotactic reactions of inorganic oxy-compounds show that many hydroxides and oxide-hydroxides, such as magnesium hydroxide, have layer structures based on sheets of hydroxyl and sometimes also oxide ions. The arrangement of these ions approximates in varying degrees to either cubic or hexagonal close packing, the cations occupying the octahedral interstices. Dehydration of these to the oxides usually occurs topotactically on heating in air. The oxides also have structures based on approximately close packed oxide ions e. g. magnesium oxide. Because there are no hydrogen ions, more interstices are occupied by metal ions than in the hydroxides. The orientation relationships observed in the dehydration reactions seem always to allow the best possible fit between close packed oxygen planes of starting material and product. Other hydroxides and oxide-hydroxides which undergo topotactic reactions on heating are those of aluminium and iron.[45, 47, 48]

Another good example of a topotactic reaction is the dehydration of gypsum[49] which takes place in three steps

$$\underset{\text{gypsum}}{CaSO_4 . 2H_2O} \rightleftharpoons \underset{\text{hemihydrate}}{CaSO_4 . \tfrac{1}{2}H_2O} \rightleftharpoons \gamma\text{-}CaSO_4 \longrightarrow \underset{\text{anhydrite}}{CaSO_4} \qquad 1.30$$

The first two steps are reversible as indicated. Orientation is well preserved in the second and third steps, but only partly preserved in the first. The reaction has been interpreted in terms of the preservation of the chains of Ca^{2+} and SO_4^{2-} ions which occur in all four structures. The structures of the hemihydrate, γ -$CaSO_4$ and anhydrite can alternatively be described in terms of analagous sheets of Ca^{2+} and SO_4^{2-} ions. One structure can then change into another by small relative displacements of these sheets, together with loss of water.[50]

The occurrence of γ-calcium sulphate, metastable under all conditions, is an example of the structural control over the phase formed.

In general, for a topotactic transformation to take place there must be a three-dimensional similarity between the structures of the starting material and the product. If there is only two-dimensional similarity in the structures then the reaction is epitactic. This similarity need not be very great and the compositions may differ radically. The mere similarity between structures is, however, not in itself sufficient to guarantee that a reaction will occur topotactically. Experimental evidence is always needed.

Some reactions are topotactic under all conditions, some only under certain conditions and others not at all. Factors which may influence the degree of orientation in any particular reaction include temperature, pressure, physical state, surrounding atmosphere and other specific experimental conditions such as time and rate of heating used to induce thermal changes.

It is interesting to note that almost all of the topotactic reactions which have been studied are endothermic and thus are potentially reversible. This is what would be intuitively expected since, for a reaction to be reversible, there should be no profound structural change during the reaction i. e. the structure of the starting material and of the product should be similar. This does not mean that all endothermic reactions will be topotactic or vice versa, but it does suggest that when an endothermic reaction is being investigated attention should be focussed on the possible topotactic nature of the transformation in order to elucidate the mechanism of the reaction.

1.3 Endothermic Decompositions

Previous reviews of the thermal decompositon of solids[1,2] have been divided into considerations of exothermic and of endothermic decompositions. The reviews by Garner[1] and by Young[2] cover mainly the endothermic dissociations of hydrates and of carbonates. Some coverage has, however, also been given to the dissociation of the sulphates[53], hydroxides[54] and oxides[55].

The DTA traces of Erdey et al[51] and Taniguchi and Ingraham[52] indicate that the thermal decomposition of NH_4VO_3 (AMV) to form V_2O_5 can be classified as an endothermic process, and some aspects of work on endothermic decompositions will be reviewed.

1.3.1 Endothermic Decompositions of Compounds Containing Ammonia

Endothermic decompositions which involve the evolution or absorption of ammonia are of special interest, and compounds which undergo this type of reaction are the ammoniates[56], nickel hexamine perchlorate[57], ammonium phosphate[58] and the ammonium-exchanged Y zeolite[59].

The decompositon curves of the isothermal decomposition of ammonium phosphate and the initial stage of the decomposition of nickel hexamine perchlorate are both best fitted by the contracting sphere equation (Section 1.1.3). The reverse reaction for the initial stage of the decomposition of nickel hexamine perchlorate has also been investigated[57] and the progress of the reaction was found to be proportional to the square-root of the time. This together with the

low activation energy (< 2kcal/mole) (1kcal ≡ 4. 184 kJ) implies that the reaction is a diffusion controlled process.

The thermochemistry of ammonium-exchanged Y- zeolite has been studied by Bolton and his co-workers[59]. They found that the deamination, dehydroxylation and desorption of physically absorbed water which constitute the thermal decomposition of ammonium-exchanged zeolite overlap to a considerable extent and separate steps for the evolution of ammonia and water vapour cannot be isolated.

1. 3. 2 Endothermic Decomposition of the Carbonates and Hydrates

There are many features which the present investigation has in common with the investigations performed by various workers on the carbonates and hydrates, and it is necessary to discuss these further in order to provide a background for the discussion of the results of the present investigation.

In the endothermic solid reactions of these compounds the energy of activation is often approximately equal to the overall enthalpy change e. g. dehydration of Alum crystals[62]. This means that the reverse reaction must occur with a very small energy of activation, provided that no profound structural change takes place during the decomposition. There are, however, notable exceptions to this general rule e. g. the dissociation and recombination of zinc carbonate[63] and of magnesite[64]. In some cases (magnesite) the formation of active products is the cause of this since they influence the overall kinetics by introducing false equilibria (one of the largest problems in carbonate studies) and raise the apparent activation energy.

Endothermic decompositions are almost exclusively interfacial in character. One of the very few exceptions is $MnCO_3$ where the kinetics of decomposition follows the Prout-Tompkins equation. Langmuir[65] was the first to draw attention to the importance of the interface between the two solid phases for dynamic equilibrium in systems of the type, $A_{(s)} \rightleftharpoons B_{(s)} + C_{(g)}$ and his suggestion was applied by Crowther and Coutts[66] to explain the results obtained in a study of the dehydration of certain salt hydrates. The basic assumption of the interface type of mechanism is that the only molecules (ions or ionic groups) which react are those in a layer immediately adjacent to the molecules (ions or ionic groups) in the space lattice of the resultant solid phase. Furthermore it can be assumed that the actual commencement of the change is restricted to the surface of the particles, which are mutually independant. The propagation of the change then takes place from the surface inwards. The different types of decomposition curve to be expected in these circumstances have been discussed by Topley and Hume[67] and are as follows:

(i) The surface rapidly becomes covered with nuclei of the product phase and the resulting interface will move inwards at a constant rate. The type of equation that holds in any specific case of this sort is dependent on the geometry of the particles and the interface. By far the most common expression is the contracting sphere equation.

(ii) If the rate at which the change spreads through the particle is very much larger than the rates of formation of nuclei on the surface, then the average curve will conform to the unimolecular law.

(iii) A case which is intermediate between these two is also possible i. e. when the rates of nucleus formation and propagation of the interface are such that the majority of the particles have at least one nucleus before more than a very small fraction of the total reaction has taken place. If this is the case then the area of the interface must pass through a maximum as the reaction proceeds and the rate of the reaction will be proportional to this area.

The recombination or reverse reaction has not, especially in the case of the hydrates, had much attention devoted to it; the rehydration of the zeolites has, however, been studied in some detail. Seyewitz and Brissaud[68] classified the products of dehydration into five main groups according to whether dehydration proceeded (i) fully, (ii) partially and independently of the percentage relative water vapour pressure, P_{rel}, over the crystal, (iii) to an extent dependent on P_{rel}, (iv) until the product was deliquescent, or (v) not at all. They studied numerous salts and found that the rate of rehydration (under fixed conditions) was constant for considerable periods but that in some cases inflexions in the rate curves indicated the possibility of the formation of intermediate hydrates. This possibility has also been noted by other authors working with $NiSO_4$[69] and $CuSO_4$[70] but these inflexions did not correspond to the composition of any stable hydrates. In the case of the carbonates the reverse reaction is a single stage and no intermediates are suspected to be formed in the recombination, but the recombination can be divided into three consecutive sections viz., (i) the chemisorption of CO_2, (ii) the production of nuclei, and (iii) the occurrence of an interface

reaction.

Thus for hydrates one usually has decomposition via several stable intermediate hydrates while recombination occurs without the formation of any stable hydrate. In the case of the carbonates both the decomposition and the recombination involve a single stage. One of the few exceptions to this is lead carbonate which has been shown[71] to decompose via several stable intermediate carbonates.

The kinetics and mechanism of the reverse reaction have been studied in isolated cases and can conveniently be divided into two main groups.

(i) The recombination is a diffusion controlled process (the rehydration of alum crystals[62])

(ii) The recombination is an interface type of reaction (the recombination of Ag_2CO_3[27])

(i) A diffusion controlled reaction

Bielanski and Tompkins[62] found that the rehydration of alum crystals at constant temperature and relative water vapour pressure follows the relationship

$$\alpha' = (kt)^{\frac{1}{2}} + B \qquad 1.31$$

(where α' is the fraction of the material recombined)

over most (~ 80%) of the reaction until a recrystallisation process occurs. The applicability of this relationship indicates that the hydration is not the inward progress of a well-defined interface and that the rate determining process is not the formation and growth of nuclei of the hydrated product, since this would give a sigmoid plot

of α' against t, which was not obtained. The applicability of this relationship is, however, consistent with diffusion along a network of interstitial channels such as are present in dehydrated zeolites. They concluded that the rate-controlling process was the diffusion of water molecules from higher adsorbed layers but could not accurately assess, by the weighing technique employed, the number of molecules in these layers. It was for this reason that Benson and Tompkins[72] later investigated the sorption of ammonia by dehydrated potash alum using measurements of the pressure of gaseous ammonia.

They found that the amount of ammonia sorbed at constant pressure is a linear function of $(\text{time})^{\frac{1}{2}}$ but that a process involving either diffusion into non-interconnecting channels or of diffusion from a network of interconnecting channels into spherical zones is inadequate. An alternative theory involving the concept of different types of sorption sites, however, was found to be consistent with the experimental results. There are likely to be many different sites for ammonia attachment where the energy of binding of the sorbate molecule varies with the nature of the site. For simplicity the authors considered these sites to comprise two main categories (X and Y) which differ in the degree of order and thus in the sorption energy of the site. Using this model they show that the equation

$$a^2 = 2kKNCp^{\frac{1}{2}} \qquad 1.32$$

is valid for the complete reaction.

Where a = moles of ammonia adsorbed/mole of alum/min.$^{\frac{1}{2}}$
k = rate constant of the sorption reaction
K = equilibrium constant for the exchange of residual H_2O between the two types of site.
C = constant form the Freundlich absorbtion isotherm of ammonia at the surface
p = pressure of ammonia

Application of this equation yields an activation energy of 9 kcals/mole (1 kcal = 4. 184 kJ). This energy term however is a composite one reflecting the temperature coefficient of the product K, k and C and is thus the algebraic sum of; the activation energy of the reaction,

$$X + NH_3 \longrightarrow X:NH_3$$

the heat of reaction of,

$$Y + X.H_2O \rightleftharpoons Y.H_2O + X$$

and also a term involving the heat of absorption of NH_3 at the surface.

The results also suggest that the process is initiated by a critical quantity of sorbed ammonia and is then accelerated by the heat released during sorption. The process has, in fact, the properties of a metastable phase transition. It seems likely that it involves a disintegration of the amorphous zones and a creation of sorption sites. Similar disintegrations are obtained by the sorption of polar molecules in other systems e. g. ammonia by chabasite[73] and water by silica gel[74].

(ii) An interface type of reaction

A good example of this type is the reaction

$$Ag_2CO_3 \rightleftharpoons Ag_2O + CO_2 \qquad 1.33$$

which was studied by Spencer and Topley[27]. They found that the contracting sphere expression held for both the forward and reverse reactions. Further evidence that the reactions are essentially interfacial in character is supplied by the fact that both the decomposition and the recombination curves were sigmoid in shape under the best experimental conditions i. e. low temperature for the decomposition and pressure of

CO_2 not greatly in excess of the equilibrium pressure for the recombination. The mechanism which they proposed for the reverse reaction involves the adsorption of CO_2

$$Ag_2O + CO_2 \rightleftharpoons Ag_2O(CO_2)_{adsorbed} \longrightarrow Ag_2CO_3 \qquad 1.34$$

The formation of the carbonate only occur where the adsorbed CO_2 happens to be in immediate juxtaposition to the ions vibrating from the oxide onto the carbonate lattice. This type of mechanism depends on the assumption that there is rapid diffusion of the adsorbed molecules in the interface. This mechanism was tested by applying an equation of the Langmuir type.

Another example of an interface-type of reaction is the decomposition and recombination of calcite studied by Britton, Gregg and Windsor[75]. One factor of interest to the present investigation which arose during their investigation was the fact that when calcium oxide, which had been formed by decomposition of calcite in vacuo, is exposed to CO_2 (at a pressure of one atmosphere) at 850°C it rapidly absorbs 50-70% of its original CO_2 content. When such a reformed specimen is subsequently decomposed in vacuo at the original decomposition temperature, a rate 4-6 times the original rate is obtained but the contracting sphere expression is still obeyed. Repetition of this procedure does not further enhance the rate. This behaviour is quite consistent with the findings of Zawadzki.[63]

1.4 Previous Work

1.4.1 The Thermal Decomposition of Ammonium Metavanadate

Although there have been a number of investigations of the thermal decomposition of ammonium metavanadate [75-84], and it is clear that the decomposition is complex and involves several stages, there is no general agreement on the stoichiometry of these stages and little information on the mechanism of the reaction. Previous investigations may be conveniently summarized and compared by dividing them according to the atmosphere prevailing during decomposition. See Table 1.2.

1.4.1.1 The Decomposition in Air or Oxidising Atmospheres

There is overall agreement [75-77, 52] that ammonium metavanadate (AMV) decomposed to $(NH_4)_2\ V_6O_{16}$ (ammonium hexavanadate or AHV) below 200°C and further to V_2O_5 above 250°C. Trau[77] has detected another intermediate, $(NH_4)_2V_4O_{11}$, (ammonium bivanadate) which is formed at lower temperatures. Lamure and Colin[78] found that formation of this intermediate (ammonium bivanadate) is dependent on the sample mass, the heating rate and the carrier gas flow rate used in a thermogravinetric analysis. Small samples, a slow heating rate and a rapid flow of carrier gas favoured its formation. Dubois and Breton[79] found that in addition to AHV there was some indication of the formation of another intermediate of variable composition which approximates to $(NH_4)_2\ O.(V_2O_5)_{8.3}$ at higher temperatures. Dilatometric examination gave similar results.

Taniguchi and Ingraham (52) have pointed out the danger of using any technique based entirely on thermogravimetric methods to determine the stoichiometry of the decomposition stages, as, for example, the formation of AHV, HVO_3 and $NH_3.\ H_2O.\ (V_2O_5)_2$ from AMV would all result in almost identical mass-losses. Thus we find Duval[80] and Erdey, Gal and Liptay[51] incorrectly reporting that all the ammonia is lost between 130°C and 200°C and that the residue is HVO_3 which is unstable. Above 200°C dehydration begins and the conversion to V_2O_5 is complete by 450°C.

The intermediate $(V_2O_5)_2.NH_3.H_2O$ has been reported by Sesbes[81] who states that this intermediate was formed between 280°C and 320°C. This then decomposes further above 320°C and by 460°C was entirely transformed into V_2O_5.

1.4.1.2 The Decomposition in Inert Atmospheres

Taniguchi and Ingraham[52] found that the intermediate formed during the decomposition in flowing N_2 was the same as that formed when O_2 was used as the carrier gas. The first stage of the reaction, in the temperature range 210-215°C, takes place in two steps. A gaseous product is evolved in both steps, but the gas analysis trace does not differentiate between the gas evolved from each step. The intermediate formed (AHV) is stable up to 260°C after which the material undergoes an endothermic reaction, evolving a gaseous product at maximum rate at about 325°C. The solid product then undergoes a further exothermic reaction at 375°C. The final solid product is a dark-coloured vanadium oxide in which the average vanadium valence is very slightly less than 5.

Under the conditions of inert atmosphere used by Satava[76] AMV decomposed in three successive stages. The mass-loss of 16.5% and the X-ray diffraction pattern for the first stage corresponded to partially reduced AHV. The second stage (350°C), with a mass-loss of 20.5%, resulted in an intermediate of the approximate formula $NH_4V_6O_{15}$. The final product (500°C), with a mass-loss of 26.5%, corresponded to $VO_{2.17}$ or V_6O_{13}. When this product was heated above 750°C the powder lines due to V_6O_{13} disappeared and those of VO_2 and V_2O_5 appeared. The DTA trace showed a double endotherm around 700°C which probably corresponds to this stage.

1.4.1.3 The Decomposition in Ammonia or Reducing Atmospheres

Satava[76] found stages similar to those in inert atmosphere for the decomposition in ammonia. The product of the first stage (150-200°C, mass-loss 15.5%) is partially reduced AHV which decomposes further at about 300°C to give $NH_4V_6O_{15}$. The product at 400°C was V_6O_{13} and further reduction of this to V_2O_3 occurs in three stages. By 500°C the V_6O_{13} is converted to VO_2 which decomposes above 600°C to give $VO_{1.67}$. The final product of the decomposition is V_2O_3 which is formed at 700°C with a total mass-loss of 36.1%.

The decomposition in hydrogen was very similar to that in ammonia[76, 82]. The products of the first three stages were identical to those formed during the decomposition in ammonia, but none of the intermediates in the further reduction of V_6O_{13} to V_2O_3 could be isolated.

Sata, Komada and Ito[82] reported a new intermediate oxide which they found to be a modification of VO_2.

1.4.1.4 The Decomposition in Vacuum

Only Deschanvres, Nouet and Raveau[83] have studied the decomposition of AMV in vacuum. They found that AMV decomposed to give AHV at first (180°C),

$$6NH_4VO_3 \longrightarrow (NH_4)_2 V_6O_{16} + 4NH_3 + 2H_2O \qquad 1.35$$

and that at higher temperatures (230°C) the hexavanadate decomposed without intermediate to give the bronze of limiting composition $NH_4V_4O_{10}$

$$2(NH_4)_2V_6O_{16} \longrightarrow 3NH_4V_4O_{10} + \tfrac{1}{2}N_2 + 2H_2O \qquad 1.36$$

When this intermediate was heated further (300-350°C) a new phase, $VO_2 \cdot yH_2O$, resulted with $Y_{max} = 0.04$. On heating to 500°C monoclinic VO_2 was formed.

Deschanvres and Nouet[84] studied the kinetics and mechanism of the first stage of the decomposition in vacuum, i.e. the conversion of AMV into AHV, reaction (1.35) above and used a mass spectrometer connected directly to the decomposition vessel to follow the gas evolution. Ammonia and water vapour were evolved simultaneously in the ratio of 2:1. The contracting sphere model (Equation 1.20), i.e. rapid surface coverage by reaction product followed by progression of the reactant-product interface at a constant rate into approximately spherical particles, held fairly well for the major portion of the decomposition. The apparent activation energy for the process over temperature range 130°C - 180°C was found to be 28 kcal mol^{-1}.

TABLE 1.2

Summary of Previous Work on the Thermal Decomposition of Ammonium Metavanadate

Atmosphere	Flow rate (ℓ/hr)	Type of analysis	Temperature range (°C)	Heating rate (°C/hr)	Sample mass (g.)	Product	Reference
Oxidising	3	DTA, EGA X-ray	210-215	180	-	$(NH_4)0.3V_2O_5$ V_2O_5	Taniguchi and Ingraham[52]
	-	TGA, DTA X-ray	250 340 420	360-600	0.25-0.50	$(NH_4)0.3V_2O_5$ unspecified V_2O_5	Satava[76]
	-	TGA	200 225 285	25-300	0.10	$(NH_4)_2O.2V_2O_5$ $(NH_4)_2\ 3V_2O_5$ $_2O_5$	Trau[77]
	30	TGA, X-ray	100-250 250-350	17-300	0.10-0.40	$(NH_4)_2=.2V_2O_5$ or $(NH_4)_2$ $0.3V_2O_5$ depending on conditions V_2O_5	Lamure and Colin[78]
	-	TGA	198-200 206-450	Not linear	0.20	HVO_3 V_2O_5	Duval[80]
	-	DTA, DTG	130-270 270-470	300	0.10-0.20	HVO_3 V_2O_5	Erdey, Gal and Liptay[51]

TABLE 1.2 (continued)

Atmosphere	Flow rate	Type of analysis	Temperature range	Heating rate	Sample mass	Product	Reference
Oxidising	-	TGA, DTA	280-320	240	-	NH_3H_2O $2V_2O_5$ V_2O_5	Sesbes[81]
Reducing NH_3	-	DTA, TGA X-ray	150-200 300 400 500 600 700	360-600	0.25-0.50	partially reduced AHV $(NH_4)_2O.2VO_2$ $5V_2O_5$ V_6O_{13} VO_2 $VO_{1.67}$ V_2O_3	Satava[76]
H_2	12	DTA, TGA	300	300	0.30	2 unspecified intermediates V_2O_5 V_2O_3 via V_6O_{13} and modified VO_2 V_2O_3 via modified VO_2 and new unspecified oxide	Sata, Komada and Ito[82]

TABLE 1.2 (continued)

Atmosphere	Flow rate	Type of analysis	Temperature range	Heating rate	Sample mass	Product	Reference
Inert	-	DTA, TGA	250	360-600	0.25-0.50	partially reduced AHV $(NH_4)_2O2VO_25V_2O_5$ V_6O_{13} $VO_2 + V_2O_5$	Satava[76]
	3	DTA, EGA X-ray	210-215 260-375	180	-	AHV V_2O_5	Taniguchi and Ingraham[52]
Vacuum	-	Isothermal	130-180 230 300-350 500	-	order of several mg.	$(NH_4)_2O.3V_2O_5$ $NH_4V_4O_{10}$ VO_2yH_2O VO_2	Deschanvres, Nouet and Raveau[83]

At the end of the stage represented by reaction (1. 35) a linear portion as a function of time appeared, corresponding to a slower reaction than if it were controlled by the rate of advancement of the interface. This phenomenon was attributed to the diffusion of gas across the layer formed by the hexavanadate on the surface of each grain.

1. 4. 2 The Crystal Structure of Some Vanadates and Vanadium Oxides

1. 4. 2. 1 The Metavanadates

The structure of AMV, proposed by Lukesh[85], and later confirmed and refined[87, 88, 89], consists of tetrahedral chains of VO_4 groups (Fig. 1. 2) linked by vertices. Evans[88] pointed out that all the anhydrous metavanadates, with the exception of $NaVO_3$, the structure of which has been shown[86] to resemble that of diopside $CaMg(SiO_3)_2$, are isostructural with AMV, with space group Pbcm. In AMV the NH_4^+ cation is irregularly surrounded by ten oxygen atoms at distances varying from 2. 85 to 3. 40 Å and while there are several relatively short N-O distances the oxygen atoms do not approach any tetrahedral configuration around the ammonium ion, thus it is not obvious where the hydrogen bonds, if any, lie.

In the chains of tetrahedra there are two types of V-O bond. Within the tetrahedron, two bonds of one type extend to the oxygen atoms which link the tetrahedra together and have a length of 1. 81 $\pm$ 0. 01 Å $V\text{-}O_I$ (Fig. 1. 3.) Two other bonds of the second type extend to unlinked oxygens in the mirror plane $V\text{-}O_{II}$ and $V\text{-}O_{III}$. Although

Figure 1.2

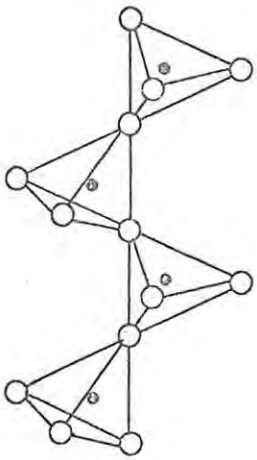

Figure 1.3

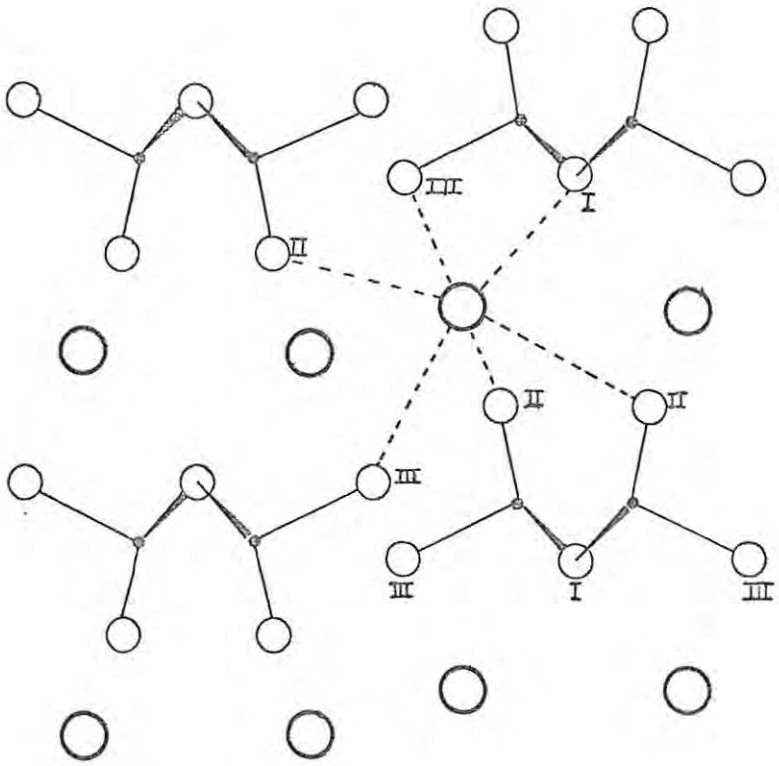

Vanadium

Oxygen

Nitrogen

these are not crystallographically related, they all have lengths of 1.66 ± 0.01 Å. The configuration of the chains is similar to that of the silicate chain in diopside, with the bonds on the linked oxygen bent at an angle of approximately 144° (angle $V\hat{O}_I V$) (143° in KVO_3, 145° in NH_4VO_3 and 141° in diopside). In the silicate chain, all the tetrahedral bonds are nearly equal in length and in character, in contrast to those in the metavanadate chain. The assymmetry of the vanadium tetrahedron must result from the tendency of vanadium to form multiple bonds with oxygen.

It has been shown[90] that in a tetrahedral environment the d shell is split so that the d_ε orbitals have a higher energy close to the 4s and 4p shells. Therefore it may be expected that the three d_ε orbitals of vanadium may form a hybrid for bonding of the $d_\varepsilon^3 s$ type, which has tetrahedral configuration. The d_γ orbitals may play an additional role in the formation of π bonds about two of the tetrahedral σ bonds, thus accounting for the severe shortening of these bonds which is observed.

1.4.2.2 The Hexavanadates

Kelmers[91] prepared $K_2V_6O_{16}$, AHV, $Rb_2V_6O_{16}$ and $Cs_2V_6O_{16}$ as precipitates from acidified solutions of the metavanadates. They are all monoclinic, space group $P2_{1/m}$ and undergo a linear expansion in the a and c dimensions as the ionic radius of the cation increases. The cell dimensions for AHV are estimated to be $a = 7.87$ Å, $b = 8.43$ Å, $c = 5.01$ Å and $\beta = 96°45'$. These were estimated on the assumption that β remains unchanged for all the

hexavanadates (β for $K_2V_6O_{16}$ was obtained from the results of Block[92]. Small changes in β would not affect the calculation since β is close to 90^o.

The structure of $K_2V_6O_{16}$ is a clearcut layer type consistent with the perfect (100) cleavage and large negative birefringence observed for this crystal. The layers consist of highly distorted VO_6 octahedra linked together by sharing corners and edges. The cations occupy positions between the layers, in irregular 12- fold co-ordination with neighbouring oxygen atoms. In $K_2V_6O_{16}$ the V_{II} atoms (in Fig. 1.4a) are in double pyramidal groups V_2O_8, in which the pyramids are joined by an edge with apices directed opposite to each other. These double groups are joined into zig-zag chains along the b axis by sharing corners, through O_{II}, and these chains are linked into sheets by VO groups represented by V_I and O_I (Fig. 1.46). This V_I - O_I distance is equal to the apical V-O distance $V_{II}O_{IV}$, while the opposite V-O distances (A and B) through the pyramidal base are correspondingly longer and shorter.

AHV has been reported[52, 75-78] to be one of the intermediates in the thermal decomposition of AMV. There is some disagreement in the x-ray powder diffraction data reported for AHV. (See Table 1.3)

Figure 1.4a

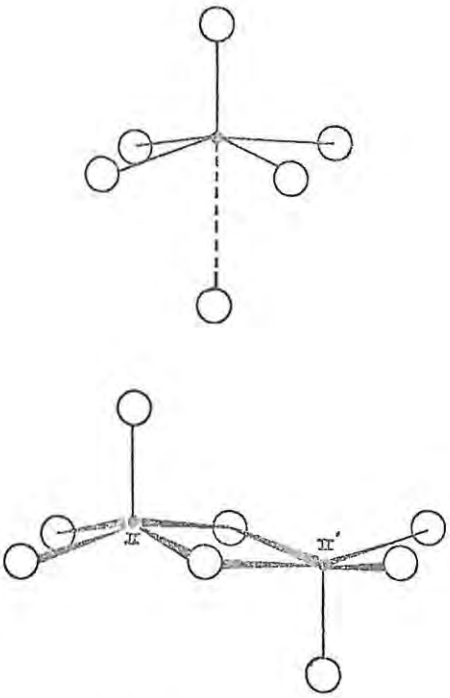

Figure 1.4b

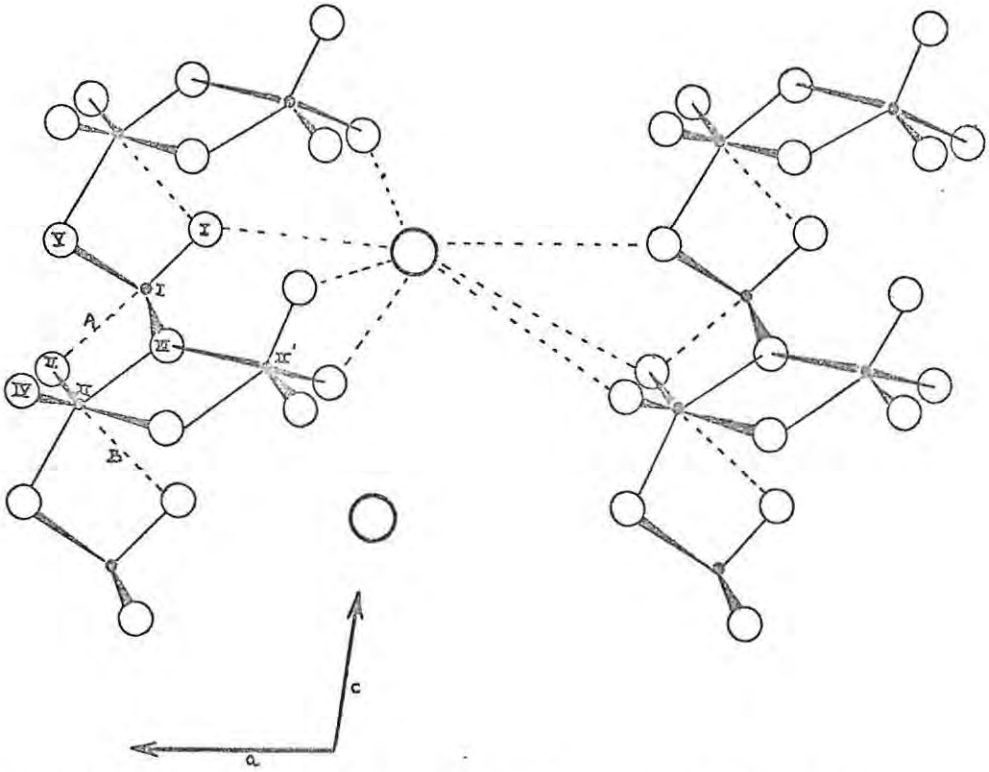

The symbols for vanadium oxygen and nitrogen atoms are the same as for figure 1.3

TABLE 1.3

Reported X-ray Powder Data for AHV Using Cu K_α Radiation

Lamure & Colin[78] and Kelmers[91]	Satava[76]	Taniguchi & Ingraham[52]
7.84 vs		8.2 vs
	7.3s	
		6.2 vw
5.75 s		5.7 vw
	5.3 m	
4.98 w		
4.21 w		
		4.1 m- broad
3.91 m		
3.55 s		
		3.46 m
	3.39 m	3.34 m
3.26 m		
3.21 m	3.22 w	3.17 s
3.04 w	3.05 vs	
2.92 m		
2.90 m		
2.87 m	2.86 m	2.88 vw broad
	2.71 m	2.61 m
2.49 w		
2.40 w	2.12 s	2.21 m
1.80 w	1.97 s	1.80 s
	1.48 s	

w = weak
m = medium
s = strong

1.4.2.3 The Vanadium Oxides

Vanadium Pentoxide

Two basic crystal structures for vanadium pentoxide which differ in space group and, to some extent, in atomic parameters have been proposed [94-98] (Fig. 1.5a and b).

Ketelaar[94], on the basis of the known crystal class and the systematically absent reflections, deduced the space group to be either $Pmn2_1$ or Pmnm. On the basis of the hemimorphic symmetry of some of his crystals; the difference in the rates of solubility in dilute sodium hydroxide solution at opposite ends of the y-axis and some of the etch figures produced by this reagent on the (010) face, he concluded that the space group must be the non-centrosymmetric $Pmn2_1$.

Ketelaar interpreted his structure in terms of chains of oxygen tetrahedra around V, sharing corners and extending parallel to (001) (Fig 1.5a), and cross-linked by additional corner sharing along (100) to form two-dimensional nets. This constitutes four-fold co-ordination of O around V (O_I, O_{II}, O_{III} & O_{IV}) (V-O, 1.57-1.83 Å) although he does point out that inclusion of an oxygen atom (O_V) in an adjacent cell, and at a slightly greater distance from V, would increase the co-ordination to five-fold. Machatski[97] contends on morphological grounds that Ketelaars structure should be considered solely in terms of single chains of tetrahedra parallel to (001) linked laterally along (100) by oxygen bridges.

Byström et al[95], dissatisfied with the very short (2.14 Å) distance between certain pairs of oxygen atoms (O_{II} and O_{III} Fig. 1.5a) in the structure proposed by Ketelaar, repeated the structure determination

1.5a is structure according to Ketelaar

1.5b is structure according to Byström et al

Both are projections on (001). The arabic figures denote the height of the atoms in per cent of C. Superimposed oxygen atoms are symmetrically displaced. Roman numerals are used to denote O atoms referred to in the text.

Figure 1.5a

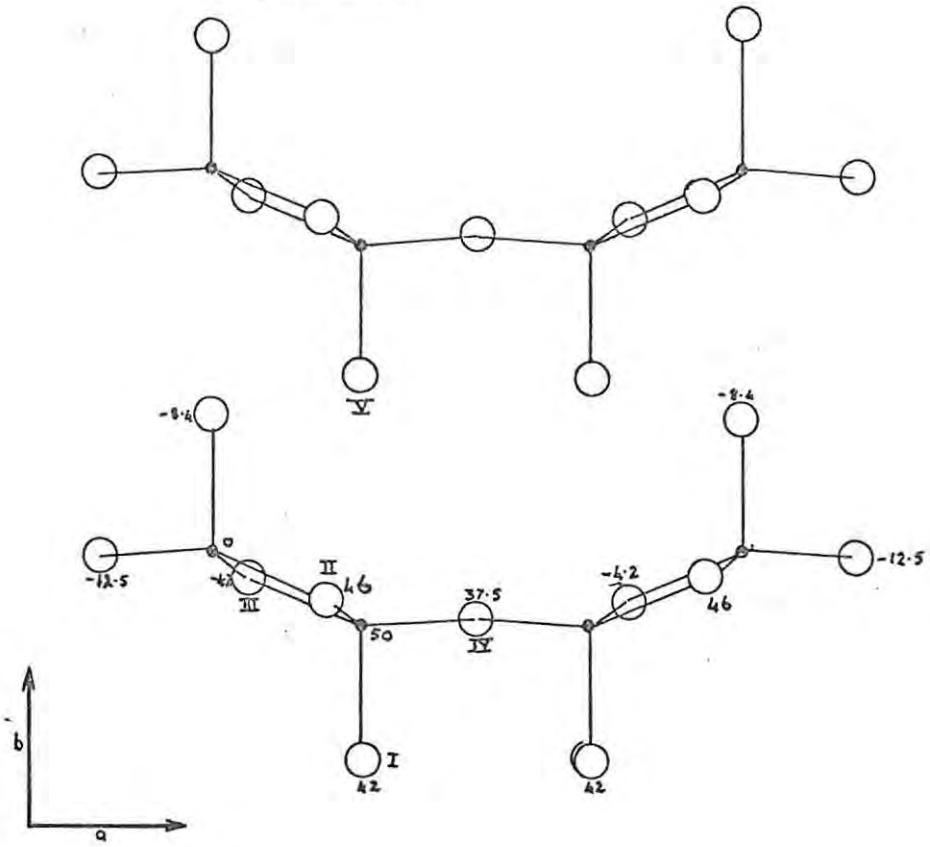

Figure 1.5b

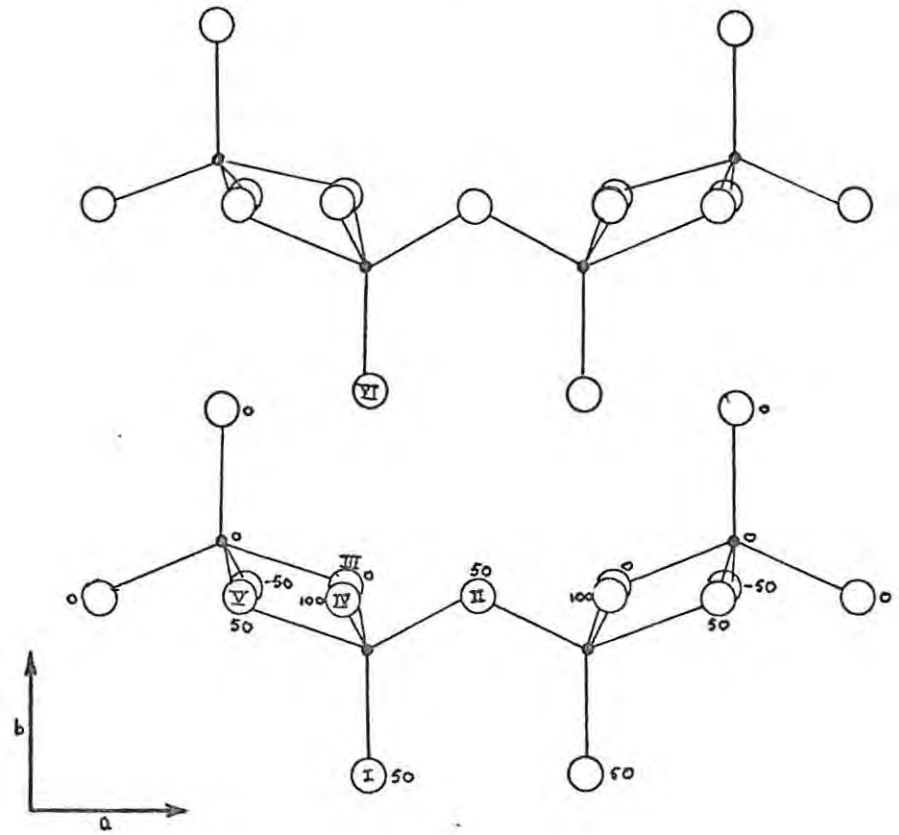

and found nothing to suggest that the space group should be $Pmn2_1$ rather than Pmnm. They did not consider that arguments for hemihedral symmetry based on crystal habit were valid for V_2O_5 grown from the melt because of the manner in which the crystals are attached to the walls of small cavities.

Byström et al describe their structure in terms of distorted trigonal bipyramids sharing corners along (100) and (001) (Fig. 1.56). Thus the oxygen atoms ($O_I \rightarrow O_V$) are considered to be five-fold co-ordinated in V_2O_5. They also show that a very distorted octahedral co-ordination could be achieved by the inclusion of a sixth oxygen atom (O_{VI}) at the very much greater V-O distance of 2.81 Å but that this would imply stronger bonds between successive V-O layers along (010) than would be expected from the perfect (010) cleavage. Finally it may be noted that the adjacent pairs of corners of the trigonal bipyramids of Byström et al which are shared along (001) define the edges of the bipyramids so that it is more convenient to describe the structure as composed of double, or zig-zag, chains of trigonal bipyramids sharing edges along (001) and cross-linked along (100) through shared corners. Bachmann, Ahmed and Barnes[96] and Magnéli and Blomberg[98] agree that the structure proposed by Byström et al is the correct one.

Vanadium Dioxide

Andersson[99] investigated the crystal structure of VO_2 by x-ray methods and found that it belongs to the monoclinic space group $P2_1/c$, with unit cell dimensions of a = 5.743 Å, b = 4.517 Å, c = 5.375 Å, β = 122.6° and a density of 4.65 gcc^{-1}, corresponding to a cell

Figure 1.6

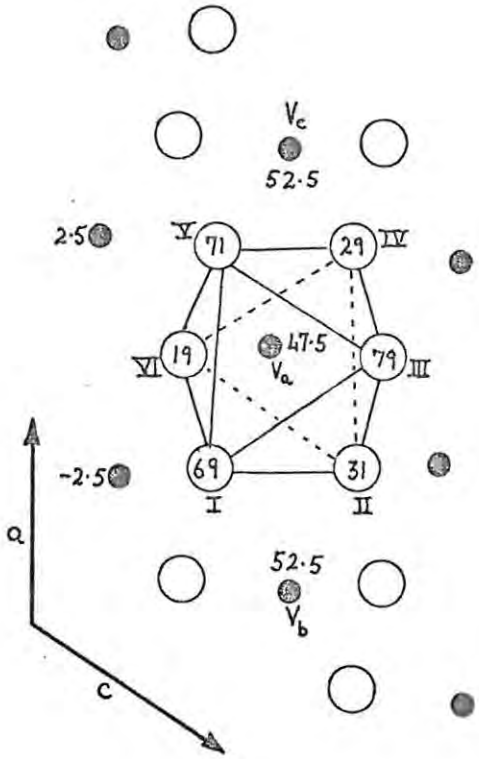

Projection of the structure on (010). The Arabic numerals give the levels of the atoms in per cent of b . One VO_6 octahedron is marked out and its 0 atoms are denoted with Roman numerals.

content of four formula units of VO_2. The structure may be described as built up of distorted VO_6 octahedra joined by edges to form strings, which are mutually connected by corners to form a three dimensional network of a deformed rutile type (Fig. 1. 6). The metal atoms within the strings are grouped pairwise to form doublets, as in the M_oO_2 structure.

The interatomic distances and angles in the VO_6 octahedra of VO_2 are comparable to those in the T_iO_6 octahedra (rutile) in spite of the distortion of the rutile type of the former structure. Thus the oxygen atoms of VO_2 (O_I & O_{II}) (Fig. 1. 6) forming the edge common to the two VO_6 octahedra of a metal atom pair (V_a & V_b) are somewhat forced apart when compared with the corresponding oxygen atoms of T_iO_2 whereas all the other O atoms in the VO_6 octahedra are closer together than the corresponding O atoms in the T_iO_6 octahedra of rutile. The conservation of the fairly regular arrangement of the oxygen atoms implies that the metal atom in vanadium dioxide is somewhat removed from the centre of gravity and approaches one face of the VO_6 octahedron.

1. 4. 3 Infrared Spectra of the Vanadates and Vanadium Oxides

Structural assignments for the infrared spectra of a large number of vanadium-oxygen compounds have been made by Fredrickson and Hansen[100].

1. 4. 3. 1 The Metavanadates

A wide variation in individual patterns for changes in the substituted cation was found for these compounds. The substituted cation has no consistent effect on the spectra. Several absorptions, (825 - 975cm^{-1}) appear which are apparently the result of V-O stretching modes for each of several, different oxygen atoms according to the particular location or arrangement within the lattice. No attempt has been made to explain the variation of the V-O stretching frequency with the arrangement within the lattice. At lower frequencies, (600cm^{-1} - 750cm^{-1}), a broad general absorption occurs.

Some of the metavanadates gave slightly different spectra depending on whether the KBr disc or the Nujol mull technique was used. Sodium and ammonium metavanadates are partially metathesized in KBr discs. These KBr pellet spectra of the metavanadates are, in most instances, reproducable and suitably distinctive for use in qualitative identification.

1. 4. 3. 2 The Hexavanadates

Two strong absorptions in the V-O stretching frequency region of these polyvanadates occur near 1000cm^{-1}, and near 960cm^{-1}. These bands are little affected by the mass or radius of the cation. The spectra also show the presence of a strong V-O band of lower frequency, located near 750cm^{-1}, with minor variation in its location from compound to compound. No attempt has been made to assign these frequencies to particular V-O bonds in the hexavanadates.

1. 4. 3. 3 The Vanadium Oxides

Two strong bands are observed[100, 101] in the infrared spectrum of V_2O_5, one located at 1020cm^{-1} and the other, which is a broad band, centered at 825cm^{-1}. The V_2O_5 structure has been described[95] as a double chain of distorted, trigonal bipyramids joined at the corners to form layers, the latter held together by lattice or residual forces. The 1020cm^{-1} band has been assigned to the V-O bond which is considerably shorter than the other bonds in the structure, viz., that contained in the V=O groups projecting perpendicularly to the V-O-V net plane, i. e. the (010) plane. The 825cm^{-1} band arises from the stretching modes of the longer V-O bonds, i. e. those in the V-O-V net plane.

In addition to the primary oxide V_2O_5, the oxide VO_2 has been shown[100] to possess an infrared spectrum. The bands appearing in this spectrum are weak when compared with those in the spectrum of V_2O_5. The main absorptions occur at 900cm^{-1} and 850cm^{-1} respectively but no assignments have been made to these absorptions.

1. 4. 3. 4 The Infrared Spectrum of the NH_4^+ ion

The fundamental vibrations of the NH_4^+ ion have been assigned from a comprehensive study[102] of the infrared spectra of ammonium chloride, bromide and the corresponding deuterated compounds. The low frequency bands at 1403cm^{-1} in the chloride is assigned to the triply degenerate bending mode ν_4 of the tetrahedral model. The triply degenerate stretching mode ν_3 is assigned to the doublet mean

Figure 1.7 Infrared absorption/structure correlation chart,
N-H and V-O vibrations

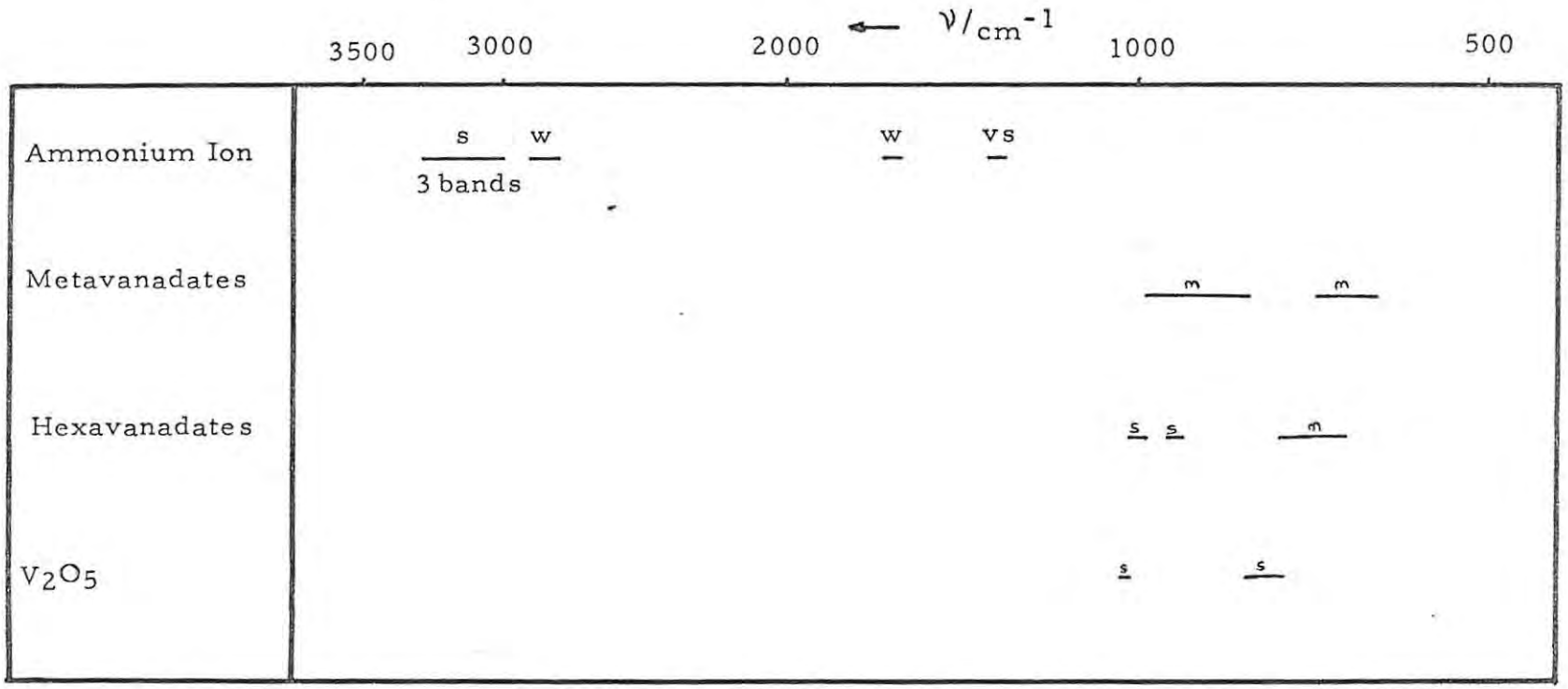

at 3080cm^{-1}. The band at 1794cm^{-1} is NH_4Cl has sometimes been assigned[103] to the doubly degenerate bending vibration ν_2. Wagner and Hornig[102], however, showed by means of the frequency ratio between the deuterated and the undeuterated compounds, that the wave-number 1683cm^{-1} should be assigned to ν_2 for NH_4Cl. The band at 2828cm^{-1} is assigned to the first overtone of ν_4 but the bands observed at 1794cm^{-1}, 2020cm^{-1} and 3223cm^{-1} cannot be accounted for in terms of intramolecular frequencies. These can, however, be interpreted as a combination between the totally symmetric mode ν_1 of the NH_4^+ ion (assigned to 3048cm^{-1} on the basis of the Raman spectrum[104]) and the optical branch of the lattice spectrum.

1. 4. 4 Relative Order of the Environment of the NH_4^+ ion and its Effect on the Infrared Spectrum

Co-operative order-disorder phenomena associated with the relative orientations of adjacent ammonium ions in ammonium halide crystals have been the subject of many investigations[105-114]. The fact that the phase transitions are order-disorder phenomena and not the onset of essentially free rotation has been firmly established[101, 104, 108, 115-118].

On studying the infrared spectra of these halides it is found that associated with the strong ν_4 fundamental band ($\sim$ 1400cm^{-1}) there is an anomalous high-wave-number component ($\sim$ 1435cm^{-1}) the intensity of which has an unusual temperature dependance. The behaviour of this component has been carefully studied for NH_4Cl[114] and clearly related to the breakdown of translational symmetry caused by the

disordering of the NH_4^+ ion orientations. The intensity of this component is proportional to p(1-p) where p is the probability that a nearest-neighbour NH_4^+ - NH_4^+ pair are orientated "parallel" to each other. Similar results have been obtained for NH_4Br[113].

The fact that this splitting of the ν_4 mode is an extremely sensitive measure of the distortion of the crystal lattice is shown by the splitting of $28cm^{-1}$ in the case of NH_4Br where it is known from x-ray data that the Br^- ions are displaced only two percent of the unit lattice dimension from their lattice position in a simple CsCl cubic lattice in which ν_4 would be degenerate.

The triply degenerate stretching mode, ν_3 , also loses its degeneracy with distortion of the lattice. This change is more difficult to detect in the infrared spectrum as the splitting is smaller (of the order of $10cm^{-1}$) and the resolution in this region is not as good.

2. OBJECTS OF THE RESEARCH

The investigation of the stepwise thermal decomposition of AMV to form V_2O_5, for which the overall reaction is

$$2NH_4VO_3 \rightleftharpoons V_2O_5 + 2NH_3 + H_2O \qquad 2.1$$

was undertaken since the preparation of V_2O_5 by this method is of some commercial importance as V_2O_5 is used extensively as a catalyst in oxidation reactions.

This research was thus undertaken with three primary aims;

(i) to investigate fully the stoichiometry of, and some of the structural changes involved in, both the forward and the reverse reactions under various conditions of surrounding atmosphere;

(ii) to obtain as many of the kinetic parameters for both the forward and the reverse reactions as possible and, using these, together with the results from (i);

(iii) to postulate probable mechanisms from the kinetic point of view for part, if not the whole of the forward and reverse reactions.

It is also intended, since the decomposition is endothermic, to investigate the possibility of illustrating the mechanism for part of the forward reaction from the molecular point of view by consideration of the crystal structures of ammonium metavanadate and ammonium hexavanadate.

Figure 3. 1

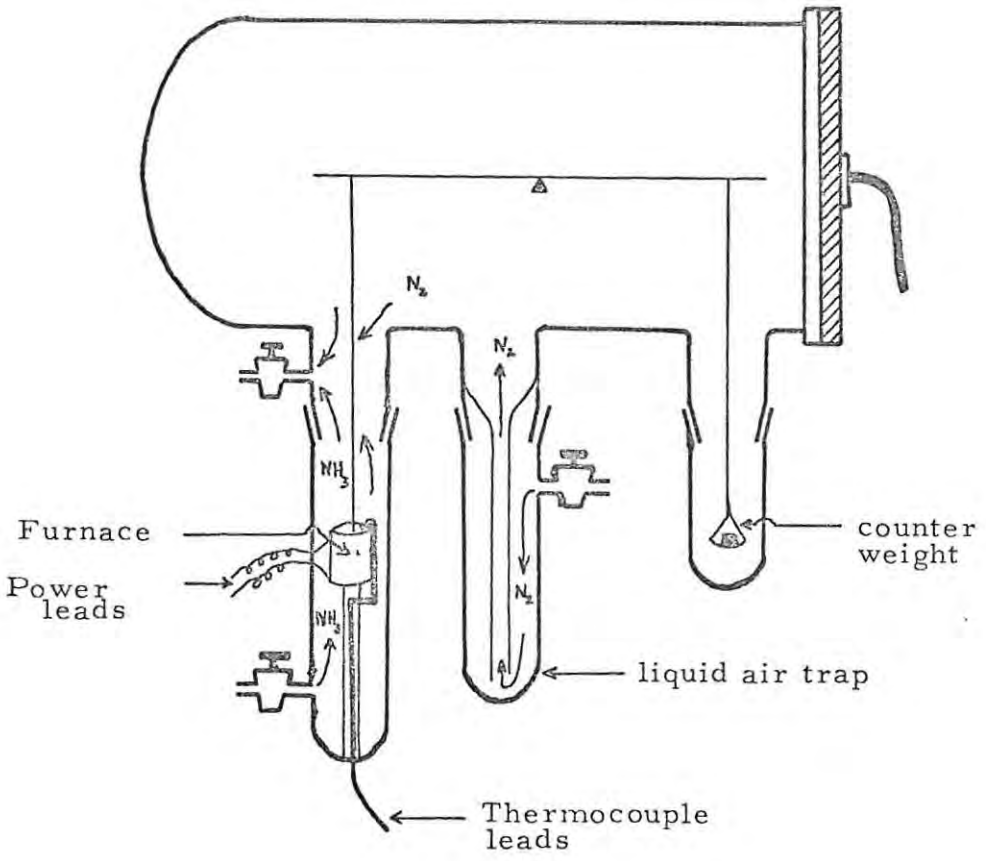
N_2
N_2
NH_3
Furnace
Power leads
NH_3
N_2
counter weight
liquid air trap
Thermocouple leads

3. APPARATUS AND GENERAL EXPERIMENTAL PROCEDURES

3.1 The Isothermal Decomposition and Recombination

Powder samples of AMV (BDH) were used throughout the investigation since powder samples from another manufacturer (Hopkins and Williams) gave similar results and attempts to obtain suitable single crystals according to the method of Lukesh[85] were unsuccessful. Deschanvres and Nouet[84] have reported that even when larger single crystals were prepared, these tended to break up at the start of the decomposition into small crystals with dimensions and decomposition kinetics similar to the material before recrystallization.

The AHV samples were prepared according to the method of Kelmers[91] except that instead of preparing the one molar starting solution of AMV from $(NH_4)_2CO_3$ and V_2O_5, it was prepared from BDH Analar AMV.

The commercial samples of V_2O_5 used in some of the recombination experiments were powder material from Hopkins and Williams. Large crystals of V_2O_5 were prepared from this material by slow cooling of the melt.

A Cahn R.G. Automatic Electrobalance was used in conjunction with a Beckman 10" linear recorder (model 1005) in order to follow the isothermal decomposition of AMV by means of the mass-loss of the sample with time. The sample was placed in a platinum bucket suspended by fine platinum wire from the balance. The balance was contained in a thick walled glass bottle (Fig 3.1) which could be

Figure 3.2

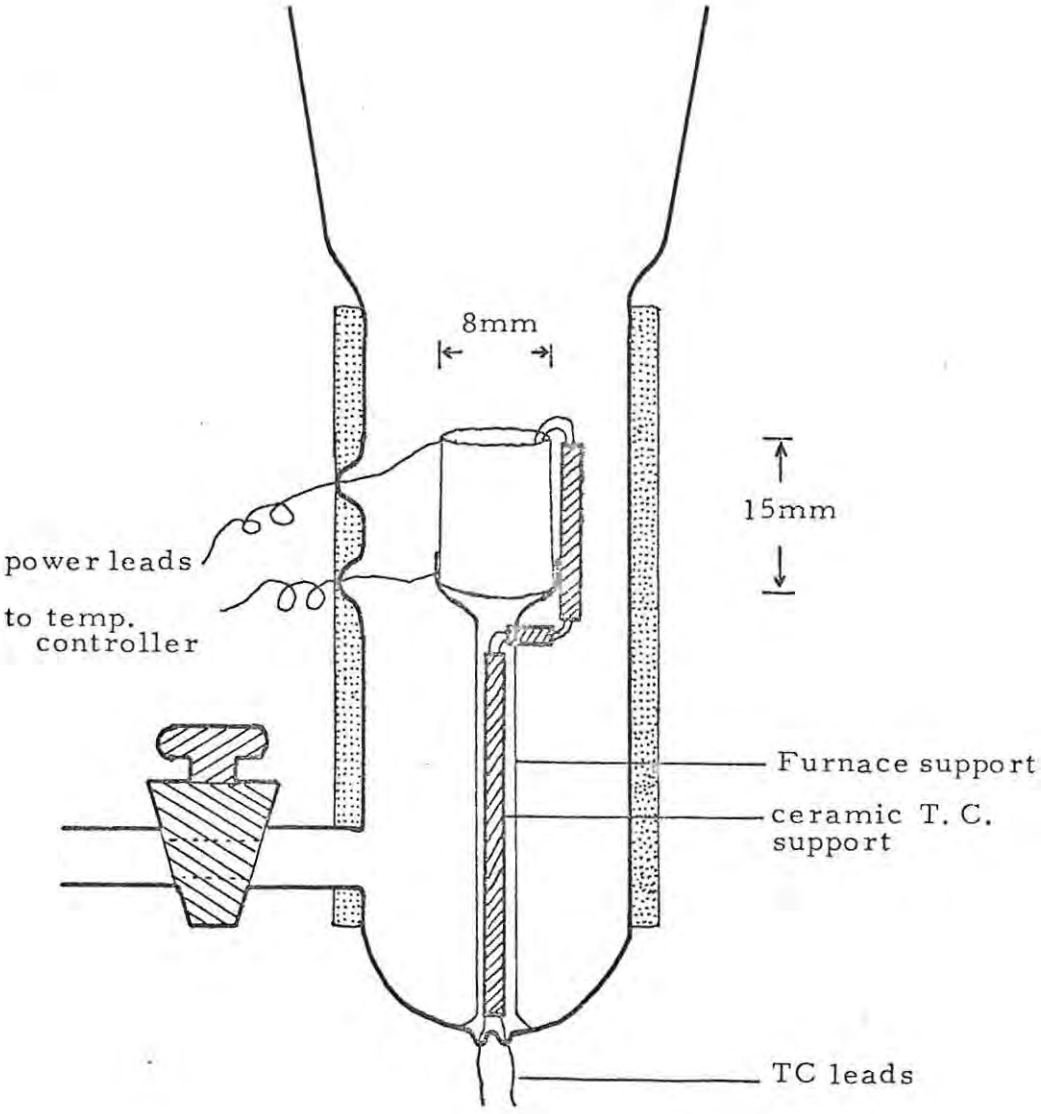
8mm
15mm
power leads
to temp.
controller
Furnace support
ceramic T. C.
support
TC leads

evacuated to 10^{-6} mmHg (throughout this thesis 1mmHg = $13.595 \times 980.665 \times 10^{-1}$ Nm^{-2}) through a vacuum line consisting of an Edwards Speedivac three-stage oil diffusion pump (model 203B), backed by an Edwards Speedivac gas ballast rotary high vacuum pump (model 25C20A). The pressure of the system was measured with a Pirani gauge (Pye Instruments Cat. No. 11018), a McLeod gauge, and a mercury manometer. The volume of the bulb of the McLeod gauge was 108.0 cm^3 at 25°C. Liquid air traps were incorporated into the system in order to protect the decomposition chamber and the backing pump from contamination by mercury vapour and the product gases.

The sample bucket was suspended in the centre of a microfurnace based on the one used by Perkin-Elmer in their TSG-1 thermogravimetric analysis system (see Fig. 3.2). The furnace element (18 gauge Nichrome wire) was wound in a spiral and this spiral element was wound onto a ceramic cylinder to form a coiled coil to yield a non-inductively wound furnace. The whole cylinder was then given a thin coat of Alundum cement to fix the element onto the cylinder. A Pt/Pt 10% Rh thermocouple was cemented into position as shown in the diagram. The furnace power leads were sealed onto heavy gauge Pt wire and the furnace and thermocouple sealed in position in a "Pyrex" glass hangdown tube which was fixed by a ground-glass joint (B34) onto the glass vacuum bottle containing the balance. The axial temperature profile of this furnace at 200°C is given in Fig 3.3. The temperature of the furnace was controlled by means of a Eurotherm digital temperature controller (model DHS/PID/SCR/FC). Calibration curves of sample temperature against set millivoltage for each of the atmospheres used during decomposition were determined

Figure 3.3

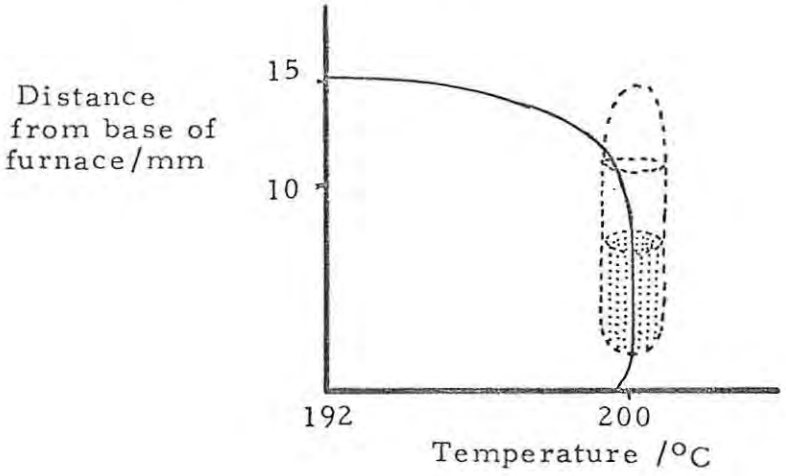

Figure 3.4

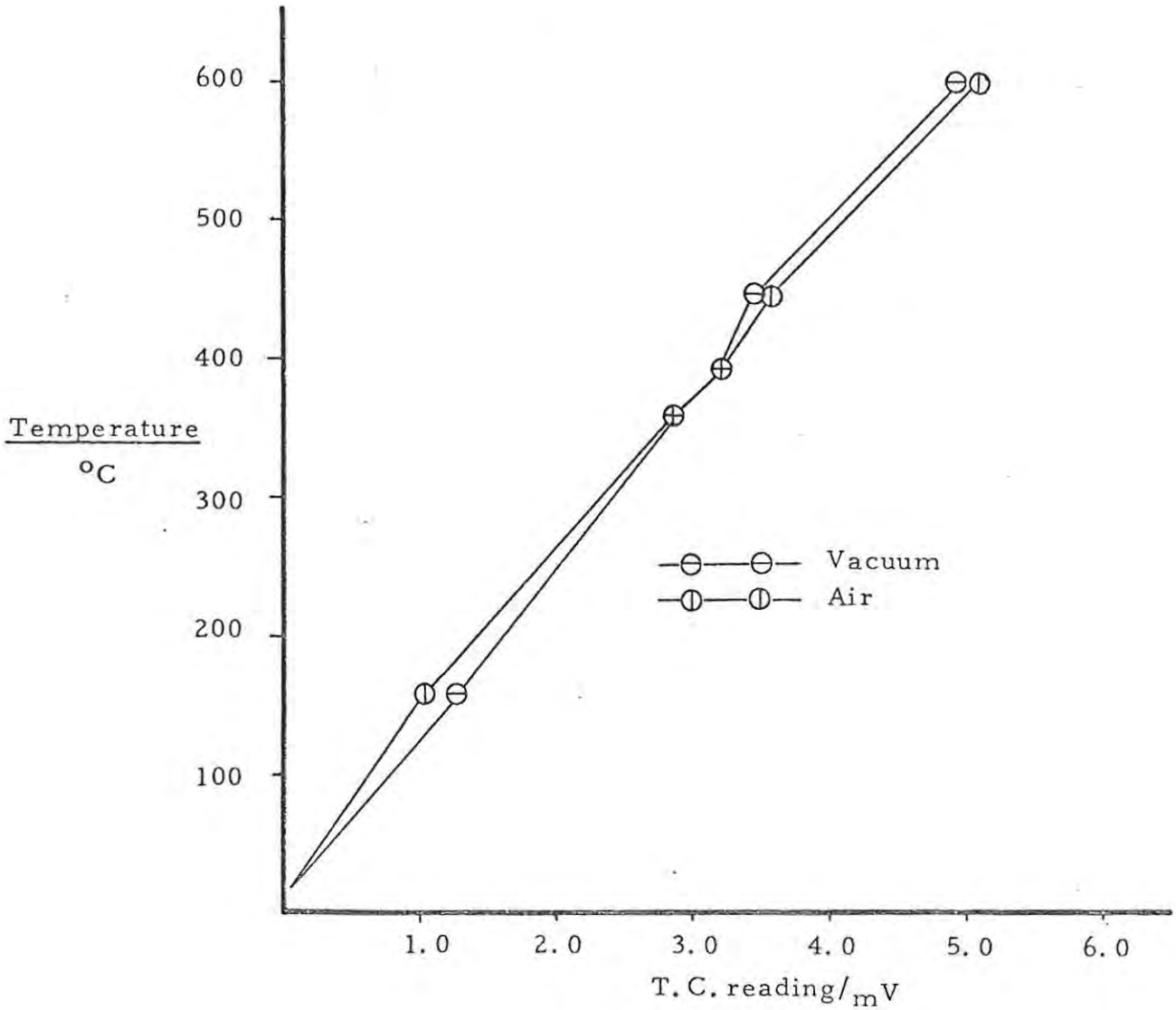

by making use of the Curie point method[119]. An example of these curves is given (Fig. 3.4).

The sample (12.00 mg $\mp$ 0.10 mg in all cases) was weighed in a platinum bucket in position in the furnace, and the apparatus was evacuated. During any decomposition in vacuo the decomposition chamber was evacuated continuously to prevent the accumulation of the product gases in the region around the sample. The furnace was then switched on and the mass-loss curve at the relevant temperature recorded.

During decomposition in flowing streams of various gases (N_2, O_2, Ar or NH_3), the liquid air trap was not used in order to prevent condensation in the decomposition chamber of any of the gases used. After the decomposition chamber had first been evacuated and isolated from the pumping system, the required gas was bled in via a moisture trap (liquid air, P_2O_5 or BaO) until the pressure of the gas in the decomposition chamber was slightly greater than one atmosphere, when the outlet tap was opened. The flow of gas adjusted to 6 litre/hr, the furnace switched on, and the mass-loss at the relevant temperature recorded.

A slightly different procedure had to be adopted for the experiments performed in flowing NH_3 since prolonged exposure of the balance to NH_3 would be detrimental to its performance. After evacuation the decomposition chamber was filled with dry N_2, taps B and C (Fig. 3.1) were opened and the flow rate was adjusted to 15 litre/hr. Ammonia was then passed into the decomposition chamber through tap B at a flow rate of 6 litre/hr. After NH_3 had been detected at tap C for $\mp$ 10 minutes the furnace was switched on and the decomposition performed as before. The gas flow in this case is shown by the arrows

Figure 3.5

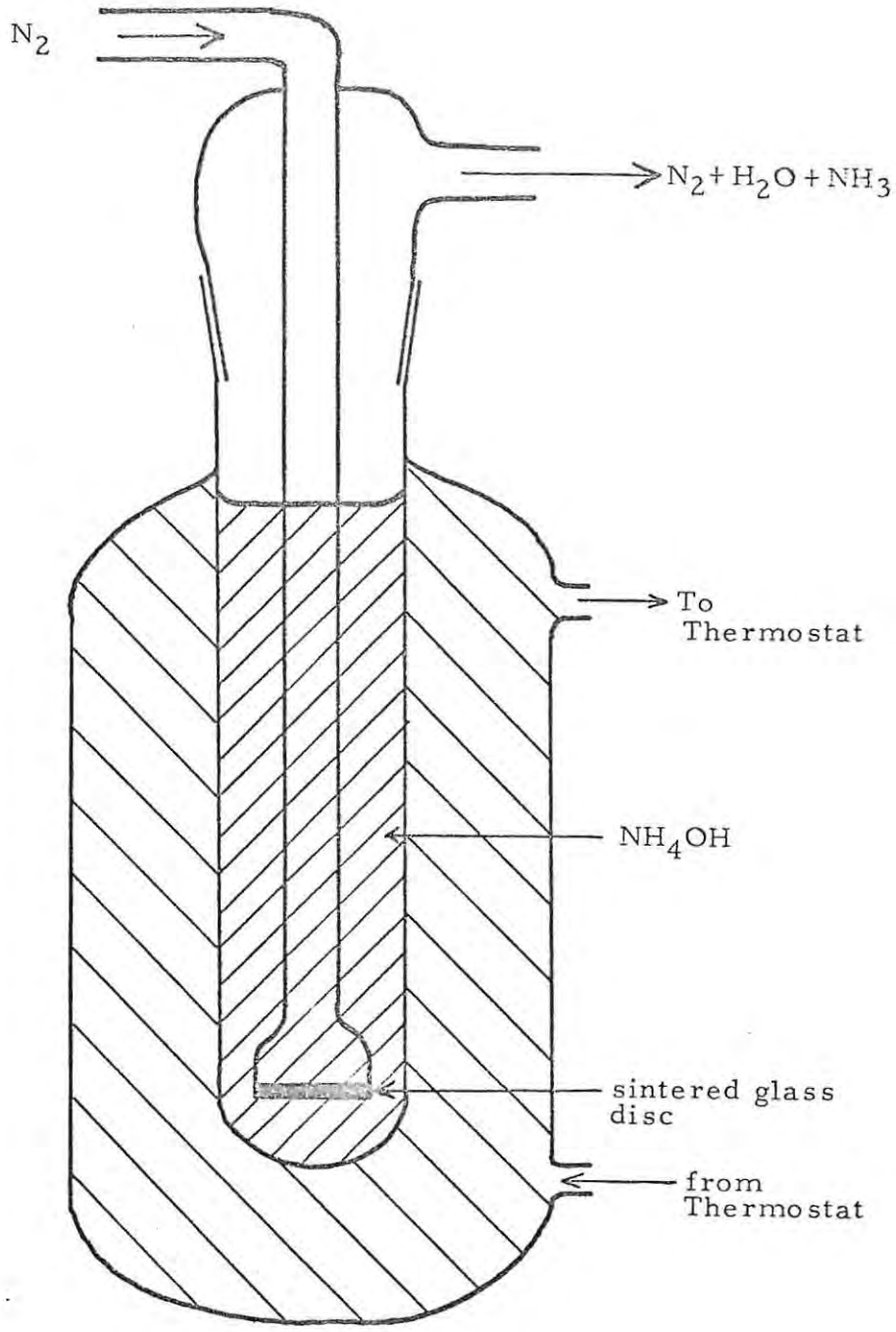
N_2
$N_2 + H_2O + NH_3$
To
Thermostat
NH_4OH
sintered glass
disc
from
Thermostat

in Fig. 3. 1.

When an atmosphere of varying pNH_3 (partial pressure of NH_3) or pH_2O (partial pressure of H_2O) was required, use was made of the apparatus shown in Fig. 3. 5. Dry N_2 was used as the carrier gas which was bubbled thrugh ammonium hydroxide of known concentration kept at a constant temperature by means of a thermostat. The partial pressures of ammonia and water vapour in the nitrogen carrier were determined from tables in Lange-Handbook of Chemistry 10th edition page 1455. The concentration of the ammonium hydroxide solution was checked before and after the experiment by the following volumetric method. An excess of standard HCl was added to an aliquot of the ammonium hydroxide. This excess was then back-titrated with standard sodium hydroxide using the mixed indicator methylred-bromocresol green. The determination was always performed in triplicate.

3. 2 The Analysis of Samples

The above method of following the isothermal reaction by means of mass loss or gain with time facilitated the interruption of the reaction at fixed points in any stage of the reaction in order to obtain samples for x-ray, infrared or micro-Kjeldahl analyses.

The x-ray investigation of the samples was confined to standard powder diffraction techniques. A Hilger-Watts microfocus and semimicrofocus x-ray generator (model Y33) and a Unicam single crystal goniometer (model S25) were used with Cu K_α radiation. The

separation of the reflections was measured by a travelling microscope and the intensity of the reflections was estimated by eye relative to that of the reflection with the highest intensity on the photograph.

The infrared investigation was performed using a Beckman IR 8 spectrophotometer in the double beam mode with a range of 625-4000 cm^{-1}. The instrument was calibrated using a standard polystyrene film. The spectra of all samples were taken using the KBr disc technique with a concentration of 1 mg of sample to 400 mg of KBr.

The nitrogen content of the samples was determined by a standard micro-Kjeldahl method[120]. The percentage vanadium was calculated directly from the initial composition of AMV and the mass loss for the particular sample, assuming no vanadium loss. The calculation of the empirical formulae of the intermediates is based, as far as possible, on the mass spectroscopic evidence of Deschanvres and Nouet[84] that, at least in the earlier stages of the decomposition NH_3 and H_2O are evolved in the mole ratio of 2:1.

The samples used for the analyses were the combined products of several replicate decompositions for the maximum sample mass used in a particular run was limited by the dimensions of the bucket and furnace. It was deemed undesirable to use different heating conditions, e. g. larger furnaces, for preparation of larger samples for analysis as, on account of self cooling, these samples could then not be accurately correlated with those prepared on a small scale; Lamure and Colin[78] have demonstrated that the nature of the products obtained is dependent on the sample mass.

4. RESULTS

Throughout this thesis 1 kcal = 4.184 kJ

4.1 The Isothermal Decomposition of Ammonium Metavanadate (AMV)

The decomposition of AMV is an endothermic reaction and as such can be expected to show some degree of reversibility. The results for the decomposition in vacuum, where recombination will be minimized, will thus be of particular importance. These results will be compared, in later sections, with those of parallel studies in inert, oxidising and reducing atmospheres.

4.1.1 The Isothermal Decomposition of AMV in Vacuum

The decomposition of AMV in vacuum occurs in three separate stages which occur over different temperature ranges. The total mass-losses at the ends of these stages are 14.7-14.9%; 16.9-17.2%; and 22.3-22.4% respectively. These mass-losses were found from the decomposition experiments performed near the lower limits of the temperature ranges given in Table 4.1, since at temperatures near the upper limit of the range there is a tendency for some of the stages to overlap.

4.1.1.1 Characterisation of the Intermediates

The products formed at the end of each stage were characterized by their x-ray powder diffraction patterns, infrared spectra and nitrogen analysis. The empirical formulae and the nitrogen content of the

Figure 4.1 X-ray powder patterns of the intermediates formed in vacuum

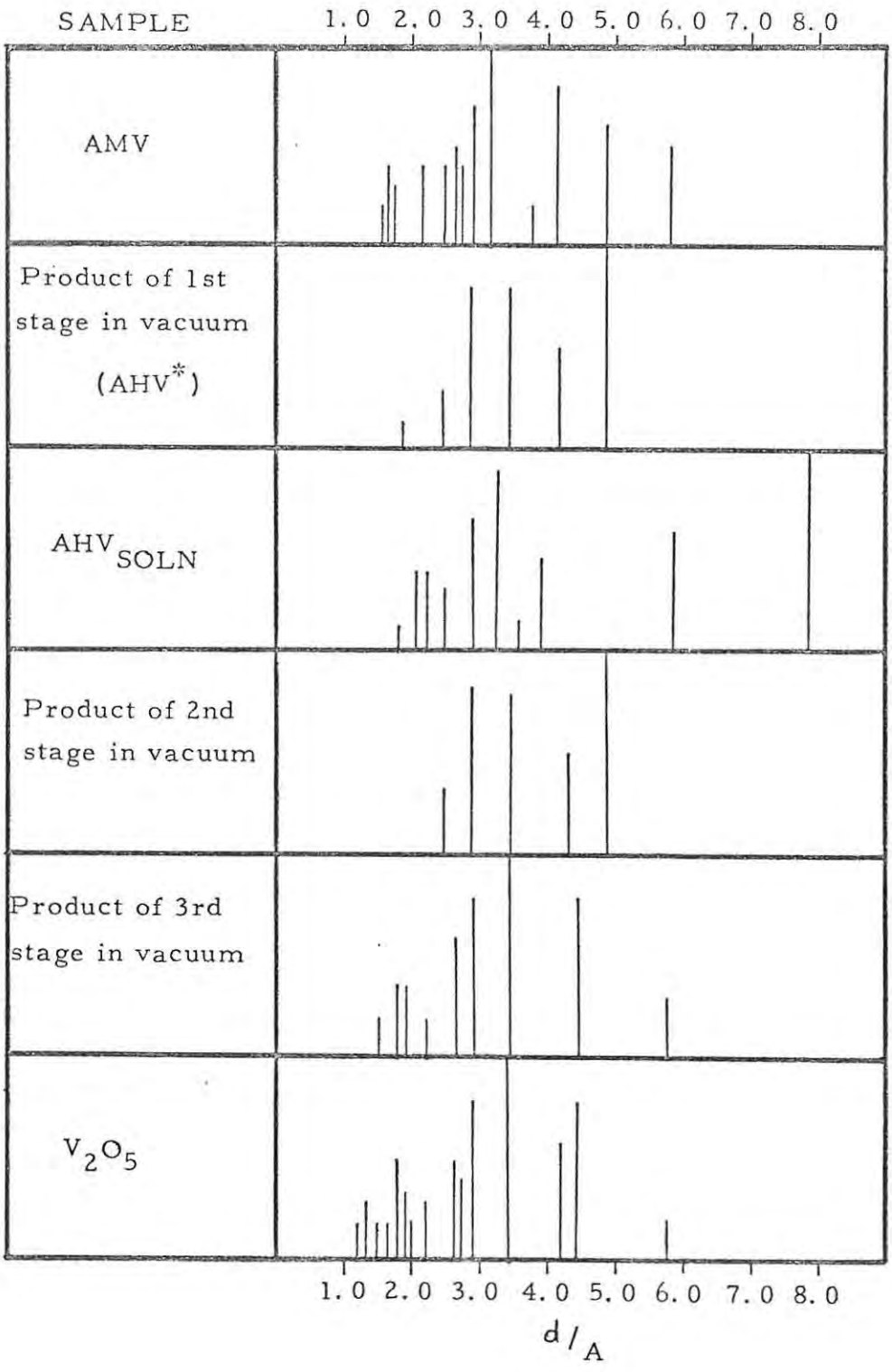

intermediates, together with the total mass-losses at the end of each stage are listed in Table 4. 1

TABLE : 4. 1

The Thermal Decomposition of AMV in Vacuum

Stage	Temp. Range / °C	Empirical formula of product	Mass loss (%)		Nitrogen (%)	
			expected	found	expected	wt found
1	105-135	$NH_4V_3O_8$ (AHV*)	14. 83	14. 7-14. 9	4. 68	4. 77
2	135-155	$NH_4V_4O_{10.5}$	16. 66	16. 9-17. 2	3. 59	3. 48
3	165-200	V_2O_5	22. 23	22. 3-22. 4	0	0

Thus the course of the reaction vacuum is:

$$NH_4VO_3 \xrightarrow[1]{\text{stage}} NH_4V_3O_8 \xrightarrow[2]{\text{stage}} NH_4V_4O_{10.5} \xrightarrow[3]{\text{stage}} V_2O_5$$

$$\text{AMV} \longrightarrow \text{AHV}^* \longrightarrow NH_4V_4O_{10.5} \longrightarrow V_2O_5$$

with the removal of ammonia and water in the ratio 2 : 1 during each stage.

The x-ray powder patterns of the first two stages in vacuum have few reflections and are complicated by fluorescence from the CuK_α radiation, and also by the broadness of the lines resulting from the smallness of the particles of material formed during the first stage in vacuum (see surface area measurements, section 4. 1. 9). The x-ray powder diffraction pattern and infrared spectrum of the product of the first stage (AHV*) shows that, even though it has the same formula, it cannot be ammonium hexavanadate (AHV) (Figure 4. 1). There are no significant changes in the x-ray powder diffraction pattern of the sample

Figure 4.2 Changes in the infrared spectrum during decomposition in vacuum

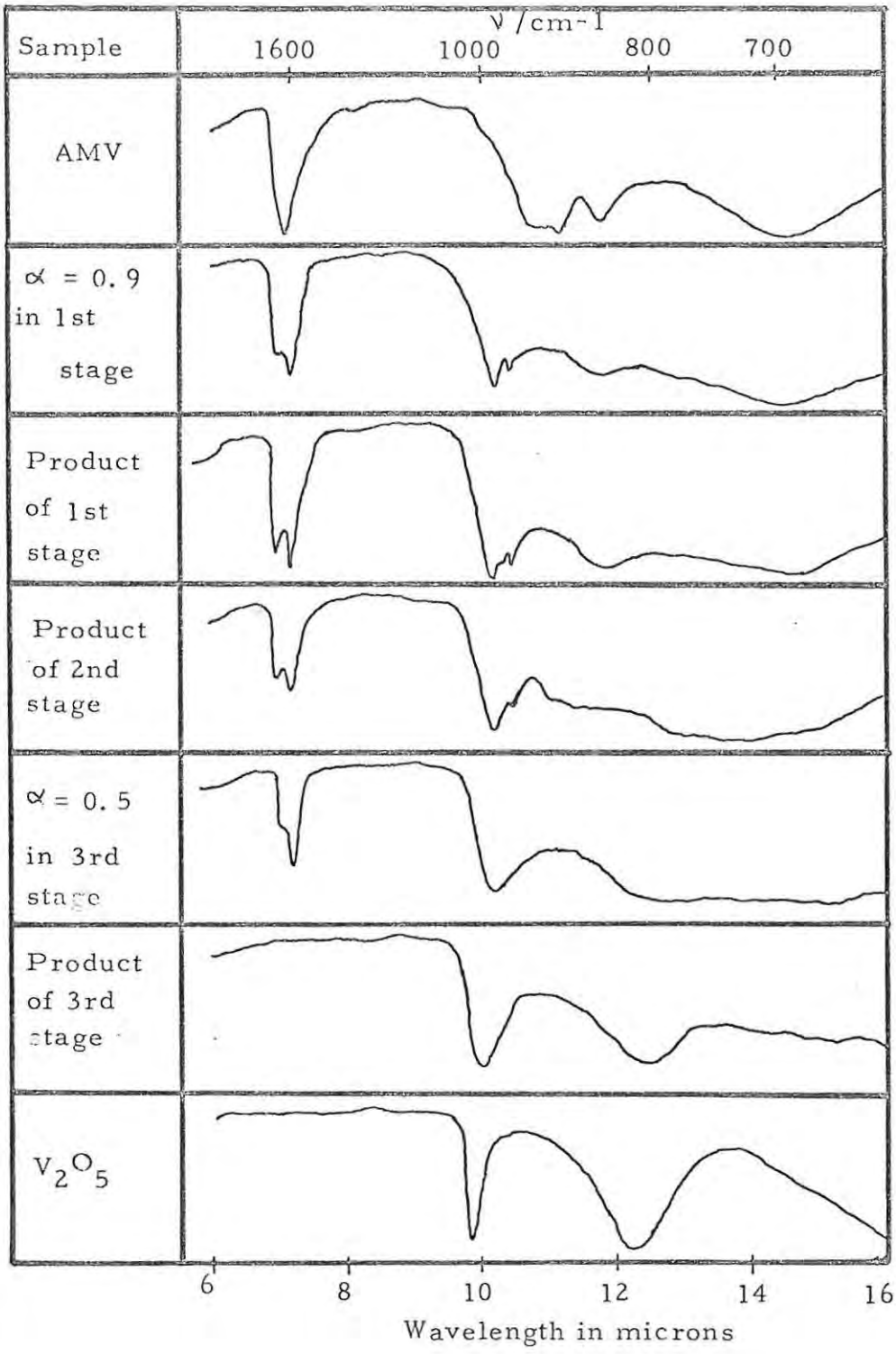

material in going from the end of the first stage to the end of the second.

The x-ray powder diffraction pattern and infrared spectrum of the product of the third stage show it to be similar to V_2O_5, the only difference in the powder patterns being the absence of the strong reflection at $d = 4.21\text{Å}$ and of the reflection at $d = 3.15\text{Å}$, which are present in the powder pattern of V_2O_5. (The x-ray powder diffraction patterns of the products of each stage as well as those of AMV, AHV and V_2O_5 are given in Figure 4.1.) Tables of the x-ray powder diffraction patterns of all the materials investigated are given in Appendix B.

4.1.1.2 Changes in the Infrared Spectrum of the Material during Decomposition in Vacuum

The changes in the infrared spectrum of the material during the decomposition in vacuum are shown in Figure 4.2. The samples used to obtain these spectra were collected by interrupting the decomposition at known values of α during each stage. Points of interest which arise from these results are:

(i) The similarity of the spectra of the products of the first and the second stage of the decomposition (and the x-ray patterns are also very similar).

(ii) The broadness of the bands in the spectrum of the final product in comparison to the bands in the spectrum of commercial V_2O_5. (Hopkins and Williams.)

(iii) The appearance and disappearance of the anomalous high frequency component at 1435cm^{-1}, associated with the triply degenerate bending mode of the NH_4^+ ion at $\sim 1400\text{cm}^{-1}$, during the first and third stages of the decomposition respectively.

Figure 4.3 Changes in the infrared spectrum of V_2O_5 formed in vacuum on annealing it in air at 360°C

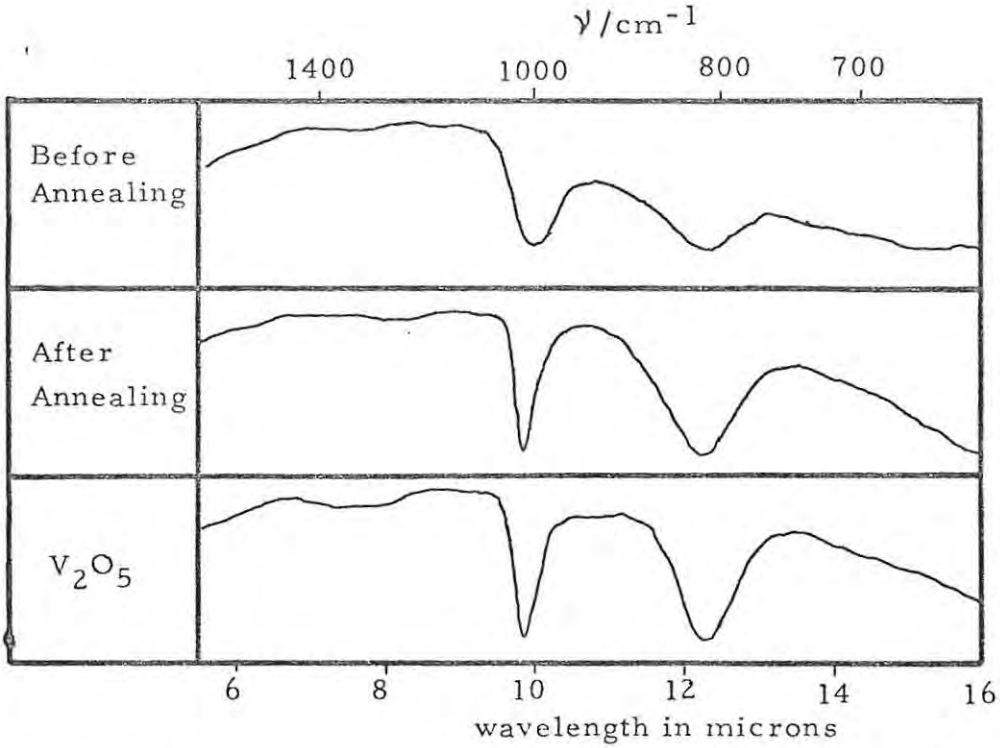

Figure 4.4 Changes in the x-ray pattern of V_2O_5 formed in vacuum on annealing it in air at 360°C

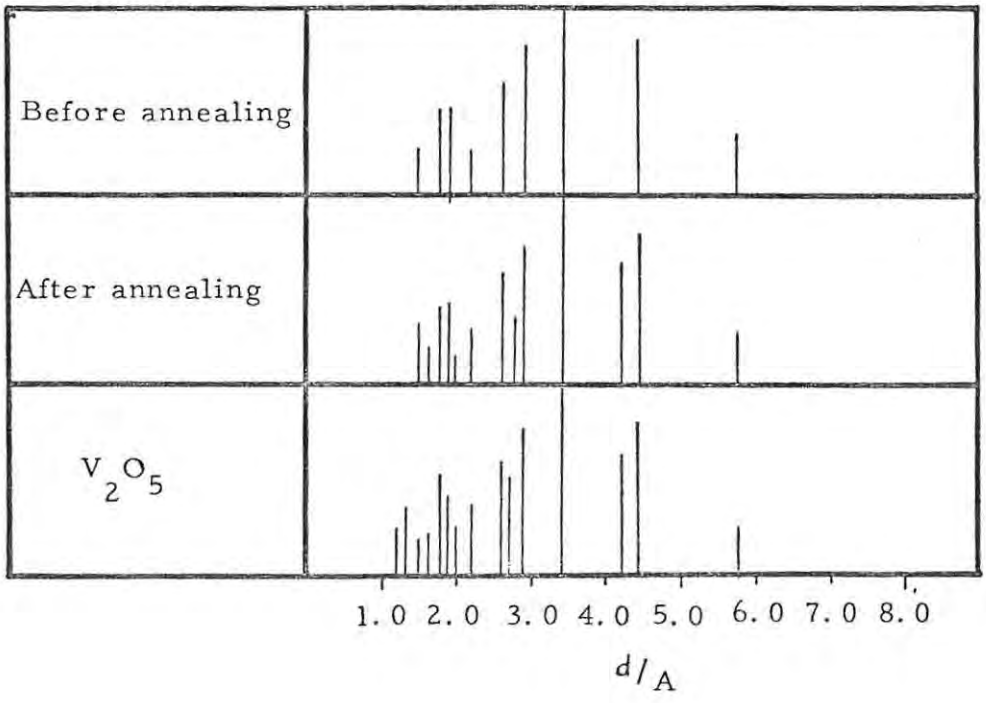

Figure 4.5 Changes in the infrared spectrum of V_2O_5 formed in vacuum on annealing it in vacuum at 550°C

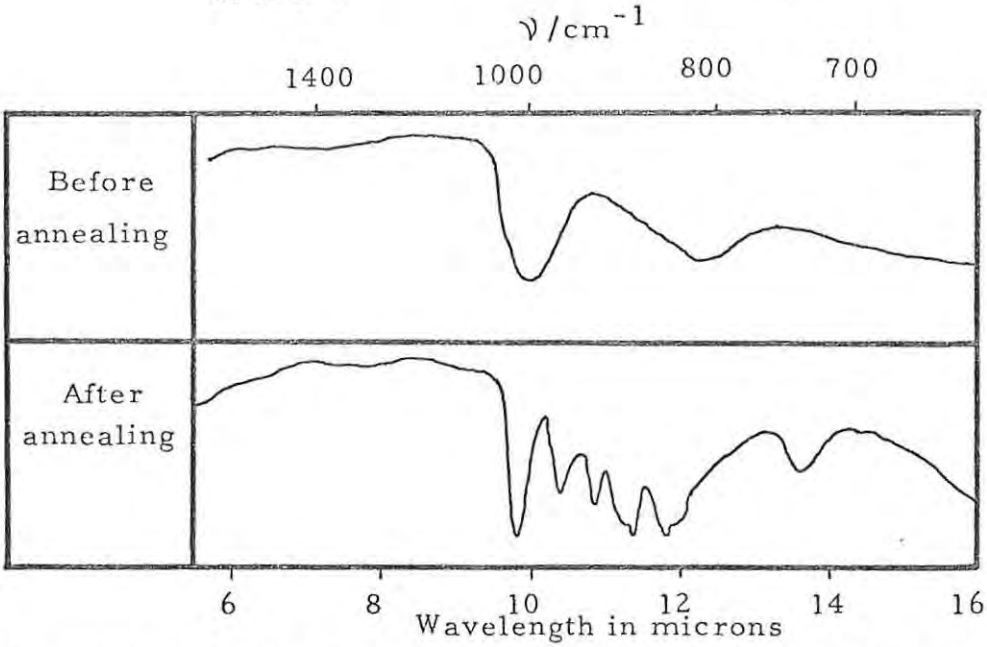

Figure 4.6 Changes in the X-ray powder pattern of V_2O_5 formed in vacuum on annealing it in vacuum at 550°C

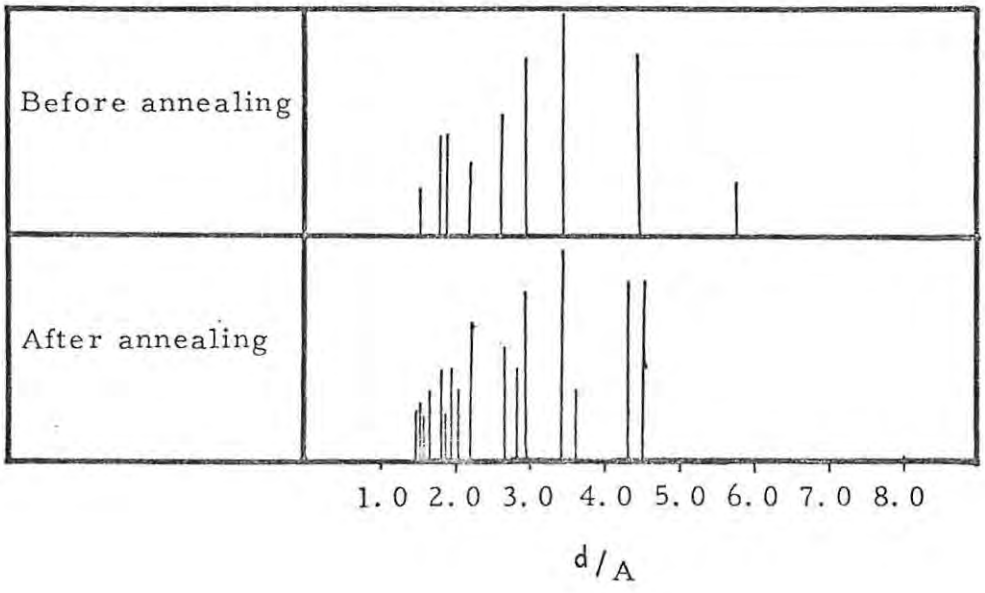

4. 1. 1. 3 The Effect of Annealing the Final Product of the Decomposition in Vacuum

As can be seen from the X-ray powder diffraction patterns and the infrared spectra, the product of the third stage in vacuum is a defective form of V_2O_5. The effect on this product of annealing at higher temperatures was thus investigated.

The V_2O_5 product of the third stage in vacuum was first annealed in air at 360°C for two hours. There was no further mass-loss but the x-ray powder diffraction pattern and infrared spectrum of the product obtained in this manner are compared with those of the same material before annealing and with those of commercial V_2O_5 (Hopkins and Williams, Laboratory Reagent) in Figures 4. 3 and 4. 4 respectively. Annealing for longer periods had no further effect on the material.

When the product was annealed in vacuum at 550°C for 30 minutes there was again no mass-loss but the x-ray powder diffraction pattern and the infrared spectrum are changed (Figures 4. 5 and 4. 6). Annealing at 550°C for longer periods in vacuum had no further effect on the product but if this product (after annealing in vacuum) is annealed in argon at 550°C for 30 minutes then the infrared spectrum and the x-ray powder diffraction pattern are found to have become identical to that found normally for V_2O_5. Annealing the V_2O_5 formed in vacuum at 400°C for several hours did not, however, have any effect on the structure of this material.

4. 1. 1. 4 The Isothermal α - time Curves for the Decomposition in Vacuum

The α - time curves, where α is the fraction of the total mass-loss

Figure 4.7 First stage of the decomposition in vacuum at 123.3°C
(Type I curve)

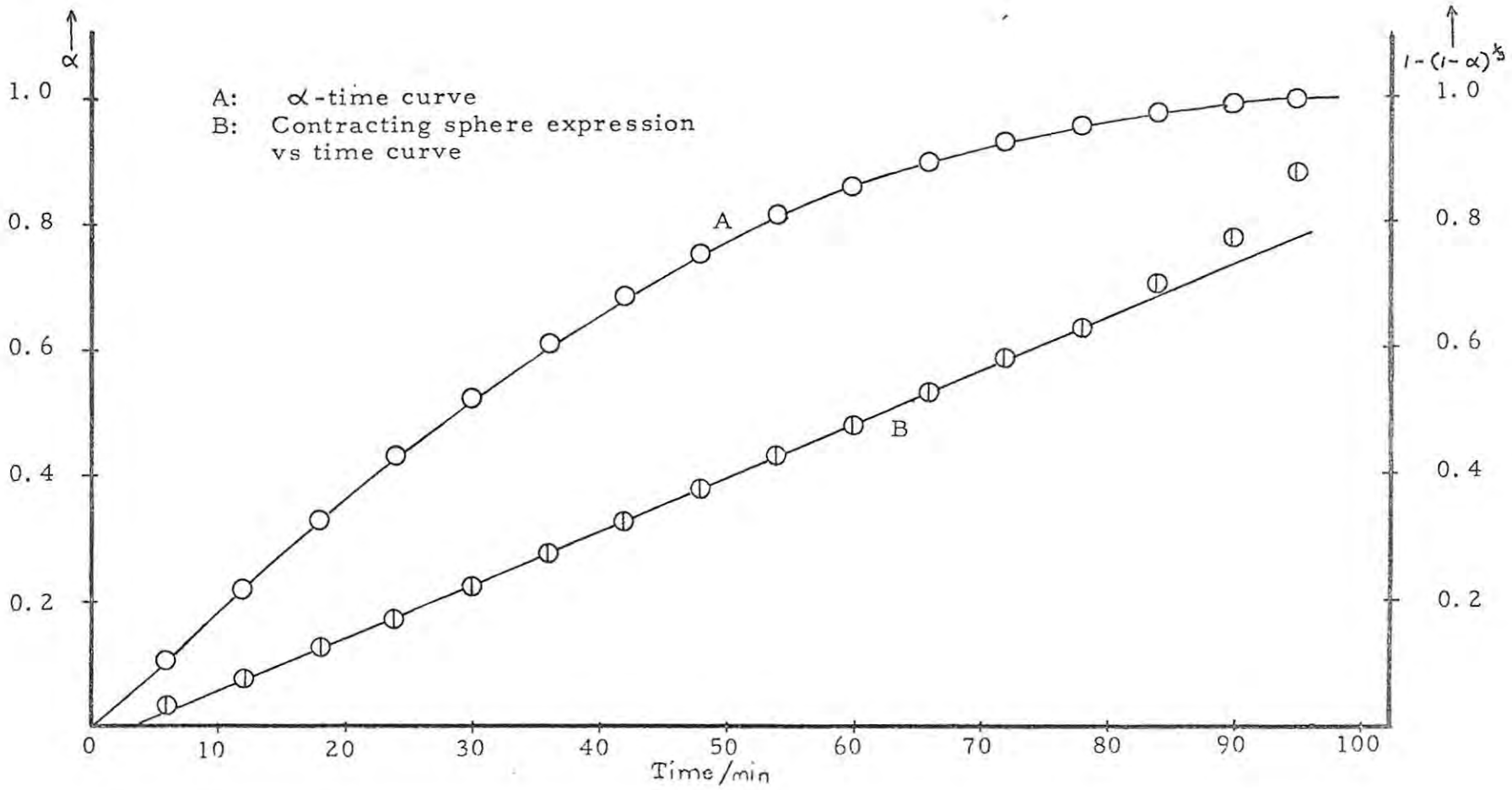

for the particular stage, for each of the three stages in the decomposition in vacuum are deceleratory throughout. The α - time curve for the first stage is shown in Figure 4.1 curve A; this type of α - time curve will be referred to as a "Type I" curve. Each of the curves were tested with the usual mathematical expressions for kinetic models of solid decompositions (See Chapter 1). The contracting sphere expression,

$$1 - (1 - \alpha)^{\frac{1}{3}} = kt + C \qquad 4.1$$

(where $k = (\frac{k''}{a})$ and a is the radius of the particles)

was found to apply over virtually the complete curve for each stage ($0.10 < \alpha < 0.95$) (Figure 4.7 curve B) with, of course, different values of the constants k and C for each stage at each particular temperature. The reproducibility of the rate constants obtained from the above expression were tested for the first stage in vacuum and found to be satisfactory; for three decomposition experiments at $123.3 \mp 0.3^{o}C$ the k''/a values were 7.8, 8.1, 8.0×10^{-3} min^{-1} respectively.

4.1.1.5 The Effect of Temperature

The effect of temperature on the rate of each stage of decomposition has been studied. The temperature ranges which gave conveniently measurable rates of decomposition for each of the three stages have been already given in Table 4.1 and the variation of the rate constant for the first stage of the decomposition with temperature is given in Table 4.2.

Figure 4.8 Arrhenius plot for the 1st stage of the decomposition in vacuum

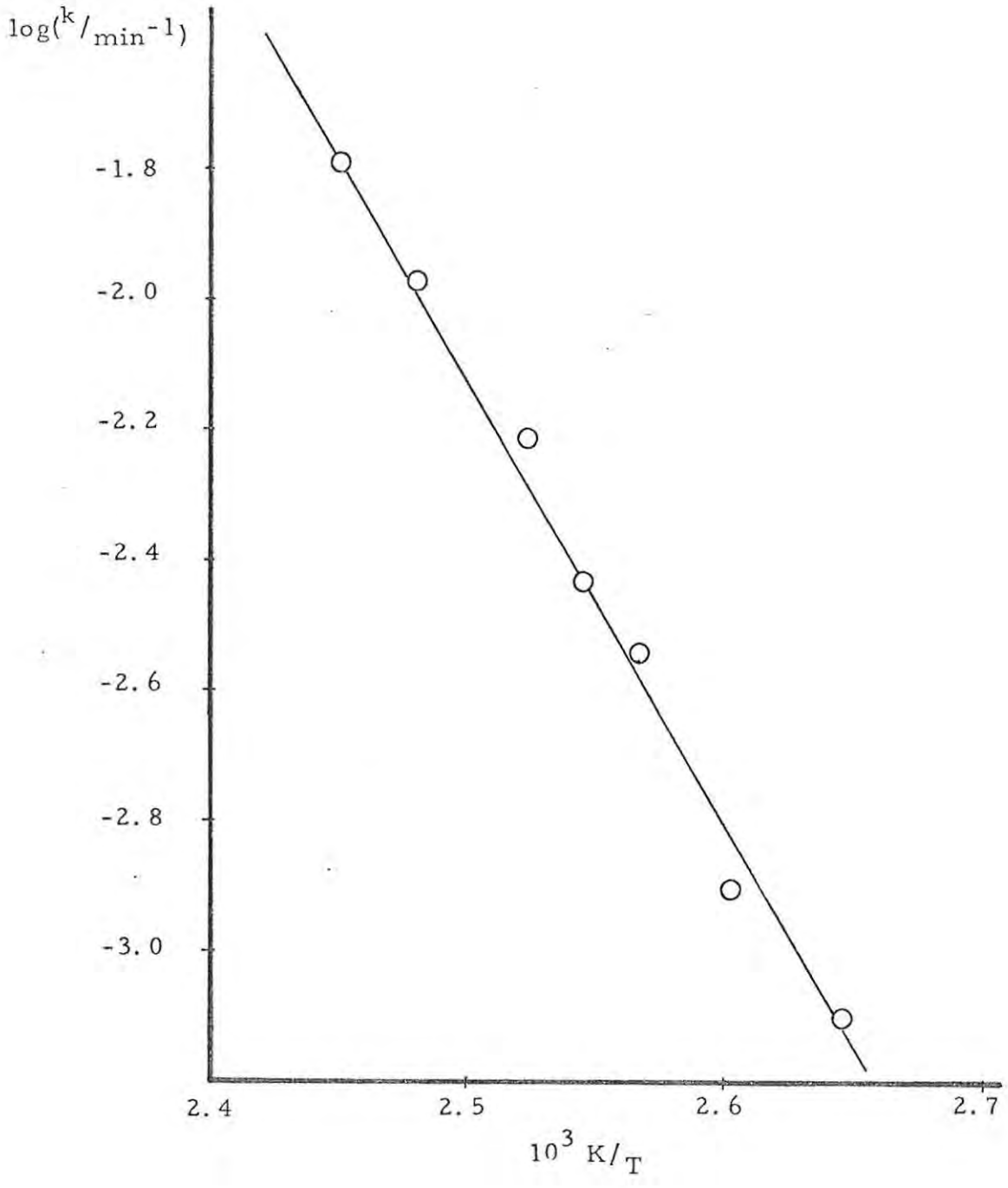

TABLE : 4.2

The Effect of Temperature on the Rate of Decomposition of the First Stage in Vacuum

Rate/(min^{-1})	Temperature/°C
0.78×10^{-3}	105.0
1.30×10^{-3}	110.0
2.90×10^{-3}	116.6
3.72×10^{-3}	120.0
7.95×10^{-3}	123.3
11.50×10^{-3}	126.6
10.71×10^{-3}	130.0
16.20×10^{-3}	135.0

Application of the Arrhenius equation,

$$k = Ae^{-E/RT}$$

i.e. $$\log k = -2.303 \, E/RT + A' \qquad (4.2)$$

results in an approximately linear plot (Figure 4.8) from which an apparent activation energy for the first stage in vacuum of 30.8 kcal mol^{-1} (was obtained). The apparent activation energies for the second and third stages in vacuum obtained in this manner are 38.2 kcal mol^{-1} and 23.4 kcal mol^{-1} respectively.

4.1.2 The Isothermal Decomposition of AMV in Inert Atmospheres

There are again three separate successive stages in the thermal decomposition of AMV in inert atmospheres (argon or nitrogen). The

total mass losses, with respect to AMV, at the end of each stage are 11.7-11.8%, 15.9-16% and 22.3-22.4% respectively. The products of and structural changes involved in each of these stages as well as the kinetic analysis of the α -time curves have been investigated in the same manner as for the decomposition of AMV in vacuum.

4.1.2.1 Characterisation of the intermediates from the decomposition in Inert Atmospheres

The products formed at the end of each stage were characterized by nitrogen analyses, x-ray powder diffraction patterns, and infrared spectra. The empirical formulae together with the nitrogen content of the intermediates are given in Table 4.3.

TABLE : 4.3

The Thermal Decomposition of AMV in Inert Atmospheres

Stage	Temp. Range/°C	Empirical formula of product	Mass-loss (%)		Nitrogen wt (%)	
			expected	found	expected	found
1	160-180	$(NH_4)_2V_4O_{11}$ (ABV)	11.10	11.7-11.8	6.74	6.82
2	180-210	$NH_4V_3O_8$ (AHV)	14.83	15.9-16.0	4.68	4.45
3	270-300	V_2O_5	22.23	22.3-22.4	0	0

The course of the decomposition reaction in inert atmospheres is thus

$$NH_4VO_3 \xrightarrow[1]{\text{stage}} (NH_4)_2V_4O_{11} \xrightarrow[2]{\text{stage}} NH_4V_3O_8 \xrightarrow[3]{\text{stage}} V_2O_5$$

i.e. AMV $\longrightarrow$ ABV $\longrightarrow$ AHV $\longrightarrow$ V_2O_5

Figure 4.9 X-ray powder patterns of the intermediates formed in argon

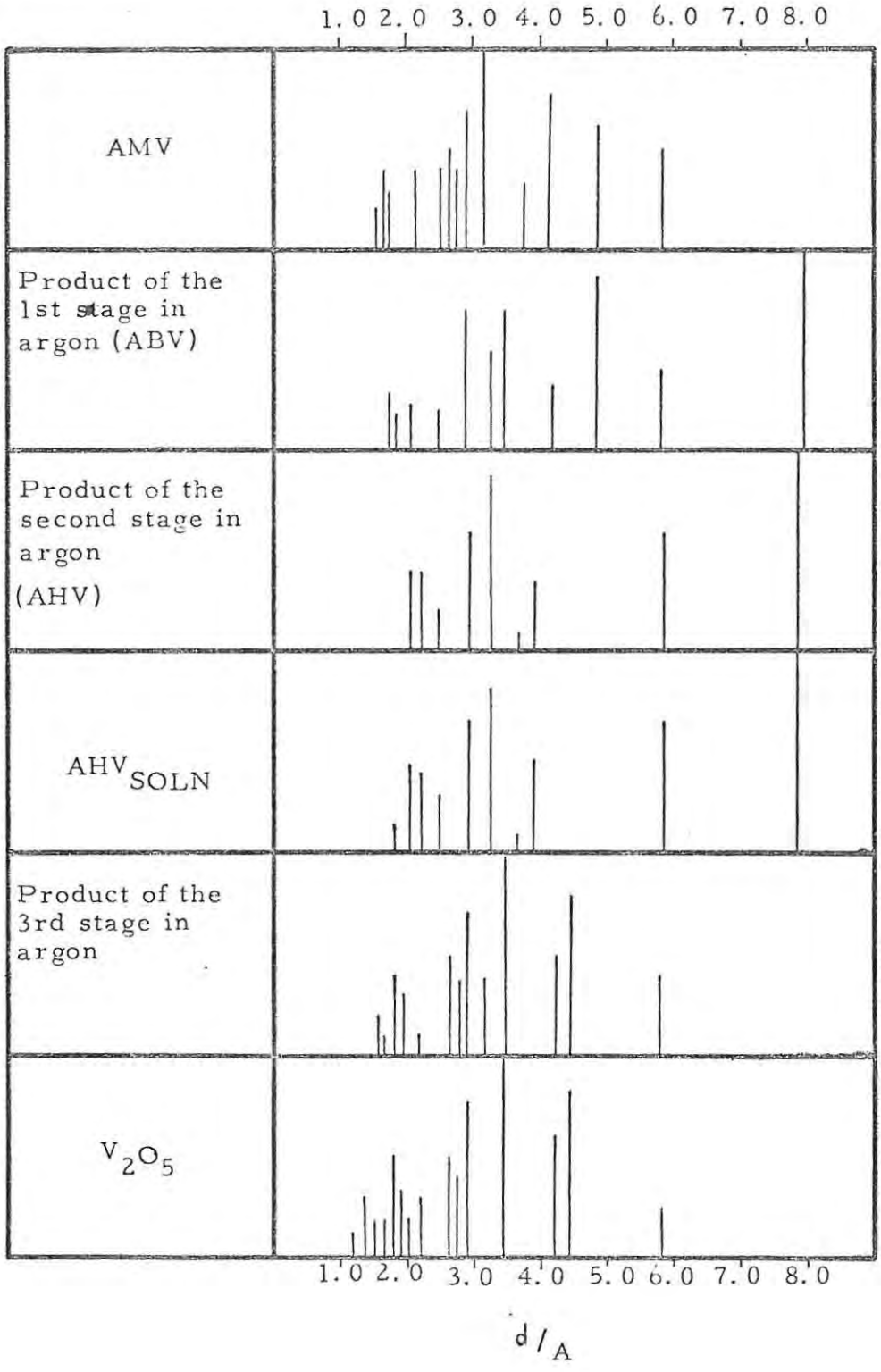

with the removal of ammonia and water in the ratio of 2 : 1 during each stage.

The x-ray powder diffraction patterns of the intermediates were fairly clearly defined (Figure 4. 9) and showed more reflections than the x-ray powder photographs of the intermediates formed in vacuum.

The x-ray powder diffraction pattern of the intermediate (ABV) formed at the end of the first stage in inert atmospheres shows that it is structurally similar to the intermediate formed at the end of the first stage in vacuum (AHV*).

The x-ray powder diffraction pattern and infrared spectrum (see next section) of the intermediate formed at the end of the second stage in inert atmospheres, together with its empirical formula, show it to be identical to AHV (prepared by Kelmers method[91]).

The powder pattern of the V_2O_5 formed at the end of the third stage in argon shows that it is similar in defectiveness to that formed in vacuum; this is shown by the absence of the reflections at d = 4. 20 Å and d = 3. 15 Å present in the x-ray powder pattern of a commercial sample of V_2O_5 (Hopkins and Williams).

4. 1. 2. 2 The Changes in the Infrared Spectrum of the Material During Decomposition in Inert Atmospheres

The changes in the infrared spectrum of the material during the decomposition in inert atmospheres are shown in Figure 4. 10. The sample materials used for these spectra were obtained at the end of each of the stages and by interrupting the decomposition at the indicated values of α during each stage.

Figure 4.10 Changes in the infrared spectrum during decomposition in argon

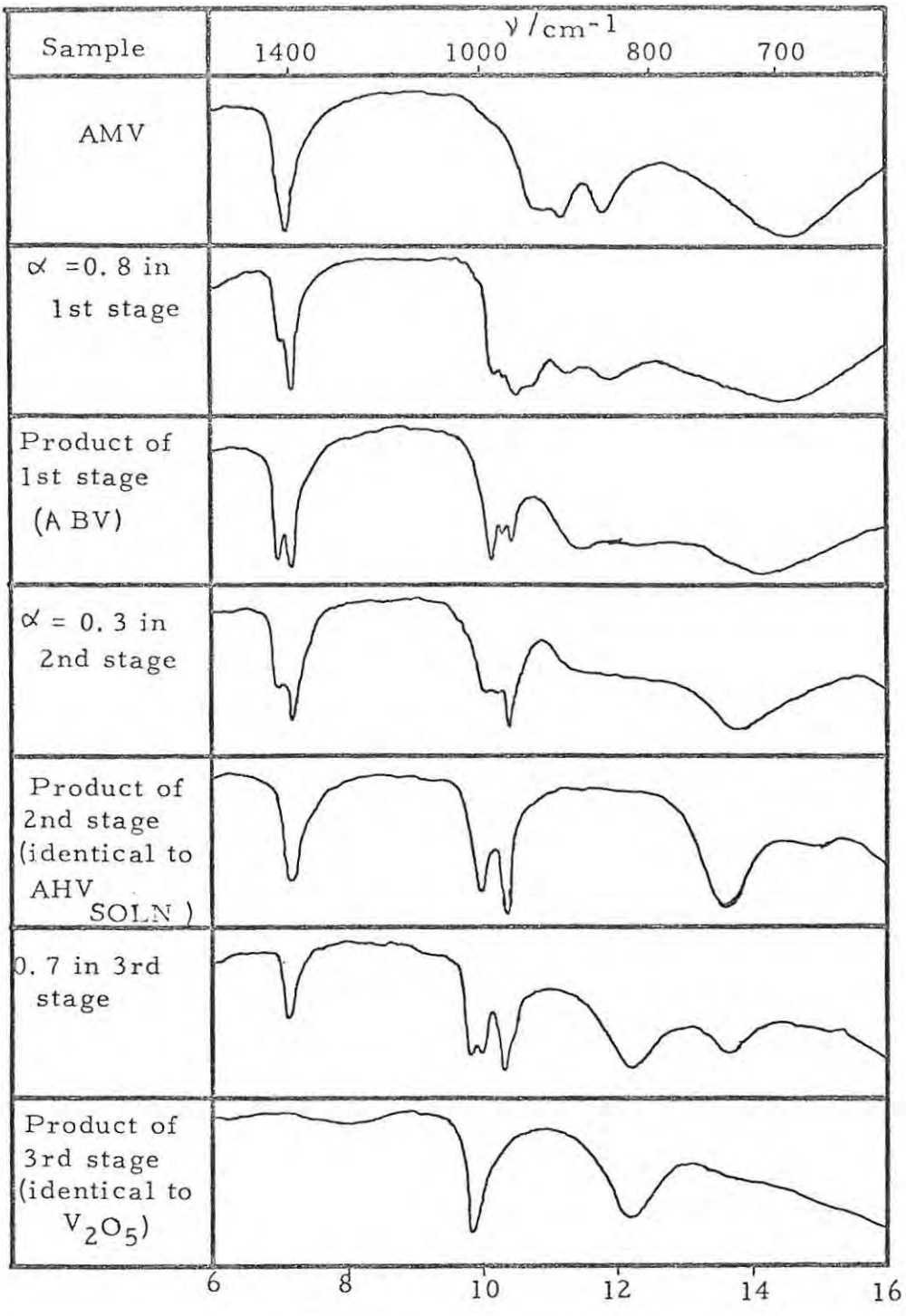

Points to be noted in these spectra are:

(i) The similarity of the spectrum of ABV formed at the end of the first stage to that of AHV formed at the end of the first stage in vacuum, even though the empirical formulae of the two intermediates are completely different.

(ii) The narrowness of the bands in the spectrum of the final product formed in inert atmospheres compared with the bands in the spectrum of the final product formed in vacuum.

(iii) The appearance and disappearance of the anomalous high frequency component associated with the triply degenerate bending mode of the NH_4^+ ion at ca. 1400 cm^{-1} during the first and second stages of the decomposition.

(iv) The gradual appearance of the bands due to V_2O_5 as the bands due to AHV disappear.

4. 1. 2. 3 Annealing the Final Product Formed in Inert Atmospheres

Annealing the final product formed in argon in air at 360°C results in no further mass loss, but the x-ray powder diffraction pattern shows that, as for the final product in vacuum, the defective nature of the structure is reduced; this is shown asbefore, by the appearance of the reflections at $d = 4.20$ Å and $d = 3.15$ Å.

The fact that the final product formed in an inert atmosphere is not as defective as the corresponding product formed in vacuum is evident since, when the inert atmosphere is annealed in vacuum at 550°C for several hours, there is no change in the infrared spectrum and the only change in the x-ray powder diffraction pattern is the appearance

Figure 4.11 First stage of the decomposition in argon (Type II curve) at 165°C

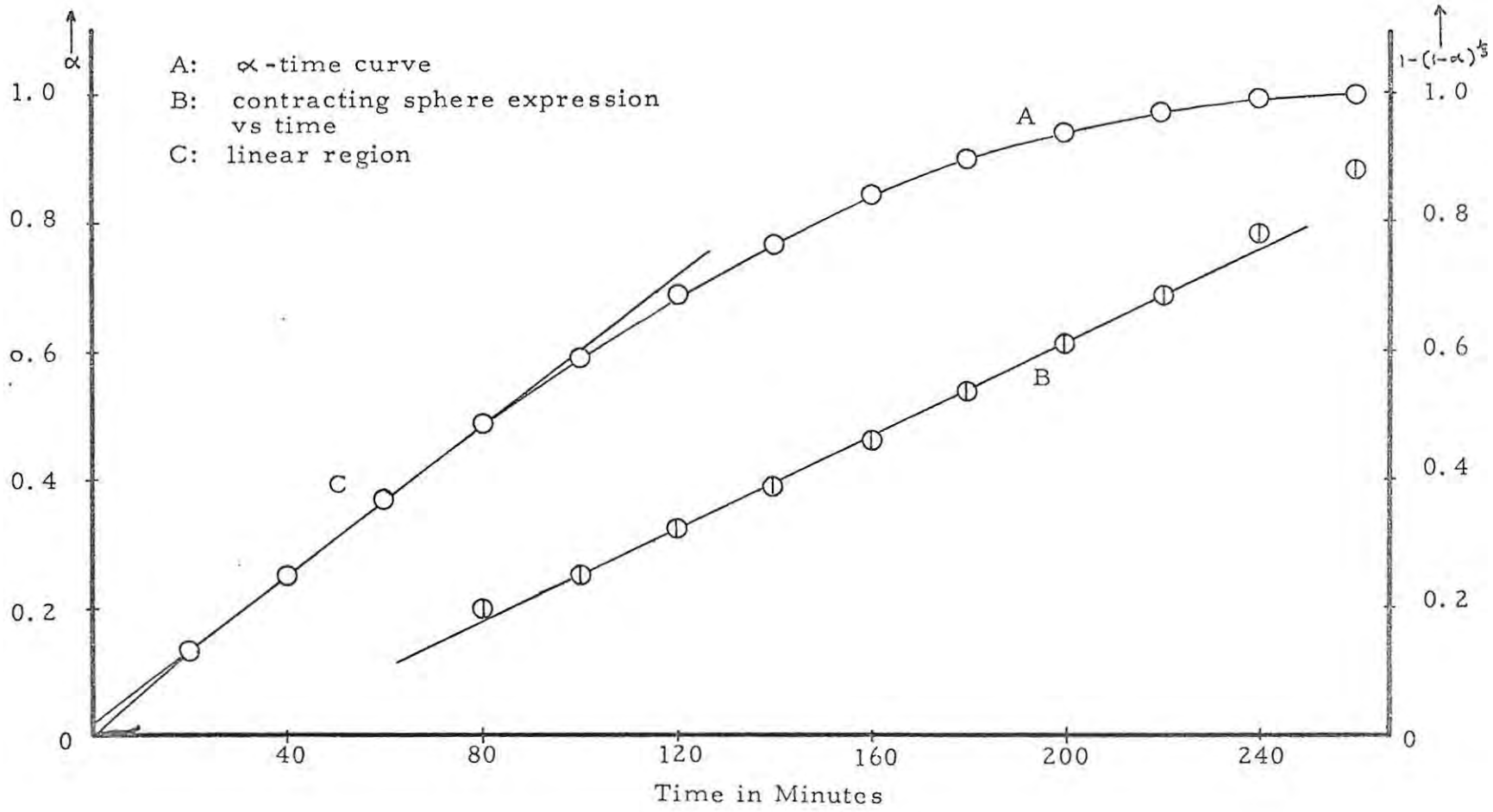

of the strong reflection at $d = 4.20$ Å which has been assumed to be associated with the formation of a more regular structure.

4. 1. 2. 4 The Isothermal α-time curves

The α-time curves for all three stages of the decomposition in inert atmospheres consisted of a linear region

$$\alpha = k't + C' \qquad 4.3$$

followed by a deceleratory region (Figure 4. 11 curve A). This type of curve will be referred to as a "Type II" curve. The linear region for the first and third stages extended over $0.01 < \alpha < 0.6 \pm 0.1$ and for the second stage over the reduced range $0.05 < \alpha < 0.35$. The contracting sphere expression (equation 4. 1) was found to apply over almost the whole of each deceleratory region (Figure 4. 11 curve B).

4. 1. 2. 5 The Effect of Temperature on Decomposition in Inert Atmospheres

Activation energies were estimated from the slopes of Arrhenius plots of the temperature variation of the rate constants $k \left(=\frac{k''}{a}\right)$ (equation 4. 1) and k' (equation 4. 2) for each stage except the second, where the linear region is too short for accurate measurement of k'.

The results are listed in Table 4. 4.

Figure 4. 12 Arrhenius plot for 1st stage of decomposition in argon

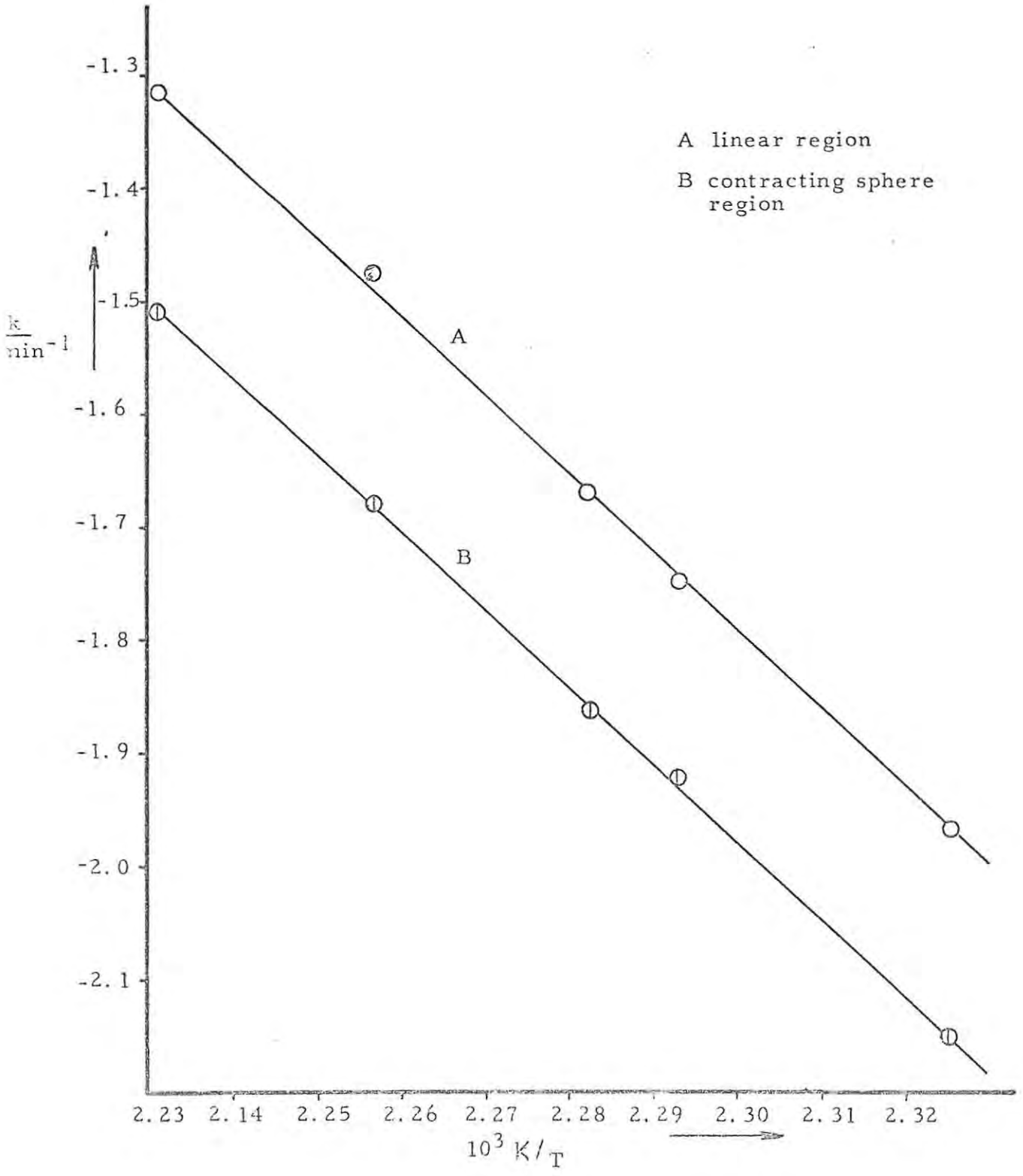

TABLE : 4.4

The Activation Energies for all of the Stage of the Decomposition of AMV in Inert Atmospheres

Stage	Atmosphere	Region	Activation Energy ($kcal\ mol^{-1}$)
1	dry argon	linear	31.9
		contracting sphere	
1	dry nitrogen	linear	32.0
		contracting sphere	31.6
1	nitrogen + 55mmHg	linear	32.1
	water vapour	contracting sphere	31.8
2	dry argon	contracting sphere	25.2
3	dry argon	linear	28.4
		contracting sphere	28.6

It is seen from Table 4.4 that the apparent activation energies for the linear and deceleratory regions of the curves for any particular stage are identical, within the limits of experimental error. The Arrhenius plots for both of these regions for the first stage in argon are given in Figure 4.12. It may also be seen from Table 4.4 that changing the surrounding gas from argon to nitrogen has no effect on the activation energies.

It is also noticeable that, although the presence of water vapour in the inert atmosphere surrounding the sample reduces the rate constant for the first stage of the decomposition at a particular temperature (See Table 4.5), the activation energy of the first stage is not affected.

TABLE : 4. 5

The Effect of Water Vapour on the Rate of the Decomposition of the First Stage in Nitrogen

(Total pressure: one atmosphere)

Temp./°C	Region	Rate /(min^{-1})	
		Dry N_2	N_2 +55. 3 mmHg water vapour
157	linear	1.41×10^{-2}	1.18×10^{-2}
	contracting sphere	0.88×10^{-2}	0.71×10^{-2}
160	linear	1.88×10^{-2}	1.34×10^{-2}
	contracting sphere	1.13×10^{-2}	0.80×10^{-2}
165	linear	2.75×10^{-2}	2.06×10^{-2}
	contracting sphere	1.67×10^{-2}	1.23×10^{-2}
170	linear	4.08×10^{-2}	3.10×10^{-2}
	contracting sphere	2.52×10^{-2}	1.84×10^{-2}
175	linear	6.67×10^{-2}	4.69×10^{-2}
	contracting sphere	3.66×10^{-2}	2.79×10^{-2}

4. 1. 3 The Isothermal Decomposition of AMV in Oxidising Atmospheres

As for the decomposition in vacuum or inert atmospheres, there are three separate successive stages in the thermal decomposition in air or oxygen, with total mass losses at the ends of each stage of 11. 4 - 11. 6%, 15. 3 - 15. 6 % and 22. 3 - 22. 4 % respectively.

4. 1. 3. 1 Characterisation of the Intermediates

The empirical formulae of the products each of the stages of the decomposition of AMV in oxidising atmospheres together with the relevant data on which they are based are given in Table 4. 6.

TABLE : 4. 6

The Thermal Decomposition of AMV in Oxidising Atmospheres

Stage	Temp./°C Range	Empirical formula of product	Mass loss(%)		Nitrogen wt %	
			expected	found	expected	found
1	150-180	$(NH_4)_2V_4O_{11}$ (ABV)	11. 10	11. 4-11. 6	6. 74	6. 82
2	180-210	$NH_4V_3O_8$ (AHV)	14. 83	15. 3-15. 6	4. 68	4. 44
3	260-300	V_2O_5	22. 23	22. 3-22. 4	O	O

The x-ray powder diffraction patterns and infrared spectra of the intermediates formed at the ends of the first and second stages of the decomposition together with their empirical formulae, show them to be identical to the corresponding intermediates formed in inert atmospheres.

Thus the course of the reaction in oxidising atmospheres is identical to that in inert atmospheres

$$NH_4VO_3 \xrightarrow[1]{\text{Stage}} (NH_4)_2V_4O_{11} \xrightarrow[2]{\text{Stage}} NH_4V_3O_8 \xrightarrow[3]{\text{Stage}} V_2O_5$$

$$\text{AMV} \longrightarrow \text{ABV} \longrightarrow \text{AHV} \longrightarrow V_2O_5$$

with the removal of ammonia and water in the ratio of 2 : 1 during each stage.

The V_2O_5 product formed at the end of the third stage is shown by its infrared spectrum and x-ray powder diffraction pattern to be identical to a commercial sample of V_2O_5 (Hopkins & Williams,

Figure 4. 13 Comparison of the x-ray powder patterns of the final products formed in vacuum, argon and air

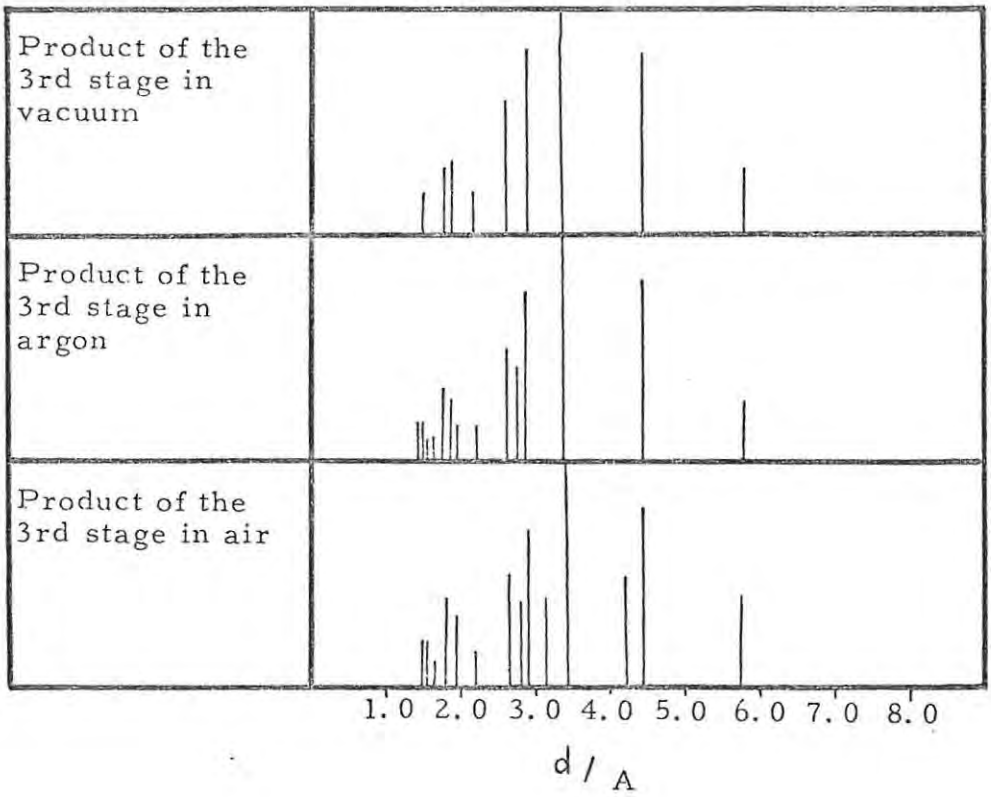

Laboratory Reagent). Annealing in air or in vacuum at 550°C for several hours had no effect on the x-ray powder diffraction pattern or the infrared spectrum of this product. It is thus not as defective as the final products in either vacuum or in inert atmospheres. The x-ray powder diffraction patterns of these final products are compared in figure 4. 13.

4. 1. 3. 2 The Isothermal α -time Curves

The α -time curves found for the decomposition in oxidising atmospheres differ from those found in inert atmospheres only in the third and final stage; thus, the α -time curves for the first two stages of the decomposition in oxidising atmospheres are "Type II" curves. The linear region extends over $0.01 < \alpha < 0.6 \pm 0.1$ for both stages and is followed, for both stages, by a decelaratory region over which the contracting sphere equation again applies.

The α -time curves for the third stage of the decomposition, however, consist of several regions:

(i) an initial burst of gas to $\alpha = 0.15 \pm 0.03$

(ii) an apparently acceleratory region to $\alpha = 0.50 \pm 0.5$

(iii) an approximately linear region ($0.50 < \alpha < 0.60$), leading into

(iv) the deceleratory region.

This type of curve will be referred to as "Type III". (Figure 4. 14 curve A.)

The contracting sphere expression was once again found to apply over almost the whole of the deceleratory region, Figure 4. 14 curve B.

Figure 4. 14 Third stage of the decomposition in air at 265°C
(Type III curve)

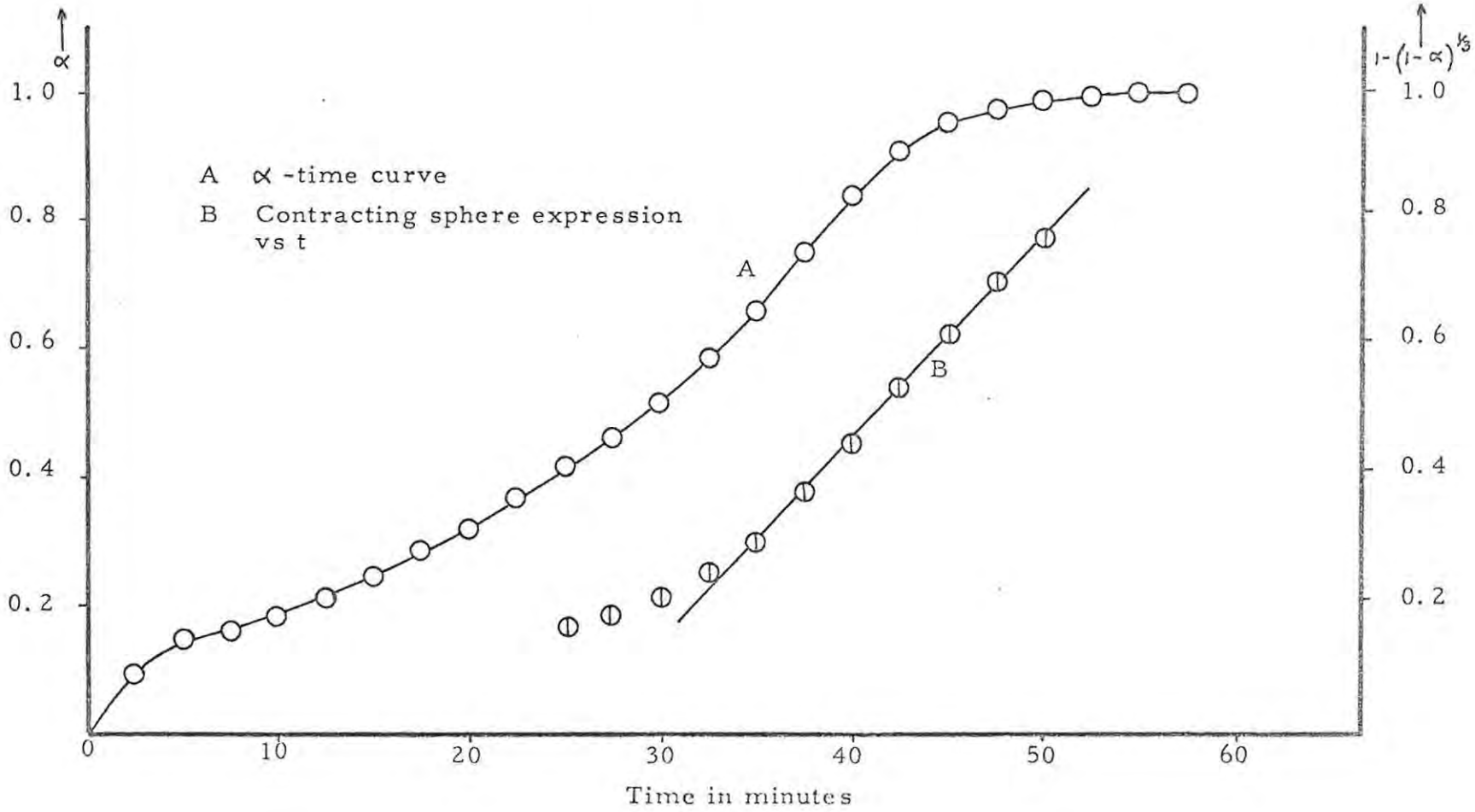

No attempt was made to make a detailed mathematical analysis of the initial stages of the "Type III" curves as it is apparent that overlapping processes are occurring. This region is only found in oxidising atmospheres and any conventional approach involving formation and growth of nuclei at this stage seems inappropriate when there may be changes in the nature and or ratio of gaseous products through possible interaction of oxygen with the vanadium-oxygen lattice; continuous mass spectrometric analysis of the gases is clearly indicated for these conditions. The infrared spectrum of material obtained by interrupting the decomposition after the initial burst of gas was found to be unchanged from that of AHV.

4. 1. 3. 3 The Effect of Temperature on the Decomposition in Oxidising Atmospheres

It was found that when the precautions of predrying the air or oxygen and facilitating the removal of the product gases by the presence of a liquid air trap adjacent to the decomposition chamber were neglected then the same mathematical expressions and regions of fit applied but the activation energy for each stage was altered. The results of the investigations performed using a predried atmosphere are obviously the more important since most control over the reaction was exercised in this case.

The study of the effect of temperature on the rate constants for the decomposition determined from both the linear and deceleratory regions of the first two stages in air, of the first stage in flowing oxygen and from the deceleratory region of the third stage in air, led to the activation energies in Table 4. 7.

TABLE : 4.7

The Activation Energies of all of the Stages of the Decomposition in Oxidising Atmospheres

Atmosphere	Stage	Region	Activation Energy/(kcal mol^{-1})	
			liquid air trap present	no liquid air trap
flowing O_2	1	linear	41.8	
		contracting sphere	42.0	
air	1	linear	40.8	53.2
		contracting sphere	42.1	53.4
air	2	linear	32.0	38.9
		contracting sphere	31.2	36.1
air	3	contracting sphere	34.2	15.6

Details of the variation of the rate constants with temperature for the first stage in air (predried) are given in Table 4.8

TABLE : 4.8

The Effect of Temperature on the Rate of Decomposition of the First Stage in Dry Air

Temperature/°C	Rate constant/(min^{-1})	
	linear	contracting sphere
152	6.73×10^{-3}	4.41×10^{-3}
155	0.06×10^{-3}	6.08×10^{-3}
158	13.60×10^{-3}	9.58×10^{-3}
162	19.32×10^{-3}	13.90×10^{-3}
167	32.82×10^{-3}	22.83×10^{-3}

Figure 4.15 Arrhenius plot for the first stage of the decomposition in air

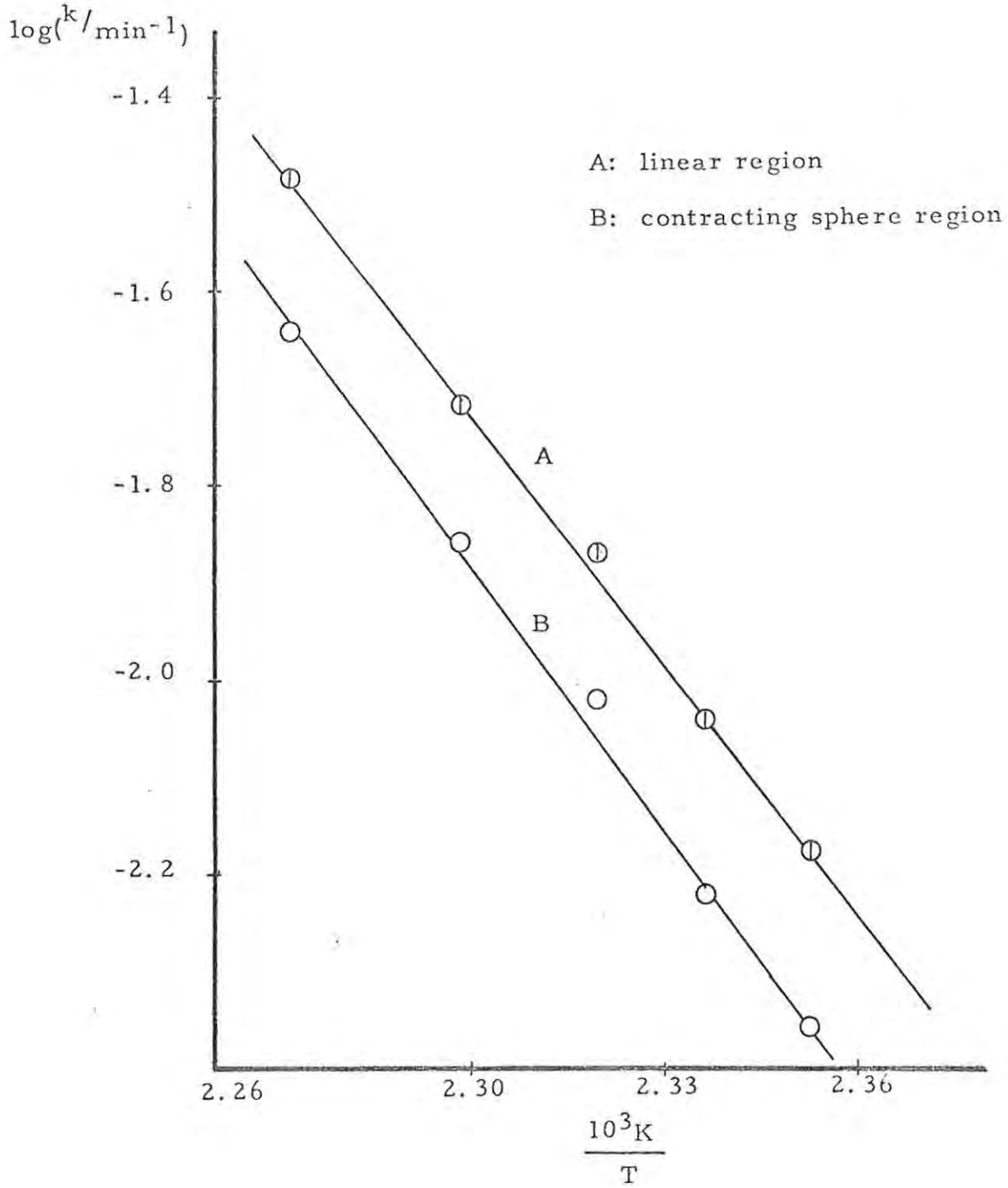

An Arrhenius plot for these two regions shows that the activation energy for both the linear and the deceleratory region are again virtually identical (Figure 4. 15).

4. 1. 4 The Isothermal Decomposition of AMV in Reducing Atmospheres (Ammonia)

This investigation was of interest since ammonia is the major product gas evolved during the decomposition of AMV, the other being water. There are again three stages in the decomposition of AMV in ammonia at temperatures below 400°C. The total mass-losses at the end of each of these stages are 14. 6-14. 8%, 19. 8-20. 0% and 28. 2-28. 6%. It has been shown (Section 1) that at temperatures above 400°C the reaction involves first the formation of the lower oxides, followed by the formation of VN. The present investigation was confined to the first three stages of the decomposition in NH_3 below 400°C.

4. 1. 4. 1 Characterisation of the Intermediates Formed in NH_3

The products formed at the end of each stage in NH_3 were characterized by nitrogen analyses, x-ray powder diffraction patterns, and infrared spectra. The empirical formulae and the nitrogen-contents of the intermediates together with the total mass-losses at the end of each stage are listed in Table 4. 9.

Figure 4.16 X-ray powder patterns of the intermediates formed in ammonia

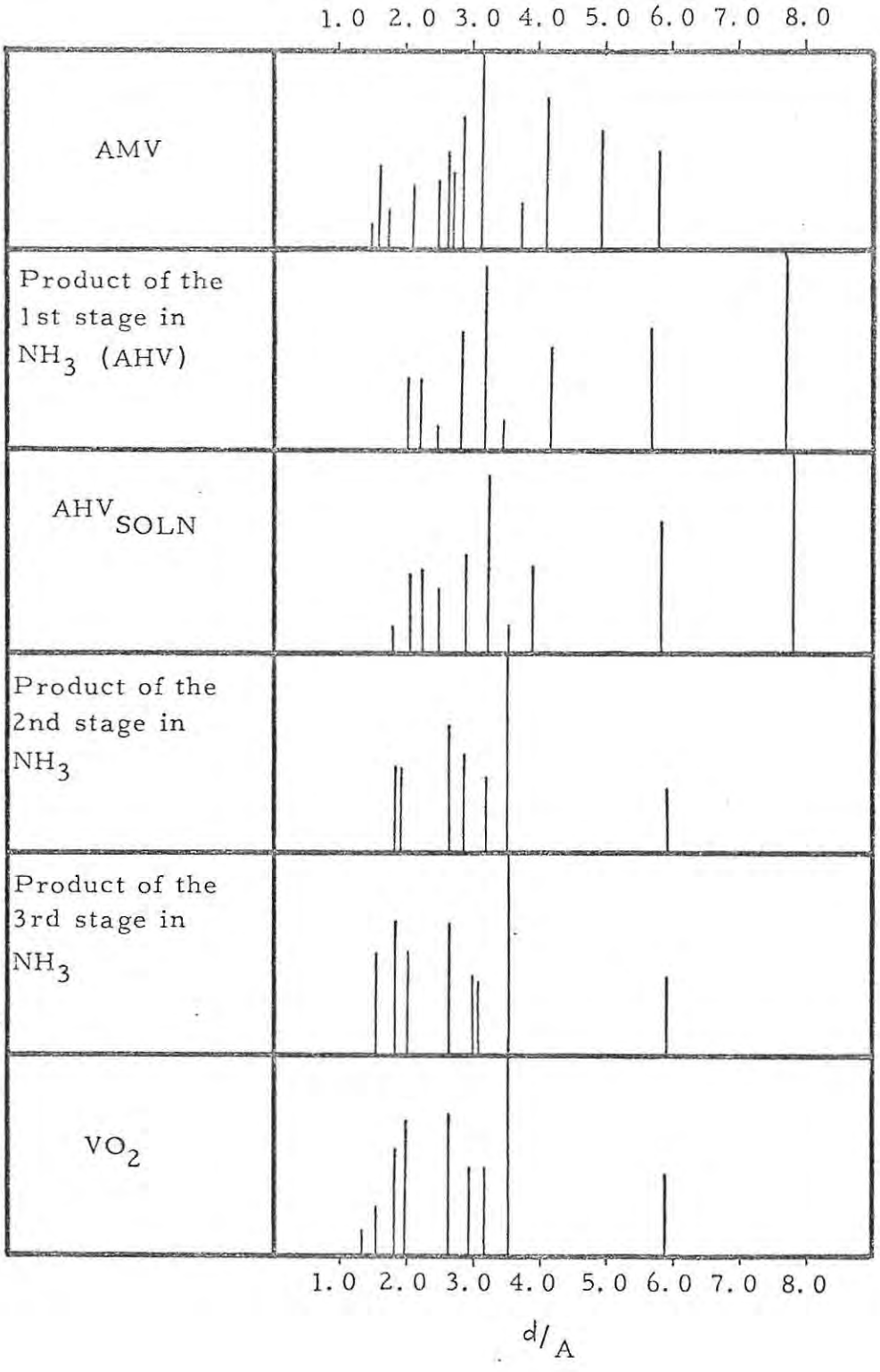

TABLE: 4. 9

The Thermal Decomposition of AMV in Ammonia

Stage	Temp. Range ^{o}C	Empirical formula of product	Mass-loss(%)		Nitrogen wt (%)	
			expected	found	expected	found
1	170-190	$NH_4V_3O_8$ (AHV)	14. 83	14. 6-14. 8	4. 68	4. 27
2	280-300	$NH_4V_6O_{15}$	19. 95	19. 8-20. 0	2. 48	2. 63
3	340-360	VO_2	29. 05	28. 2-28. 6	0	0

The course of the reaction in ammonia up to $400^{o}C$ is thus

$$NH_4VO_3 \xrightarrow[1]{\text{Stage}} NH_4V_3O_8 \xrightarrow[2]{\text{Stage}} NH_4V_6O_{15} \xrightarrow[3]{\text{Stage}} VO_2$$

ie. $$\text{AMV} \longrightarrow \text{AHV} \longrightarrow NH_4V_6O_{15} \longrightarrow VO_2$$

with ammonia and water being evolved in the ratio of 2 : 1 during the first stage only.

The x-ray powder diffraction patterns and infrared spectra of the products formed at the end of the first and third stages show them to be identical to AHV (prepared by the method of Kelmers[91]) and to VO_2 (Alpha Inorganics Ventron) respectively as outlined in the reaction scheme above (See Figure 4. 16 and 4. 17).

4. 1. 4. 2 The Changes in the Infrared Spectrum of the Material during Decomposition in NH_3

The changes in the infrared spectrum of the material during the decomposition in ammonia are shown in Figure 4. 17.

Figure 4.17 Changes in the infrared spectrum during decomposition in ammonia

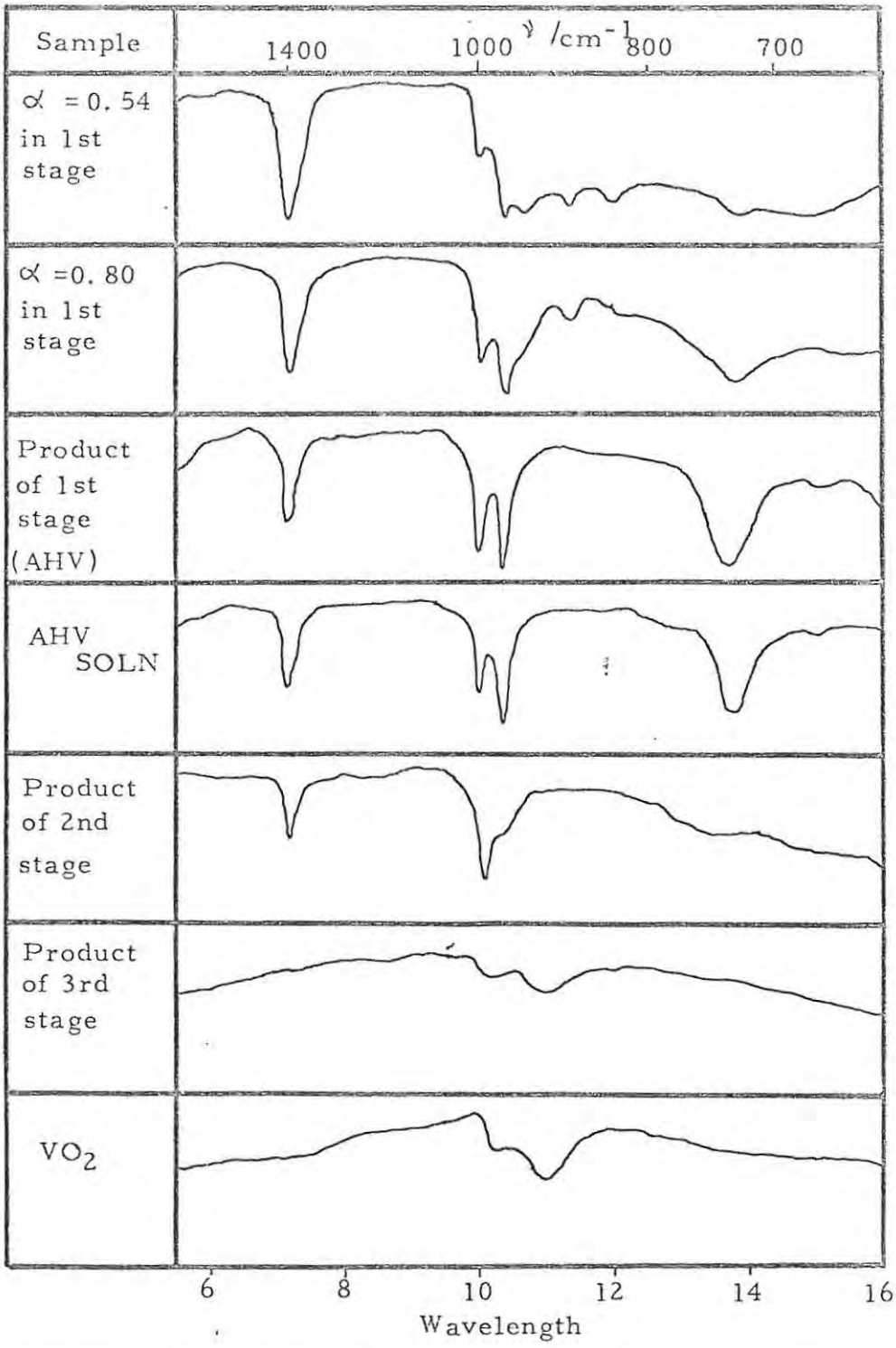

NOTE: ∝ = 0.80 in the first stage of the decomposition corresponds to a mass loss of 11.7% which is the mass loss undergone in the formation of ABV during decomposition in air or argon

It is interesting to note the total absence of the anomalous high frequency component associated with the triply degenerate bending mode of the NH_4^+ ion at $\sim$ 1400 cm^{-1} during the first stage of the decomposition.

4. 1. 4. 3 The Isothermal α -time Curves

The curves are basically "Type II" for all the three stages studied, i. e., a linear and a deceleratory region. In the first stage the linear region extends up to $\alpha = 0.75 \mp 0.05$ while in the second and third stages it is very short, i. e., only to $\alpha = 0.40$. The fit of the contracting sphere expression is not as good as it is for the decomposition in other atmospheres, but it still provides the best fit of any of the usual mathematical expressions for kinetic models of solid decompositions, i. e. those described in Chapter 1. The reason for the poor fit is apparently that during the later stages of the decomposition in ammonia the material is being reduced as well as decomposed.

4. 1. 4. 4 The Effect of Temperature

Analysis of the variation of the rate constants for decomposition with temperature for each region (linear and deceleratory) of the first stage and for the deceleratory regions of the second and third stages, by application of the Arrhenius equation (Equation 4. 2), enabled the activation energy for each stage to be calculated (See Table 4. 10).

TABLE 4.10

The Activation Energies for all of the Stages in the Decomposition of AMV in Ammonia

Stage	Region	Activation Energy/(kcal mol^{-1})
1	linear	32.5
	contracting sphere	35.0
2	contracting sphere	80.2
3	contracting sphere	67.3

Accurate values for the activation energies for the short linear regions of the second and third stages of the decomposition could not be calculated.

The activation energies for the second and third stages of the decomposition in ammonia are seen to be much greater than any of the activation energies for any of the stages of the decomposition in the other atmospheres studied.

Comparison of the Results for the Decomposition of AMV in the Various Atmospheres

The results described in detail in sections 4.1.1 to 4.1.4 are summarized in Table 4.11 and presented diagrammatically in Figure 4.18. The products are classified according to their structural similarities in the last column of the table; the subscripts indicate that the product possesses a relatively disordered structure, and different subscripts for the same general structure type, i.e. $(ABV)_a$ and $(ABV)_b$ indicate minor differences in the relative degree of structural disorder, as shown by the infrared and x-ray powder studies.

The abbreviations in the penultimate column of Table 4.11 are clearly defined by the empirical formulae of the corresponding products.

Figure 4.18 Diagrammatic representation of the course of the reaction in the various atmospheres

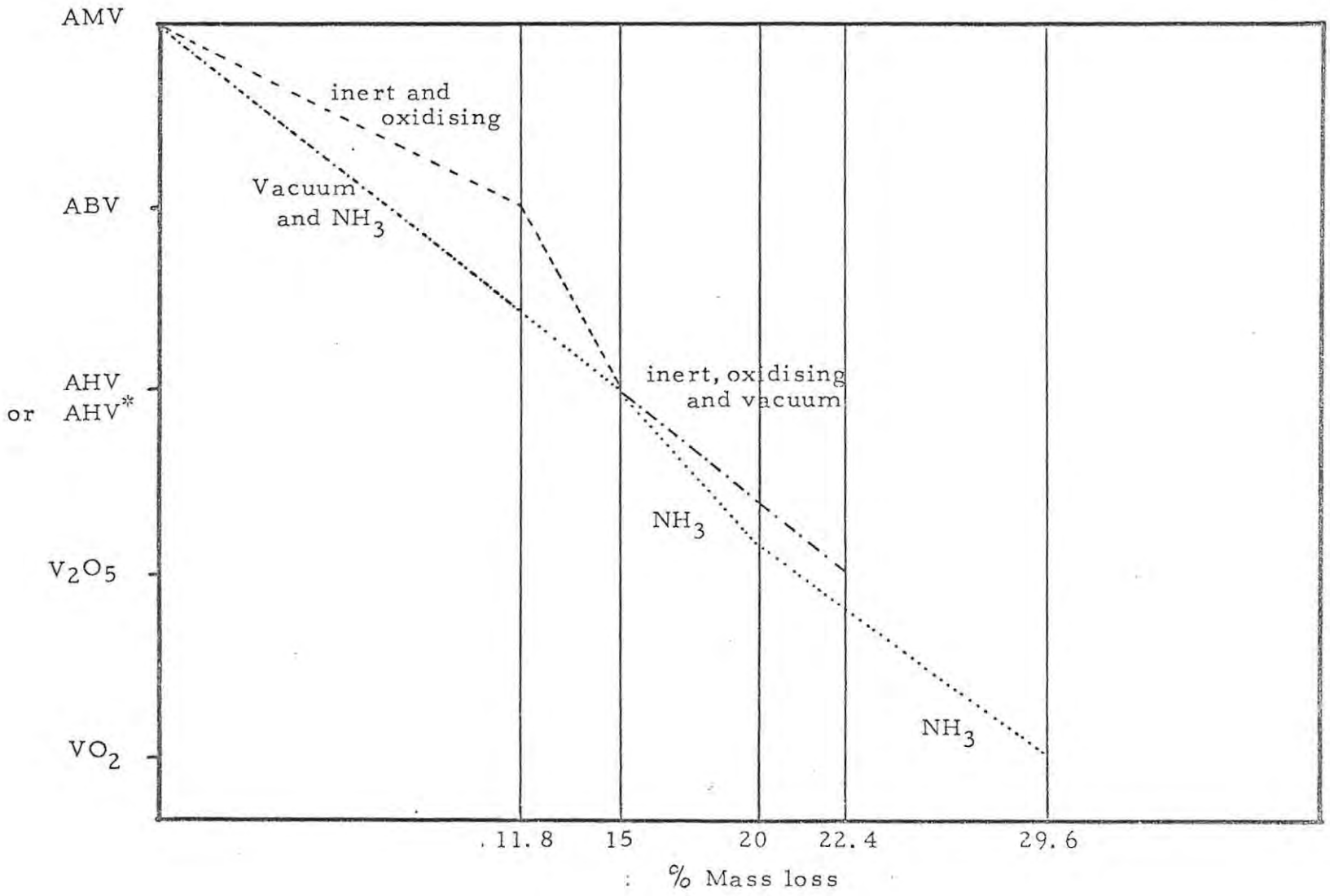

TABLE 4.11 : Summary of the General Results of the Decomposition of AMV in Various Atmospheres

Atmosphere	Stage	Temp. Range °C	Activation Energy kcal mol^{-1}		Total mass loss %		Empirical formula of product		Product type according to structural analysis
			Region	Value	Expected	Found	Formula	Abbreviation	
Vacuum	1	105-135	cont. sphere	30.8	14.83	14.7-14.9	$NH_4V_3O_8$	AHV	$(ABV)_a$
	2	135-155	cont. sphere	38.2	16.66	16.9-17.2	$NH_4V_4O_{10.5}$	-	
	3	165-200	cont. sphere	23.4	22.23	22.3-22.4	V_2O_5	-	
Inert	1	160-180	linear cont. sphere	32.9 31.6	11.10	11.7-11.8	$(NH_4)_2V_4O_{11}$	ABV	$(ABV)_b$
	2	180-210	cont. sphere	25.2	14.83	15.9-16.0	$NH_4V_3O_8$	AHV	(AHV)
	3	270-300	linear cont. sphere	28.4 28.6	22.23	22.3-22.4	V_2O_5	-	$(V_2O_5)_b$
Oxidising	1	150-180	linear cont. sphere	40.8 42.1	11.10	11.4-11.6	$(NH_4)V_4O_{11}$	ABV	$(ABV)_b$
	2	180-210	linear cont. sphere	32.0 31.2	14.83	15.3-15.6	$NH_4V_3O_8$	AHV	(AHV)
	3	260-300	cont. sphere	34.2	22.23	22.3-22.4	V_2O_5	-	(V_2O_5)
Ammonia	1	165-190	linear cont. sphere	32.5 34.0	14.83	14.6-14.8	$NH_4V_3O_8$	AHV	(AHV)
	2	280-300	cont. sphere	80.2	19.95	19.8-20.0	$NH_4V_6O_{15}$	-	
	3	340-360	cont. sphere	67.3	29.05	28.2-28.6	VO_2	-	

4. 1. 5 The Isothermal Decomposition of Ammonium Hexavanadate and of "AHV-type" Intermediates

Since the empirical formulae of several products (product types $(ABV)_a$ and (AHV) in Table 4. 11) were all $NH_4V_3O_8$, and since AHV can also be prepared from solution, it was decided to compare the kinetics of decomposition of the various compounds of this empirical formula in each of the atmospheres studied.

The AHV preparation (AHV_{SOLN}) and the intermediates formed in air (AHV_{Air}) and in inert atmospheres (AHV_{Inert}) all have similar structures, as shown by their virtually identical infrared spectra and x-ray powder data. Each of these samples was decomposed in air, argon and vacuum. Decomposition to V_2O_5 takes place in a single stage under all conditions.

$$2NH_4V_3O_{8\,(s)} \longrightarrow 3V_2O_{5\,(s)} + 2NH_{3\,(g)} + H_2O_{(g)}$$

The rate constants and the activation energies for the decomposition under various conditions of atmosphere were determined for each sample.

The general shape of the α-time curves depends largely on the conditions of atmosphere under which the decomposition is performed. The α-time curves for all of the decompositions performed in vacuum were Type I curves, those performed in argon were Type II curves and those performed in air were Type III curves.

A comparison of the rate constants $k(=\frac{k''}{a})$ for the contracting sphere regions of decomposition curves of the various AHV-type samples in each of the atmospheres is given in Table 4. 12, together with the corresponding activation energies.

TABLE 4.12 : The Isothermal Decomposition of Various AHV's in Various Atmospheres

		AHV prepared in:					
		AIR		ARGON		SOLUTION	
Atmosphere	Temperature °C	Rate constant x10^2 (min^{-1})	Act. Energy (kcal mol^{-1})	Rate constant x 10^2 (min^{-1})	Act. Energy (kcal mol^{-1})	Rate constant x 10^2 (min^{-1})	Act. Energy (kcal mol^{-1})
Vac	220	2.37		2.39		0.46	
	225	3.30		2.98		0.34	
	235	5.97	28.2	3.58	15.2	0.80	28.6
	240	8.45		4.57		1.15	
	245			5.32		1.38	
Air (dry)	265	1.58		0.997		0.62	
	270	2.15		1.14		0.84	
	275	3.35	cont. sphere region	1.35	cont. sphere region	1.12	cont. sphere region
	280	3.45	34.2	1.70	22.0	1.49	34.6
	285	4.99		1.96		1.96	
Argon	268.5	0.38	linear region	0.94	linear region	1.41	linear region
	273	0.60	37.5	1.14	29.2	2.19	44.3
	279	0.89	cont. sphere reg.	1.514	cont. sphere reg.	3.49	cont. sphere reg.
	284.5	1.22		1.95	28.6	5.27	
	295.5	2.32	36.4	3.22		11.67	45.4

The infrared spectrum and x-ray powder diffraction data for the intermediate formed at the end of the first stage in vacuum (AHV*) indicate that this sample is structurally different from the AHV-type samples described above, and corresponds to the bivanadate in structure. The further decomposition of this sample is also considerably different in argon or in air. Decomposition to V_2O_5 occurs in two stages. At about 220°C, decomposition to a total mass loss of 19.6% occurs and the final stage to V_2O_5 (22.4% mass loss) takes place at about 300°C. The infrared spectrum of the intermediate formed at 19.6% mass loss shows that it is not the same as the $NH_4V_6O_{15}$ formed in ammonia, even though the total mass loss involved in the formation of these two intermediates is the same.

When AHV* is decomposed further in ammonia then three further stages are detected in the decomposition. At about 220°C, decomposition to a total mass loss (with respect to AMV) of 16.17% occurs. The infrared spectrum of this intermediate is similar to that of AHV. Further decomposition leads to a total mass loss of 19.8-20.4% at 310°C, and to a total mass loss of 29.6% at 350°C. The products formed during these two stages are identical to the products formed at the end of the second and third stages of the decomposition of AMV in ammonia i.e. $NH_4V_6O_{15}$ and VO_2 respectively.

The x-ray powder data and infrared spectrum of AHV* (mass loss 14.9%) suggest a structural similarity to the intermediates formed at the end of the first stages in air or argon (ABV) (mass loss 11.7%), i.e., all of the reflections in the powder photograph of AHV* are present in the powder photograph of ABV. The powder diffraction pattern of ABV has, however, many more reflections than has the powder pattern of AHV*. There are virtually no differences in the infrared spectra in

the region 600-4000cm^{-1}. ABV, formed at the end of the first stage in air, however, decomposes further in vacuum in a single stage at about 180°C to give a defective form of V_2O_5, similar to the product of the third stage in vacuum.

4. 1. 6 The Effect of Pressure on the First Stage of the Decomposition

The mass loss involved in the first stage of the decomposition in oxidising or inert atmospheres is different to that of the first stage of the decomposition in vacuum although these intermediates ABV and AHV* are structurally similar. A series of decompositions were thus performed under various pressures of nitrogen. The results are given in Table 4. 13.

TABLE 4. 13

First Stage of the Decomposition under Various Total Pressures of Nitrogen

Pressure(mmHg)	Temp. °C	% Mass loss
10^{-5}	105-135	(AHV*) 14. 7-14. 9
0. 18	137	15. 0
0. 49	143	15. 0
1. 31	147	14. 2
52. 9	151	12. 68
202	153	12. 18
402	154	12. 08
720 (atmospheric pressure)	160-180	(ABV) 11. 7-11. 8

The series of decompositions could not be performed at a single temperature since the temperature at which decomposition commences is approximately 30°C higher at atmospheric pressure than in vacuum (See Table 4. 11).

It can be seen from Table 4. 13 that under these conditions of sample size (cf. Lamure and Colin[78]) the pressure under which the decomposition is performed has little effect on the mass loss of the first stage of the decomposition, below about 1. 0 mmHg.

4. 1. 7 The Effect of the Pressure of NH_3 in the Surrounding Atmosphere on the First Stage of the Decomposition

An ABV intermediate, which is the product of the first stage of the decomposition in inert or in oxidising atmospheres, cannot be isolated when the decomposition is carried out in an atmosphere of ammonia. AHV is formed directly from AMV in ammonia and the infrared spectrum of the sample after interruption at the appropriate mass loss did not correspond to ABV (Figure 4. 19).

A series of decompositionsunder various partial pressures of NH_3 in the nitrogen carrier gas were performed and the changes in the infrared spectra with partial pressure of ammonia for a mass loss of 11. 8% in the formation of the samples are given in Figure 4. 19.

It can be seen from the infrared spectra that ABV can be isolated during the decomposition if the partial pressure of ammonia in the nitrogen is less that about 200 mmHg. If the partial pressure of ammonia in the nitrogen is greater than about 350mmHg then ABV

Figure 4.19 Changes in the infrared spectrum during decomposition with increasing P_{NH_3}

Total pressure: 1 atmosphere

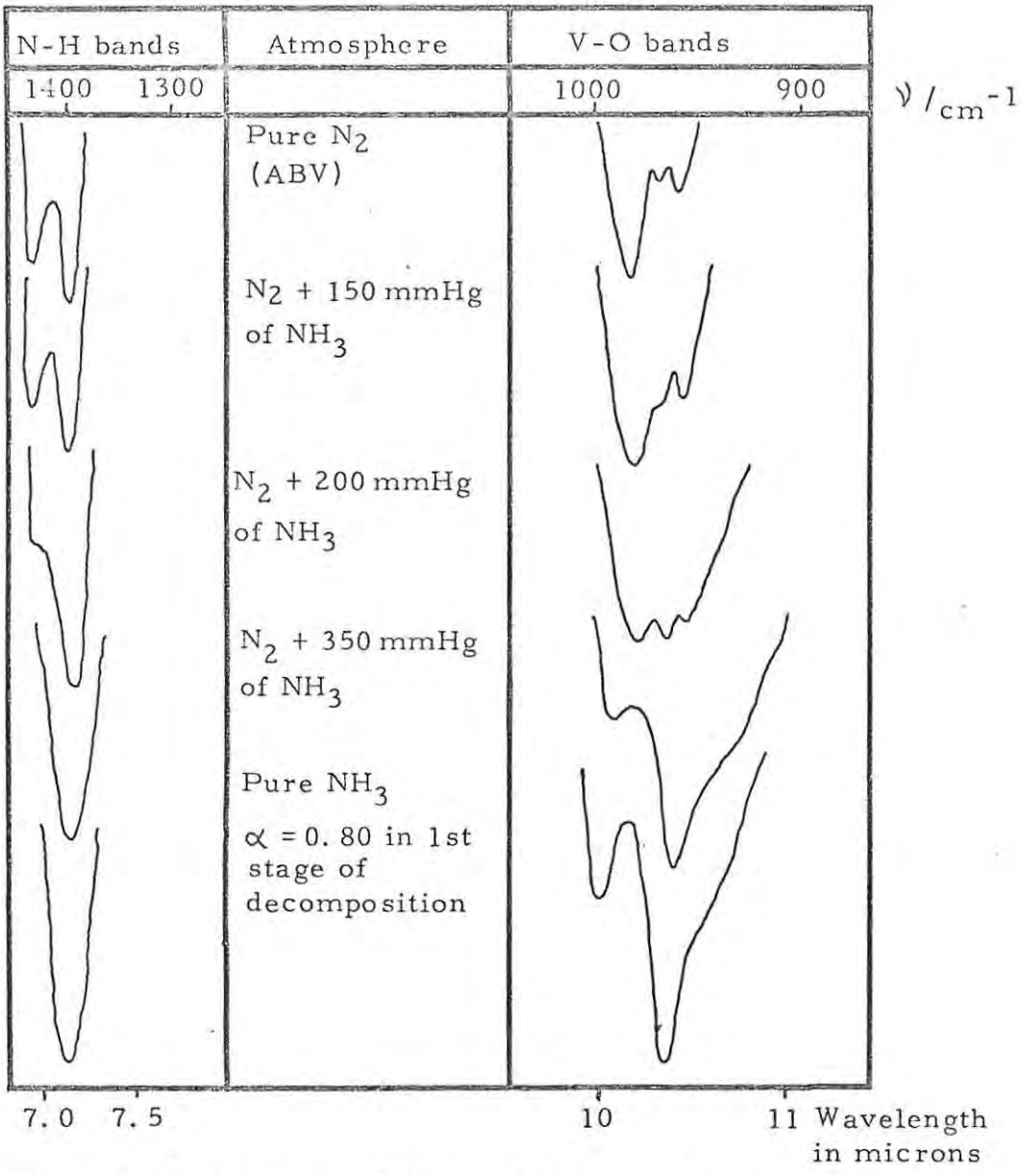

The mass loss from AMV in each case was 11.8 %

cannot be isolated at all.

4. 1. 8 The Effect of Pre-irradiation on the Decomposition of AMV

Samples (10g) of AMV were sealed in Pyrex ampoules under vacuum and were given a 100 Mrad dose of γ-rays in the ^{60}Co source at the Atomic Energy Board, Pelindaba.

Only the first stage of the decomposition in vacuum was studied and compared with that of control samples. The α -t curves were found to be of Type I (i. e. deceleratory throughout) as before. The rate constants of decomposition determined from the application of the contracting sphere expression to the α -t curves are given in Table 4. 14.

TABLE 4. 14

The Effect of Pre-irradiation on the Rate of Decomposition of the First Stage in Vacuum

Sample	Temperature	Rate constant $x10^3/(min^{-1})$
irradiated	123. 5	6. 94
control	123. 5'	7. 11
irradiated	120. 0	3. 70
control	120. 0	3. 62

It is thus apparent that pre-irradiation with γ -rays has no significant effect on the kinetics of the first stage of the decomposition in vacuum.

4. 1. 9 The Surface Areas of Various Intermediates and Products

The surface areas of some of the intermediates and final products formed during the decomposition were determined by Dr V. M. Lovell at the National Institute for Metallurgy by the B. E. T. method using krypton adsorption. The results are given in Table 4. 15.

TABLE 4. 15

The Surface Areas of Various Intermediates and Products

Sample	Surface area ($m^2 g^{-1}$)
1. NH_4VO_3 (AMV)	0. 365
2. V_2O_5 from 3rd stage in air	5. 26
3. V_2O_5 from 3rd stage in vacuum	25. 9
4. (3) annealed in air	27. 6
5. V_2O_5 from decomposition of AHV in air	2. 86
6. V_2O_5 from decomposition of AHV in vacuum	3. 20
7. V_2O_5 from Hopkins and Williams	3. 15
8. AHV prepared from solution	1. 30
9. AHV from 2nd stage in air	3. 82
10. AHV* from 1st stage in vacuum	18. 58

4. 1. 10 Differential Enthalpic Analysis

Differential enthalpic analyses (DEA) were performed by Dr M. E. Brown at Queens University, Belfast, using a Perkin Elmer DSC-IB scanning calorimeter. Heating rates of 20°C/min and gas flow rates of 0. 2 l/min were used.

Figure 4.20 DEA thermograms of AMV in N_2 and in air

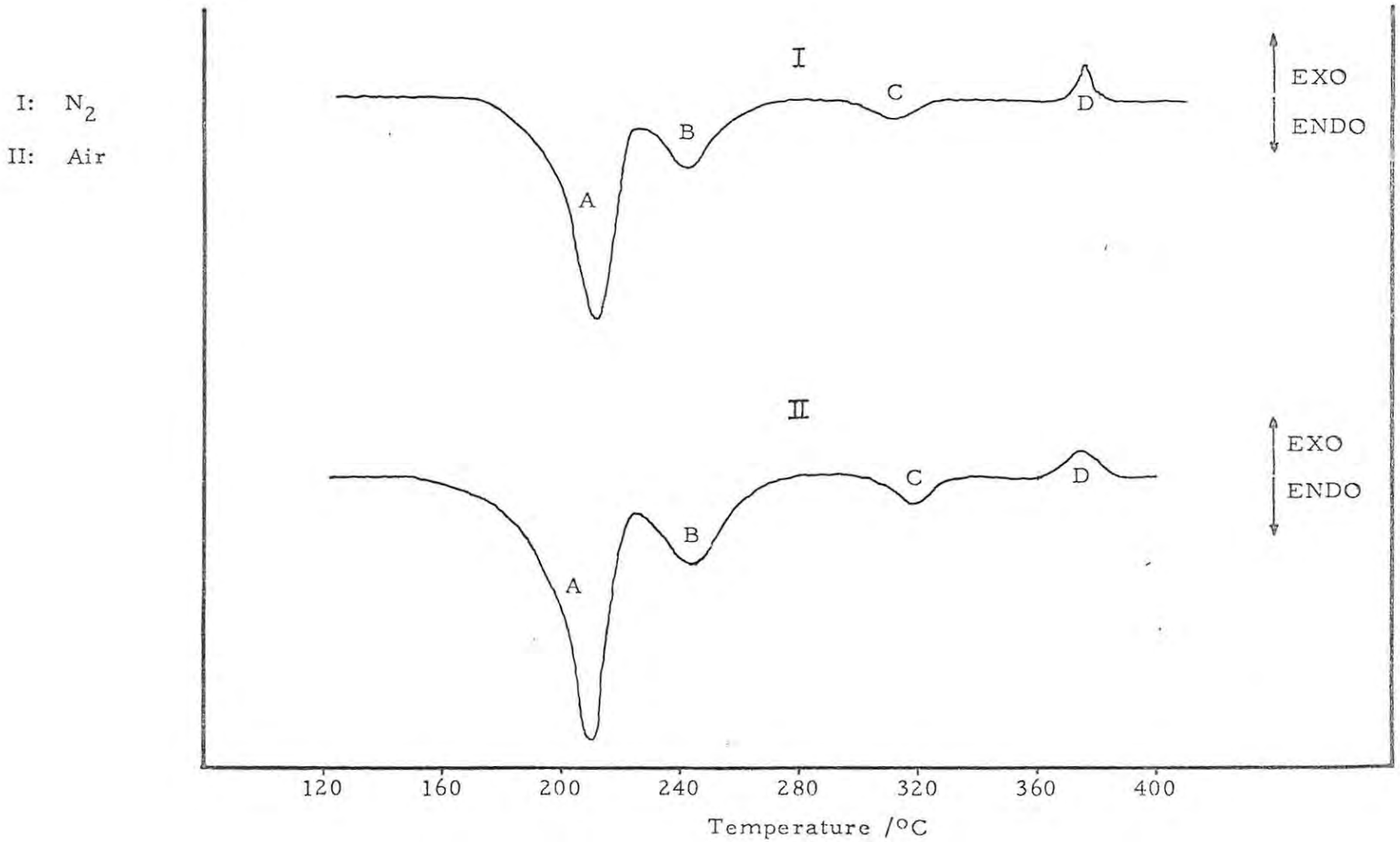

In order to correlate the endotherms with the various stages obtained in the isothermal study of the decomposition, infrared spectra of the samples obtained by interrupting the thermograms after each endotherm were recorded in the range 4000-250cm^{-1}.

The DEA thermograms for AMV in nitrogen and in air are illustrated in Figure 4.20. The thermograms are basically the same, and are in agreement with published DTA results [51, 52]. Measurement of the areas under the "peaks" and relation to thermograms of samples with known enthalpies of fusion, run under similar conditions, yielded the values for the enthalpy changes given in Table 4.16, all referred to one mole of NH_4VO_3.

Infrared spectra show that endotherm A corresponds to decomposition reaction (4.4).

$$4NH_4VO_{3(s)} \longrightarrow (NH_4)_2V_4O_{11\,(s)} + 2NH_{3\,(g)} + H_2O_{(g)} \qquad 4.5$$

$$4AMV \longrightarrow ABV + 2NH_3 + H_2O$$

If the enthalpy change for reaction (4.3) is taken as 12.5 $\pm$ 0.2 kcal/mole AMV, (calculated from area under "peak" A), the enthalpy of formation of the intermediate ABV; $(NH_4)_2V_4O_{11}$ over the temperature range (150-210°C) is -870 $\pm$ 5 kcal/mole.

Infrared spectra show that endotherm B represents further reaction to form AHV i.e. reaction (4.4)

$$3(NH_4)_2V_4O_{11\,(s)} \longrightarrow 2(NH_4)_2V_6O_{16\,(s)} + 2NH_{3\,(g)} + H_2O_{(g)} \qquad 4.4$$

$$3ABV \longrightarrow 4AHV + 2NH_3 + H_2O$$

From Table 4.16 it can be seen that the scatter in the ΔH values for endotherm B is far greater than for endotherm A. For this reason the

enthalpy of formation of AHV was calculated from the DEA of a crystalline sample of AHV prepared from solution[91]. A single endotherm only, corresponding to endotherm C in the DEA of AMV (and a very small subsequent exotherm : D) appears in the thermogram, and this is ascribed to reaction(4. 6)

$$(NH_4)_2V_6O_{16\,(s)} \longrightarrow 3V_2O_{5\,(s)} + 4NH_{3\,(g)} + 2H_2O_{\,(g)} \qquad 4.6$$

$$2AHV \longrightarrow 3V_2O_5 + 4NH_3 + 2H_2O$$

From a measured enthalpy of reaction of 8. 1 $\pm$ 0. 2 kcal/mole AMV and the standard enthalpies of formation of the products[121], the enthalpy of formation of AHV in the temperature range 300-340°C is estimated to be -625 $\pm$ 2. 5 kcal/mole AHV.

Now, using the estimated enthalpies of formation of ABV and AHV leads to an expected value for the enthalpy change for reaction (4. 5) of the order of 4 kcal/mole AMV. This is slightly lower than the measured values of 4. 9 - 9. 5 kcal.

The standard enthalpy of reaction (4. 7)

$$2NH_4VO_{3\,(s)} \longrightarrow V_2O_{5\,(s)} + 2NH_{3\,(g)} + H_2O_{(g)} \qquad 4.7$$

$$\text{i.e. } 2AMV \longrightarrow V_2O_5 + 2NH_3 + H_2O$$

calculated from the standard enthalpies of formation[121] in 26. 5 kcal/ mole AMV.

ΔCp^{θ} for reaction (4. 7)[121] is -5. 8 cal K^{-1}.

If it is assumed that ΔCp^{θ} is independent of temperature over the range 298-500 K then ΔH^{θ} (500k) for reaction (4. 7) is given by

$$\Delta H^{\theta}(500k) = \Delta H^{\theta}(298k) + \Delta Cp^{\theta} . \Delta T$$

$$= 25.9 \text{ kcal/mole AMV}$$

The difference between ΔH^{θ} and ΔH, the enthalpy of reaction under the actual conditions, is likely to be less than the experimental errors involved[122].

This standard value is slightly greater than the maximum value of about 21.5 kcal obtained in the present study.

The exotherm D has been ascribed[52] to the oxidation of the last traces of ammonia trapped in the V_2O_5 product. It could also be a recrystallisation effect, as has been observed in DTA studies of the dehydration of hydrates[123], or, of course, a combination of these two processes.

TABLE 4.16

Enthalpy Changes Associated with the Stages of Decomposition of Ammonium Metavanadate.

(Δ H/kcal (mol AMV)$^{-1}$

Sample	Atmosphere	Endotherm			Exo-therm	Total
		A	B	C	D	
AMV	N_2	12.8	5.3-9.5	0.8	1.4	17 - 21.5
	Air	13.0	4.9-8.0	1.0	1.0	17.5-20.5
AHV	N_2	-	-	8.1-9.2	0	-

TABLE 4. 17

Standard Enthalpies of Formation

	Temperature / K	ΔH_f^θ / kcal mol^{-1}	Reference
NH_4VO_3 (s) (AMV)	298	-251.1	121
V_2O_5 (s)	298	-373	121
NH_3 (g)	298	-11.04	121
H_2O (g)	298	-57.84	121
$(NH_4)_2V_4O_{11}$ (s) (ABV)	420-480	-870± 5	this work
$NH_4V_3O_8$ (s) (AHV)	570-610	-625±2.5	this work

4.2 The Recombination, or Reverse Reaction

The endothermic nature of the thermal decomposition of AMV is well established[52,78]. It was decided to study the reversibility of the overall reaction because of the results obtained for other endothermic decompositions such as the dehydration of crystal hydrates[62] and the decomposition of hydroxides[54] and carbonates[27]

$$2NH_4VO_3\,(s) \rightleftharpoons V_2O_5\,(s) + 2NH_3(g) + H_2O(g) \qquad 4.8$$

Each of the intermediates formed in nonreducing atmospheres recombined on exposure to damp ammonia to form a product with infrared spectrum and x-ray data identical to AMV. (Figures 4.21 and 4.22). Although the decomposition to V_2O_5 involves several stages, it was found that the recombination reaction occurred in a single stage. Of the decomposition intermediates in ammonia, only the product of the first stage recombines completely to form AMV. This is expected as

4.21 Comparison of the infrared spectra of "recombined" AMV and "normal" AMV

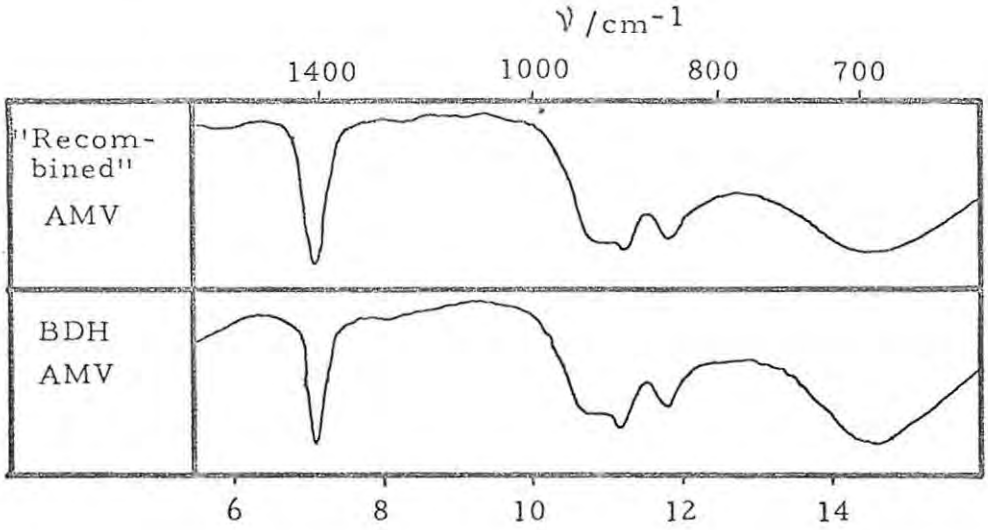

4.22 Comparison of the x-ray powder patterns of "recombined" AMV and "normal" AMV

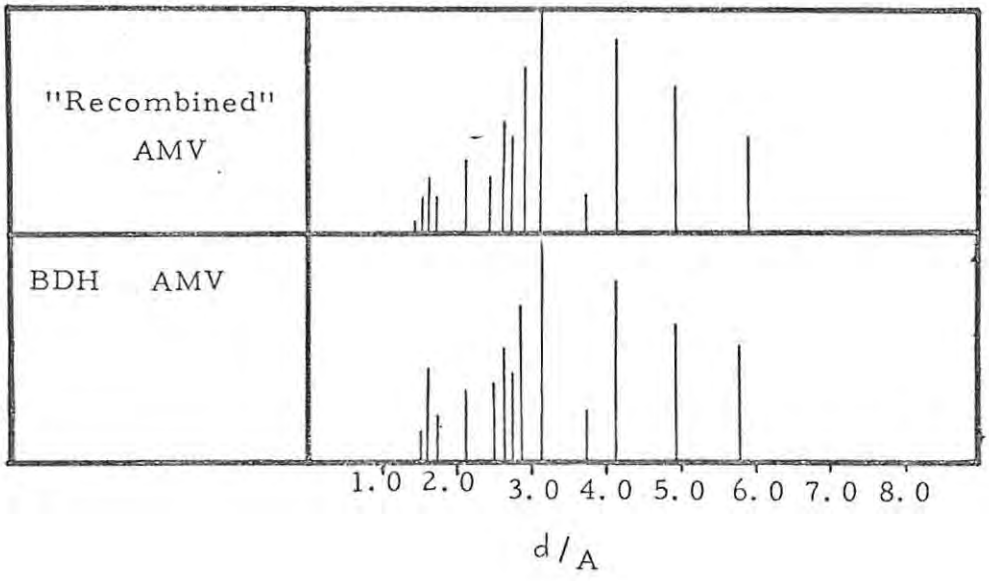

Figure 4.23

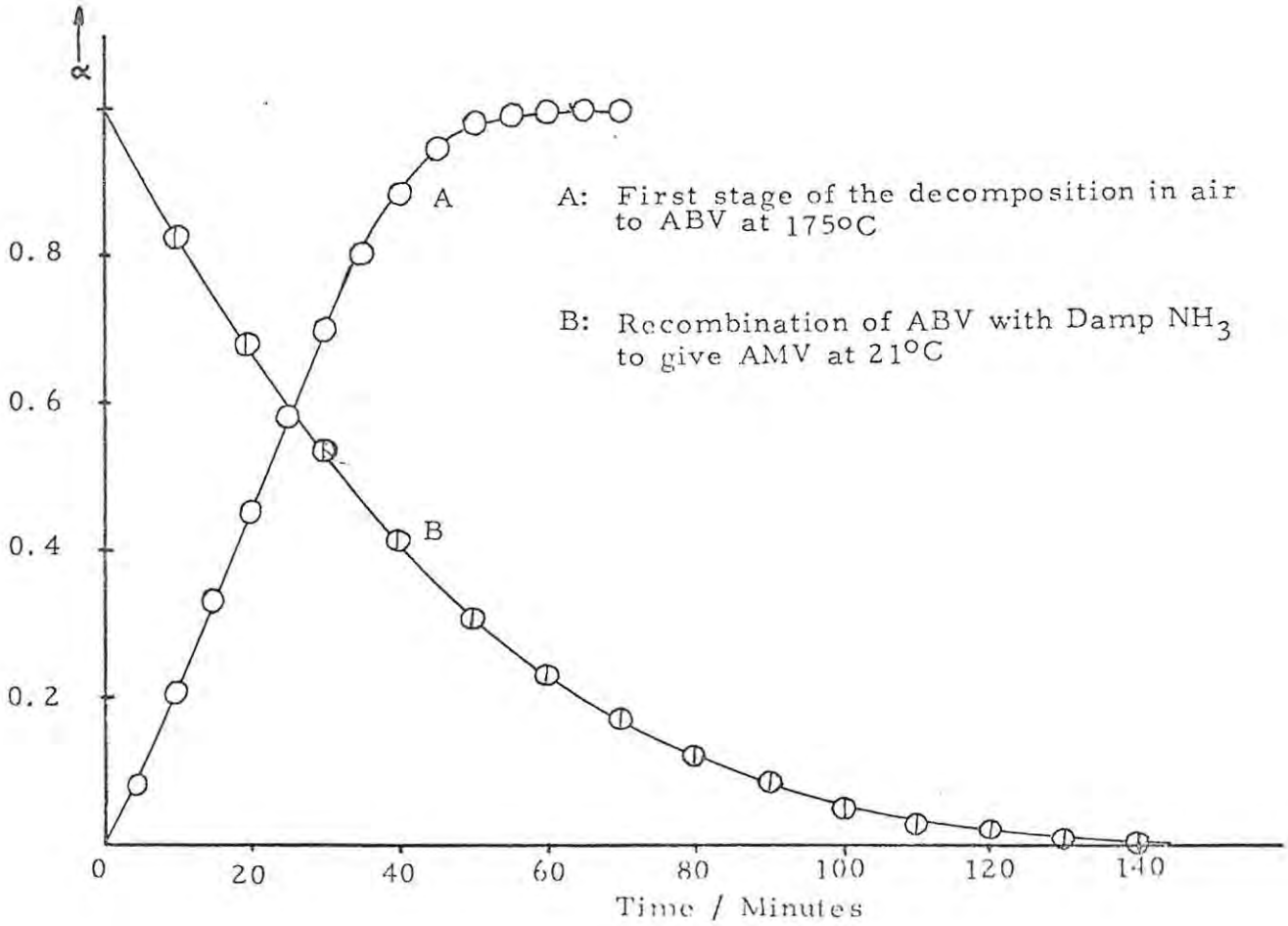
α
0.8
0.6
0.4
0.2
A
B
A: First stage of the decomposition in air to ABV at 175°C
B: Recombination of ABV with Damp NH_3 to give AMV at 21°C
0
20
40
60
80
100
120
140
Time / Minutes

reduction occurs during the later stages of the decomposition in ammonia. The product of the second stage of the decomposition in ammonia $NH_4V_6O_{15}$, only gains 57.3% of the mass expected if it were to recombine completely to AMV, and the product of the third stage of the decomposition in ammonia, VO_2, does not react with damp ammonia at room temperature.

In Figure 4.23, the decomposition of AMV to ABV, in air at 175°C i.e.

$$4NH_4VO_3\,(s) \rightleftharpoons (NH_4)_2V_4O_{11}\,(s) + 2NH_3\,(g) + H_2O\,(g) \qquad 4.9$$

$$\text{i.e. } 4\text{AMV} \rightleftharpoons \text{ABV} + 2NH_3 + H_2O$$

is represented by curve "A" and the reaction of the solid product of reaction 4.9 with damp ammonia at 21°C, by curve "B".

The AHV intermediates formed do not recombine as readily as does the bivanadate (ABV). The infrared and x-ray powder photographs indicate that the AHV has the more ordered structure. AHV prepared from solution[91], AHV_{SOLN}, combines extremely slowly with damp ammonia. The V_2O_5 product formed by decomposing AHV_{SOLN} in air recombines with damp ammonia, in a single stage to give AMV and not the hexavanadate. AHV cannot be isolated by interrupting the recombination of any sample of V_2O_5 at the appropriate mass gain and the infrared spectrum (Figure 4.24) and x-ray powder photograph (Figure 4.25) of the sample at this point correspond to a mixture of AMV and V_2O_5.

4.2.1 The α'-t Curves

It was found more convenient to plot α'-t curves rather than α-t

Figure 4.24 Comparison of the infrared spectra of AHV and the material obtained by interrupting the recombination at the mass gain corresponding to the formation of AHV

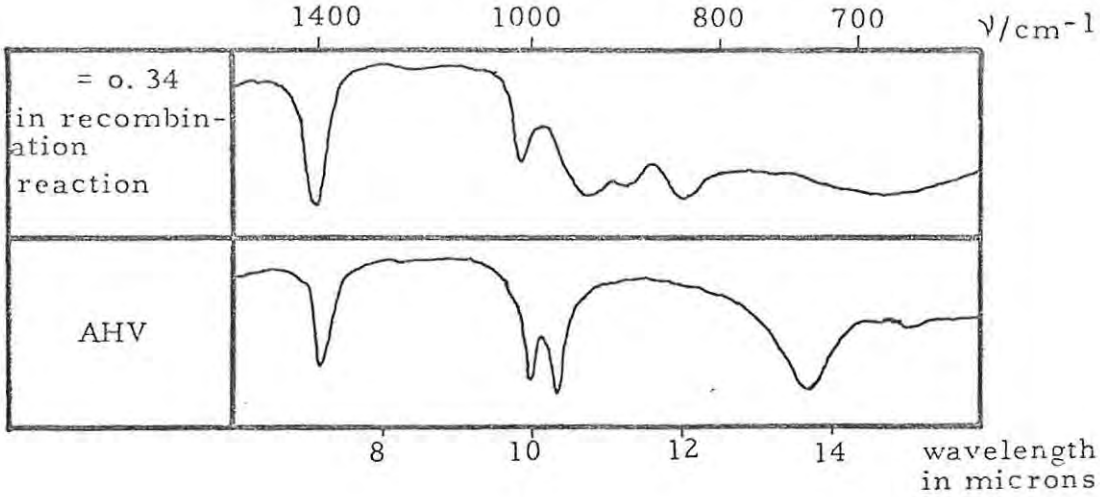

Figure 4.25 Comparison of the x-ray powder patterns of AMV, V_2O_5 and the material obtained by interrupting the recombination at the mass gain corresponding to the formation of AHV

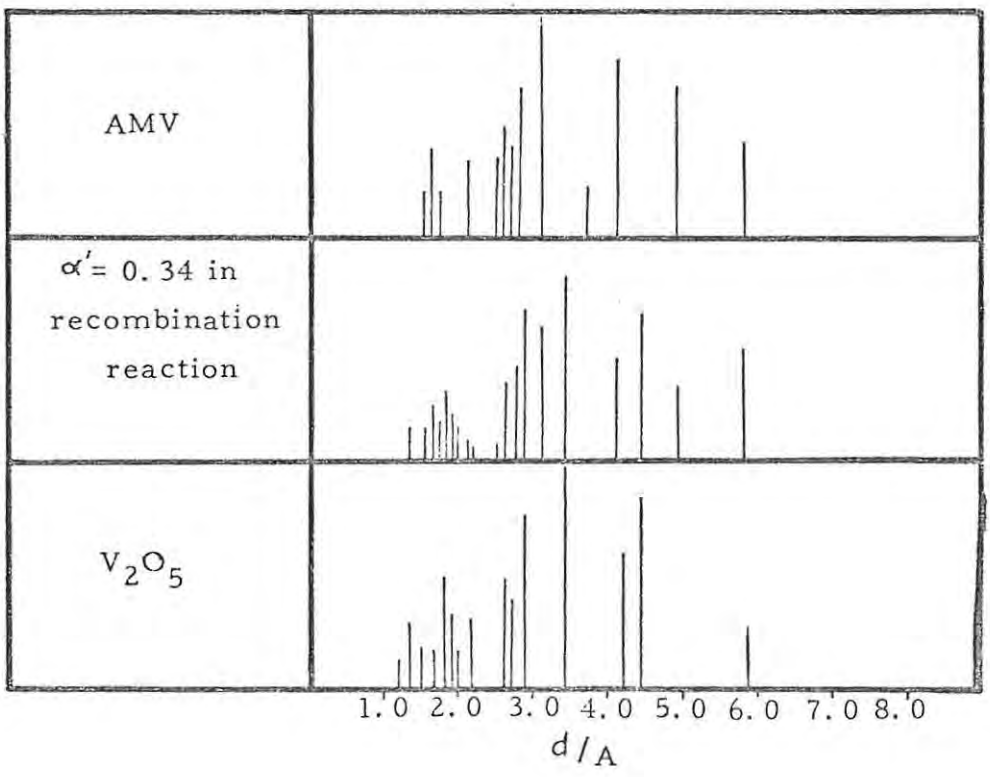

curves when analysing the recombination reaction, where $\alpha' = (1- \alpha)$ and α is the fraction of the decomposition reaction completed. The curves so obtained were tested with the usual mathematical expressions for both an interface and a diffusion controlled process (see Section 1.1.4). The parabolic law

$$\alpha' = (kt)^{\frac{1}{2}} \qquad 4.10$$

was found to apply over almost the whole reaction ($0.2 \leqslant \alpha' \leqslant 0.96$). This is consistent with diffusion along interstitial channels as is found for the zeolites[59] and alums[62]. A plot of α' against $t^{\frac{1}{2}}$ for the recombination of V_2O_5 (obtained from the final product of the decomposition in air) to give AMV at 21°C is shown in Figure 4.26 as curve B.

4.2.2 Dependence of the Rate of Recombination on the Defectiveness of the Starting Material

A commercial sample of V_2O_5 (Hopkins and Williams) combined, at 21°C, with damp ammonia to give AMV, with a rate constant which could be increased somewhat by preheating the sample to 300°C in vacuum, followed by cooling, but which was still less than the rate constant for recombination of the V_2O_5 decomposition product.

TABLE 4.18

Sample	Rate constants for recombination / $(min)^{-1}$
Final product of decomposition in air	1.42×10^{-2}
Hopkins and Williams V_2O_5	1.19×10^{-2} (1)
Hopkins and Williams V_2O_5 preheated in vacuum	1.32×10^{-2} (2)

(1) Only recombines to $\alpha' = 0.85$
(2) Recombines completely

Figure 4.26 The recombination of V_2O_5 to form AMV

P_{NH_3} = 35 mmHg; P_{H_2O} = 16.4 mmHg

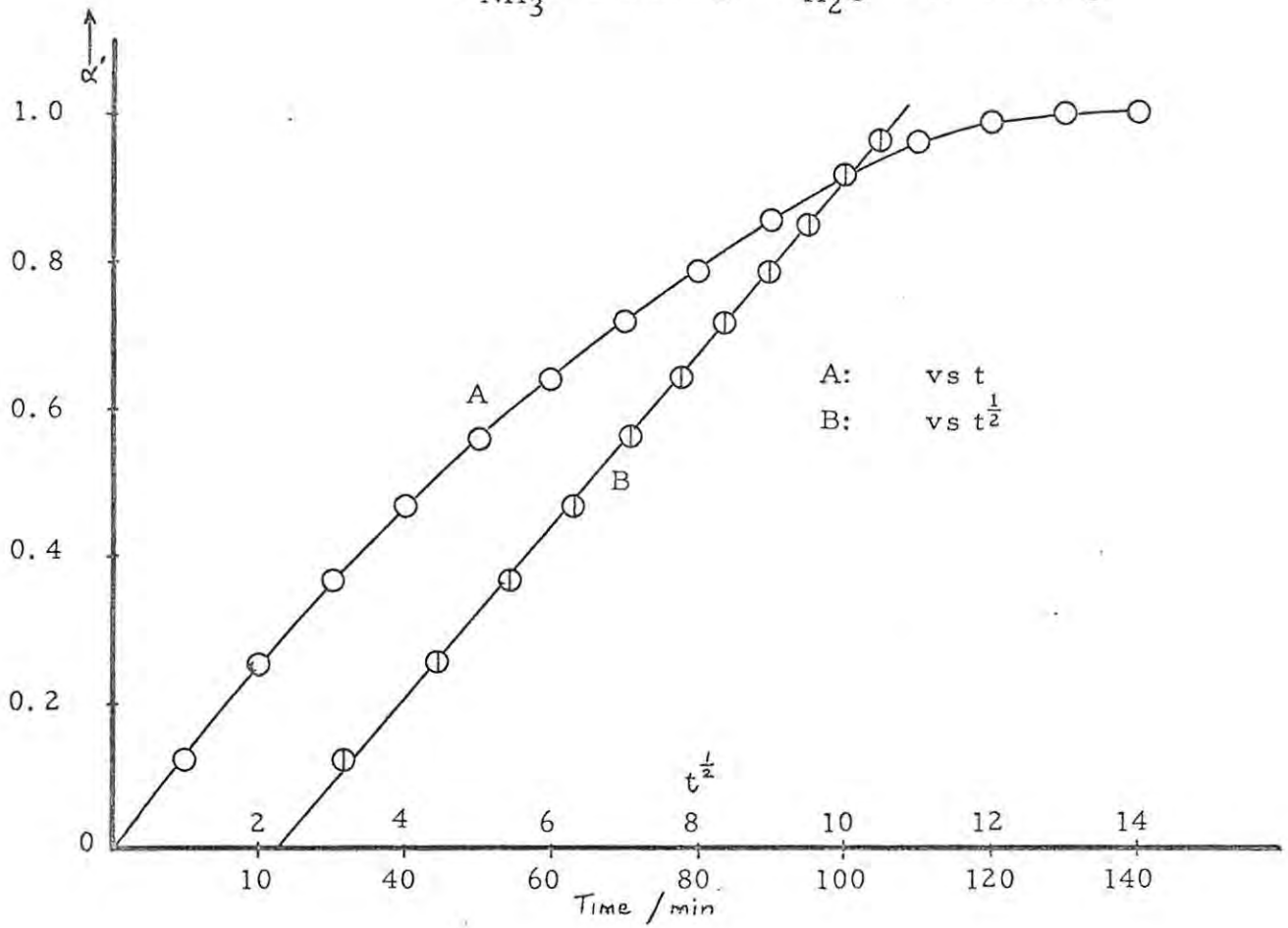

4. 2. 3 The Temperature Dependence of the Rate of Recombination

The value of the rate constant for the recombination of V_2O_5 (final product of the decomposition in air) with damp ammonia ($P_{H_2O} = P_{NH_3} = 70$mmHg) is seen from Figure 4.27 curve A to pass through a maximum with increasing temperature and then to decrease. The position of the maximum value of the rate constant is at about 35°C for this material. An arrhenius plot of log k from equation 4.2 against 1/T for the temperature interval 15-30°C for this material yields an activation energy of 2.0-4.0 kcal mol^{-1} for the recombination process at these temperatures.

It is also seen from Figure 4.27 curve E that the rate of physical adsorption of H_2O vapour (P_{H_2O} = 70 mmHg) on V_2O_5 formed in air decreases with increasing temperature over the same temperature range (the mass of H_2O adsorbed during a fixed time interval was taken as a measure of the rate of absorption of H_2O vapour). It should be noted that curve E is parallel to the last portion of curve A.

If relatively dry ammonia (P_{NH_3} = 720 mmHg, $P_{H_2O} < 0.1$mmHg) is used for the recombination of V_2O_5 (final product of the decomposition in air) then the rate constant for the recombination increases with increasing temperature over the temperature range 35-70°C (Figure 4.27 curve C). Application of equation 4.2 again yields an activation energy of about 3 kcal mol^{-1}, which suggests that curve C is equivalent to the initial portion of curve A.

The rate constant for the recombination of V_2O_5, formed at the end of the decomposition in vacuum, with damp ammonia (P_{NH_3} = 12.5 mmHg, P_{H_2O} = 70 mmHg) was however found to decrease with increasing temperature over the temperature range 15-30°C

Figure 4.27 Temperature dependence of the rate constant for recombination of various samples and under various experimental conditions

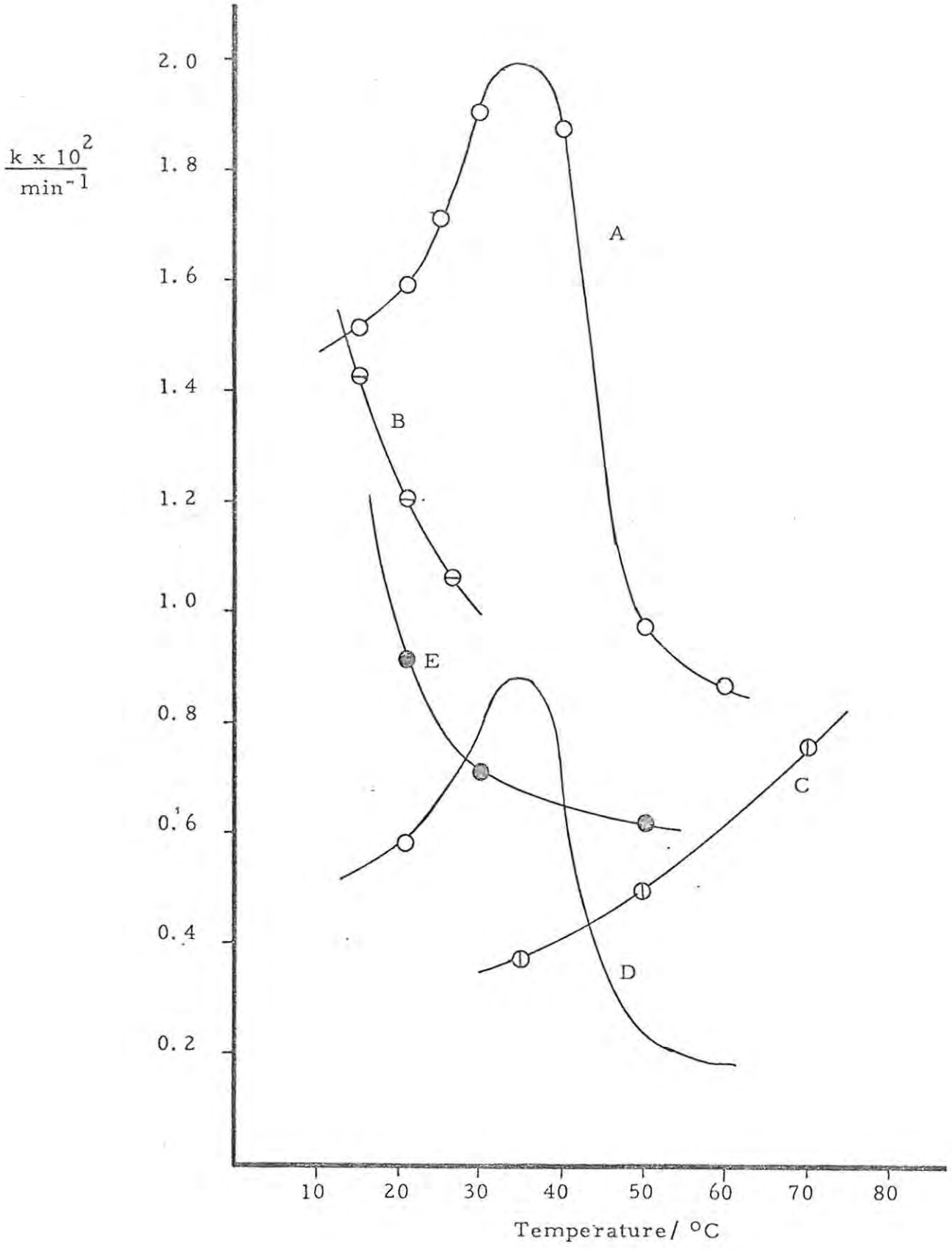

(figure 4.27 curve B) and thus to parallel curve E and the initial portion of curve A.

Curve D was estimated in order to illustrate the effect that P_{NH_3} would have on the position of the curve. The estimation of the position of this curve was based on the results of the investigation into the effect that P_{NH_3} would have on the rate constant for recombination at constant temperature which is discussed in the next section.

4. 2. 4 The Effect of Surrounding Atmosphere on the Recombination

Water vapour alone can be physically absorbed at 20°C on the V_2O_5 product in amounts greater than stoichiometrically required for the recombination reaction. It was not possible to establish that ammonia alone is <u>not</u> absorbed by V_2O_5, on using the normal experimental procedure of a flowing gas stream, since with the driest ammonia used ($P_{H_2O} \approx 0.004$ mmHg) recombination still occurred, although at a much reduced rate (total recombination took several days). To test whether this recombination occurs because, with the gas flowing, enough H_2O eventually passes over the sample for recomibation to occur, a sample of V_2O_5 was placed in a vacuum desiccator which was evacuated and baked to remove all traces of moisture. Dry ammonia ($P_{H_2O} \approx 0.004$ mmHg) was then bled in until the pressure inside the desiccator was one atmosphere. Over a period of ten days the sample gained only 2% of the mass corresponding to complete recombination. X-ray and infrared investigation of this material showed that it was a mixture of V_2O_5 with a small amount of AMV.

Figure 4.28 Section of figure 4.29 at p_{H_2O} = 70 mmHg

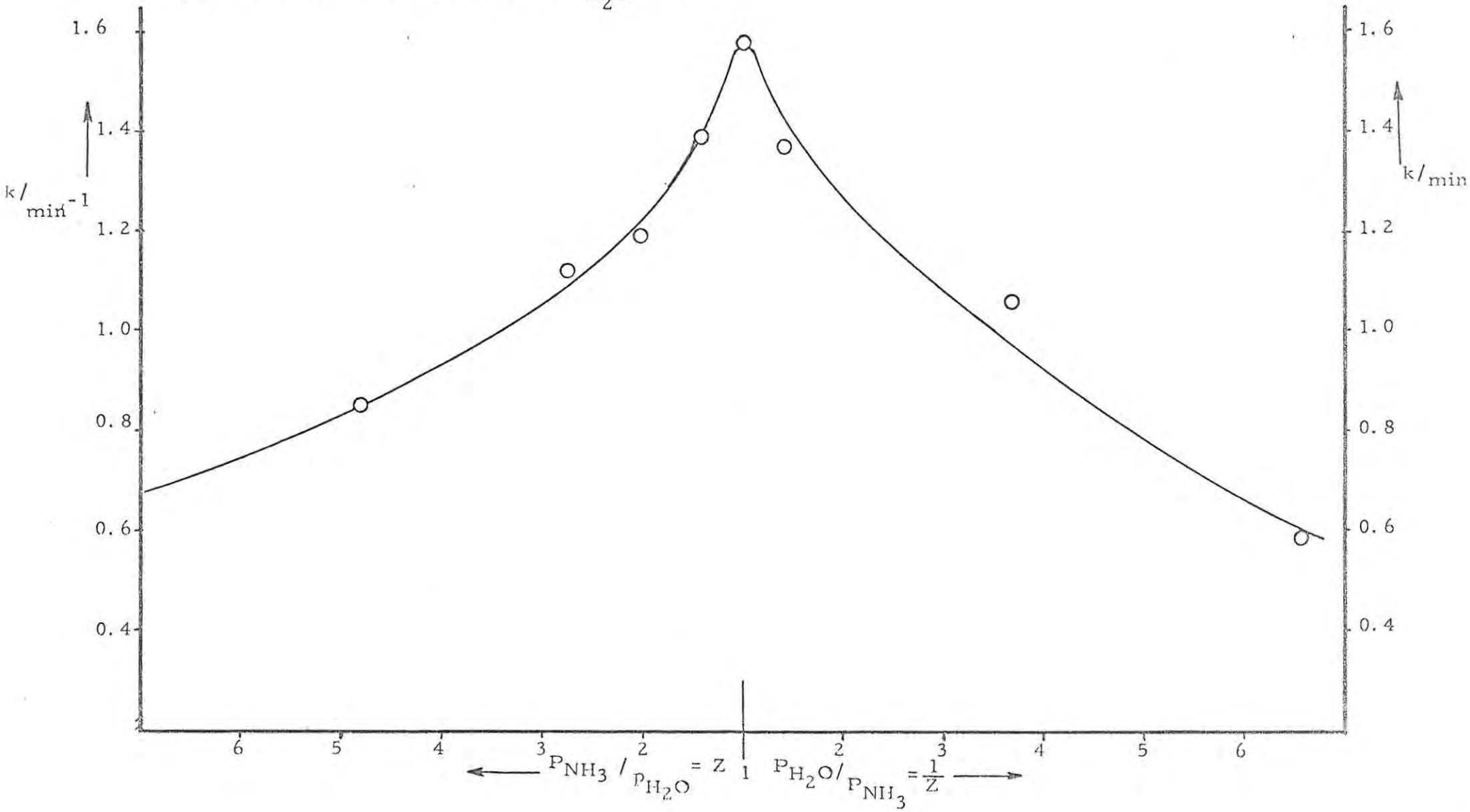

It thus seems conclusive that ammonia alone cannot be absorbed by V_2O_5 to any substantial degree but only reacts with it in the presence of water vapour, to form AMV.

The rate constants for a series of recombinations at constant temperature (21°C) and constant water vapour pressure (P_{H_2O} = 70 mmHg) are plotted against the ratio $Z = P_{NH_3} / P_{H_2O}$ and $\frac{1}{Z}$ in figure 4.28. It is clear that under these conditions the rate constants for the recombination pass through a maximum when $Z = \frac{1}{Z} = 1$ i.e. i.e. $P_{NH_3} = P_{H_2O}$.

This investigation was extended further and recombinations were performed over a wide range of values of Z and $\frac{1}{Z}$. A contour map of the reaction was estimated on the basis of these results (Figure 4.29). In this map, contours of constant values for the rate constants for recombination are plotted against the ratio Z, or its reciprocal, and the water vapour pressure P_{H_2O}.

The map may be divided into two regions as shown. It is clear that in region I the value of the rate constant for the recombination depends almost entirely on P_{NH_3} and is virtually independent of P_{H_2O}. In region II the position is more complex and it appears as though the value of the rate constant for the recombination depends on both P_{NH_3} and P_{H_2O}.

The overall dependence of the rate constant for recombination on the ratio Z is also clear and over a wide range of $P_{combined}$, = $P_{NH_3} + P_{H_2O}$ maximum values of the rate constant for recombination were obtained for Z approximately equal to one i.e. $P_{NH_3} = P_{H_2O}$.

It is also clear from the map that at low P_{H_2O} values in region II,

Figure 4.29 Contour map of the recombination reaction at 21°C (Total pressure 1 atmosphere)

Contours of constant k drawn at every 0.2×10^{-2} min^{-1}

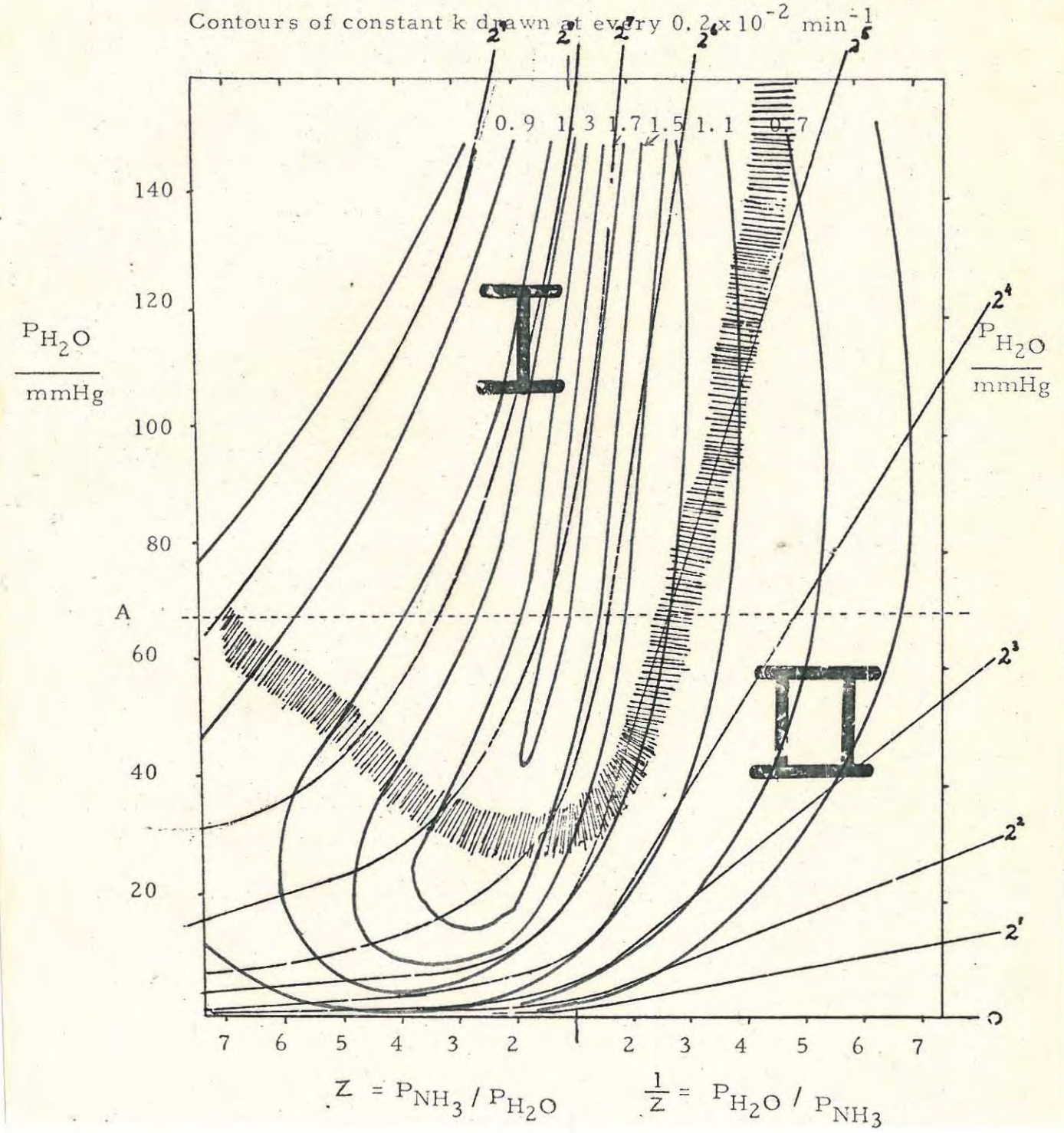

A: Section displayed in figure 4.28

Contours on overlay are lines of constant P_{NH_3}

the decrease in the rate constant for recombination, with a fixed P_{H_2O}, as Z decreases below one i. e. low proportions of NH_3, is more marked than is the decrease for high proportions of NH_3.

4. 2. 5 The Effect of Preadsorption of H_2O on the Recombination

When the stoichiometric amount of H_2O required for the complete recombination was preadsorbed on the V_2O_5 product before ammonia was admitted, the kinetics of the subsequent reaction with ammonia were found to depend on both the pressure of the ammonia and the partial pressure of water in the ammonia. In discussing the results the time when the ammonia was admitted has been taken as t = O.

4. 2. 5. 1 Damp Ammonia

When damp ammonia ($P_{NH_3} = P_{H_2O} = 70$ mmHg) is admitted after preadsorption of half of the stoichiometric amount of water required for the complete recombination then equation 4. 10 still applies over the whole reaction and the rate constant for recombination is identical to that obtained with no preadsorption of H_2O. If all the water required for recombination is preadsorbed then the rate constant for recombination is slightly reduced. (See Table 4. 19.)

A: α'-t curve for recombination of V_2O_5 without preabsorption of H_2O

B: α'-t curve for recombination of V_2O_5 after preabsorption of $\frac{1}{2}H_2O$/mole V_2O_5

C: α'-t curve for recombination of V_2O_5 after preabsorption of $1H_2O$/mole V_2O_5

Figure 4.30 Effect of Pre-Absorption of H_2O Vapour on V_2O_5 in various Stoichiometric Proportions on the α^1-t Curve for the Recombination

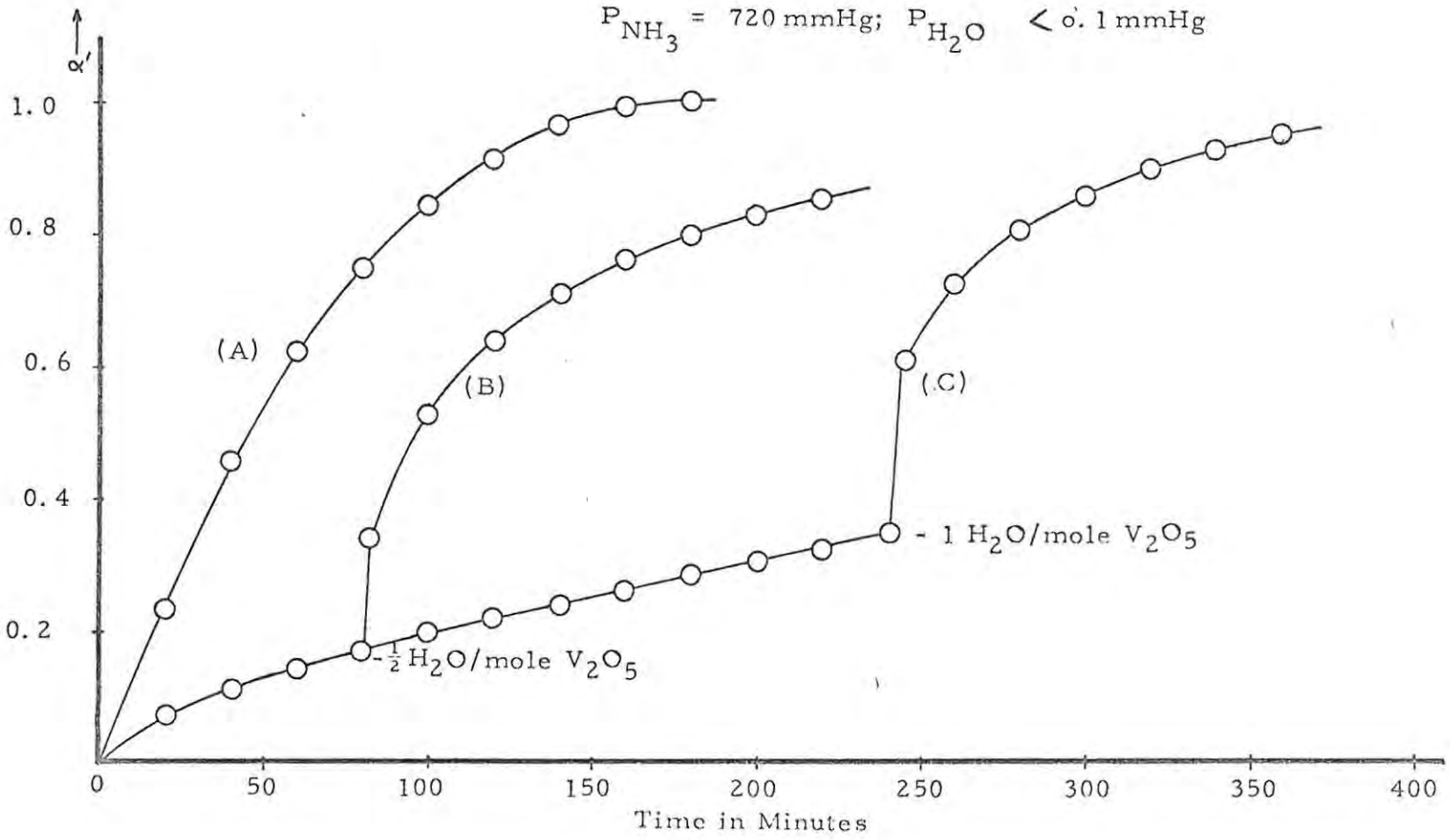

4. 2. 5. 2 Dry Ammonia

When dry ammonia (P_{NH_3} = 70 mmHg, $P_{H_2O} < 0.1$ mmHg) was admitted after preadsorption of amounts of water ranging from a half to the full amount required for recombination, the $\alpha' - t^{\frac{1}{2}}$ plots for the reaction showed two distinct regions. The rate constant, k_1 for the earlier period is greater than that, k_2, for the later part of the reaction. Both rate constants are independent of the amount of preadsorbed water. (See Table 4. 19.)

The point at which the change in slope occurs, however, does depend on the amount of preadsorbed water, and corresponds approximately to unity for the ratio (NH_3 reacted)/(H_2O preadsorbed).

4. 2. 5. 3 Dry Ammonia at Atmospheric Pressure

When dry ammonia (H_2O < 0. 1 mmHg) at atmospheric pressure is admitted after preabsorption of either half (Figure 4. 30 curve B) or all of the water (Figure 4. 30 curve C) required for recombination there are again two successive processes. Initially there is a very rapid reaction (duration < 60 secs.) followed by a slower reaction for which equation 4. 10 for a diffusion controlled process applies with a single value of k. In both cases, the rapid reaction holds until the ratio (NH_3 reacted) / (H_2O preadsorbed) is approximately one. The infrared spectrum of the material obtained by interrupting the recombination reaction at the end of the rapid process is given in Figure 4. 31. The x-ray powder diffraction pattern of this material is compared with those of AMV and V_2O_5 in Figure 4. 32.

Figure 4. 31

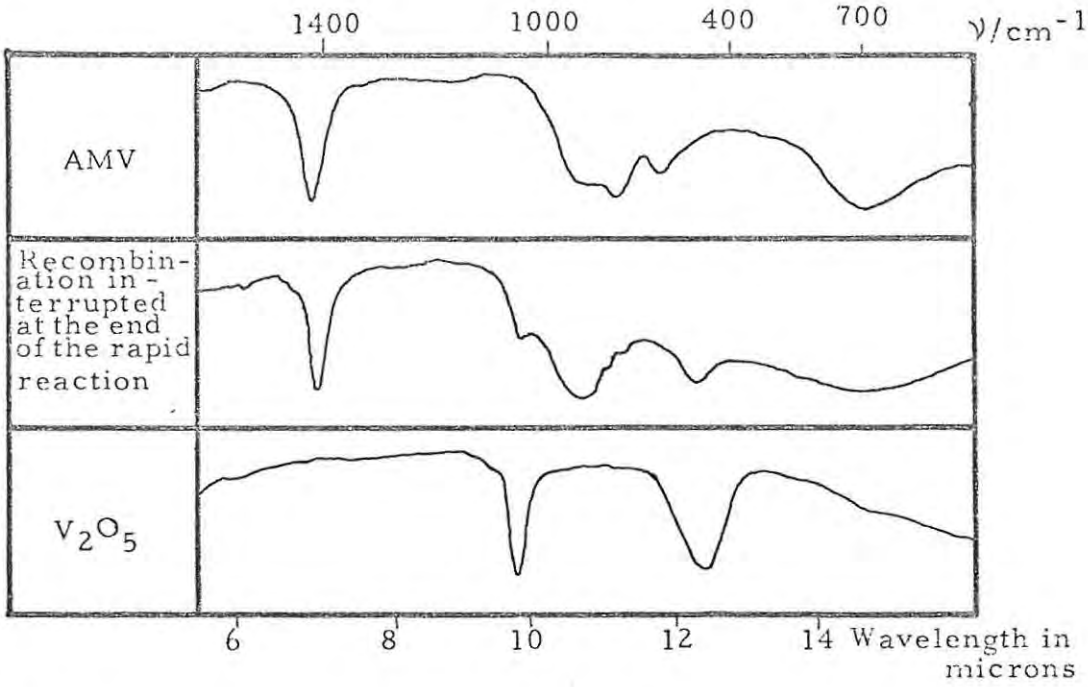

Figure 4. 32

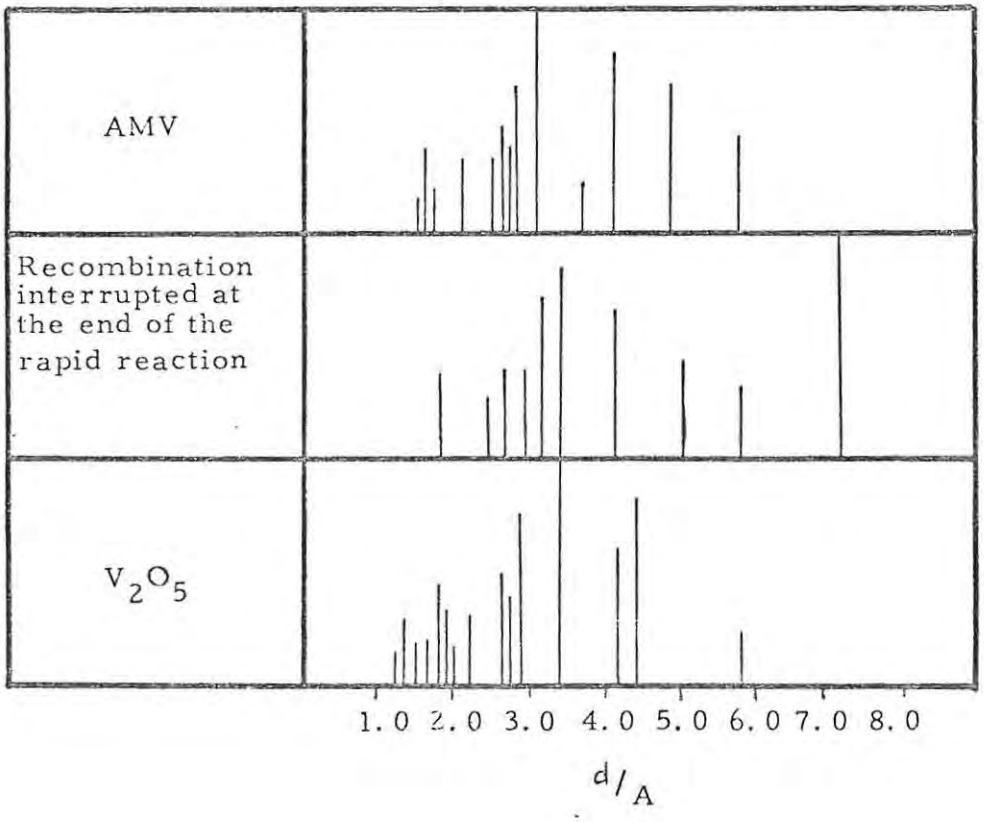

When an excess of H_2O was preadsorbed onto the V_2O_5 ($1\frac{1}{2}$ times the stoichiometric amount of H_2O required for complete recombination) and then dry NH_3 at one atmosphere pressure admitted, rapid reaction occurred until 1 mole of NH_3 per mole of V_2O_5 had reacted with the V_2O_5 and water. Further reaction with another mole of NH_3 to form AMV is slow.

Thus when preadsorption of H_2O is followed by the admission of dry NH_3 to the system, the course of the reaction appears to be:

$$V_2O_5 + H_2O \longrightarrow V_2O_5 \cdot H_2O \xrightarrow[\text{rapid}]{+NH_3} V_2O_5 \cdot H_2O \cdot NH_3$$

$$\xrightarrow[\text{slow}]{+NH_3} 2NH_4VO_3 \qquad 4.11$$

Adsorption of an equimolar quantity of water onto the surface of the V_2O_5 product of the decomposition in air, (surface are = $5.26 m^2 g^{-1}$) would correspond to the formation of approximately 30 layers (calculated by considering the water molecules to be spheres each with an effective radius[124] equal to 1.31×10^{-10} m).

4. 2. 6 The Effect of Surface Area on the Recombination Reaction

Single crystals of V_2O_5, grown from the melt, did not react with damp ammonia over several hours. When crushed, the finely powdered fragments showed signs, under the microscope, of reaction on the damaged surface. Grinding in a vibrating ball mill gave a sample similar in reactivity to the commercial sample of V_2O_5. The rate constant for recombination were 1.14 and $1.18 \times 10^{-2} min^{-1}$ respectively.

TABLE 4. 19

The Effect of Pre-adsorption of the Stoichiometric Proportion of Water Indicated on the Rate Constant for Recombination

Composition of the gas admitted after preadsorption		Rate constants for recombination after preadsorption of the stoichiometrically calculated proportions of water indicated ($min^{-1}.10^{-2}$)						
P_{NH_3} / mmHg	P_{H_2O} / mmHg	No H_2O	$\frac{1}{2}H_2O$		$^3/_4$ H_2O		1 H_2O	
		k_1	k_1	k_2	k_1	k_2	k_1	k_2
70	70	1. 90	1. 96	-	-	-	1. 30	-
70	< 0. 1	0. 10	0. 27	0. 020	0. 23	0. 026	0. 25	0. 014
720	< 0. 1	1. 30	50. 0	0. 19	-	-	50. 0	0. 14

k_1 refers to rapid process)
) - Both are for diffusion controlled reaction
k_2 refers to slow process)

The V_2O_5 product of the decomposition in vacuum has a surface area approximately five times that of the product formed in air (25.9 and 5.26 $m^2\ g^{-1}$ respectively, see section 4. 1. 9) but because of the difference in structural order of these materials the effect of surface area alone could not be assessed. The rate of recombination, under the same conditions, is however found in general to be greater for the material with the larger surface area.

4. 2. 7 Sealed Tube Experiments

When AMV is heated in an evacuated sealed tube to 210°C, followed by cooling, the product is recombined AMV of a light grey-brown colour. A temperature of 210°C in vacuum would lead to complete decomposition of AMV to V_2O_5 (Table 4. 11), but in the tube used, complete decomposition of the AMV present would result in a total pressure of about 3 atmospheres of ammonia and water vapour. From the results for the decomposition in damp ammonia (1 atmosphere) (Table 4. 11), only the first stage of the decomposition of AMV to AHV will have occurred at 210°C.

On heating to higher temperatures (300°C), the infrared spectrum of the solid product was similar to that of the product of the second stage of the decomposition of AMV in ammonia which had recombined as far as possible. i. e. partial reduction had occurred and complete recombination to AMV was no longer feasible.

The infrared spectrum of the product obtained on heating an equimolar mixture of AMV and V_2O_5 to 210°C in an evacuated sealed

tube corresponded to a mixture of AMV, AHV and V_2O_5. This shows that this treatment is equivalent to the first stage of the decomposition in ammonia, as AHV is not formed on recombination of V_2O_5. The ammonia and water released in this stage combine with the V_2O_5 to form AMV.

4. 3 Decomposition of the Recombined Material

4. 3. 1 General

Throughout this section, "normal" AMV refers to AMV before any decomposition has taken place; "recombined" AMV refers to AMV prepared by the following reaction:

$$V_2O_5 + 2NH_3 + H_2O \longrightarrow 2AMV$$

and "combined" AMV refers to AMV prepared by

$$AHV + 2NH_3 + H_2O \longrightarrow 3AMV.$$

The following results clearly show that the formation of AHV during the decomposition is the point of highest structural order reached during the reaction and once this has been destroyed by further decomposition it cannot be regained. During the decomposition in vacuum AHV is never formed and the degree of structural order is low throughout the reaction. We thus find that on decomposing "normal" AMV in vacuum to V_2O_5, recombining and decomposing the material a second time, the intermediates found are identical to those formed during the first decomposition in vacuum.

Figure 4. 33

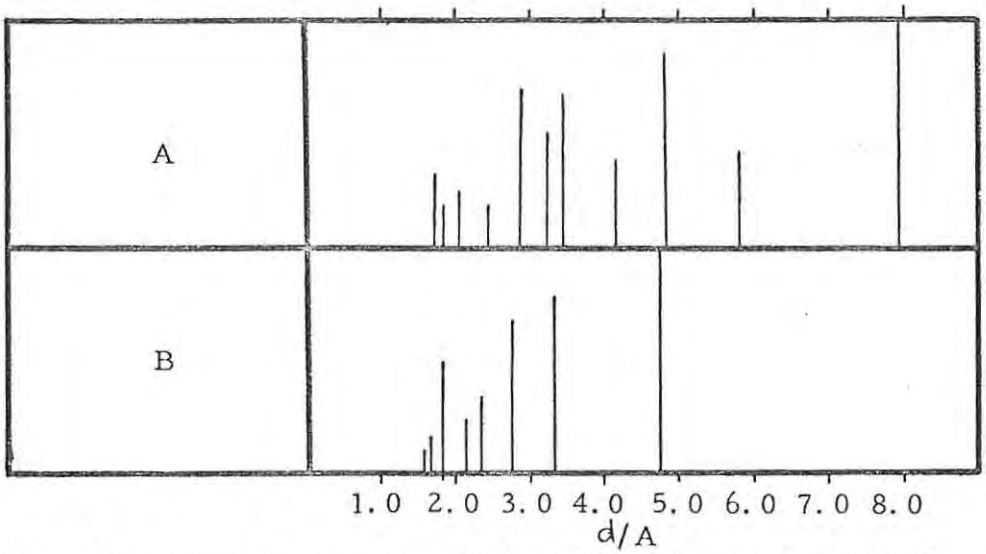

A : Intermediate formed at the end of the first stage of the decomposition of AMV in Air

B: Intermediate formed at the end of the first stage of the decomposition of "recombined" AMV in air

(i) When AMV is decomposed to V_2O_5 in air, recombined and then decomposed a second time in air, the decomposition is again found to proceed via the formation of two intermediates to a final product of V_2O_5. The mass loss involved in the formation of, and the infrared spectrum of the intermediate isolated at the end of the first stage of the decomposition of "recombined" AMV in air, are identical to those for the material isolated at the end of the first stage of the decomposition of "normal" AMV in air. The x-ray powder pattern of this material is, however, different (Figure 4.33).

(ii) Neither the mass loss nor the infrared spectrum of the intermediate formed at the end of the second stage of the decomposition of "recombined" AMV correspond to those of AHV (the product of the second stage of the decomposition of "normal" AMV in air) (Figure 4.34 spectrum A).

(iii) When the decomposition of the "recombined" AMV in air is interrupted at a mass loss of 15% (corresponding to the formation of AHV in the decomposition of "normal" AMV) then the infrared spectrum (Figure 4.34 spectrum B) shows the presence of an anomalous high frequency component at $\sim 1440cm^{-1}$ associated with the triply degenerate bending mode of the NH_4^+ ion at $\sim 1400cm^{-1}$. This is only found below a mass loss of 13% in the decomposition of "normal" AMV in air.

(iv) When the "recombined" AMV is decomposed in ammonia to the end of the first stage (14.9% mass loss) then the product formed has again a different infrared spectrum to that of AHV (Figure 4.34 spectrum C). If the successive decomposition in air is repeated then no further changes are observed in the intermediates formed.

Figure 4.34 Infrared spectra of intermediates isolated during decomposition of recombined material

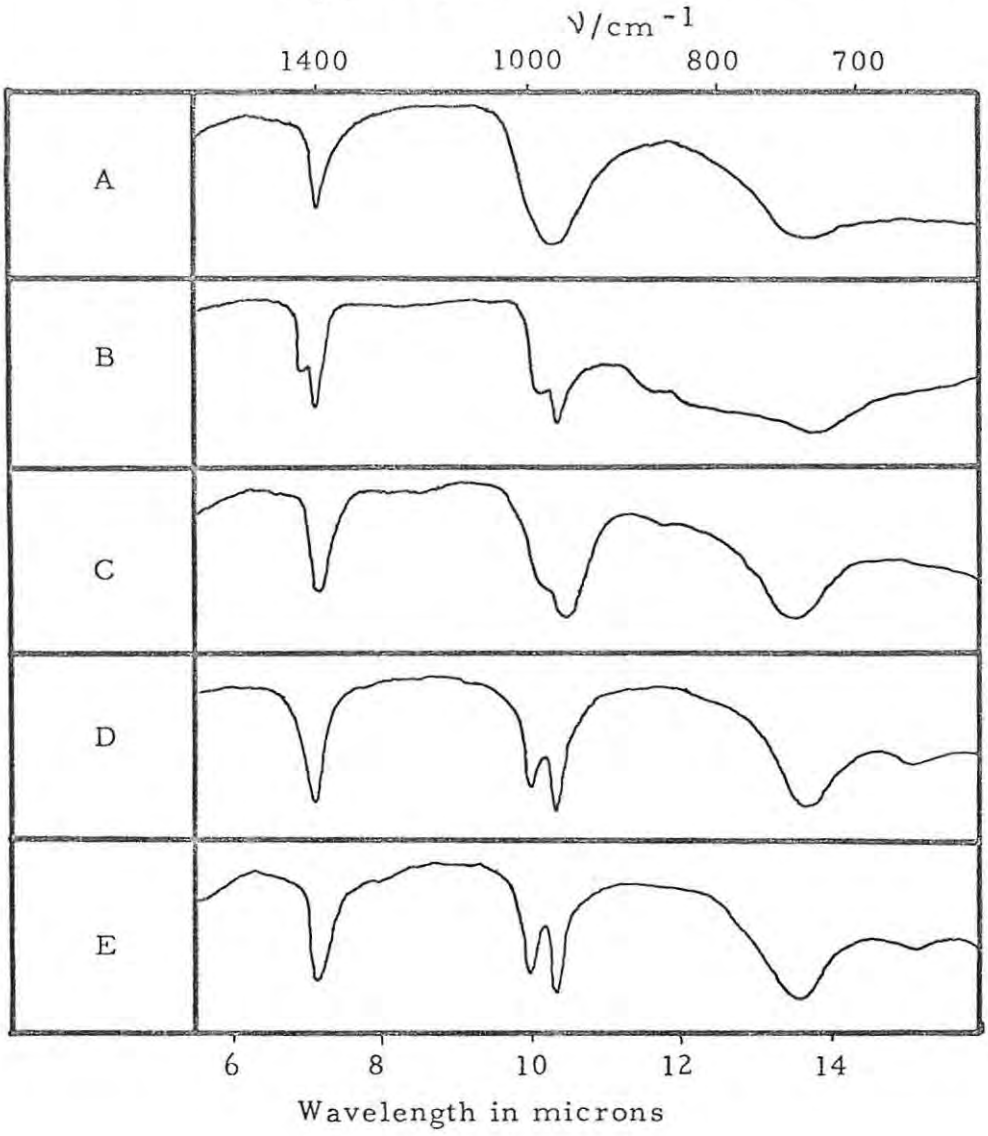

(v) If the initial decomposition is only carried out as far as the end of the second stage in air, i.e. to form AHV, (Figure 4.34 spectrum D), then on recombining to form "combined" AMV and performing the decomposition a second time, the intermediates formed are found to be identical to those formed during the decomposition of "normal" AMV (Figure 4.34 spectrum E).

4.3.2 The Effect of Repeated Recombination and Decomposition on the Rate Constant for the First Stage of the Decomposition of AMV in Air

The rate constant for the forward reaction of the first stage when AMV is decomposed in air,

$$4\ \text{AMV} \underset{\text{reverse}}{\overset{\text{forward}}{\rightleftharpoons}} \text{ABV} + 2NH_3 + H_2O$$

is increased considerably on decomposing the material obtained from the reverse reaction (Figure 4.35). On repeating the successive decomposition and recombination processes, no further increase in the rate constant was observed (Table 4.20).

TABLE 4.20

Increase of the Rate Constant of Decomposition with Successive Decomposition and Recombination of the First Stage of the Reaction in Air

	Rate constant / $(min)^{-1} \times 10^{-2}$
1st decomposition	2.53
2nd decomposition	6.06
3rd decomposition	6.08
4th decomposition	6.05

Figure 4.35 Successive Decomposition to AMV in Air at 175°C

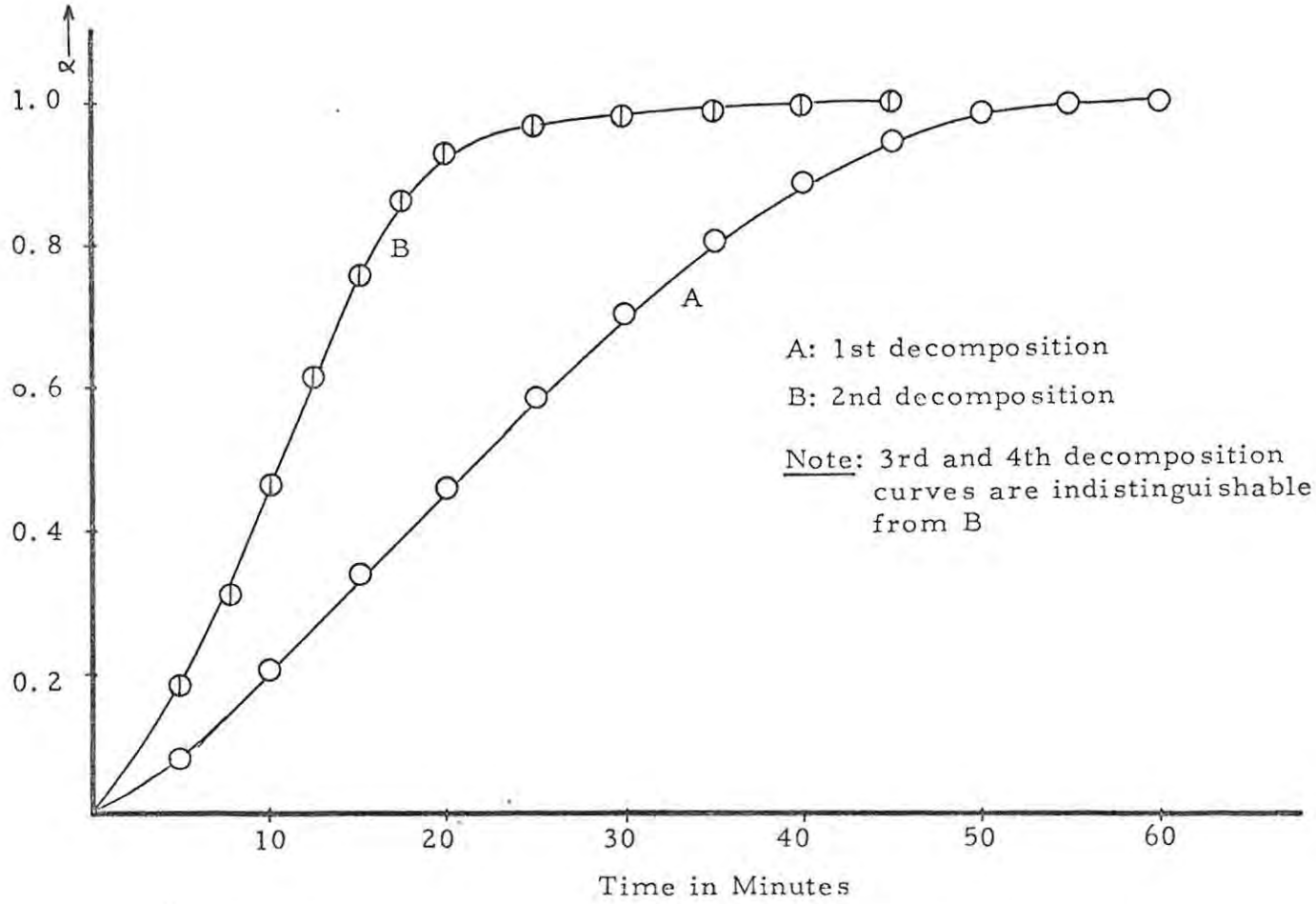

The rate constant for the recombination was, however, found to remain unchanged during the series of successive decompositions and recombinations.

4. 3. 3 Differential Enthalpic Analysis of the Recombined Material

This work was performed by Dr M. E. Brown at Queens University, Belfast using a Perkin-Elmer DSC-IB scanning calorimeter. The flow of dry N_2 was 0. 2 litres / min and the heating rate was $20^{\circ}C$/min.

The DEA thermogram of "recombined" AMV from V_2O_5 formed by the decomposition of "normal" AMV in air does not show the third endotherm C see Figure 4. 36 curve I (c. f. section 4. 1. 10). The Δ H values for the endotherms A and B and exotherm D are given in Table 4. 21 below. These values are very close to those for the decomposition of "normal" AMV. A further recombination after decomposition does not alter these values significantly although the exotherm D is diminished.

AHV prepared from solution also combines with ammonia and water vapour to give AMV. The DEA thermogram of this "combined" AMV does however show endotherm C. (Figure 4. 36 curve II)

The most noteworthy point arising from the differential enthalpic analyses of the "recombined" AMV and the "combined" AMV is thus the absence of the endotherm C in the thermogram of the former.

Figure 4.36 DEA Thermograins of "recombined" AMV and "combined" AMV in N_2

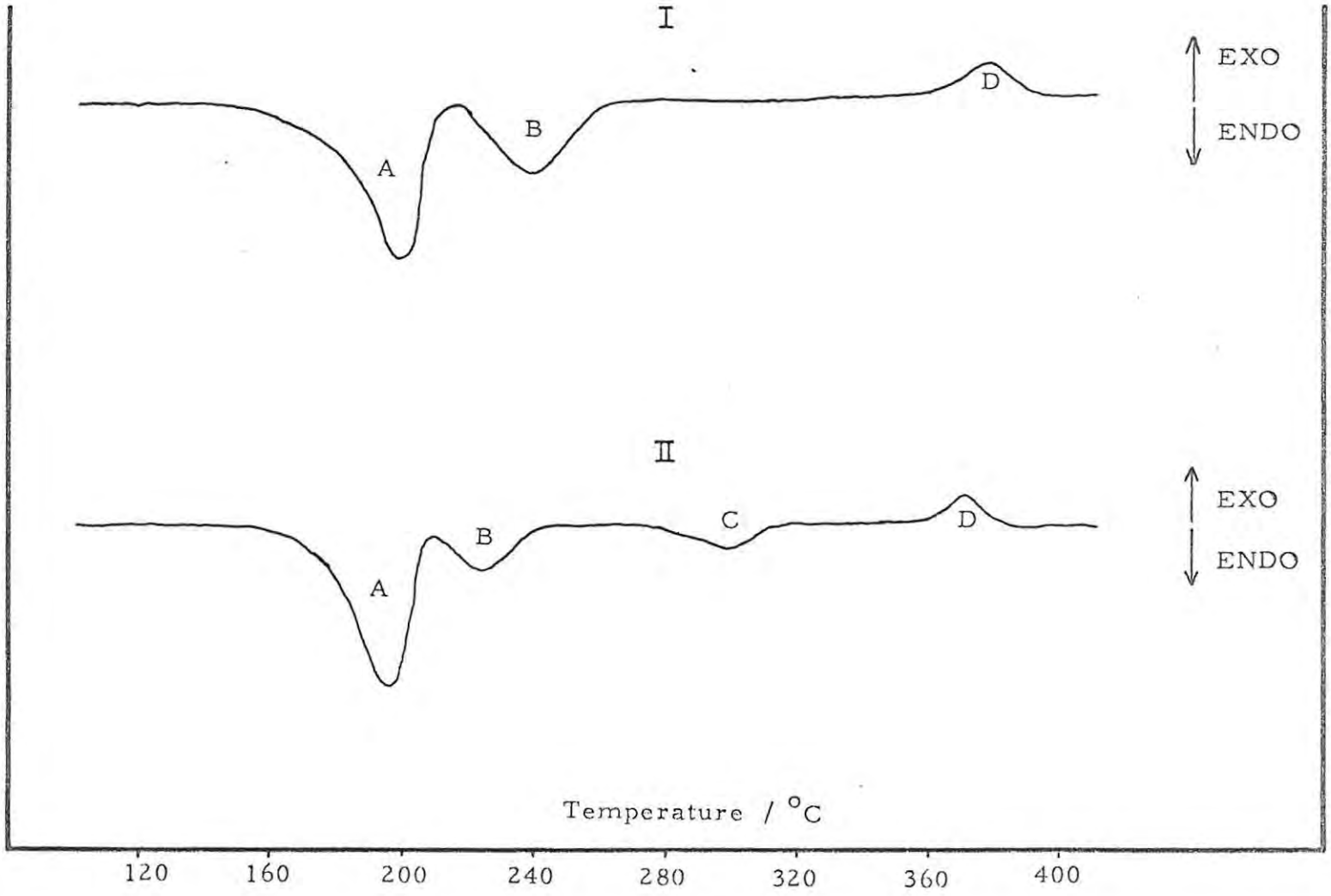

I: "Recombined" AMV

II: "Combined" AMV

TABLE 4.21

Enthalpy Changes Associated with the Stages of Decomposition of Recombined Material in N_2

($\triangle H$/kcalmol^{-1} AMV)

Sample	Endotherm				Exotherm	Total
	A	B	A + B	C	D	
"normal" AMV	12.8	5.3-9.5	17.8-22.3	0.8	-1.4	17-21.5
"combined" AMV	12.3	5.2	17.5	2.1-3.0	-1.7	18-19
"recombined" AMV	11.8	6.8	18.6	0	-1.3	17.3
"twice recombined" AMV	11.8	6.0	17.8	0	-0.8	17

4. 4 Electron Microscopy

The electron microscopy was performed by Dr M. E. Brown at Queens University, Belfast. Two replication methods were used:

(a) direct application on cellulose acetate which had been softened with acetone, and

(b) replication via a preliminary imbedding stage in Perspex heated to about 120°C.

There was very little difference in the results obtained with the two different methods of replication except that on the harder Perspex the crystallites did tend to lie flat for replication.

The electron micrographs illustrated in Plates 1-4 are:

Plate 1 - the original samples of AMV and AHV,

Plate 2 - the final products of the decomposition of AMV under low vacuum (~ 0. 1mmHg) and in nitrogen,

Plate 3 - the final products of the decomposition of AMV and AHV in air, and

Plate 4 - recombined AMV and combined AMV.

The original AMV Plate 1 consisted mainly of fairly well-formed crystallites with smooth surfaces and edges, some intergrowth and attachment and very little irregular material. The crystallites of AHV are similar in size to those of AMV but are less regular. The faces of the crystallites are generally smooth with some fine "needle" type growth and the edges are rounded.

The micrograph of the product of the decomposition in vacuum (Plate 2) shows that basically the crystalline form is retained and some faces on replication are as smooth as the original while others

PLATE 1

AMV 7100 x

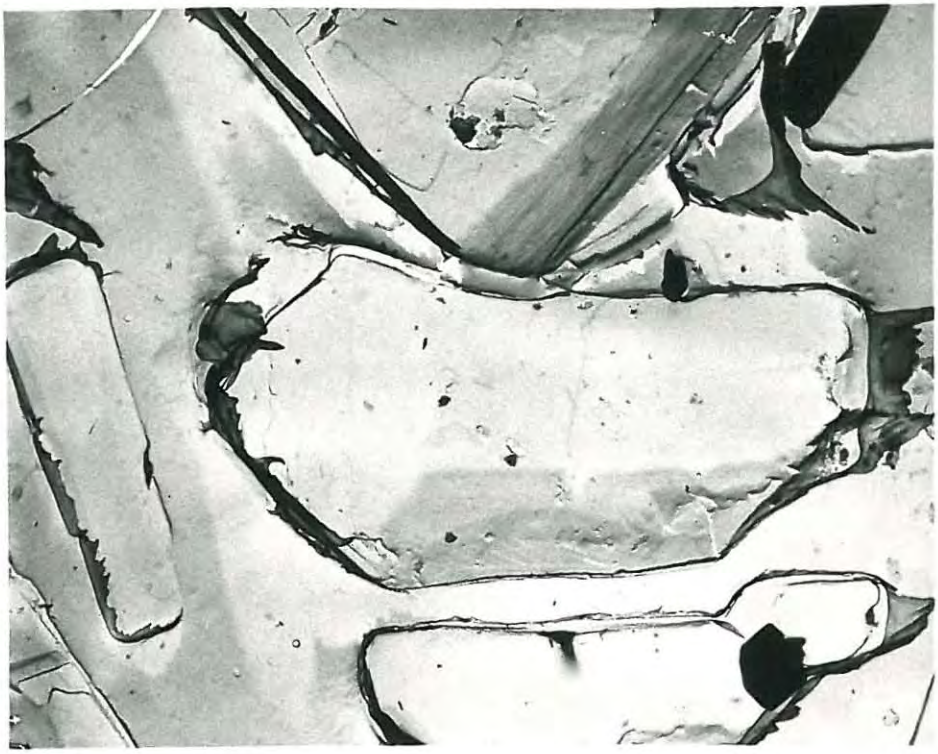

AHV 14200 x

PLATE 2

PRODUCT IN VACUUM 21300 x

PRODUCT IN NITROGEN 21300 x

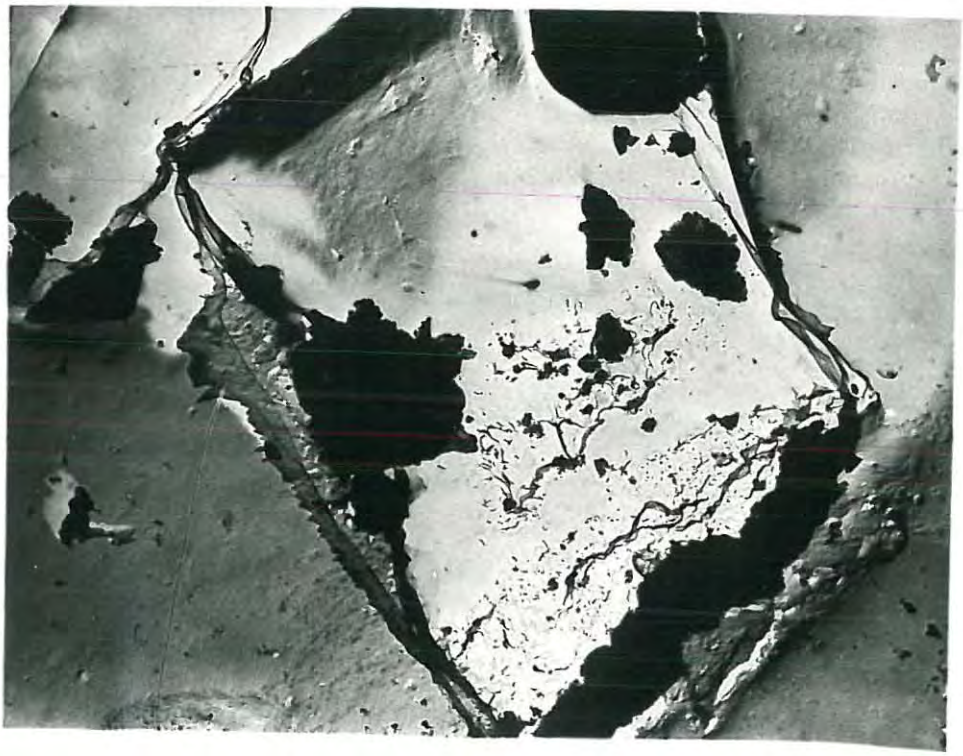

PLATE 3

AMV DECOMP. IN AIR 14200 x

AHV DECOMP. IN AIR 14200 x

PLATE 4

RECOMBINED AMV 14200 x

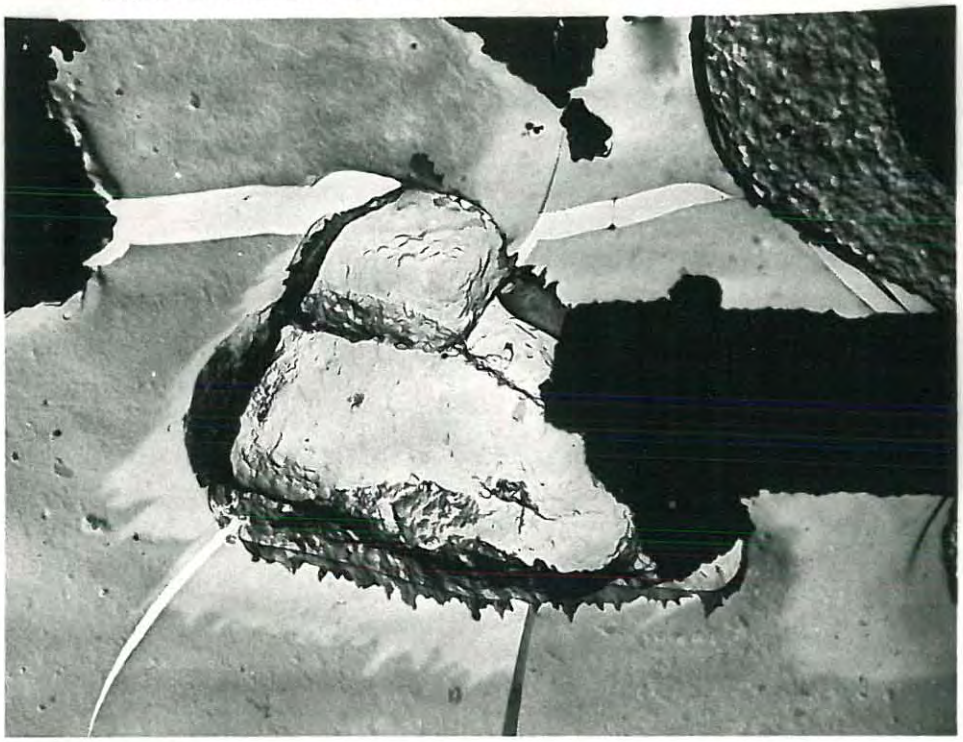

COMBINED AMV 35500 x

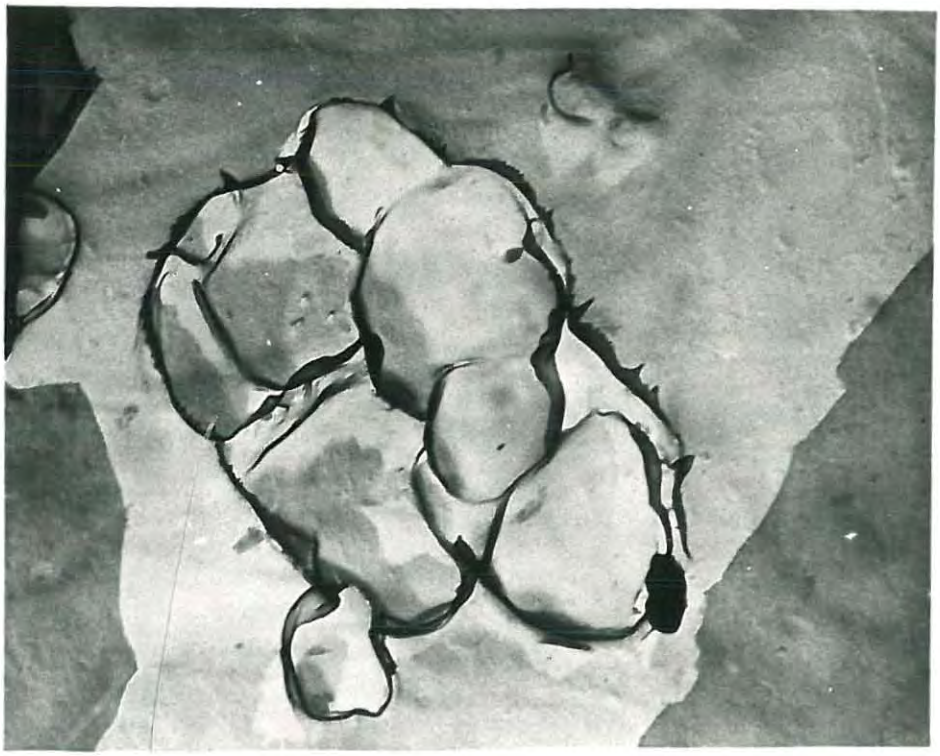

show considerable pitting. Fracture of some of the crystallites does occur (either during decomposition or during replication) and the surfaces exposed are very rough. There is also a considerable amount of material of small particle size.

The micrograph of the product formed in nitrogen (Plate 2) shows that, while some faces are again more pitted than others, the crystallites seem less susceptible to fracture.

The micrographs of the product formed on decomposing either AMV or AHV in air (Plate 3) show that the surface appears to have been etched. The crystallites are well formed and show little tendency to crumble.

The micrographs of "recombined" AMV and "combined" AMV are completely different to one another (Plate 4). Some of the crystallites of "recombined" AMV remain unshattered and have very rough surfaces, but the main tendency is to break up (either during reaction or during replication). There does not seem to have been any recrystallisation during the recombination of V_2O_5 to form AMV The particles of "combined" AMV show no direct relationship to either AMV or AHV in either shape or size. There is definitely a recrystallisation process in the recombination of AHV to form "combined" AMV. This is shown by the fact that the crystallites are intergrown with smooth surfaces and rounded edges.

The main points of interest arising from this investigation are:-

1. The product formed in vacuum appears to be more distrupted than the product formed in nitrogen, but as this was a relatively soft vacuum ($\sim$ 0. 1mmHg) the full effect of vacuum conditions on the

decomposition is unlikely to be noticeable. The product formed in air is the least disrupted of all, and the etching is definite evidence of a specific interaction of air with the surface of the material. From the micrograph of the product formed by decomposing AHV (prepared from solution) in air it is seen that this interaction certainly occurs during the third stage of the decomposition of AMV in air. Whether this interaction also occurs during the earlier stages of the decomposition cannot be verified without micrographs of the earlier intermediates, ABV and AHV.

2. It is obvious from the retention of general shape and size by the crystallites, during the decomposition and recombination that there can be no profound changes in the basic structure of the material. The removal and re-admission of gaseous products appear to be from a basically unaltered V-O framework. This is evidence that the decomposition and the recombination reactions are effectively topotactic or at least epitactic in nature.

3. The fact that the "combined" AMV is obviously recrystallised material while the "recombined" AMV is not, lends strength to the hypothesis that AHV is the point of maximum structural order reached during the decomposition and that once decomposition has proceeded beyond this point, such a degre of structural order is never regained by subsequent recombinations and decompositions.

5. DISCUSSION

5. 1 The Stoichiometry of the Decomposition

The intermediates formed during the decomposition of AMV in vacuum, argon, ammonia and air have all been characterized by means of x-ray powder diffraction photographs, infrared spectra and chemical analyses, as well as by the mass-losses involved in their formation. It is only by combining all of these techniques that it is possible to differentiate among the courses of the decompositions under the various conditions of surrounding atmosphere; the results of the above investigations permit detailed discussion of the stiochiometry of the decomposition under the various atmospheric conditions. Some of the structural changes occurring during the decomposition, illustrated by the changes in the infrared spectra and x-ray powder diffraction photographs of the sample material, will also be discussed under this heading.

5. 1. 1 Summary

The stoichiometry of the decomposition in the various atmospheres studied is:

In vacuum, $NH_4VO_3 \xrightarrow{\text{1st Stage}} NH_4V_3O_8 \xrightarrow{\text{2nd Stage}} NH_4V_4O_{10.5} \xrightarrow{\text{3rd Stage}} V_2O_5$

(disordered) (disordered) (defective)

i. e. AMV $\longrightarrow$ AHV* $\longrightarrow$ $NH_4V_4O_{10.5} \longrightarrow V_2O_5$ VAC

In inert or oxidising atmospheres

$NH_4VO_3 \xrightarrow{\text{1st Stage}} (NH_4)_2V_4O_{11} \xrightarrow{\text{2nd Stage}} NH_4V_3O_8 \xrightarrow{\text{3rd Stage}} V_2O_5$

(disordered) (ordered)

i. e. AMV $\longrightarrow$ ABV $\longrightarrow$ AHV $\longrightarrow$ V_2O_5 INERT

In ammonia, $NH_4VO_3 \xrightarrow{\text{1st Stage}} NH_4V_3O_8 \xrightarrow{\text{2nd Stage}} NH_4V_6O_{15} \xrightarrow{\text{3rd Stage}} VO_2$

(ordered) (ordered)

i. e. AMV $\longrightarrow$ AHV $\longrightarrow$ $NH_4V_6O_{15} \longrightarrow VO_2$

Each stage of the decomposition in non-reducing atmospheres is accompanied by the evolution of ammonia and water in the molecular ratio 2:1.

5. 1. 2 The Formation and Decomposition of Ammonium Bivanadate (ABV)

ABV is the product of the first stage of the decomposition of AMV in both inert and oxidising atmospheres,

$$4NH_4VO_3 \longrightarrow (NH_4)_2V_4O_{11} + 2NH_3 + H_2O$$

or

$$4AMV \longrightarrow ABV + 2NH_3 + H_2O$$

The infrared spectrum of ABV (figure 4. 10) is seen to include a satellite NH_4^+ band near 1440cm^{-1}. This satellite band has been shown (Section 1. 4. 4) to have its origin in the loss in degeneracy of the asymmetrical bending mode of the NH_4^+ ion near 1400cm^{-1}, and can be interpreted as indicating a disordered, non-degenerate structure in terms of the NH_4^+ ion arrangement. This interpretation of the presence of the satellite band will be used throughout the discussion and the use of the term "disordered" when referring to the structure of any of the intermediates will mean that the structure is disordered with respect to the NH_4^+ ion arrangement.

The satellite band is only detected in the infrared spectrum near the end of the first stage in inert or in oxidising atmospheres, when $\alpha > 0.75$. Further decomposition of the bivanadate (ABV) in inert or in oxidising atmospheres first leads to the formation of ammonium hexavanadate, AHV (see below). When ABV is decomposed in vacuum, however, a single stage at about 180°C occurs with the formation of a form of V_2O_5 which is shown to be highly defective, by the broadness of the bands in the infrared spectrum and by the absence of the strong reflections at $d = 4.21$ Å and $d = 3.15$ Å which are present in the x-ray powder diffraction photograph of a commercial sample of V_2O_5 (Hopkins and Williams).

5. 1. 2. 1 The Formation of Ammonium Hexavanadate (AHV) from ABV

The formation of AHV from ABV forms the second stage of the decomposition in inert and in oxidising atmospheres, with the stoichiometry:

$$3(NH_4)V_4O_{11} \longrightarrow 4NH_4V_3O_8 + 2NH_3 + H_2O$$

or $$3ABV \longrightarrow 4AHV + 2NH_3 + H_2O$$

The satellite band near $1440cm^{-1}$ in the infrared spectrum cannot be detected after about the halfway mark for this stage ($\alpha > 0.5$). The hexavanadate is thus not disordered in terms of the NH_4^+ ion arrangement. The AHV intermediate is seen to be structurally identical to AHV prepared from solution[91] by their infrared spectra and x-ray powder patterns.

5. 1. 3 The Formation of AHV-type Intermediates Directly from AMV

AHV-type intermediates are formed at the end of the first stage in vacuum,

$$3NH_4VO_3 \longrightarrow NH_4V_3O_8 + 2NH_3 + H_2O$$

or $$3AMV \longrightarrow AHV^* + 2NH_3 + H_2O$$

and in ammonia

$$3\ AMV \longrightarrow AHV + 2NH_3 + H_2O$$

AHV^* is shown by its infrared spectrum and x-ray powder pattern to be structurally different to AHV and is disordered (as shown by the presence of the sattelite NH_4^+ band at $1440cm^{-1}$), but AHV^* is structurally similar to ABV according to these same criteria.

The satellite NH_4^+ band at about $1440cm^{-1}$ and hence a disordered structure in terms of the NH_4^+ ion arrangement is not detected during the decomposition in ammonia if, for a sample of about 12 mg, the partial

pressure of ammonia in the atmosphere surrounding the sample exceeds about 300 mmHg. This is clearly ssen from figure 4.19. This formation of AHV without the prior formation of a disordered structure has also been reported [78] to occur during the decomposition of AMV in nitrogen and in air when large samples (> 200 mg), a rapid heating rate and a slow flow of carrier gas are used during the thermogravimetric analysis.

5.1.4 The Further Decomposition of the Two Types of Intermediate, AHV* and AHV

The further decomposition of the two types of intermediate, AHV* and AHV, takes place in considerably different stages reflecting their different structures. When the decomposition of AHV* is continued in air, two stages are detected: at about 220°C, decomposition to a total mass loss of 19.6% occurs and the final stage to V_2O_5 takes place at about 300°C. AHV, however, decomposes in a single stage in air to form V_2O_5 (see below). If AHV* is decomposed further in ammonia then three further stages in the decomposition are found. First, an intermediate with an infrared spectrum identical to that of AHV is formed (mass loss 16.9% empirical formula $NH_4V_4O_{10.5}$) at about 220°C, after which the decomposition proceeds via identical intermediates to those formed at the ends of the second and third stages in ammonia (see below). It thus appears that under sufficient ammonia pressure an ordering process can occur.

When the decomposition of AHV* is continued in vacuum, two stages are detected: at 135-160°C decomposition to a total mass loss of 16.9 - 17.2% occurs, with the formation of the disordered intermediate

$NH_4V_4O_{10.5}$. Further decomposition in the range 165-200°C leads to the formation of a highly defective form of V_2O_5 (as seen from the infrared spectrum and x-ray powder pattern). The x-ray powder photographs of the products of the first and second stages in vacuum (AHV* and $NH_4V_4O_{10.5}$) are very similar (figure 4.1), and this, together with the constancy of the V-O bands in the infrared spectra figure 4.2, suggests that the changes during decomposition in vacuum are occurring within a basically unaltered V-O framework.

5.1.5 The Formation of V_2O_5 from AHV

Further decomposition of AHV, in any of the atmospheres studied, leads directly to V_2O_5. The relative defectiveness of the final product is dependent upon the conditions of the surrounding atmosphere used during its formation. This will be discussed further below.

$$2NH_4V_3O_8 \longrightarrow 3V_2O_5 + 2NH_3 + H_2O$$

or

$$2\,AHV \longrightarrow 3V_2O_5 + 2NH_3 + H_2O$$

In addition to forming the third stage in inert and in oxidising atmospheres, this reaction may also be studied by decomposing AHV in vacuum although it is not formed in the vacuum decomposition of AMV. It may also be studied directly in the single stage of the decomposition of the AHV material prepared from solution. The AHV* intermediate formed as the product of the first stage in vacuum, however, decomposes further, in vacuum and in atmospheres of air and argon, in two stages.

The relative defectiveness of the final V_2O_5 product as shown by the x-ray powder diffraction patterns and infrared spectra is very dependent on the conditions of atmosphere that surrounded the AHV starting

material during the decomposition (see section 4.1). The V_2O_5 formed in air ($V_2O_5{}_{AIR}$) is the least defective, and the V_2O_5 formed under conditions of hard vacuum ($V_2O_5{}_{VAC}$) is the most defective, while the V_2O_5 formed in inert atmospheres ($V_2O_5{}_{INERT}$) is intermediate between the two in its degree of defectiveness.

These differences in the final products formed are clearly shown by the relative structural changes which occur on annealing in vacuum or in air.

(i) $V_2O_5{}_{VAC}$. When $V_2O_5{}_{VAC}$ is annealed in <u>air</u> at 360°C for two hours the defectiveness is removed, although no mass loss occurs; the infrared spectrum and x-ray powder pattern of the annealed sample are identical to those of $V_2O_5{}_{AIR}$.

When $V_2O_5{}_{VAC}$ is annealed in <u>vacuum</u> at 550°C for 30 minutes then x-ray powder pattern and infrared spectrum are again changed, also with no mass loss (figures 4.5 and 4.6 respectively). The changes are most noticeable in the infrared spectrum of the vacuum annealed $V_2O_5{}_{VAC}$ where the band at 825cm^{-1}, assigned[100] to the stretching modes of the longer V-O bonds in the V-O-V net plane in the standard spectrum of V_2O_5, has been replaced by a large number of bands. This implies that the structural changes occurring during the annealing of $V_2O_5{}_{VAC}$ in vacuum are likely to involve the fracture of at least some of the V-O-V cross-linkages which occur in V_2O_5. If this material is now further annealed in either inert or oxidising atmospheres at 550° C then the defectiveness is entirely removed and the infrared spectrum and x-ray powder diffraction pattern are again identical to those of $V_2O_5{}_{AIR}$.

(ii) $V_2O_{5_{INERT}}$. Annealing $V_2O_{5_{INERT}}$ in air at 360°C or in vacuum at 550°C results merely in removing the defectiveness of the structure with no accompanying mass loss and without the appearance of the large number of bands found in (i) above.

(iii) $V_2O_{5_{AIR}}$. Annealing $V_2O_{5_{AIR}}$ in air or vacuum at high temperatures has no effect on either the infrared spectrum or on the x-ray powder diffraction pattern of the sample.

The relative defectiveness of the V_2O_5 samples formed in vacuum and in inert or oxidising atmospheres is also shown by the electron micrographs of the samples (Plates 2 and 3, Section 4.4). The tendecny to crumble and the degree of disruption of the material is seen to be greatest for the $V_2O_{5_{VAC}}$ and least for $V_2O_{5_{AIR}}$. The brittleness and degree of disruption of $V_2O_{5_{INERT}}$ lies between these two.

5.1.6 The Further Stages of the Decomposition of AHV in Ammonia

Further decomposition in ammonia of the AHV intermediate involves partial reduction of the sample and formation of VO_2 as the product at the end of the third stage. AHV thus decomposes in ammonia in the temperature range 280-300°C to form $NH_4V_6O_{15}$ (total mass loss 19.9%). The third stage of the decomposition to VO_2 (total mass loss 28.4-28.6%) occurs in the temperature range 340-360°C. That partial reduction of the sample has occurred during the second and third stages of the decomposition in ammonia is clear since complete recombination of the products formed at the ends of these stages with Ammonia and water, to reform AMV, is no longer possible.

5. 1. 7 AHV - The Highest Point of Structural Order Reached During the Decomposition

The point in the decomposition at which AHV is formed is clearly shown by the results in section 4. 3 to be the point of maximum structural order (relative to the NH_4^+ ion) reached in the decomposition of AMV to form V_2O_5. Once decomposition has proceeded beyond this point, such a degree of order cannot be regained during a second decomposition, after recombination with ammonia and water vapour.

AHV is, however, never isolated during the decompostion in vacuum. It is thus found (section 4. 3. 1), on recombining $V_2O_{5_{VAC}}$ with ammonia and water vapour and decomposing the "recombined" AMV so formed in vacuum once more, that the intermediates isolated during this second decomposition are identical to those formed during the first decomposition.

5. 2 The Kinetics and Mechanism of the Decomposition Reaction

The results of the kinetic studies have been reported in sections according to the nature of the surrounding atmosphere. In discussing the significance of these results, however, valid detailed comparisons of kinetic behaviour can only be made for reactions involving similar reactants and products. Some general trends are, however, apparent.

The inhibiting effect of a gaseous atmosphere on the decomposition, which has been shown to be endothermic and reversible, is evident from the fact that decomposition in vacuum, where gaseous products are continuously removed, commences at a measurable rate some $50^{\circ}C$ below the temperature required for the decomposition in the various gases.

The shape of the isothermal α -time curves is also altered from "Type I" for all stages in vacuum, to "Type II" for all stages in gaseous atmospheres (except for the third stage of the decomposition in oxidising atmospheres, for which the curves are "Type III").

The contracting sphere equation (equation 4. 1), which applies over the complete "Type I" curve and over the deceleratory region of the "Type II" and "Type III" curves, is based on the model[26] of a narrow size-range of approximately spherical (or cubic) particles which decompose by initial rapid coverage of the surface with product, followed by progression of the reactant product interface inwards at constant rate towards the centre of the particle. With continuous rapid removal of gaseous products it appears that this model is closely obeyed as the movement of the reactant/intermediate I interface is followed by a similar process for the intermediate I/intermediate II interface and so on, with little overlap of the stages. The surface area accessible to krypton increases dramatically during decomposition in vacuum from the original AMV (0. 36 $m^2 g^{-1}$) to AHV* (18. 6 $m^2 g^{-1}$) to V_2O_5 (26 $m^2 g^{-1}$) showing that there will be little resistance to removal of the gaseous products through the solid products infrared and x-ray data confirm the disordered nature of these intermediates.

When the removal of gaseous products is impeded by the presence of a surrounding atmosphere the decomposition follows a different course, via more structurally - ordered solid intermediates. The "Type II" α -time curves obtained for all stages in gaseous atmospheres, except the third stage of the decomposition in oxidising atmospheres, comprises an initial approximately linear region and a deceleratory or decay region. The extent of the linear region depends on the conditions of surrounding atmosphere under which the decomposition is performed, being greater the higher the pressure of NH_3 surrounding the sample.

Two interpretations of this linear region are possible. One[125] is that it has its origin in initial decomposition along dislocation lines into the crystallites. The other is that it has its origin in the effect of the ordering or re-crystallisation process on the rate of evolution of the gaseous products. The latter explanation is not acceptable in the light of the present results since this would require an ordering or re-crystallisation process to occur during each stage of the decomposition, under all except hard vacuum conditions. Since this would be an exothermic process it would be entirely different to the decomposition process, which is endothermic, and the activation energy for this process would not be expected to be the same as the activation energy for the decay region of the Type II curves which is what is observed. It would also modify the values of the enthalpies of reaction for the various stages of the decomposition and it will be shown in section 5.2.2.3 that this modification only definitely occurs during the third stage of the decomposition in inert or oxidising atmospheres.

It will be shown in section 5.2.1, however, that an adaptation of the former explanation (decomposition along dislocation lines) is consistent with the experimental observations.

The activation energies for the various regions of each of the stages in each of the atmospheres studied have been obtained from the temperature dependence of the relevant rate constants. It is noticeable that, for any particular stage with a "Type II" curve, the activation energies calculated from the temperature variation of the rate constants of the linear (k') and the contrasting sphere ($k=\frac{k''}{a}$) regions are the same, within experimental error.

Self-cooling is often a problem in studying the kinetics of endothermic decompositions, but the small samples used (12mg) and the resulting

reasonable linearity of the Arrhenius plots obtained show that any self-cooling effect is not marked.

The enthalpies of reaction have been determined for each of the stages of the decomposition in inert and in oxidising atmospheres, by differential enthalpic analysis. This investigation has permitted the calculation of the enthalpies of formation of the intermediates formed during the decomposition in inert and in oxidising atmospheres.

5. 2. 1 The Mechanism of the First Stage of the Decomposition, from the Kinetic Point of View

The mechanism of only the first stage of the decomposition under the various conditions of surrounding atmosphere

i. e. vacuum	AMV $\longrightarrow$ AHV*
oxidising or inert atmospheres	AMV $\longrightarrow$ ABV
ammonia	AMV $\longrightarrow$ AHV

will be discussed below, since it is only for the first stage of the decomposition that a common starting-point occurs, in that the sample material is identical in all atmospheres at the commencement of the stage.

It can be seen from the electron microscopic investigation (section 4. 4) that even at the end of the third stage of the decomposition the external shape of the crystallites has been maintained, although the surface area has increased by a factor of at least ten (section 4. 1. 5. 6). This implies that there must be pores and/or channels into the material created during the decomposition reaction. It must be noted that the

increase in surface area is greatest during the decomposition in vacuum.

It can be seen from Table 4.11 that the apparent activation energies for both the linear and deceleratory regions of the Type II curves are always equal, although the rate constant k' for the linear region is always greater than k ($=\frac{k''}{a}$), the rate constant for the deceleratory region, for any one curve. It is also seen that the apparent activation energies for the first stage of the decomposition in vacuum (30.8 kcal mol^{-1}), N_2 (30.9 kcal mol^{-1}), $N_2 + H_2O$ (32.1 kcal mol^{-1}) Ar (31.8 kcal mol^{-1}) and NH_3 (33 kcal mol^{-1}), are identical within the limits of experimental error. The activation energy for the first stage of the decomposition is much greater in air (53.4 kcal mol^{-1}). When the removal of evolved product gases is facilitated, and the atmosphere is dried, the activation energy in oxidising atmospheres is lowered (Air 42.0 kcal mol^{-1}, O_2 41.8 kcal mol^{-1}) but it is still greater than $E^{\neq}_{ammonia}$ (where $E^{\neq}$ represents the activation energy).

These results suggest that the rate determining step is the same for the first stage of the decomposition in vacuum, inert atmospheres and ammonia but is different for the decomposition in oxidising atmospheres.

The existence of an initial linear region in the α/time curve for the decomposition of solids has previously been explained[125] as being caused by initial decomposition along dislocation lines (of which there must be many in a microcrystalline powder, such as the sample material used during the present investigation), which must result either in the production of pores and channels into the crystallites or in the fracture of the crystallites. It was found in the present investigation that during the decomposition in vacuum (where the evolution of the product gases is not hindered, and NH_3 and H_2O are evolved simultaneously[84] in the molecular ratio 2:1), the linear region was absent altogether, while

during the decomposition in Ar, N_2 and N_2+H_2O it extended to $\alpha = 0.50 \mp 0.10$. During the decomposition in ammonia, however, the linear region extended right to $\alpha = 0.75 \mp 0.10$. From this it is clear that it is the hinderance of the evolution of NH_3 which influences the extent of the linear region and not the hinderance of the evolution of H_2O, which is consistent with the information from $E^{\neq}$.

The rate controlling process is probably the same for both the linear and the contracting sphere regions since the activation energy is the same for both regions. The frequency, A, in the Arrhenius equation will however, be different for each of the regions and from the values of the relative first-order rate constants for the linear and contracting sphere regions it is seen that the frequency factor is always greater for the linear region (see Table 5.1 below).

The rate determining step for both the linear and contracting sphere regions of the decomposition in non-oxidising atmospheres is thus the evolution of ammonia.

The mechanism of the first stage of the decomposition in non-oxidising atmospheres, from the kinetic viewpoint, is expected to be as follows. Initial decomposition on the surface of the crystallites and along dislocation lines creates pores into the material, with the diffusion of NH_3 and H_2O to the internal surfaces of these pores. Once the pressure of NH_3 in these pores and channels has risen to such a point that decomposition via the formation of further pores is no longer more rapid than evolution of the product gases from the external surface of the crystallites(during the decomposition in ammonia or inert atmospheres) or when the material is so porous that there is no difference between the evolution of the product gases via these pores and the

evolution across the product layer formed on the external surface of the crystallites (the decomposition in vacuum) then the product-reactant interface advances inwards into the remaining undecomposed material of the particles, and the contracting sphere equation applies. The reason for having differing explanations for the termination of the linear region of the kinetic curve in inert atmospheres or in ammonia, and in vacuum is that the surface area increases most during the decomposition in vacuum and the linear region, if present at all, is found only for $\alpha < 0.10$. The crystallites thus break up at the beginning of the decompositon reaction in vacuum, since the removal of the evolved gases from the region around the sample is rapid. This disruption of the sample material at the beginning of the decomposition has also been observed by Deschanvres and Nouet[84] in their study of the decomposition of larger crystals in vacuum.

The same general mechanism applies to the decomposition in oxidising atmospheres as that discussed above for non-vacuum conditions since the α/time curves are again Type II curves and the intermediates formed at the end of the first stage of the decomposition in oxidising and in inert atmospheres is the same i.e. ABV. The rate determining process must, however, be different since the activation energy for the first stage of the decomposition in oxidising atmospheres (53.4 kcalmol^{-1}) is much greater than that for the decomposition in non-oxidising atmospheres (maximum value of 33 kcal mol^{-1}). When the removal of the evolved product gases is facilitated and the atmosphere surrounding the sample (air or oxygen) is dried then the activation energy is lowered (42 kcal mol^{-1}) from its high value, but is still higher than when NH_3 evolution is rate-determining. The values for A, the frequency factor, are also much greater for the first stage of the decomposition in pre-dried oxidising

atmospheres ($\sim 10^{21}$ sec^{-1}) than for the decomposition in non-oxidising atmospheres ($\sim 10^{16}$ sec^{-1}) while the frequency factor is greatest for the decomposition in undried air ($\sim 10^{26}$ sec^{-1}). This suggests that the evolution of H_2O is the rate determining process in oxidising atmospheres. The value of 42 kcal mol^{-1} obtained for the activation energy for the first stage of the decomposition in dry oxidising atmospheres is thus the activation energy for the evolution of H_2O via the pores and cracks created during the linear region, and across the product layer formed on the external and internal surfaces for the contracting sphere region.

The ability of the oxygen atoms in the V_2O_5 lattice to exchange with gaseous oxygen and with water is well known [126] and is responsible for the catalytic activity of V_2O_5 in oxidation. It must be an interaction of this type which is preventing the escape of the ammonia and which thus forces the rate determining process to change from the evolution of NH_3 to the evolution of H_2O.

In general, the strong interaction between the solid decomposition product and atmospheric oxygen could

(i) hinder the removal of gaseous products

or (ii) facilitate the crystallisation or ordering process resulting in a more stable product, which in turn has a higher activation energy for its further decomposition

or (iii) alter the nature of the activated complex involved in the decomposition stage (see later).

The activation energy for the evolution of H_2O might be expected to be higher than the activation energy for the evolution of NH_3, since the formation of H_2O requires the fracture of strong V-O bonds whereas the generation of NH_3 merely requires the fracture of hydrogen bonds.

5. 2. 2 The Thermodynamics of the Decompositon

5. 2. 2. 1 The First Stage of the Decompositon

The decomposition is assumed to be a homogeneous, unimolecular process. It is thus valid to use the following relationships[127]

$$k' = \frac{ekT}{h} \cdot e^{\Delta S^{\ddagger}/R} \cdot e^{-E_{exp}/RT} \qquad 5.1$$

$$k' = A^{-E_{exp}/RT} \qquad 5.2$$

(where k' is the rate constant in sec^{-1} for the decomposition at temperature T) to calculate values for the entropy of activation ($\Delta S^{\ddagger}$) and the frequency factor (A) using the experimentally determined activation energies. Values of A and $\Delta S^{\ddagger}$ for the first stage of the decompositon are given in Table 5. 1.

TABLE 5. 1

Values of the Frequency Factor and Entropy of Activation for the First Stage of the Decomposition under the Various Conditons of Atmosphere

Atmosphere	A/sec^{-1}		$\Delta S^{\ddagger}/cal\ K^{-1}mol^{-1}$
	linear region	contracting sphere region	contracting sphere region
Vacuum	-	44.7×10^{15}	15. 8
Ar	21.5×10^{15}	13.7×10^{15}	13. 5
N_2	10.9×10^{15}	6.7×10^{15}	12. 0
$N_2 + H_2O$	14.9×10^{15}	10.2×10^{15}	12. 9
NH_3	8.2×10^{15}	1.1×10^{15}	8. 5
O_2	1.3×10^{21}	1.0×10^{21}	35. 6
Air	1.8×10^{21}	1.2×10^{21}	36. 1
undried Air	12.4×10^{25}	6.8×10^{25}	57. 7

If the first stage of the decompositon in vacuum, N_2, $N_2 + H_2O$, Ar, and NH_3, for which it has been shown that the mechanism and rate determining step are identical in each atmosphere, are considered then it is noticeable that the ΔS^* values decrease in the order

$$\text{Vacuum} > A_r \approx N_2 + H_2O \approx N_2 > NH_3$$

If the relative order of the intermediates formed at the end of the first stage of the decomposition with respect to the ammonium ion arrangement (from infrared spectra) isnow considered it is seen that the relative order increases.

$$\text{Vacuum} < A_r \approx N_2 + H_2O \approx N_2 < NH_3$$

These trends are as would be expected from the hypothesis drawn in Section 5. 2. 1 that the rate determining step for the first stage of the decomposition in these atmospheres is the evolution of ammonia.

5. 2. 2. 2 The Formation of V_2O_5 from AHV

It has been found that AHV, in addition to being one of the intermediates formed during the decomposition in both inert and oxidising atmospheres, can be prepared from solution[91]. The decompositon of AHV_{INERT}, AHV_{AIR} and AHV_{SOLN}, each in vacuum, argon and air were thus investigated.

The activation energies and hence the frequency factors and entropies of activation were calculated in each case, as before, for the contracting sphere region of the curves. The values of these parameters are given in Table 5. 2.

TABLE 5.2 : Activation energies, frequency factors and entropies of activation for the decomposition of each of the AHV's in each of the atmospheres

Sample	Atmosphere	$E^{\neq}/kcalmol^{-1}$	A/sec^{-1}	$\Delta S^{\neq}/calK^{-1}mol^{-1}$
AHV_{SOLN}	Vacuum	28.6	5.3×10^{9}	-15.9
	Argon	45.4	5.2×10^{15}	11.4
	Air	34.6	1.7×10^{11}	- 9.0
AHV_{AIR}	Vacuum	28.2	1.9×10^{10}	-13.4
	Argon	36.5	5.1×10^{11}	- 6.9
	Air	34.2	1.8×10^{13}	0.2
AHV_{INERT}	Vacuum	15.6	6.2×10^{4}	-38
	Argon	28.6	9.8×10^{11}	-5.5
	Air	22.0	1.7×10^{11}	-9.0

In the first instance, only the decomposition of the AHV's in argon and in vacuum will be considered since it has been seen from the electron microscopy investigation (Plate 3 Section 4.4) and from the shape of the kinetic curves that the decompostion in air involves some strong interaction between the oxygen in the air and the surface of the material. It has been shown by other workers[126] that V_2O_5 readily exchanges its oxygen atoms with those in the surrounding atmosphere at these temperatures (280-300°C) and it must be this interaction which alters the decomposition process in air. The decomposition process in vacuum and argon are, however, assumed to be the same, with the evolution of the product gases being hindered in argon and not in vacuum.

The relative values of the activation energies for the decomposition of the AHV's in argon, vacuum and air are illustrated in figure 5.1.

The following explanation is an attempt to rationalise these values and their relationship to one another, but it must be borne in mind that other explanations are possible and, without more data, a definitive mechanism for the decomposition of AHV and a positive explanation of these values is not possible.

The AHV and AHV_{AIR} may be considered to have had the same oxidising pretreatment, i.e. previous interaction of the surface with the solution in the one case and with the air in the other case. The AHV_{INERT}, on the other hand, has undergone no such interaction in its formation. If this pretreatment and consequently the state of the surface of the material has a strong influence on the decomposition process in vacuum then it would explain why the activation energies for the decomposition of AHV_{SOLN} and AHV_{AIR} in vacuum are similar and greater than the activation energy for the decomposition of AHV_{INERT} in vacuum.

The decomposition in argon, on the other hand, must depend more on the relative physical nature of the AHV's than on the pretreatment since, in this case, the activation energy for the decomposition of AHV_{SOLN} (surface area = 1.30 m^2g^{-1}) is greater than the activation energy for the decomposition of AHV_{AIR} (Surface area = 3.82 m^2g^{-1}). This dependence must be linked to the fact that the evolution of the product gases during the decomposition is hindered in argon and not at all hindered during the decomposition in vacuum.

It is seen from Table 5.2 that the relative values of the entropies of activation for each of the AHV's are less for the decomposition in

Figure 5. 1 Activation energies of the decomposition of the AHV intermediates in argon, vacuum and air

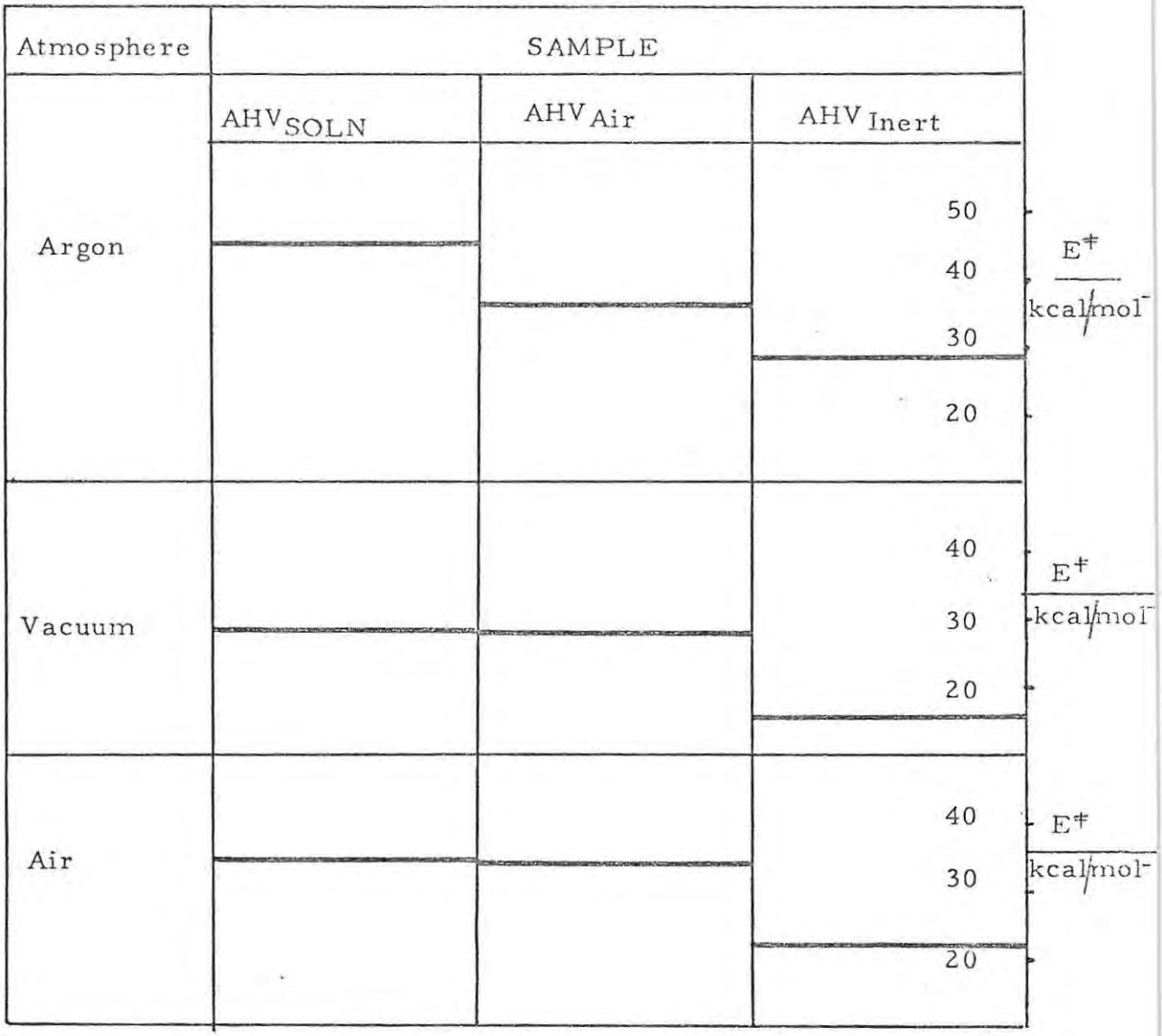

vacuum than for the decomposition in argon. It has been assumed above that the decomposition processes in argon and in vacuum are essentially the same. However, the trend in the $\Delta S^{\neq}$ values suggests that the activation process is different, viz., that the activation process in vacuum is a concerted process and so slower that the activation process in argon.

The decomposition of each of the AHV's in air has been shown, by the shape of the kinetic curves (Type III) and the electron micrographs (Plate 3 Section 4.4), to proceed through an entirely different process to the decomposition in either argon or vacuum. It is thus not possible to compare the activation energy or entropy of activation valves for the decomposition in air with those for the decomposition in either argon or vacuum. It is seen from Table 5.2, however, that the activation energies for the decomposition of AHV_{SOLN} and AHV_{AIR} are equivalent (within the limits of experimental error) and are greater than the activation energy for the decomposition of AHV_{ARGON} in air. It will be assumed that the above explanation for the relative values of the activation energy for the decomposition of the various AHV's in vacuum and in argon is also true for the decomposition in air. It is clear on the basis of this assumption that the rate determining process for the decomposition of the various AHV's in air is also dependent on the oxidising pretreatment or lack of it that the AHV's have undergone.

5.2.2.3 The Application of Absolute Reaction Rate Theory to the Decomposition of AMV in inert atmospheres

Some of the difficulties encountered in the application of absolute

reaction rate theory (ARRT) to reactions in solids have been discussed by Shannon.[128] A basic assumption of ARRT is that the whole reaction consists of the repetition of a fundamental unit step wherein a small number of atoms or molecules form a new configuration via an intermediate of higher energy than the initial or final states. There is a critical configuration which must be attained if the final state is to be reached and the energy required to form this configuration is supplied by a local fluctuation in the thermal energy of the assembly. In solids the energy increase should be treated as a temporary local concentration of phonons, caused by interference of wave packets, and the theory requires that the lifetime of the transition state should be long in comparison with the time of thermal relaxation in the lattice. It is doubtful if this is so. The reactants thus necessarily interact with all the other atoms, molecules or ions present in forming the activation complex and the approximation involved is thus that of treating a many-body problem as a single-body problem. Such treatments have, however, proved fairly successful.

The experimental activation energy for a decomposition stage then may be assumed to refer to a "mole" of activated complex for that particular stage. The enthalpies of reaction, however, determined from DEA (Section 4. 1. 10) and related by infrared data to particular stages, are measured with respect to the sample mass and thus have to be suitably scaled for inclusion on a potential energy diagram.

i. e. $E^{\neq}$ represents an activation energy in kcal/mol of <u>activated complex</u>

ΔH represents an enthalpy change in kcal/mol of <u>starting material</u>

and $\frac{E^{\neq}}{\Delta H} = n$, the number of moles of starting material needed for the formation of 1 mole of activated complex, where n

is some integer such that n . Δ H does not exceed $E^{\ddagger}$ and will be assumed to be the largest such integer.

It is convenient in this section to write the formula for the starting material (AMV) in the form $(NH_4)_2$ O. V_2O_5 since emphasis will be placed on the concept of "$(NH_4)_2$ O units" (i. e. $2NH_3 + H_2O$) and "V_2O_5 units" (note that $(NH_4)_2O\ V_2O_5 = 2NH_4VO_3 = 2AMV$).

For the first stage of the decomposition in inert atmospheres, ΔH is 26 kcal/mol $(NH_4)_2\ OV_2O_5$ and $E^{\ddagger}$ is 32 kcal mol^{-1}. The value of the integer n is thus one and the formula of the activated complex is $(NH_4)_2O.\ V_2O_5$.

ΔH for the second stage of the decomposition, although variable, is approximately half that of the first stage (say 12 kcal/mol$(NH_4)_2\ OV_2O_5$) while the activation energy $E^{\ddagger}$ for the second stage (26 kcal mol^{-1}) is only slightly less than for the first stage. The value of n is thus two and two moles of starting material ($2(NH_4)_2$ O V_2O_5) are needed for the formation of the activated complex. It is known from the discussion of the stoichiometry of the reaction that NH_3 and H_2O are evolved in the ratio of 2:1 in every stage of the reaction i. e. there is a gradual reduction in the ratio of "$(NH_4)_2$ O" to V_2O_5 units from the original 1:1 ratio in AMV to pure V_2O_5. It is thus not unreasonable to assume that the activated complex for each stage will contain one "$(NH_4)_2$ O unit" and this will, in any event represent the empirical composition of the activated complex. The formula for the activated complex for the second stage of the decomposition is thus taken to be $(NH_4)_2$ O. $2V_2O_5$ (or ABV).

The Δ H value for the third stage of the decomposition is very small (~ 2. 0 kcal/mol $(NH_4)_2$ O. V_2O_5), while $E^{\ddagger}$ remains at approximately at the same level as before. The low Δ H value for the third stage of

the decomposition is proposed to be the resultant of concurrent exothermic and endothermic processes, the exotherm(s) possibly arising from some form of recrystallisation. It would thus not be valid to calculate n from this value of ΔH. The values of ΔH of 16-18 kcal/mol $(NH_4)_2 O\ V_2O_5$ and the activation energy (45 kcal mol^{-1}) obtained for the decomposition of AHV_{SOLN} in inert atmospheres have thus been used to calculate the formula of the activated complex for the third stage. It is seen that n = 3 and, if the activated complex is again assumed to contain one "$(NH_4)_2$ O unit", then the formula of the activated complex is $(NH_4)_2$ O. $3V_2O_5$ (or AHV).

The enthalpy change accompanying the decomposition reaction in inert atmospheres is thus approximately 8 kcal/mol $(NH_4)_2O$ and the total energy barrier to be surmounted is of the order of 40-50 kcal. The reaction scheme for the formation of one mole of V_2O_5 is thus

$$2AMV \longrightarrow 2AMV' \longrightarrow \tfrac{1}{2}ABV \longrightarrow \tfrac{1}{2}ABV' \longrightarrow \tfrac{2}{3}AHV \longrightarrow \tfrac{2}{3}AHV' \longrightarrow V_2O_5$$

where the superscript indicates the activated complex. In order to illustrate this reaction scheme by means of a potential energy diagram, the experimental values of both the activation energy and the enthalpy of reaction must be adjusted to refer to one mole of V_2O_5. The potential energy curve for the formation of one mole of V_2O_5 by the decomposition of AMV in inert atmospheres is given below.

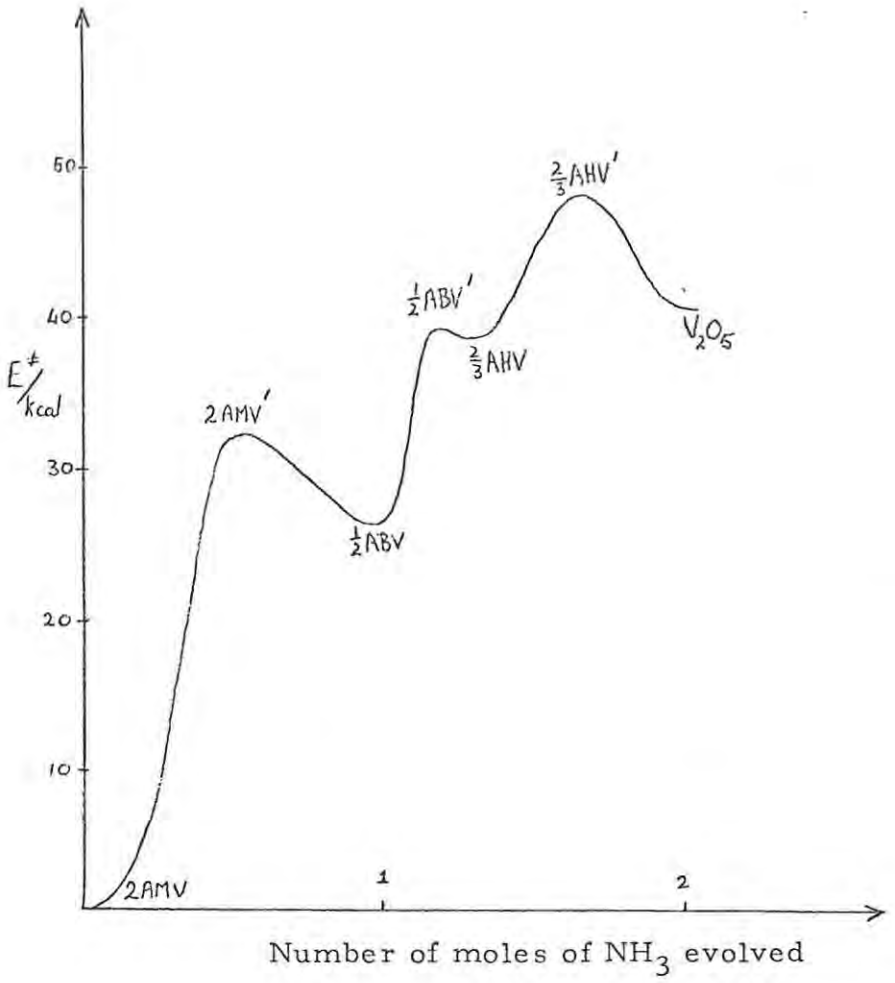

5. 2. 3 The Mechanism of the Decomposition from the Molecular Point of View

The first stage of the thermal decomposition of AMV is ammonia,

$$3NH_4VO_3 \longrightarrow NH_4V_3O_8 + 2NH_3 + H_2O \qquad 5.3$$

has been chosen from the present work to examine in detail in respect of the atomic movements since it is a reversible process, without complete disruption of the structure. The possibility of this analysis hinges on the fact that the crystal structures of both reactant and product materials is known.

Legend for Figure 5.2

Figure 5.2 is an illustration of the crystal structure of AMV viewed in the direction


V atoms in forward chain


V atoms in the rear chain


O atoms in the forward chain


O atoms in the rear chain


N atoms in front of the forward V-O chain


N atoms behind the forward V-O chain


N atoms in front of the rear V-O chain


N atoms behind the rear V-O chain

Figure 5.2

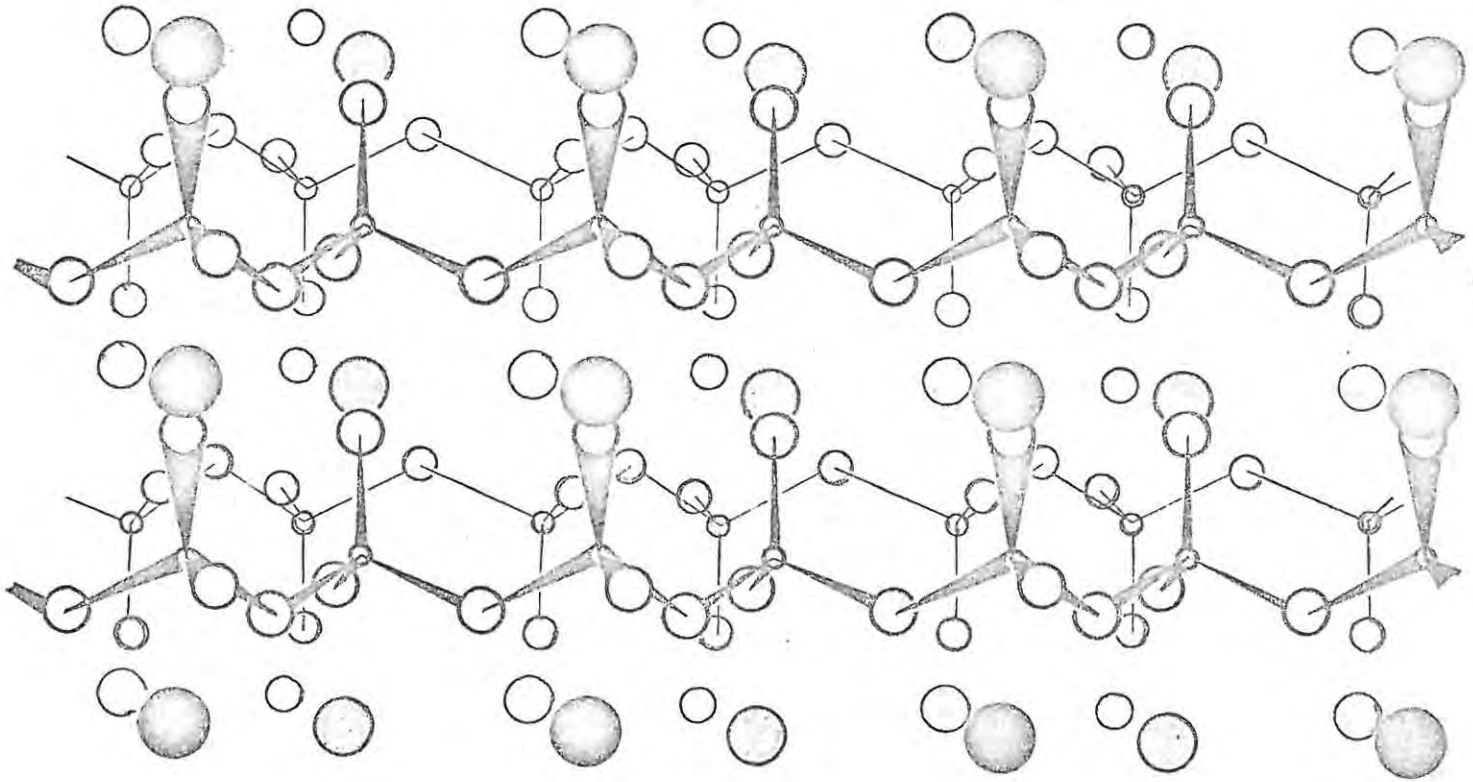

Legend for Figure 5.3

Figure 5.3 is an illustration of the crystal structure of AHV viewed in the a direction

V atoms

Forward O atoms

Rear O atoms

Forward N atoms

Rear N atoms

Figure 5.3

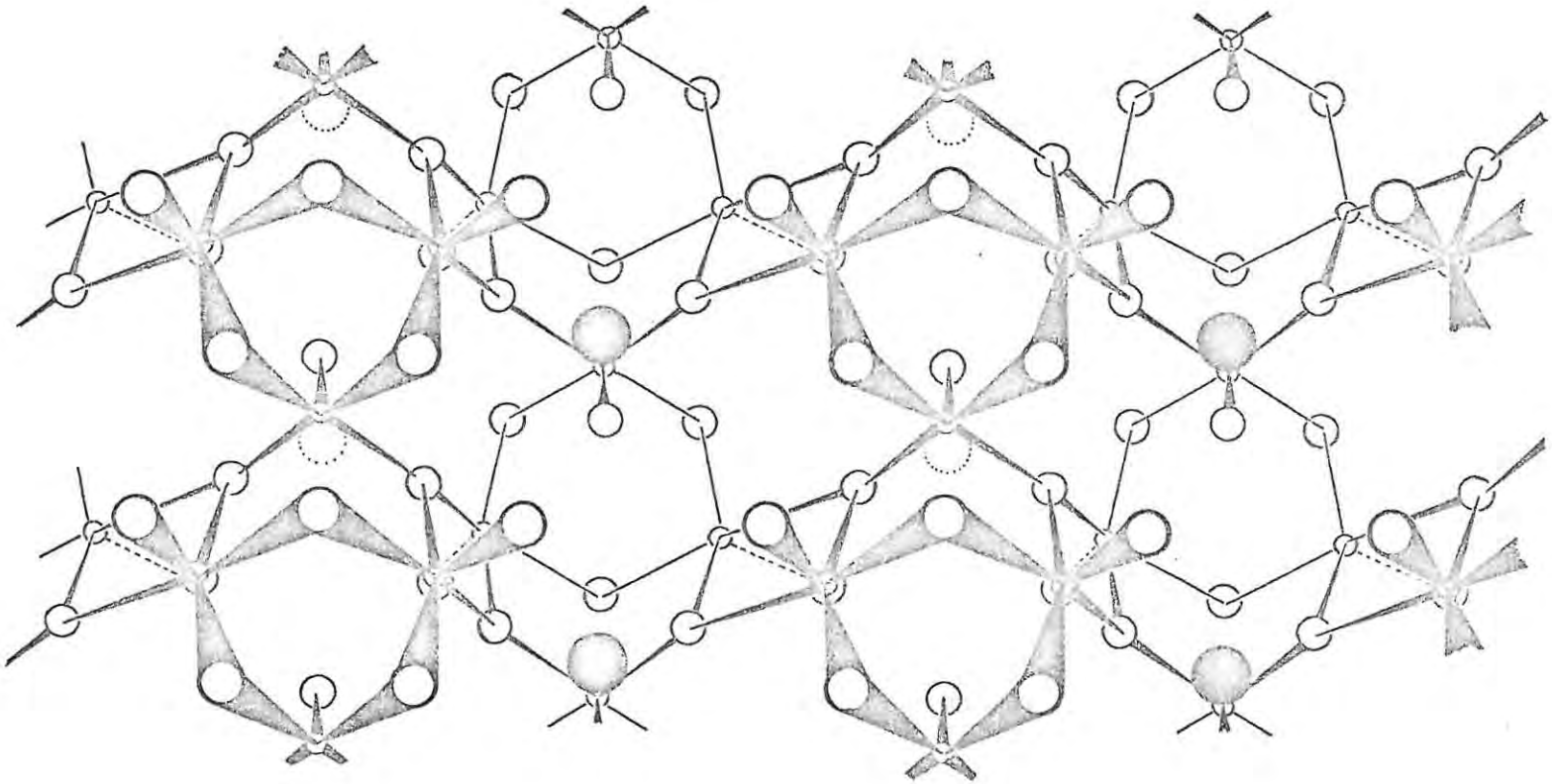

The crystal structures of AMV and AHV are illustrated in Figures 5.2 and 5.3 respectively. These structures have already been discussed in some detail in section 1.4.2 and it will suffice here merely to delineate the major features of each structure.

(i) AMV, Figure 5.2, consists of zig-zag chains of tetrahedra of oxygen about vanadium, linked by their corners and stretching in the 'a' direction.

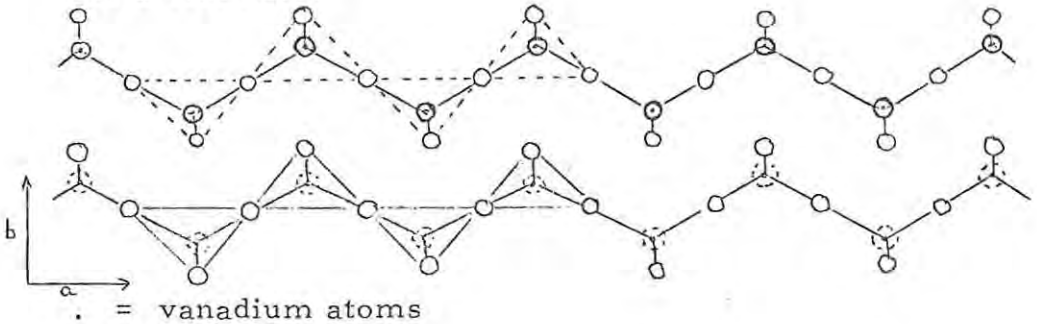

. = vanadium atoms

o = oxygen atoms

It is seen from Figure 5.2 that the apices of the tetrahedra in any one chain point in the same direction and that the apices of the tetrahedra in neighbouring chains in the 'b' direction are pointing in directions opposite to one another.

(ii) AHV, Figure 5.3, consists of square pyramids of oxygen about vanadium joined by corners and edges to form sheets stretching in the 'b' and 'c' directions; (Only the basic outline of the sheets is given)

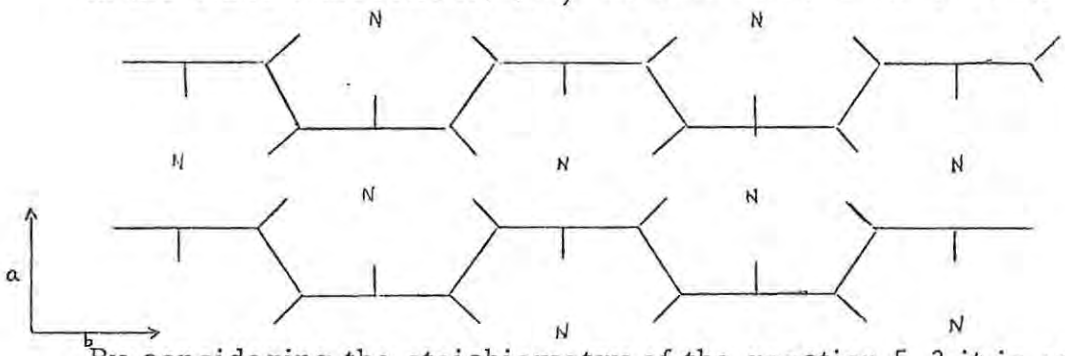

By considering the stoichiometry of the reaction 5.3 it is seen that the tetrahedral chains of the AMV must break into units comprising three vanadium and eight oxygen atoms each, as shown in Figure 5.4.

Legend for Figure 5.4

Figure 5.4 is an illustration of how the tetrahedral chains of AMV break up during the decomposition in ammonia

V atoms in the forward chain

V atoms in the rear chain

O atoms in the forward chain

O atoms in the rear chain

N atoms in front of the forward V-O chain

N atoms behind the forward V-O chain

N atoms in front of the rear V-O chain

N atoms behind the rear V-O chain

Figure 5.4

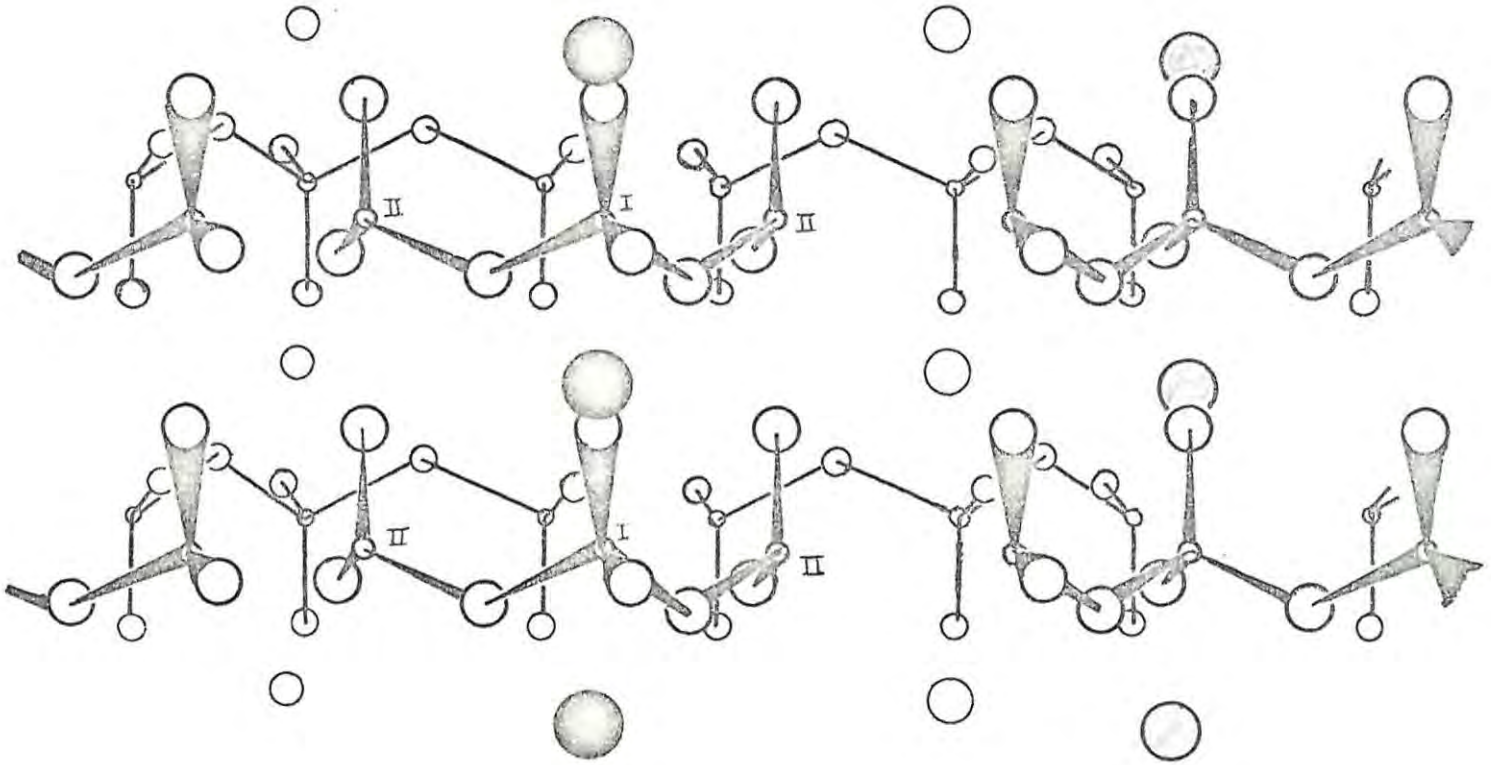

This fracture of the chains is accompanied by the evolution of two moles of ammonia and one of water for every three moles of AMV. On this basis, a detailed mechanism is proposed. The relative positions at which the neighbouring chains are chosed to break is arbitrary and the positions for fracture shown in Figure 5.4 were chosen simply to facilitate the rearrangement to form AHV, with the minimum amount of atomic movement. For this to occur, the fracture of the chains must be assumed to be a co-operative process. It is felt that this assumption is reasonable since it would be energetically favourable for the decomposition and subsequent rearrangement to involve the least possible atomic movement consistent with the change in structure.

Each of these V_3O_8 units rotates (about an imaginary axis joining the two terminal vanadium atoms (V_{II})) in the opposite direction to that in which the apices of the tetrahedra point through either 135^o or 45^o alternately. This rotation is followed by a contraction in the 'a' and 'b' directions resulting in the orientation of these units shown in Figure 5.5.

The orientation is followed by the cross linking of these units to form AHV.

ABV is formed during the first stage of the decomposition in oxidising or inert atmospheres according to the reaction.

$$4NH_4VO_3 \rightleftharpoons (NH_4)_2V_4O_{11} + 2NH_3 + H_2O \qquad 5.4$$

$$4AMV \rightleftharpoons ABV + 2NH_3 + H_2O$$

i.e. the evolution of two moles of ammonia and one of water for every four moles of AMV.

The detailed crystal structure of ABV has not, to the author's knowledge, been determined but it is seen from the infrared spectrum of the material that the arrangement of the surroundings about the

Legend for Figure 5. 5

Figure 5. 5 illustrates the arrangement of the (V_3O_8) units prior to cross linkage to form AHV

V atoms

Forward O atoms

Rear O atoms

Forward N atoms

Rear N atoms

Figure 5.5

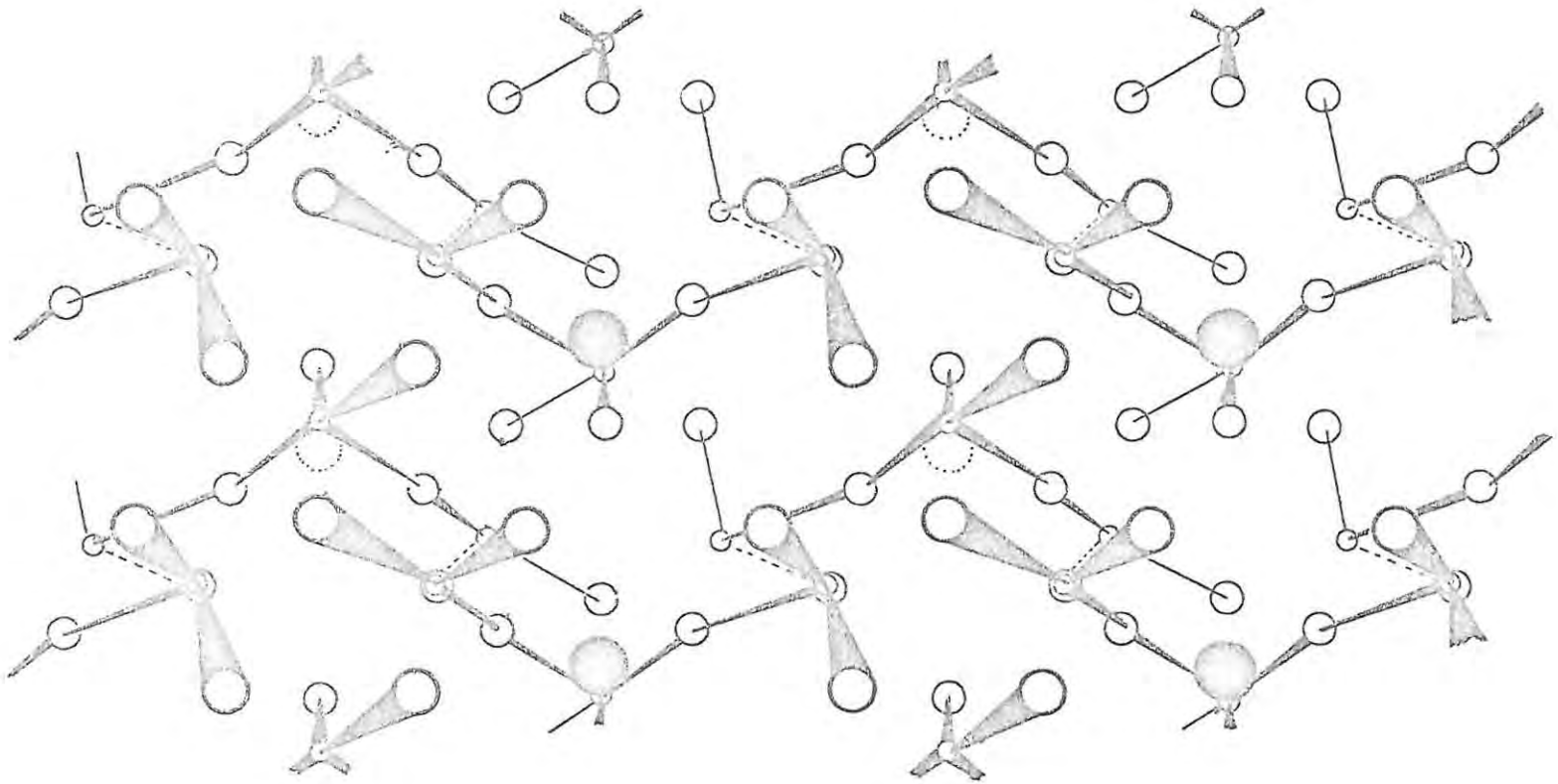

NH_4^+ ion must be asymmetrical in order to result in the loss of degeneracy of the asymmetrical bending mode of the NH_4^+ ion at about 1400 cm^{-1}. It is also known from the present work that the intermediate formed at the end of the first stage of the decomposition in vacuum (AHV^*), although having the same empirical formula as AHV, is structurally similar to ABV. Since further decomposition of ABV in inert or oxidising atmospheres results in the formation of AHV,

$$3(NH_4)_2V_4O_{11} \longrightarrow NH_4V_3O_8 + 2NH_3 + H_2O \qquad 5.5$$

$$3ABV \longrightarrow 4AHV + 2NH_3 + H_2O$$

it is felt that the structure of ABV must be intermediate between that of AMV and AHV.

Lamure and Colin[78] have found that ABV is relatively much more soluble in water than are AMV, AHV or V_2O_5. This suggests that the structure of ABV is unlikely to consist of infinite groups of vanadium and oxygen atoms but rather of discrete ionic $n(V_4O_{11})^{2-}$ units, where n is some integer. There is also a strong possibility, from a consideration of the stoichiometry of reaction 5.5, that n is 3 or some multiple of 3.

It does not seem possible to predict a definite structure for ABV, merely from consideration of the above factors, and all that is really clear is that the decompositon of AMV to form ABV must be essentially a "bond-breaking" process, while further decomposition of ABV to form AHV must be essentially a "bond-making" process.

5.3 The Kinetics and Mechanism of the Recombination Reaction

In order to facilitate the discussion of the recombination reaction

$$V_2O_{5(s)} + 2NH_{3(g)} + H_2O_{(g)} \longrightarrow 2NH_4VO_{3(s)} \qquad 5.6$$

$$V_2O_5 + 2NH_3 + H_2O \longrightarrow 2AMV$$

the following points arising from the results should be noted.

(i) The fact that the α'-time curves for the recombination can be analysed by application of the parabolic law (equation 4.10) implies that the reaction is controlled by the diffusion of some species into the V_2O_5 rather than by the advancement of the product-reactant interface.

(ii) Both ammonia and water are needed for the reaction to occur, but the water must be adsorbed before the ammonia can react, since it is seen (section 4.2.3) that dry ammonia neither reacts with nor is adsorbed onto V_2O_5.

(iii) If the stoichiometric amount of water required for the reaction is adsorbed onto the surface of the V_2O_5 (product of the decomposition in air) then this would correspond to ca. 30 layers of water molecules. This, together with the fact that more water than the stoichiometrically required amount can be adsorbed, leads to the conclusion that the water must be diffusing into the V_2O_5.

(iv) It is seen from the results of section 4.2.4 that preadsorption of the stoichiometric amount of H_2O required for recombination onto the V_2O_5, followed by reaction with NH_3, results in an initial rapid reaction until the amount of NH_3 reacted is such that the mole ratio in the sample of $V_2O_5 : H_2O : NH_3$ is about 1 : 1 : 1. This is followed by a slower reaction until AMV is formed. It is thus likely that the recombination reaction progresses via the formation of an "active" complex in which the mole ratio of $V_2O_5 : H_2O : NH_3$ is about 1:1:1. This is supported by the results of section 4.2.3 where it was found that, over a wide range of combined pressures, the rate constant for recombination is a maximum for a ratio of $P_{NH_3} : P_{H_2O}$ in the

atmosphere surrounding the sample of approximately 1 : 1, when p_{H_2O} is not very low.

(v) From Figure 4. 30 it can be seen that the time required for the adsorption of the amount of water stoichiometrically required for reaction 5. 6 is greater than the time required for complete recombination to AMV using damp ammonia.

(vi) The temperature dependence of the rates of recombination of samples of V_2O_5 (Figure 4. 27) shows that the surface area of the material and/or the relative order of the structure play a major part in determining the rate of recombination.

(vii) The roughness of the surface and the tendency to crumble of the "recombined" AMV (Plate 4, section 4. 3) which, unlike the "combined" AMV, has not undergone a definite recrystallisation process, suggests that when the V_2O_5 is recombined with damp ammonia some strain, possibly resulting in cracks, is introduced into the material.

The overall mechanism of the recombination reaction, derived by consideration of the above points together with the detailed results in Chapter 4, is that (i) the adsorption and (ii) diffusion of H_2O into the V_2O_5 followed by (iii) the formation of the "active" complex $V_2O_5.H_2O.NH_3$ are the rate determining steps of the reaction.

If Figure 4. 27 curve A is considered, it is seen that the rate constant for recombination passes through a maximum with increasing temperature and then decreases. At low temperatures and high p_{H_2O} the rate determining step is thus (ii) above. The low activation energy of 2-4 kcal mol^{-1} for the process at low temperatures is in keeping with this.

As the temperature is raised in the range 15-60°C the rate begins to be controlled by the desorption of H_2O. This is shown by the similarity of Curve E (temperature dependence of the rate of desorption of water from V_2O_5) to the last part of Curve A.

Since the sample material (V_2O_5 formed in vacuum) used for the determination of Curve B in Figure 4.27 has a much smaller particle size and a relatively disordered structure, diffusion of water in the lattice is rapid and the desorption of water from the material becomes the rate controlling factor at much lower temperatures than for curve A. Thus temperature, structural order and particle size all influence the rate of recombination, and various curves are possible. The influence of p_{NH_3} on the position of the curve is shown by curve D. The influence of p_{H_2O} on the curve is more marked. When relatively dry ammonia is used for the recombination it would be expected, on the basis of the above mechanism, that diffusion of water would remain dominant to higher temperatures, although the activation energy for the process should remain unchanged. This is found experimentally (curve C).

Complete recombination with damp ammonia is more rapid than is the adsorption of the stoichiometric amount of water required for recombination. Thus when damp ammonia is used for the recombination, the adsorption of water and the reaction with ammonia probably occur in close sequence and the resulting formation of a nucleus of AMV at an active site creates strain, which distorts the lattice, most probably creating cracks or channels which facilitate further diffusion of the reactant gases into the material. This explanation does not imply that the early part of the α'-time curve should be acceleratory as there is an initial rapid period.

The results of the investigation into the effect of preadsorption of

water onto the sample material on the recombination (Section 4.2.4) show that the recombination proceeds via the formation of a complex in which the mole ratio of V_2O_5 : H_2O : NH_3 is 1 : 1 : 1. The formation of this complex is very rapid if the water has been preadsorbed, while further reaction of this complex with ammonia is relatively slow.

If the contour map for the recombination at a fixed temperature (21°C) (Figure 4.29) is considered it is seen that it may be divided into two regions. In region I it is clear that the rate constant is strongly dependent on p_{NH_3} and virtually independent of p_{H_2O}. In region II, however, the rate constant is dependent on both p_{NH_3} and p_{H_2O} in some complex way. It is evident, however that the average effect in both regions I and II is that the rate constant is dependent on the ratio $Z = p_{NH_3} / p_{H_2O}$. The influence of the formation of the 1 : 1 : 1 complex on the rate constant for recombination at this temperature is clear since over a wide range of combined pressures the rate constant is a maximum when Z is approximately one.

The process of recombination of V_2O_5 with ammonia and water to give AMV thus first involves the absorption and diffusion of water into the sample material. This is controlled by the particle size and order of the structure at lower temperatures and by desorption of the water from the material at elevated temperatures. These processes are followed by the formation of the complex V_2O_5. H_2O. NH_3, and finally there is reaction of this complex with more ammonia to give AMV.

i.e. $V_2O_5 + H_2O \rightarrow \underset{(A)}{(HO)_2\ V_2O_4} \xrightarrow[K_1]{NH_3} [(HO).OV_2O_4]^-\ NH_4^+$

$$\xrightarrow[K_2]{NH_3} 2NH_4VO_3$$

where A acts rather like a dibasic acid with $K_2 << K_1$

6 FURTHER INVESTIGATIONS

Although it has been possible to give rational explanations for many experimental observations it has not been possible to propose a definite mechanism for the whole of the decomposition reaction. It is believed, however, that the present work has indicated several profitable lines for further investigation into the reaction:

$$2NH_4VO_3 \rightleftharpoons V_2O_5 + 2NH_3 + H_2O$$

In connection with the decomposition, or forward, reaction, a continuous determination of the gases evolved throughout the decomposition in each of the atmospheres studied is imperative in order to elucidate the mechanism in more detail.

It has been shown that it is possible to propose a mechanism, from the molecular point of view, for the first stage of the decomposition of AMV in ammonia by consideration of the crystal structures of AMV and AHV. The detailed crystal structure of ABV is now needed in order to carry this investigation further. There are, however, inherent difficulties in this investigation since ABV is only obtained as a microcrystalline powder and any attempts to recrystallise it have led to the formation of AHV. It would also be of interest to extend these ideas further and to see whether the mechanism of other endothermic decompositions could be explained in terms of the atomic or molecular movements involved in proceeding from the starting to theproduct material.

In connection with the reverse or recombination reaction, the main investigation of interest would be into the structure of the intermediate "compound" $V_2O_5.H_2O.NH_3$. Determination of its structure would lead to the proposal of a mechanism outlining the atomic movements during

recombination, on the same lines as has been proposed for the first stage of the decomposition in ammonia.

An investigation into the effect that relative structural order and particle size of the V_2O_5 sample have on the rate of recombination would also be interesting. It should be possible to separate these two effects since V_2O_5 formed in vacuum and annealed in air has a larger surface area than, but appears to be as ordered as, V_2O_5 formed in air.

7. BIBLIOGRAPHY

1. Jacobs and Thompkins - Chemistry of the solid state - Ed Garner (Butterworths 1955) chapter 7.
2. Young - Decomposition of solids (Pergamon Press 1966) chapters 1 & 2.
3. Harvey - Trans. Far. Soc. 29, (1933), 653.
4. MacDonald - J. Chem. Soc. (1936), 832.
5. Hailes - Trans. Far. Soc. 29, (1933), 544.
6. Prout and Thompkins - Trans. Far. Soc. 43, (1947), 148.
7. Garner and Gomm - J. Chem. Soc. (1931) 2123.
8. Garner and Marke - J. Chem. Soc. (1937), 657.
9. Garner and Haycock - Proc. Roy. Soc. A211, (1952), 335.
10. Bright and Garner - J. Chem. Soc. (1934), 1872.
    Garner and Pike - J. Chem. Soc. (1937), 1565.
11. Bagdassarian - Acta. Phys. Chim. USSR 20, (1945), 441.
12. Herley - M. Sc. Thesis (Rhodes University, 1959).
13. Young and Thompkins - Trans. Far. Soc. 52, (1956), 1245.
14. Bartlett, Thompkins and Young - J. Chem. Soc. (1956), 3323.
15. Fischbeck and Spengler - Z. Anorg. Chem. 241, (1939) 209.
16. Finch, Jacobs and Tompkins - J. Chem. Soc. (1954), 2053.
17. Garner and Hailes - Proc. Roy. Soc. A139, (1933), 576.
18. Prout and Thompkins - Trans. Far. Soc. 40 (1944) 488.
19. Young - Decomposition of solids (Pergamon Press 1966) page 51.
20. Haynes and Young - Disc. Far. Soc. 31 (1961) 229.
21. Prout and Thompkins - Trans. Far. Soc. 42 (1946) 482.
22. Avrami - J. Chem. Phys. 7 (1939) 1103; 8 (1940) 212; 9 (1941) 177.
23. Erofeyev - Acad. Sci. URSS 52, (1946), 511.

24. Sharples - Introduction to Polymer Crystalisation (Arnold, London 1966) chapter 4.

25. Gent - Trans. Inst. Rubber Ind. 30 (1954) 139.

26. Hume and Colvin - Proc. Roy. Soc. A132, (1932), 548.
Topley - Proc. Roy. Soc. A132, (1932), 413.
Bradley, Colvin and Hume - Phil. Mag. 14 (1932), 1102.
Bradley - Phil. Mag. 12 (1931), 290.

27. Spencer and Topley - J. Chem. Soc. (1929) 2633.

28. Gregg and Razouk - J. Chem. Soc. (1949) 536.

29. Jacobs and Thompkins - Chemistry of the solid state - Ed. Garner (Butterworths 1955) p. 203.

30. Harrison - Comprehensive chemical kinetics - Ed. Bamford and Tipper (Elsevier, 1969) vol. 2, chapter 5.

31. Crank - The Mathematics of Diffusion (Oxford University Press, 1956).

32. Wagner - Z. Physik. Chem. B21 (1933) 25; B32 (1936) 447.

33. Deb - Trans. Far. Soc. 62 (1966) 3032.

34. Giess - J. Am. Ceram. Soc. 46 (1963) 374.

35. Jander - Z. Anorg. Allgem. Chem. 163 (1927) 1.

36. Ginstling and Brounstein - J. Appl. Chem. USSR 23 (1950) 1327.

37. Dünwald and Wagner - Z. Physik. Chem. B24 (1934) 53.

38. Stone and Tilley - Reactivity of solids - Proc. 5th Int. Symp. - Munich 1964 (Elsevier, Amsterdam, 1965) p. 583.

39. Harrison, Catton and Rantoma - Reactivity of solids - Proc. 6th Int. Symp. - Schenectady, New York 1968 (Wiley) p. 65.

40. Cohen and Schmidt - J. Chem. Soc. (1964) 1996.

41. Cohen and Schmidt - Reactivity of the photexcited organic molecule (Interscience, London 1967) p. 227.

42. Jacobs - Reactivity of solids - Proc. 6th Int. Symp. - Schenectady, New York 1968 (Wiley) p. 207.

43. Renshaw and Thomas - Nature 209, (1966), 1196.

44. Renshaw and Thomas - J. Chem. Soc. (London) A (1967) 2058.

45. Taylor, Glasser and Dent-Glasser - Quart. Rev. 16 (1962) 343.

46. Mackay - Proc. 4th Int. Symp. - Amsterdam 1960, p. 571.

47. Saalfeld - Proc. 4th Int. Symp. - Amsterdam 1960, p. 310.

48. Brindley and Choe - Amer. Min. 46 (1961) 771.

49. Van Oosterhout - Acta Cryst 13 (1960) 932.

50. Flörke - Neues Jahrb Mineral 84 (1952) 189.

51. Erdey, Gal and Liptay - Talanta 11 (1964) 913.

52. Taniguchi and Ingraham - Can. J. Chem. 42 (1964) 2467.

53. Ingraham and Marier - Trans. Metall. Soc. of Aime 242 (1968) 2039.

54. Mikhail, Brunauer and Copeland - J. Colloid and Interface Sci. 21 (1966) 394.

55. Herley and Prout - J. Amer. Chem. Soc. 82 (1960) 1540.

56. Hartoulari and Dufour - Bull. Soc. Chim. France 9 (1969) 3017

57. Sherriff and Galwey - J. Chem. Soc. A (1967) 1705.

58. Liteanu, Margineau and Kröbl - J. Thermal Analysis 2 (1970) 119.

59. Bolton and Lanewala - J. Catalysis 18 (1970) 154.

60. Rabo, Pickert, Stamires and Boyle - Acts. Congr. Intern. Catalyse 2 (1960) 2055.

61 Uitehoeven, Christner and Hall - J. Phys. Chem. 60 (1956) 220.

62. Bielanski and Tompkins - Trans. Far. Soc. 46 (1950) 1072.

63. Zawadzki - Festskrift Tillägnad - J. A. Hedvall (Göteborg 1948). Hüttig, Meller and Lehmann - Zeits. Phys. Chem. B19 (1932) 1.

64. Cremer and Gatt - Radex Rundschau (1949) 144. Bischoff - Zeit. Anorg. Chem. 262 (1950) 288.

65. Langmuir - J. Amer. Chem. Soc. 38 (1916) 2263.

66. Crowther and Coutts - Proc. Roy. Soc. A106 (1924) 215.

67. Topley and Hume - Proc. Roy. Soc. A120 (1928) 210.

68. Seyewitz and Brissaud - Bull. Soc. Chem. 47 (1930) 690. - Acad. Sci. Paris 190 (1930) 690.

69. Ghosh - J. Indian Chem. Soc. 18 (1941) 472.

70. Davis and Eyre - Proc. Roy. Soc. A 104 (1923) 1131.

71. Glasner and Hodara - Bull. Res. Council (Israel) 7A (1958) 66.

72. Benson and Tompkins - J. Phys. Chem. 60 (1956) 220.

73. Evans - Proc. Roy. Soc. (London) A134 (1931) 97.

74. Zsigmondy - Z. Anorg. Allgem. Chem 71 (1911) 356.

75. Britton, Gregg and Windsor - Trans. Far. Soc. 48 (1952) 63.

75a. Tamara, Teranishi and Miyazaki - J. Chem. Soc. Japan 55 (1952) 68.

76. Satava - Coll. Czech. Comm. 24 (1959) 2172.

77. Trau - Roczniki Chemii 36 (1962) 1365. Zeszyty Naukowe Politechniki Krakowskiej 21 (1966) 113.

78. Lamure and Colin - C. R. Acad. Sci, Paris, 258, (6433.

79. Dubois and Breton - C. R. Acad. Sci. Paris, 206 (1938) 1969.

80. Duval - Inorganic thermogravimetric analysis (Elsevier 1953) p. 170.

81. Sesbes - Istanbul Univ. Fen. Fak. Mecmuasi. Ser. C. 20 (1955) 272.

82. Sata, Komada and Ito - Kogyo Kagaku Zasshi 71 (1968) 643-7.

83. Deschanvres, Nouet and Raveau - C. R. Acad. Sci. Paris, 261 (1965) 3144.

84. Deschanvres and Nouet - C. R. Acad. Sci. Paris Ser. C, 264 (1967) 2041.

85. Lukesh - Acta Cryst. 3 (1950) 476.

86. Sørum - K. Norske Vidensk Selsk. Forh. 16 (1943), 39-42.

87. Swanson, Gilfrich, Cook, Stinchfield and Parks - Nat. Bur. of Stds. Circular 539, vol. 8 (1959).

88. Evans - Z. Krist. 114 (1960) 257.

89. Synecek and Hanic - Physic. J. Czech. 4 (1954) 120.

90. Griffith and Orgel - Quart. Rev. Chem. Soc. (London) 11 (1957) 381.

91. Kelmers - J. Inorg. Nucl. Chem. 21 (1961) 45.

92. Block - Thesis (John Hopkins University, 1955).

93. Evans and Block - Inorg. Chem. 5 (1966) 1808.

94. Ketelaar - Z. Krist. 95 (1936) 9.

95. Byström, Wilhelmi and Brotzen - Acta Chem. Scand. 4 (1950) 1119.

96. Bachmann, Ahmed and Barnes - Z. Krist 115 (1961) 110.

97. Machatschki - Naturwissenschaften 24 (1936) 742.

98. Magnéli and Blomberg - Acta Chem. Scand. 5 (1951) 585.

99. Andersson - Acta Chem. Scand. 10 (1956) 623.

100. Frederickson and Hausen - Anal. Chem. 35 (1963) 818.

101. Kera and Hirota - J. Phys. Chem. 73 (1969) 3973.

102. Wagner and Hornig - J. Chem. Phys. 18 (1950) 296.

103. Hornig - J. Chem. Phys. 16 (1948) 1068.

104. Krishnan - Proc. Ind. Acad. Sci. A26 (1947) 432.

105. Simon - Ann. Physik 68 (1922) 4.

106. Sorai, Suga and Seki - Bull. Chem. Soc. Japan 38 (1965) 1125.

107. Stephenson and Karo - J. Chem. Phys. 48 (1968) 104.

108. Levy and Peterson - Phys. Rev. 83 (1951) 1270;
- J. Am. Chem. Soc. 75 (1953) 1536.

109. Garland and Renard - J. Chem. Phys. 44 (1966) 1130.

110. Garland and Young - J. Chem. Phys. 49 (1968) 5282.

111. Wagner and Hornig - J. Chem. Phys 18 (1950) 296, 305.

112. Nagamiya - Proc. Math. Soc. Japan 24 (1942) 137; 25 (1943) 540.

113. Schumaker and Garland - J. Chem. Phys. 53 (1970) 392.

114. Schumaker and Garland - J. Chem. Solids, 28 (1967) 799.

115. Frenkel - Acta Phys. Chim. USSR 3 (1935) 23.

116. Lawson - Phys. Rev. 57 (1940) 417.

117. Bovey - J. Opt. Soc. Am. 41 (1951) 836.

118. Rush, Taylor and Havens - Phys. Rev. Lett. 5 (1960) 507.
J. Chem. Phys. 37 (1962) 234.

119. Perkin-Elmer Handbook - Model UU 1 Temperature Programme Control.

120. Steyn - Ph. D. Thesis (Rhodes University 1957).

121. Kubaschewski, Evans and Alcock - Metallurgical Thermochemistry-4th edition 1967, Pergamon Oxford) p. 360.
Todd and Coughlin - J. Am. Chem. Soc. 71 (1949) 317.
also
Rossini et al - Selected values of chemical thermodynamic properties, NBS circular 500.

122. Cox and Pilcher - Thermochemistry of organic and organometallic compounds - (Academic Press, London, 1970) p. 496.

123. Borg - Differential Thermal Analysis I - Ed. Mackenzie (Academic Press, London, 1970) p. 346.

124. International Critical Tables First Edition (McGraw-Hill) p. 92.

125. Jach - Nature 196 (1962) 827.
Thomas and Renshaw - J. Chem. Soc. A (1967) 2058 and (1969) 2758.

126. Winter, Sturge and Sturge - J. Chem. Soc. A (1968) 2889.
Cameron, Farkas and Litz - J. Phys. Chem. 57 (1953) 229.

127. Laidler - Chemical kinetics - 2nd Edition (McGraw-Hill, 1965) p. 90.

128. Shannon - Trans. Far. Soc. 60 (1964) 1902.

APPENDIX A THE DECOMPOSITION OF, AND RECOMBINATION TO AMV

In the tables given below α refers to the fraction of the decomposition reaction of a particular stage completed and α' refers to the fraction of the recombination reaction completed, t refers to the time in minutes. In all cases both α and α' have for convenience been multiplied by a factor of 1000, and T represents the temperature in degrees centigrade.

TABLE A1 First Stage of the Decomposition in Vacuum

T	105°C		110°C		116.6°C		120°C		123.3°C		123.3°C	
	α	t	α	t	α	t	α	t	α	t	α	t
	45	40	53	20	69	10	34	10	38	3	45	3
	106	80	113	40	141	20	143	20	104	6	115	6
	186	120	179	60	212	30	241	30	163	9	176	9
	264	160	245	80	278	40	320	40	218	12	228	12
	342	200	314	100	340	50	393	50	274	15	279	15
	416	240	383	120	400	60	472	60	327	18	327	18
	484	280	443	140	457	70	548	70	378	21	374	21
	548	320	497	160	512	80	612	80	429	24	423	24
	606	360	541	180	563	90	669	90	477	27	465	27
	655	400	582	200	609	100	725	100	521	30	508	30
	702	440	622	220	653	110	773	110	565	33	549	33
	759	480	658	240	694	120	814	120	607	36	587	36
	789	520	689	260	732	130	849	130	646	39	624	39
	812	560	719	280	765	140	879	140	683	42	661	42
	834	600	743	300	796	150	903	150	718	45	695	45
	850	640	767	320	823	160	924	160	750	48	725	48
	864	680	787	340	846	170	940	170	780	51	756	51
	876	720	804	360	865	180	952	180	809	54	783	54
	887	760	818	380	882	190	960	190	836	57	810	57
	897	800	831	400	896	200	967	200	858	60	834	60
	905	840	841	420	908	210	975	210	878	63	855	63
	912	880	849	440	918	220	981	220	895	66	877	66
	919	920	857	460	928	230	987	230	914	69	897	69
	925	960	863	480	937	240	991	240	928	72	913	72
	931	1000	868	500	946	250	995	250	942	75	942	75
	936	1040	873	520	954	260	1000	260	954	78	955	78
	941	1080	878	540	962	270			964	81	965	81
	945	1120	882	560	969	280			973	84	976	84
	949	1160	886	580	976	290			981	87	983	87
	952	1200	890	600	981	300			988	90	989	90
	955	1240			986	310			994	93	993	93
	958	1280			991	320			998	96	997	96

TABLE A1 (continued)

T	123.3°C		126.6°C		130°C		135°C	
	α	t	α	t	α	t	α	t
	41	3	56	4	24	4	44	2
	108	6	196	8	127	8	119	4
	170	9	296	12	223	12	188	6
	224	12	391	16	314	16	259	8
	276	15	482	20	399	20	325	10
	325	18	567	24	475	24	387	12
	376	21	640	28	550	28	447	14
	426	24	706	32	618	32	505	16
	471	27	760	36	681	36	561	18
	513	30	809	40	737	40	610	20
	556	33	851	44	787	44	657	22
	596	36	887	48	832	48	700	24
	636	39	916	52	869	52	743	26
	672	42	941	56	903	56	782	28
	708	45	959	60	929	60	820	30
	738	48	972	64	952	64	852	32
	769	51	980	68	970	68	881	34
	798	54	988	72	985	72	907	36
	821	57	993	76	996	76	931	38
	842	60	997	80	1000	80	956	40
	864	63	999	84			972	42
	885	66					989	44
	906	69					999	46
	920	72						
	940	75						
	952	78						
	963	81						
	975	84						
	982	87						
	989	90						
	993	93						
	997	96						

TABLE A2 Second Stage of the Decomposition in Vacuum

T

135°C		140°C		145°C		150°C		152°C		155°C	
α	t	α	t	α	t	α	t	α	t	α	t
202	5	190	3	171	2	70	$\frac{1}{2}$	121	1	137	1
328	10	352	7	317	4	183	$1\frac{1}{2}$	236	2	252	2
425	15	451	11	427	6	268	$2\frac{1}{2}$	331	3	331	3
493	20	528	15	506	8	345	$3\frac{1}{2}$	408	4	417	4
537	25	584	19	567	10	415	$4\frac{1}{2}$	478	5	496	5
582	30	634	23	622	12	479	$5\frac{1}{2}$	541	6	568	6
619	35	662	27	665	14	535	$6\frac{1}{2}$	592	7	626	7
649	40	697	31	695	16	577	$7\frac{1}{2}$	631	8	683	8
672	45	732	35	732	18	613	$8\frac{1}{2}$	669	9	727	9
694	50	761	39	762	20	648	$9\frac{1}{2}$	701	10	763	10
724	55	782	43	793	22	683	$10\frac{1}{2}$	732	11	799	11
746	60	817	47	817	24	711	$11\frac{1}{2}$	758	12	835	12
761	65	845	51	841	26	739	$12\frac{1}{2}$	783	13	870	13
784	70	866	55	866	28	761	$13\frac{1}{2}$	809	14	899	14
806	75	894	59	890	30	789	$14\frac{1}{2}$	828	15	928	15
821	80	908	63	915	32	810	$15\frac{1}{2}$	853	16	957	16
836	85	937	67	933	34	838	$16\frac{1}{2}$	873	17	978	17
858	90	965	71	951	36	859	$17\frac{1}{2}$	892	18	992	18
881	95	993	75	975	38	873	$18\frac{1}{2}$	911	19	999	19
903	100	999	79	988	40	887	$19\frac{1}{2}$	924	20		
918	105			999	42	901	$20\frac{1}{2}$	943	21		
933	110					923	$21\frac{1}{2}$	955	22		
948	115					937	$22\frac{1}{2}$	968	23		
963	120					958	$23\frac{1}{2}$	981	24		
978	125					972	$24\frac{1}{2}$	994	25		
985	130					986	$25\frac{1}{2}$	999	26		
993	135					993	$26\frac{1}{2}$				
999	140					999	$27\frac{1}{2}$				

TABLE A3 Third Stage of the Decomposition in Vacuum

165°C		170°C		175°C		180°C		185°C		190°C	
α	t	α	t	α	t	α	t	α	t	α	t
77	5	89	4	35	2	86	2	89	2	93	1
141	10	174	8	133	4	166	4	187	4	166	2
217	15	254	12	206	6	256	6	279	6	233	3
291	20	331	16	279	8	345	8	381	8	313	4
364	25	409	20	349	10	435	10	473	10	383	5
438	30	486	24	419	12	511	12	562	12	450	6
508	35	557	28	486	14	581	14	632	14	511	7
636	40	631	32	549	16	652	16	695	16	572	8
693	45	694	36	381	18	712	18	756	18	626	9
748	50	754	40	610	20	767	20	810	20	677	10
786	55	803	44	670	22	815	22	851	22	725	11
821	60	846	48	721	24	856	24	883	24	764	12
856	65	883	52	765	26	882	26	908	26	808	13
885	70	911	56	803	28	907	28	930	28	837	14
911	75	934	60	841	30	927	30	949	30	865	15
923	80	951	64	867	32	943	32	959	32	891	16
936	85	966	68	889	34	955	34	972	34	910	17
949	90	977	72	908	36	965	36	981	36	929	18
959	95	986	76	924	38	974	38	991	38	946	19
965	100	997	80	937	40	981	40	997	40	959	20
971	105	1000	84	949	42	987	42			968	21
976	110			959	44	994	44			974	22
981	115			968	46	997	46			981	23
986	120			975	48					984	24
990	125			981	50					987	25
993	130			984	52					990	26
996	135			987	54					993	27
998	140			991	56					996	28
				994	58					999	29
				997	60						

TABLE A4 First Stage of the Decomposition in Damp Air

160°C		165°C		170°C		175°C		180°C	
α	t	α	t	α	t	α	t	α	t
55	20	68	10	66	5	54	$2\frac{1}{2}$	28	2
120	40	132	20	143	10	130	5	104	4
193	60	197	30	229	15	206	$7\frac{1}{2}$	183	6
261	80	263	40	312	20	265	10	253	8
332	100	331	50	397	25	326	$12\frac{1}{2}$	315	10
407	120	380	60	477	30	379	15	380	12
477	140	437	70	546	35	434	$17\frac{1}{2}$	442	14
544	160	488	80	607	40	482	20	500	16
599	180	544	90	668	45	536	$22\frac{1}{2}$	557	18
658	200	589	100	717	50	584	25	606	20
717	220	645	110	765	55	627	$27\frac{1}{2}$	654	22
765	240	688	120	812	60	674	30	698	24
809	260	727	130	851	65	715	$32\frac{1}{2}$	736	26
849	280	766	140	883	70	754	35	774	28
884	300	800	150	914	75	791	$37\frac{1}{2}$	808	30
918	320	840	160	942	80	824	40	840	32
946	340	867	170	959	85	861	$42\frac{1}{2}$	871	34
970	360	899	180	974	90	891	45	898	36
991	380	917	190	988	95	919	$47\frac{1}{2}$	922	38
999	400	940	200	997	100	940	50	944	40
		955	210	999	105	960	$52\frac{1}{2}$	961	42
		968	220	1000	110	974	55	975	44
		983	230			984	$57\frac{1}{2}$	986	46
		989	240			993	60	992	48
		994	250			998	$62\frac{1}{2}$	996	50
		997	260			1000	65	999	52

TABLE A5 Second Stage in the Decomposition in Damp Air

185°C		190°C		195°C		195°C		200°C	
α	t	α	t	α	t	α	t	α	t
89	5	126	5	85	2	126	3	173	2
168	10	301	10	208	4	263	6	335	4
274	15	492	15	344	6	416	9	470	6
368	20	634	20	453	8	568	12	589	8
442	25	721	25	542	10	674	15	697	10
526	30	782	30	618	12	747	18	757	12
621	35	836	35	670	14	800	21	811	14
689	40	874	40	717	16	842	24	854	16
753	45	902	45	755	18	879	27	886	18
800	50	918	50	792	20	916	30	913	20
842	55	940	55	825	22	932	33	930	22
868	60	956	60	854	24	947	36	946	24
889	65	973	65	882	26	963	39	962	26
905	70	984	70	901	28	974	42	978	28
921	75	995	75	920	30	984	45	985	30
937	80	1000	80	934	34	989	48	991	32
947	85			943	36	995	51	996	34
958	90			948	38	1000	54	1000	36
968	95			958	40				
979	100			967	42				
989	105			976	44				
995	110			981	46				
999	115			986	48				
				991	50				
				995	52				
				999	54				

TABLE A6 Third Stage of the Decomposition in Damp Air

T

275°C		280°C		285°C		290° C		295°C		300°C	
α	t	α	t	α	t	α	t	α	t	α	t
24	3	24	2	28	2	43	2	29	1	23	1
56	6	39	4	81	4	97	4	55	2	65	2
98	9	78	6	116	6	133	6	83	3	127	3
144	12	112	8	144	8	169	8	107	4	190	4
176	15	139	10	162	10	225	10	131	5	245	5
263	18	163	12	202	12	305	12	154	6	301	6
334	21	198	14	233	14	387	14	187	7	359	7
410	24	239	16	284	16	470	16	232	8	414	8
507	27	293	18	349	18	562	18	280	9	475	9
607	30	346	20	419	20	654	20	334	10	537	10
707	33	410	22	500	22	743	22	393	11	590	11
805	36	476	24	584	24	823	24	450	12	644	12
890	39	549	26	675	26	896	26	502	13	704	13
944	42	622	28	756	28	949	28	552	14	759	14
968	45	695	30	835	30	968	30	614	15	810	15
978	48	768	32	900	32	981	32	668	16	852	16
985	51	837	34	949	34	988	34	718	17	896	17
990	54	898	36	975	36	993	36	763	18	931	18
993	57	934	38	982	38	995	38	813	19	961	19
995	60	956	40	989	40	998	40	858	20	975	20
998	63	971	42	996	42	1000	42	896	21	984	21
1000	66	981	44	998	44			924	22	991	22
		985	46	1000	46			950	23	993	23
		990	48					967	24	996	24
		995	50					976	25	998	25
		998	52					984	26	1000	26
		1000	54					991	27		
								995	28		
								997	29		
								1000	30		

TABLE A7 First Stage of the Decomposition in Dry Air

T	152°C		158°C		162°C		167°C	
	α	t	α	t	α	t	α	t
	42	10	69	5	41	3	44	2
	109	20	141	10	106	6	117	4
	181	30	206	15	170	9	183	6
	255	40	276	20	235	12	246	8
	322	50	347	25	297	15	314	10
	388	60	416	30	356	18	376	12
	456	70	482	35	414	21	437	14
	522	80	548	40	468	24	502	16
	584	90	612	45	520	27	556	18
	638	100	674	50	570	30	607	20
	691	110	731	55	622	33	659	22
	740	120	780	60	670	36	707	24
	790	130	825	65	712	39	755	26
	826	140	869	70	756	42	797	28
	869	150	905	75	797	45	836	30
	901	160	945	80	831	48	877	32
	930	170	971	85	865	51	910	34
	956	180	986	90	901	54	940	36
	971	190	992	95	927	57	963	38
	985	200	996	100	952	60	980	40
	990	210	999	105	971	63	990	42
	994	220	1000	110	985	66	995	44
	997	230			991	69	997	46
	999	240			996	72	1000	48
	1000	250			1000	75		

TABLE A8 Second Stage of the Decomposition in Dry Air

T

180°C		185°C		190°C		195°C	
α	t	α	t	α	t	α	t
93	6	62	4	89	3	150	2
218	12	158	8	212	6	385	4
352	18	301	12	355	9	590	6
487	24	445	16	507	12	710	8
596	30	574	20	631	15	790	10
674	36	665	24	714	18	825	12
756	42	742	28	773	21	855	14
798	48	799	32	813	24	890	16
839	54	837	36	852	27	910	18
870	60	871	40	882	30	930	20
896	66	900	44	906	33	940	22
917	72	919	48	926	36	950	24
938	78	933	52	941	39	960	26
953	84	943	56	956	42	970	28
969	90	952	60	965	45	979	30
979	96	962	64	975	48	985	32
989	102	971	68	985	51	990	34
995	108	981	72	994	54	994	36
997	114	991	76	997	57	997	38
1000	120	995	80	1000	60	1000	40
		997	84				
		1000	88				

TABLE A9 Third Stage of the Decomposition in Dry Air

T

265°C		270°C		275°C		280°C		285°C	
α	t	α	t	α	t	α	t	α	t
96	5	100	4	65	3	61	2	29	$1\frac{1}{2}$
149	10	148	8	127	6	110	4	63	3
160	15	184	12	173	9	139	6	88	$4\frac{1}{2}$
182	20	217	16	223	12	163	8	117	6
212	25	263	20	276	15	193	10	160	$7\frac{1}{2}$
247	30	315	24	341	18	227	12	216	9
289	35	375	28	424	21	268	14	249	$10\frac{1}{2}$
318	40	437	32	516	24	317	16	330	12
368	45	523	36	648	27	366	18	386	$13\frac{1}{2}$
415	50	625	40	791	30	415	20	454	15
465	55	728	44	904	33	471	22	528	$16\frac{1}{2}$
517	60	835	48	940	36	537	24	613	18
583	65	917	52	959	39	607	26	692	$19\frac{1}{2}$
658	70	948	56	969	42	685	28	764	21
750	75	957	60	973	45	766	30	836	$22\frac{1}{2}$
836	80	967	64	981	48	849	32	908	24
906	85	976	68	986	51	910	34	964	$25\frac{1}{2}$
952	90	983	72	990	54	944	36	980	27
974	95	991	76	995	57	954	38	986	$28\frac{1}{2}$
988	100	995	80	998	60	966	40	991	30
995	105	998	84	1000	63	976	42	995	$31\frac{1}{2}$
998	110	1000	88			983	44	998	33
1000	115					990	46	1000	$34\frac{1}{2}$
						995	48		
						998	50		
						1000	52		

TABLE A10 First Stage of the Decomposition in Oxygen (dry)

T	156 °C		160 °C		164.5 °C		169.8 °C	
	α	t	α	t	α	t	α	t
	74	10	58	6	63	3	29	2
	162	20	135	12	134	6	110	4
	255	30	210	18	202	9	190	6
	351	40	296	24	270	12	272	8
	441	50	380	30	336	15	359	10
	526	60	464	36	402	18	432	12
	610	70	539	42	470	21	507	14
	684	80	612	48	533	24	568	16
	746	90	681	54	597	27	633	18
	809	100	746	60	654	30	696	20
	869	110	801	66	705	33	754	22
	916	120	855	72	758	36	806	24
	948	130	900	78	806	39	855	26
	969	140	940	84	851	42	900	28
	984	150	968	90	891	45	938	30
	993	160	982	96	926	48	966	32
	997	170	993	102	961	51	984	34
	1000	180	998	108	981	54	994	36
			1000	114	990	57	997	38
					996	60	1000	40
					999	63		
					1000	66		

TABLE A11 First Stage of the Decomposition in Argon

T	157°C		163°C		165°C		170°C		175°C	
	α	t	α	t	α	t	α	t	α	t
	45	5	30	3	38	4	53	2	22	2
	122	10	75	6	104	8	119	4	86	4
	203	15	133	9	189	12	194	6	186	6
	284	20	191	12	268	16	266	8	288	8
	359	25	247	15	351	20	337	10	400	10
	436	30	304	18	442	24	410	12	508	12
	504	35	360	21	528	28	475	14	610	14
	568	40	417	24	604	32	533	16	696	16
	629	45	470	27	678	36	592	18	779	18
	689	50	522	30	745	40	654	20	852	20
	741	55	569	33	803	44	708	22	912	22
	785	60	618	36	854	48	764	24	950	24
	823	65	664	39	903	52	806	26	967	26
	855	70	709	42	938	56	849	28	976	28
	882	75	751	45	964	60	888	30	982	30
	900	80	789	48	975	64	921	32	987	32
	921	85	822	51	981	68	951	34	992	34
	938	90	854	54	986	72	971	36	996	36
	951	95	880	57	990	76	980	38	998	38
	958	100	904	60	993	80	986	40	1000	40
	966	105	925	63	996	84	989	42		
	970	110	946	66	999	88	992	44		
	976	115	963	69	1000	92	994	46		
	982	120	974	72			997	48		
	985	125	984	75			1000	50		
	988	130	988	78						
	992	135	991	81						
	995	140	994	84						
	997	145	997	87						
	999	150	1000	90						
	1000	155								

TABLE A12 Second Stage of the Decomposition in Argon

T

180°C		185°C		190°C		200°C	
α	t	α	t	α	t	α	t
53	5	74	3	201	2	82	1
127	10	197	6	392	4	155	2
212	15	345	9	539	6	233	3
323	20	463	12	637	8	318	4
423	25	571	15	711	10	392	5
503	30	653	18	760	12	465	6
582	35	714	21	799	14	559	7
646	40	764	24	833	16	625	8
704	45	803	27	873	18	661	9
751	50	842	30	897	20	694	10
799	55	872	33	917	22	727	11
831	60	895	36	931	24	755	12
857	65	917	39	946	26	784	13
889	70	938	42	956	28	812	14
910	75	955	45	966	30	837	15
926	80	970	48	976	32	857	16
942	85	980	51	985	34	878	17
952	90	987	54	990	36	894	18
963	95	993	57	995	38	910	19
974	100	996	60	998	40	927	20
984	105	998	63	1000	42	939	21
995	110	1000	66			951	22
1000	115					963	23
						972	24
						980	25
						985	26
						996	27
						1000	28

TABLE A13 Third Stage of the Decomposition in Argon

T

270°C		280°C		290°C		300°C	
α	t	α	t	α	t	α	t
45	5	44	4	45	2	30	1
90	10	148	8	101	4	73	2
144	15	259	12	172	6	118	3
202	20	375	16	242	8	170	4
259	25	489	20	327	10	225	5
311	30	590	24	409	12	285	6
373	35	691	28	489	14	360	7
435	40	778	32	565	16	425	8
500	45	852	36	638	18	500	9
572	50	901	40	699	20	568	10
642	55	926	44	760	22	635	11
709	60	951	48	812	24	693	12
776	65	965	52	864	26	753	13
836	70	975	56	906	28	795	14
891	75	985	60	944	30	838	15
931	80	990	64	974	32	870	16
958	85	993	68	983	34	895	17
968	90	995	72	991	36	918	18
975	95	998	76	995	38	933	19
983	100	1000	80	998	40	948	20
990	105			1000	42	960	21
995	110					973	22
998	115					983	23
1000	120					988	24
						993	25
						998	26
						1000	27

TABLE A14 First Stage of the Decomposition in Dry N_2

T	160°C		165°C		170°C		170°C		175°C	
	α	t	α	t	α	t	α	t	α	t
	45	3	57	3	52	2	57	2	28	1
	102	6	156	6	137	4	143	4	76	2
	160	9	270	9	221	6	225	6	137	3
	222	12	367	12	310	8	305	8	194	4
	279	15	448	15	404	10	393	10	251	5
	342	18	527	18	479	12	473	12	300	6
	397	21	598	21	545	14	545	14	354	7
	451	24	665	24	618	16	619	16	409	8
	508	27	729	27	681	18	685	18	461	9
	560	30	786	30	746	20	742	20	510	10
	611	33	841	33	805	22	800	22	564	11
	655	36	887	36	861	24	848	24	617	12
	700	39	928	39	905	26	896	26	661	13
	740	42	955	42	942	28	931	28	706	14
	778	45	971	45	973	30	960	30	747	15
	813	48	979	48	988	32	974	32	785	16
	846	51	983	51	994	34	980	34	820	17
	874	54	988	54	997	36	986	36	852	18
	901	57	992	57	999	38	992	38	885	19
	926	60	995	60	1000	40	996	40	913	20
	946	63	998	63			998	42	936	21
	960	66	1000	66			1000	44	955	22
	971	69							969	23
	977	72							978	24
	983	75							986	25
	987	78							991	26
	990	81							995	27
	993	84							998	28
	995	87							1000	29
	997	90								
	999	93								
	1000	96								

TABLE A15 First Stage of the Decomposition in N_2 + 55.3 mmHg of H_2O

T

157°C		162°C		170°C		178°C	
α	t	α	t	α	t	α	t
44	6	84	6	86	3	27	1
107	12	185	12	192	6	82	2
188	18	284	18	288	9	134	3
267	24	377	24	376	12	189	4
338	30	463	30	472	15	245	5
408	36	548	36	547	18	299	6
475	42	626	42	622	21	356	7
540	48	697	48	695	24	411	8
697	54	765	54	756	27	463	9
650	60	828	60	810	30	514	10
714	66	880	66	861	33	562	11
762	72	918	72	903	36	610	12
806	78	945	78	938	39	658	13
847	84	963	84	965	42	704	14
881	90	970	90	981	45	744	15
915	96	977	96	986	48	784	16
941	102	984	102	992	51	822	17
960	108	989	108	996	54	859	18
975	114	993	114	1000	57	892	19
986	120	996	120			921	20
993	126	999	126			941	21
997	132	1000	132			960	22
999	138					974	23
1000	144					980	24
						985	25
						991	26
						993	27
						996	28
						999	29
						1000	30

TABLE A16 First Stage of the Decomposition in Ammonia

T

172 °C		185 °C		190 °C		195 °C		200 °C	
α	t	α	t	α	t	α	t	α	t
110	10	69	5	40	$2\frac{1}{2}$	75	2	61	2
245	20	165	10	146	5	202	4	144	4
371	30	260	15	260	$7\frac{1}{2}$	341	6	255	6
505	40	351	20	379	10	492	8	357	8
617	50	439	25	493	$12\frac{1}{2}$	636	10	466	10
700	60	521	30	595	15	845	12	568	12
743	70	603	35	676	$17\frac{1}{2}$	914	14	661	14
781	80	681	40	741	20	944	16	747	16
801	90	749	45	789	$22\frac{1}{2}$	959	18	820	18
820	100	805	50	812	25	968	20	875	20
835	110	846	55	822	$27\frac{1}{2}$	973	22	924	22
853	120	883	60	832	30	978	24	955	24
866	130	909	65	844	$32\frac{1}{2}$	981	26	975	26
882	140	929	70	855	35	984	28	987	28
896	150	942	75	864	$37\frac{1}{2}$	986	30	992	30
910	160	950	80	871	40	988	32	994	32
922	170	957	85	878	$42\frac{1}{2}$	991	34	996	34
933	180	962	90	885	45	993	36	999	36
942	190	966	95	892	$47\frac{1}{2}$	995	38	1000	38
951	200	971	100	900	50	997	40		
959	210	975	105	910	$52\frac{1}{2}$	998	42		
967	220	978	110	919	55	999	44		
975	230	982	115	926	$57\frac{1}{2}$	1000	46		
982	240	985	120	934	60				
988	250	989	125	940	$62\frac{1}{2}$				
993	260	992	130	947	65				
996	270	995	135	957	70				
999	280	997	140	968	75				
1000	290	999	145	977	80				
		1000	150	985	85				
				994	90				
				1000	95				

TABLE A17 Second Stage of the Decomposition in Ammonia

T	285°C		290°C		295°C		300°C		305°C	
	α	t	α	t	α	t	α	t	α	t
	381	10	311	5	241	4	100	2	43	1
	480	20	431	10	419	8	219	4	136	2
	530	30	501	15	518	12	366	6	218	3
	556	40	555	20	578	16	459	8	296	4
	576	50	594	25	627	20	516	10	379	5
	596	60	636	30	675	24	563	12	450	6
	616	70	693	35	711	28	609	14	518	7
	642	80	725	40	747	32	644	16	575	8
	666	90	753	45	783	36	678	18	636	9
	685	100	778	50	813	40	713	20	679	10
	705	110	806	55	843	44	750	22	714	11
	725	120	831	60	873	48	781	24	750	12
	745	130	852	65	903	52	816	26	786	13
	762	140	884	70	946	56	843	28	821	14
	785	150	908	75	970	60	875	30	854	15
	805	160	922	80	982	64	906	32	882	16
	828	170	933	85	996	68	934	34	900	17
	844	180	947	90	1000	72	953	36	918	18
	864	190	954	95			975	38	932	19
	881	200	961	100			994	40	950	20
	897	210	983	105			1000	42	964	21
	911	220	990	110					975	22
	924	230	997	115					986	23
	934	240	1000	120					993	24
	944	250							997	25
	954	260							1000	26
	964	270								
	970	280								
	977	290								
	983	300								
	987	310								
	990	320								

TABLE A18 Third Stage of the Decomposition in Ammonia

T

340°C		345°C		350°C		355°C		360°C	
α	t	α	t	α	t	α	t	α	t
209	5	157	5	171	5	333	4	211	2
409	10	355	10	325	10	629	8	461	4
550	15	480	15	427	15	735	12	608	6
629	20	545	20	500	20	797	16	676	8
675	25	589	25	555	25	840	20	725	10
707	30	624	30	607	30	874	24	771	12
729	35	658	35	651	35	890	28	810	14
745	40	691	40	698	40	906	32	846	16
758	45	720	45	733	45	923	36	873	18
767	50	745	50	767	50	935	40	896	20
776	55	764	55	800	55	946	44	917	22
785	60	781	60	825	60	955	48	931	24
795	65	795	65	845	65	964	52	944	26
804	70	806	70	864	70	970	56	956	28
811	75	823	75	876	75	975	60	963	30
818	80	835	80	889	80	980	64	973	32
826	85	844	85	900	85	984	68	981	34
833	90	854	90	909	90	988	72	988	36
839	95	864	95	916	95	991	76	994	38
844	100	873	100	924	100	995	80	996	40
850	105	883	105	932	105	998	84	998	42
857	110	892	110	940	110	1000	88	1000	44
861	115	898	115	948	115				
864	120	902	120	955	120				
868	125	905	125	960	125				
872	130	911	130	965	130				
875	135	915	135	970	135				
879	140	921	140	974	140				
881	145	927	145	978	145				
883	150	931	150	982	150				
885	155	935	155	985	155				

TABLE A19 Decomposition of AHV (from the second stage in air) in Argon

T

268.5°C		273°C		279°C		284.5°C		295.5°C	
α	t	α	t	α	t	α	t	α	t
156	8	182	7	92	3	122	3	59	3
249	16	266	14	185	6	229	6	122	6
329	24	333	21	250	9	312	9	190	9
398	32	415	28	298	12	395	12	273	12
459	40	504	35	344	15	469	15	361	15
525	48	588	42	388	18	536	18	454	18
586	56	666	49	434	21	596	21	542	21
637	64	748	56	478	24	654	24	639	24
688	72	817	63	531	27	712	27	727	27
737	80	879	70	573	30	767	30	800	30
774	88	910	77	619	33	804	33	866	33
805	96	928	84	663	36	834	36	922	36
835	104	941	91	700	39	866	39	956	39
854	112	952	98	735	42	896	42	976	42
878	120	961	105	774	45	917	45	983	45
896	128	972	112	809	48	935	48	988	48
908	136	981	119	839	51	949	51	993	51
917	144	988	126	866	54	961	54	998	54
927	152	992	133	894	57	973	57	998	57
932	160	995	140	913	60	982	60	1000	60
939	168	997	147	929	63	989	63		
947	176	999	154	943	66	993	66		
952	180	1000	161	952	69	998	69		
957	192			961	72	1000	72		
				968	75				
				975	78				
				979	81				
				983	84				
				986	87				
				990	90				
				993	93				
				996	96				

TABLE A20 Decomposition of AHV (from second stage in air) in Vacuum

T

205°C		215°C		220°C		225°C	
α	t	α	t	α	t	α	t
62	4	52	4	34	3	19	2
137	8	167	8	123	6	47	4
217	12	279	12	237	9	99	6
294	16	398	16	365	12	182	8
381	20	520	20	530	15	283	10
456	24	637	24	637	18	413	12
530	28	742	28	743	21	548	14
605	32	827	32	840	24	656	16
680	36	884	36	900	27	758	18
752	40	921	40	939	30	833	20
807	44	944	44	961	33	890	22
852	48	959	48	973	36	935	24
877	52	966	52	983	39	958	26
901	56	971	56	987	42	975	28
914	60	974	60	992	45	982	30
926	64	976	64	995	48	987	32
934	68	979	68	997	51	991	34
939	72	981	72	999	54	996	36
944	76	984	76	1000	57	999	38
949	80	987	80			1000	40
954	84	990	84				
961	88	992	88				
968	92	995	92				
974	96	997	96				
980	100	999	100				
985	104	1000	104				

TABLE A21 Decomposition of AHV (prepared from solution) in Air

T	274°C		283°C		291°C		300°C	
	α	t	α	t	α	t	α	t
	42	5	33	3	12	2	14	1
	93	10	110	6	42	4	31	2
	161	15	199	9	82	6	55	3
	241	20	300	12	150	8	99	4
	322	25	405	15	217	10	166	5
	410	30	512	18	289	12	231	6
	493	35	605	21	363	14	296	7
	576	40	699	24	438	16	363	8
	661	45	776	27	524	18	421	9
	727	50	841	30	606	20	487	10
	788	55	889	33	680	22	561	11
	841	60	924	36	749	24	629	12
	886	65	953	39	810	26	698	13
	919	70	964	42	867	28	759	14
	946	75	975	45	906	30	812	15
	966	80	988	48	936	32	860	16
	980	85	993	51	961	34	898	17
	985	90	997	54	973	36	927	18
	988	95	999	57	983	38	944	19
	993	100	1000	60	986	40	954	20
	997	105			990	42	963	21
	1000	110			993	44	970	22
					996	46	975	23
					998	48	982	24
					1000	50	985	25
							988	26
							992	27
							995	28
							997	29
							999	30
							1000	31

TABLE A22 Decomposition of AHV (prepared from solution) in Argon (damp)

T	258°C		263°C		268°C		273°C		279°C	
	∝	t	∝	t	∝	t	∝	t	∝	t
	78	8	104	6	44	4	49	3	53	2
	171	16	217	12	166	8	143	6	146	4
	289	24	346	18	296	12	286	9	271	6
	423	32	489	24	431	16	432	12	406	8
	538	40	614	30	543	20	559	15	561	10
	649	48	727	36	648	24	677	18	687	12
	745	56	816	42	744	28	773	21	787	14
	823	64	875	48	819	32	848	24	863	16
	912	80	943	60	915	40	938	30	947	20
	927	88	957	66	940	44	954	33	965	22
	940	96	969	72	957	48	968	36	975	24
	952	104	978	78	968	52	978	39	983	26
	966	112	983	84	971	56	983	42	987	28
	980	120	988	90	984	60	988	45	990	30
	988	128	992	96	989	64	991	48	992	32
	995	136	995	102	992	68	995	51	993	34
	998	144	998	108	996	72	998	54	995	36
	1000	152	1000	114	1000	76	1000	57	997	38
									1000	40

TABLE A23 Decomposition of AHV (prepared from solution) in Argon (dry)

258°C		268°C		273°C		278°C	
α	t	α	t	α	t	α	t
24	10	73	6	27	4	40	2
64	20	167	12	136	8	119	4
109	30	275	18	276	12	238	6
161	40	395	24	409	16	340	8
221	50	501	30	556	20	441	10
279	60	606	36	697	24	544	12
335	70	701	42	804	28	648	14
398	80	783	48	873	32	730	16
471	90	853	54	921	36	810	18
537	100	901	60	948	40	870	20
606	110	943	66	965	44	908	22
678	120	969	72	970	48	935	24
744	130	980	78	980	52	957	26
808	140	985	84	985	56	975	28
868	150	988	90	989	60	982	30
913	160	992	96	992	64	987	32
944	170	995	102	995	68	991	34
969	180	997	108	998	72	994	36
986	190	1000	114	1000	76	996	38
992	200					998	40
998	210					1000	42
1000	220						

TABLE A24 Decomposition of AHV (prepared from solution) in vacuum

T

220°C		226°C		235°C		240°C		245°C	
α	t	α	t	α	t	α	t	α	t
169	10	111	8	67	5	135	4	84	2
353	20	294	16	193	10	291	8	179	4
510	30	313	24	375	15	445	12	282	6
637	40	639	32	568	20	574	16	420	8
734	50	744	40	719	25	676	20	534	10
804	60	818	48	811	30	756	24	629	12
849	70	875	56	865	35	820	28	709	14
886	80	908	64	904	40	865	32	763	16
910	90	933	72	931	45	893	36	806	18
931	100	947	80	941	50	917	40	843	20
945	110	963	88	949	55	938	44	873	22
955	120	970	96	959	60	953	48	896	24
962	130	975	104	968	65	964	52	915	26
969	140	982	112	974	70	969	56	929	28
974	150	987	120	978	75	977	60	943	30
980	160	992	128	981	80	984	64	953	32
985	170	996	136	985	85	988	68	963	34
988	180	998	144	988	90	991	72	971	36
992	190	1000	152	991	95	995	76	975	38
995	200			995	100	998	80	981	40
998	210			998	105	1000	84	985	42
1000	220			1000	110			988	44
								991	46
								994	48
								996	50
								998	52
								999	54
								1000	56

TABLE A25 Decomposition of AHV (from second stage in Argon) in Air

T	260°C		265°C		270°C		275°C		280°C	
	α	t	α	t	α	t	α	t	α	t
	134	8	23	6	92	5	78	3	99	3
	200	16	114	12	165	10	153	6	169	6
	234	24	177	18	199	15	182	9	211	9
	278	32	207	24	234	20	226	12	278	12
	351	40	238	30	284	25	260	15	342	15
	425	48	299	36	345	30	304	18	417	18
	505	56	369	42	401	35	355	21	501	21
	598	64	447	48	459	40	411	24	590	24
	695	72	530	54	530	45	469	27	682	27
	793	80	615	60	612	50	518	30	774	30
	869	88	702	66	685	55	576	33	851	33
	920	96	785	72	770	60	627	36	900	36
	944	104	855	78	855	65	683	39	925	39
	957	112	906	84	914	70	739	42	947	42
	964	120	936	90	957	75	790	45	960	45
	971	128	953	96	977	80	843	48	972	48
	976	136	960	102	987	85	889	51	980	51
	981	144	967	108	992	90	923	54	987	54
	986	152	974	114	996	95	943	57	992	57
	991	160	979	120	1000	100	957	60	996	60
	998	168	984	126			967	63	998	63
	995	176	989	132			977	66	1000	66
	997	184	994	138			984	69		
	999	192	996	144			991	72		
	1000	200	998	150			996	75		
			1000	156			999	78		
							1000	81		

TABLE A26 Decomposition of AHV (from second stage in Argon) in Vacuum

T

220°C		225°C		230°C		235°C		245°C	
α	t	α	t	α	t	α	t	α	t
50	3	49	3	29	2	57	2	9	$1\frac{1}{2}$
175	6	209	6	139	4	191	4	40	3
308	9	406	9	253	6	342	6	135	$4\frac{1}{2}$
463	12	610	12	411	8	513	8	253	6
608	15	761	15	564	10	665	10	448	$7\frac{1}{2}$
730	18	855	18	697	12	774	12	625	9
818	21	904	21	795	14	853	14	760	$10\frac{1}{2}$
875	24	928	24	860	16	910	16	843	12
908	27	940	27	908	18	942	18	904	$13\frac{1}{2}$
930	30	949	30	940	20	962	20	944	15
945	33	958	33	953	22	975	22	961	$16\frac{1}{2}$
960	36	966	36	962	24	985	24	972	18
970	39	973	39	970	26	990	26	977	$19\frac{1}{2}$
975	42	980	42	974	28	993	28	984	21
980	45	986	45	978	30	996	30	989	$22\frac{1}{2}$
984	48	991	48	982	32	998	32	994	24
909	51	995	51	984	34	1000	34	996	$25\frac{1}{2}$
993	54	998	54	987	36			998	27
995	57	1000	57	989	38			1000	$28\frac{1}{2}$
997	60			991	40				
999	63			994	42				
1000	66			996	44				
				998	46				
				1000	48				

TABLE A27 Decomposition of Irradiated AMV in Vacuum

Irradiated Material		Control	
T	123.5° C		
α	t	α	t
61	10	67	10
217	20	228	20
366	30	383	30
500	40	520	40
612	50	641	50
705	60	749	60
786	70	835	70
856	80	896	80
907	90	939	90
947	100	968	100
975	110	982	110
989	120	994	120
1000	130	1000	130

TABLE A28 Decomposition of Irradiated AHV (prepared from solution) in Air

Irradiated Material		Irradiated Material		Control	
T	275°C				
α	t	α	t	α	t
28	3	28	3	28	3
67	6	63	6	49	6
112	9	94	9	95	9
176	12	149	12	145	12
238	15	222	15	219	15
379	18	288	18	293	18
446	21	364	21	381	21
509	24	444	24	462	24
572	27	513	27	530	27
635	30	576	30	593	30
691	33	632	33	643	33
741	36	684	36	699	36
793	39	732	39	738	39
835	42	777	42	780	42
867	45	816	45	822	45
902	48	854	48	847	48
927	51	874	51	875	51
948	54	899	54	900	54
972	57	923	57	924	57
983	60	947	60	946	60
990	63	961	63	964	63
997	66	972	66	974	66
1000	69	982	69	981	69
		989	72	988	72
		996	75	994	75
		1000	78	997	78
				999	81
				1000	84

TABLE A29 Recombination of Various V_2O_5 Samples Under a High Pressure of Ammonia

Sample	V_2O_5 formed in air I		V_2O_5 formed in Vacuum II		V_2O_5 (Hopkins & Williams) III		V_2O_5 Hopkins & Williams pre-heated in vacuum	
	α'	t	α'	t	α'	t	α'	t
	107	10	197	20	85	20	96	20
	237	20	284	40	175	40	235	40
	358	30	362	60	260	60	362	60
	460	40	425	80	338	80	474	80
	548	50	478	100	417	100	571	100
	624	60	526	120	495	120	654	120
	691	70	564	140	567	140	726	140
	750	80	605	160	630	160	786	160
	802	90	641	180	685	180	831	180
	847	100	675	200	735	200	861	200
	883	110	703	220	775	220	883	220
	917	120	730	240	798	240	896	240
	944	130	756	260	810	260	904	260
	966	140	779	280	822	280	913	280
	984	150	800	300	830	300	918	300
	993	160	821	320	838	320	923	320
	998	170	842	340	845	340	927	340
	1000	180	870	360	852	360	930	360
			887	380	858	380	933	380
			903	400	863	400	936	400
			919	420	868	420	938	420
			934	440	873	440	940	440
			948	460	878	460	942	460
			960	480	882	480	944	480

TABLE A29 continued

Sample	V_2O_5 formed from decomposition of AHV (prepared from solution) in air IV	
	α'	t
	81	10
	166	20
	271	30
	385	40
	495	50
	582	60
	664	70
	729	80
	793	90
	839	100
	877	110
	910	120
	935	130
	951	140
	963	150
	974	160
	984	170
	992	180
	996	190
	998	200
	1000	210

TABLE A30 Recombination of Various V_2O_5 Samples under Damp Ammonia

(pNH_3=100 mmHg, pH_2O = 29 mmHg in a carrier gas of N_2)

Sample No. from Table A29	I		II		III		IV		V_2O_5 from 3rd Stage in Argon	
	α'	t	α'	t	α'	t	α'	t	α'	t
	79	5	119	5	60	5	110	5	111	5
	182	10	218	10	121	10	293	10	230	10
	266	15	290	15	183	15	402	15	333	15
	337	20	353	20	242	20	487	20	437	20
	400	25	408	25	302	25	553	25	517	25
	459	30	454	30	354	30	621	30	576	30
	514	35	502	35	401	35	682	35	628	35
	566	40	548	40	445	40	736	40	676	40
	614	45	595	45	490	45	780	45	724	45
	658	50	642	50	533	50	825	50	768	50
	713	55	689	55	576	55	862	55	810	55
	742	60	734	60	617	60	889	60	845	60
	779	65	778	65	654	65	917	65	880	65
	814	70	820	70	692	70	944	70	908	70
	845	75	858	75	725	75	966	75	931	75
	874	80	894	80	750	80	983	80	948	80
	899	85	924	85	767	85	993	85	962	85
	920	90	945	90	781	90	997	90	973	90
	937	95	959	95	793	95	1000	95	982	95
	951	100	972	100	801	100			990	100
	966	105	981	105	809	105			996	105
	974	110	987	110	815	110			999	110
	981	115	991	115	821	115			1000	115
	987	120	993	120	828	120				
	991	125	995	125	833	125				
	994	130	998	130	837	130				
	996	135	1000	135	841	135				
	998	140			844	140				
	1000	145			847	145				

TABLE A31 Recombination of V_2O_5 Formed in Air Using Damp Ammonia ($pNH_3 = pH_2O = 70mmHg$)

T

15°C		30°C		40°C		50°C		60°C	
α'	t	α'	t	α'	t	α'	t	α'	t
178	10	246	10	272	10	211	10	220	10
326	20	421	20	445	20	343	20	356	20
454	30	569	30	583	30	448	30	450	30
562	40	687	40	700	40	539	40	534	40
660	50	783	50	793	50	617	50	600	50
752	60	858	60	861	60	680	60	662	60
837	70	914	70	906	70	731	70	715	70
907	80	949	80	932	80	778	80	754	80
967	90	966	90	945	90	811	90	788	90
978	100	976	100	954	100	837	100	811	100
983	110	980	110	960	110	854	110	824	110
988	120	982	120	963	120	868	120	845	120
993	130	985	130	966	130	877	130	856	130
997	140	987	140	968	140	884	140	866	140
1000	150	989	150	970	150	891	150	873	150
		990	160	973	160	897	160	880	160
		992	170	976	170	903	170	886	170
		994	180	978	180	909	180	892	180
		995	190	980	190	914	190	898	190
						919	200	904	200
						923	210	910	210
						927	220	915	220
						931	230	919	230
						934	240	923	240

TABLE A32 Recombination of V_2O_5 Formed in Air Using Dry Ammonia (pNH_3 = 720mmHg; $pH_2O \leq 0.1mmH_5$)

T	35 °C		50 °C		70 °C	
	α'	t	α'	t	α'	t
	129	20	170	20	240	20
	190	40	300	40	411	40
	261	60	404	60	528	60
	340	80	493	80	605	80
	413	100	567	100	669	100
	468	120	629	120	721	120
	522	140	680	140	762	140
	570	160	725	160	785	160
	618	180	758	180	802	180
	659	200	787	200	815	200
	695	220	804	220	824	220
	731	240	819	240	832	240
	760	260	829	260	838	260
	786	280	840	280	844	280
	808	300	847	300		
	826	320	855	320		
	838	340	858	340		
	850	360	861	360		
	858	380	864	380		
	866	400	866	400		
	872	420				

TABLE A33 Recombination of V_2O_5 Formed in Vacuum
Using Damp Ammonia (pNH_3 = 12.5mmHg
(pH_2O = 70mmHg

T

15°C		21°C		30°C	
α'	t	α'	t	α'	t
161	15	162	15	174	15
297	25	283	25	256	25
415	35	392	35	354	35
498	45	470	45	424	45
580	55	546	55	499	55
658	65	617	65	573	65
731	75	680	75	634	75
802	85	744	85	694	85
815	95	805	95	747	95
920	105	860	105	797	105
965	115	905	115	843	115
985	125	945	125	889	125
993	135	970	135	930	135
1000	145	985	145	965	145
		994	155	989	155
		1000	165	998	165
				1000	175

TABLE A34 Recombination of V_2O_5 Formed in Air at 21°C Using Various Vapour Pressures of Ammonia and Water

pNH_3	700mmHg		700mmHg		700mmHg		700mmHg		700mmHg	
pH_2O	4.58mmHg		0.53mmHg		0.004mmHg		88.8mmHg		52 mmHg	
	α'	t	α'	t	α'	t	α'	t	α'	t
	134	10	163	20	282	120	67	5	72	5
	196	20	270	40	341	240	147	10	154	10
	274	40	357	60	387	360	223	15	218	15
	351	60	442	80	430	480	295	20	280	20
	418	80	518	100	466	600	361	25	334	25
	479	100	583	120	501	720	423	30	402	30
	532	120	642	140	531	840	480	35	467	35
	581	140	694	160	554	960	534	40	525	40
	622	160	742	180	576	1080	585	45	570	45
	670	180	776	200	595	1200	634	50	633	50
	706	200	809	220	611	1320	681	55	694	55
	741	220	843	240	624	1440	726	60	747	60
	775	240	867	260	638	1560	770	65	796	65
	807	260	897	280	650	1680	813	70	841	70
	834	280	914	300	664	1800	850	75	882	75
	861	300	927	320	675	1920	885	80	917	80
	885	320	938	340	687	2040	913	85	943	85
	909	340	949	360	697	2160	937	90	959	90
	930	360	950	380	708	2280	959	95	974	95
	948	380	961	400	720	2400	974	100	982	100
	960	400	968	420	733	2520	982	105	987	105
	971	420	974	440	742	2640	990	110	992	110
	979	440	978	460	750	2760	993	115	996	115
	983	460	981	480	760	2880	997	120	998	120
	988	480	984	500			999	125	1000	125
	990	500					1000	130		
	992	520								
	994	540								

TABLE A34 (Continued)

pNH_3	100 mmHg		100 mmHg		100 mmHg		35 mmHg		23 mmHg	
pH_2O	29 mmHg		14.7 mmHg		6.9 mmHg		16 mmHg		17 mmHg	
	α'	t	α'	t	α'	t	α'	t	α'	t
	79	5	86	5	84	5	51	5	116	10
	182	10	156	10	168	10	126	10	242	20
	266	15	216	15	237	15	193	15	357	30
	337	20	273	20	294	20	256	20	452	40
	400	25	328	25	347	25	311	25	534	50
	459	30	381	30	440	30	366	30	606	60
	512	35	429	35	485	35	415	35	668	70
	566	40	476	40	528	40	467	40	728	80
	613	45	520	45	572	45	515	45	775	90
	657	50	560	50	609	50	558	50	817	100
	700	55	599	55	647	55	601	55	852	110
	741	60	639	60	682	60	638	60	884	120
	776	65	676	65	712	65	676	65	911	130
	813	70	716	70	741	70	708	70	934	140
	845	75	753	75	771	75	748	75	954	150
	874	80	789	80	798	80	788	80	974	160
	898	85	824	85	825	85	823	85	987	170
	922	90	855	90	849	90	859	90	993	180
	936	95	884	95	873	95	892	95	998	190
	950	100	910	100	890	100	918	100	1000	200
	964	105	933	105	909	105	945	105		
	974	110	953	110	925	110	961	110		
	980	115	968	115	940	115	972	115		
	986	120	981	120	951	120	983	120		
	991	125	991	125	961	125	990	125		
	994	130	996	130	967	130	994	130		
	996	135	998	135	974	135	997	135		
	998	140	1000	140	979	140	1000	140		
	1000	145			982	145				
					986	150				
					990	155				

TABLE A35 Recombination of V_2O_5 formed in Air Using a Fixed Pressure of H_2O (= 70 mmHg) and Varying the Pressure of Ammonia

pNH_3 (mmHg)	1.56		3.13		6.25		12.5		25	
	α'	t	α'	t	α'	t	α'	t	α'	t
	216	20	132	20	112	20	64	10	63	10
	342	40	219	40	198	40	124	20	121	20
	425	60	293	60	271	60	175	30	180	30
	495	80	357	80	335	80	225	40	237	40
	552	100	417	100	395	100	268	50	291	50
	605	120	473	120	454	120	306	60	343	60
	654	140	522	140	509	140	346	70	396	70
	700	160	565	160	555	160	382	80	456	80
	742	180	608	180	602	180	417	90	511	90
	779	200	651	200	649	200	450	100	563	100
	816	220	685	220	692	220	481	110	614	110
	847	240	721	240	733	240	511	120	665	120
	877	260	757	260	774	260	542	130	713	130
	904	280	791	280	814	280	575	140	758	140
	928	300	820	300	851	300	605	150	804	150
	951	320	850	320	884	320	641	160	848	160
	975	340	877	340	917	340	677	170	891	170
	993	360	900	360	946	360	708	180	931	180
	997	380	924	380	969	380	739	190	963	190
	1000	400	946	400	990	400	769	200	986	200
			966	420	998	420	799	210	999	210
			983	440	1000	440	826	220	1000	220
			1000	460			852	230		
							878	240		
							901	250		
							923	260		
							944	270		
							963	280		
							980	290		
							996	300		
							1000	310		

TABLE A35 (Continued)

pNH_3(mmHg)	50		98		140		186		316	
	α'	t	α'	t	α'	t	α'	t	α'	t
	102	10	141	10	140	10	95	10	76	10
	219	20	265	20	240	20	187	20	153	20
	332	30	371	30	328	30	276	30	228	30
	432	40	473	40	410	40	357	40	299	40
	519	50	559	50	488	50	434	50	360	50
	604	60	637	60	561	60	501	60	419	60
	685	70	714	70	625	70	567	70	479	70
	756	80	782	80	691	80	628	80	532	80
	820	90	839	90	756	90	691	90	583	90
	880	100	891	100	813	100	745	100	632	100
	926	110	930	110	876	110	794	110	695	110
	961	120	958	120	925	120	834	120	717	120
	981	130	974	130	960	130	878	130	754	130
	993	140	984	140	982	140	909	140	791	140
	1000	150	993	150	995	150	936	150	825	150
			1000	160	1000	160	954	160	855	160
							969	170	884	170
							980	180	909	180
							992	190	928	190
							997	200	945	200
							1000	210	957	210
									964	220
									970	230
									975	240
									980	250
									984	260
									988	270
									991	280
									994	290
									997	300
									1000	310

TABLE A36 Recombination of V_2O_5 formed in air after preabsorbtion of varying amounts of water

Amount preabsorbed: Half the amount stoichiometrically required for complete recombination to AMV

pNH_3(mmHg)	70		100		720		70	
pH_2O(mmHg)	70		29		0.1		0.004	
α'	t	α'	t	α'	t	α'	t
67	10	62	10	65	10	63	10
94	20	93	20	94	20	96	20
115	30	116	30	115	30	117	30
128	40	133	40	130	40	134	40
150	50	153	50	152	50	153	50
165	60	167	60	167	60	166	60
127	70	148	70	341	63	266	70
330	80	341	80	365	65	376	80
514	90	515	90	491	75	433	90
665	100	665	100	574	85	473	100
797	110	793	110	625	95	499	110
906	120	895	120	663	105	523	120
980	130	972	130	693	115	545	130
997	140	995	140	719	125	560	140
1000	150	1000	150	743	135	573	150
				761	145	585	160
				778	155	596	170
				794	165	605	180
				808	175	614	190
				820	185	621	200
				831	195	628	210
				841	205	635	220
				850	215	640	230
				860	225	646	240
				869	235	651	250
				878	245	655	260
				885	255	659	270
				892	265	662	280
				898	275	666	290

TABLE A36 (Continued)

Amount preabsorbed: All the H_2O stoichiometrically required for complete recombination to AMV

pNH_3(mmHg)	70		720		70	
pH_2O(mmHg)	70		< 0.1		0.004	
α'	t	α'	t	α'	t
95	20	94	20	96	20
123	40	128	40	134	40
166	60	165	60	166	60
193	80	191	80	196	80
220	100	221	100	224	100
243	120	245	120	246	120
262	140	264	140	263	140
284	160	286	160	287	160
305	180	308	180	310	180
325	200	321	200	324	200
346	220	345	220	348	220
352	240	353	240	405	230
336	250	570	242	460	240
472	260	641	245	505	250
615	270	729	255	554	260
736	280	772	265	602	270
839	290	805	275	640	280
921	300	832	285	672	290
983	310	855	295	698	300
997	320	880	305	719	310
1000	330	897	315	737	320
		913	325	752	330
		924	335	765	340
		933	345	774	350
		942	355	780	360
		951	365	784	370
		959	375	788	380
		966	385	792	390
		970	395	796	400
		973	405	799	410

TABLE A37 Successive Decomposition and Recombination of AMV in Air (for Decomposition) and Dry Ammonia (for Recombination)

First decomposition to V_2O_5 in air		Second decomposition to V_2O_5 in air		Third decomposition to V_2O_5 in air		First recombination in dry NH_3		Second recombination in dry NH_3	
α	t	α	t	α	t	α'	t	α'	t
63	4	80	4	126	4	107	10	137	10
367	8	555	8	573	8	237	20	269	20
554	12	604	12	610	12	358	30	393	30
601	16	636	16	638	16	460	40	497	40
639	20	665	20	661	20	548	50	587	50
659	24	687	24	682	24	625	60	660	60
671	28	702	28	700	28	691	70	731	70
678	32	715	32	713	32	750	80	791	80
682	36	727	36	726	36	802	90	849	90
686	40	736	40	739	40	847	100	893	100
688	44	744	44	743	44	883	110	932	110
690	48	750	48	751	48	917	120	961	120
691	52	753	52	754	52	944	130	978	130
691	56	755	56	756	56	966	140	990	140
714	60	756	60	756	60	984	150	996	150
791	64	756	64	756	64	993	160	1000	160
897	68	794	68	829	68	999	170		
975	72	958	72	984	72	1000	180		
996	76	1000	76	1000	76				
1000	80								

TABLE A38 Successive Decomposition and Recombination of the First Stage in Air (pNH_3 = 715 mmHg, pH_2O < 0.1 mmHg)

First decomposition		Second decomposition		Third decomposition		First recombination		Second recombination	
α	t	α	t	α	t	α'	t	α'	t
24	2½	54	2½	53	2½	174	10	176	10
80	5	181	5	178	5	318	20	319	20
143	7½	308	7½	305	7½	464	30	465	30
204	10	462	10	459	10	588	40	585	40
270	12½	611	12½	611	12½	694	50	690	50
334	15	758	15	756	15	773	60	770	60
393	17½	873	17½	870	17½	833	70	829	70
457	20	944	20	943	20	881	80	878	80
530	22½	959	22½	960	22½	919	90	915	90
582	25	967	25	966	25	953	100	949	100
644	27½	972	27½	973	27½	972	110	971	110
700	30	977	30	978	30	986	120	985	120
750	32½	981	32½	980	32½	994	130	993	130
804	35	986	35	984	35	998	140	997	140
846	37½	988	37½	986	37½	1000	150	1000	150
885	40	991	40	990	40				
920	42½	994	42½	994	42½				
948	45	997	45	997	45				
968	47½	1000	47½	1000	47½				
982	50								
988	52½								
992	55								
995	57½								
998	60								
1000	62½								

APPENDIX B X-Ray Powder Deffraction Reflections

The radiation used for all of the photographs was Cu K_{α}

In the tables below s is the diffraction cone diameter in cm at the camera radius and . d is the interplanar separation in Angstrom units. The relative intensities of the reflections are given in the diagrams in Chapter 4.

(1 Angstrom unit = 10^{-1}nm)

TABLE B1 Reflections of Substances Related to AMV

B.D.H. AMV		AHV decomposed to V_2O_5 recombined to AMV		3rd stage air recombined to AMV		1st stage air recombined to AMV	
s	d	s	d	s	d	s	d
1.622	5.80	1.580	5.95	1.578	5.96	1.577	5.96
1.936	4.86	1.895	4.98	1.913	4.97	1.877	5.02
2.292	4.12	2.298	4.10	2.265	4.16	2.225	4.24
2.528	3.74	2.512	3.76	2.505	3.77	2.457	3.84
3.004	3.15	2.960	3.20	2.985	3.17	2.950	3.21
3.282	2.89	3.231	2.95	3.250	2.92	3.222	2.94
3.496	2.72	3.496	2.72	3.492	2.72	3.586	2.65
3.620	2.63	3.610	2.64	3.601	2.64	3.859	2.47
4.512	2.13	4.508	2.13	4.520	2.12		
5.630	1.73	5.256	1.84				
5.990	1.63	5.372	1.81				
6.322	1.55	5.582	1.74				
		5.938	1.65				
		6.296	1.56				
		6.694	1.48				

TABLE B2 Reflections of Substances Related to ABV

Product of:	1st stage of decomposition of AMV in air		1st stage of decomposition of AMV from recombined V_2O_5		1st stage of decomposition in air of AMV from recombined ABV		1st stage of decomposition of AMV in vacuum		2nd stage of decomposition of AMV in vacuum	
	s	d	s	d	s	d	s	d	s	d
	1.182	7.94	1.995	4.72	1.177	7.98	1.954	4.82	1.946	4.84
	1.630	5.77	2.855	3.31	1.610	5.84	2.278	4.14	2.182	4.32
	1.890	4.98	3.445	2.76	1.930	4.88	2.762	3.42	2.758	3.43
	1.964	4.79	4.063	2.35	2.739	3.45	3.340	2.84	3.314	2.87
	2.254	4.19	4.520	2.12	2.909	3.25	3.924	2.43	3.910	2.44
	2.748	3.44	5.416	1.79	3.310	2.87	5.268	1.84		
	2.924	3.24	5.780	1.68	3.924	2.43				
	3.270	2.90	6.095	1.60	3.728	2.03				
	3.344	2.84								
	3.924	2.43								
	4.740	2.03								
	5.266	1.84								
	5.654	1.72								

TABLE B3 Reflections of Substances related to AHV

AHV prepared from solution		2nd stage of the decomposition in air		1st stage of the decomposition in NH_3	
s	d	s	d	s	d
1.166	8.05	1.170	8.03	1.238	7.59
1.232	7.62	1.222	7.72	1.658	5.67
1.598	5.88	1.610	5.84	2.240	4.22
1.672	5.62	2.662	3.55	2.684	3.52
1.906	4.94	2.890	3.28	2.938	3.22
2.394	3.94	2.938	3.22	3.394	2.80
2.474	3.82	3.250	2.92	3.850	2.48
2.636	3.59	3.844	2.48	4.376	2.19
2.702	3.50	4.296	2.23	4.754	2.02
2.912	3.25	4.710	2.04		
2.962	3.20				
3.000	3.16				
3.292	2.98				
3.346	2.84				
3.896	2.45				
4.368	2.20				
4.796	2.01				

TABLE B4 Reflections of Substances Related to V_2O_5

Hopkins and Williams V_2O_5		3rd stage of the decomposition in air		3rd stage of the decomposition in argon		3rd stage of the decomposition in vacuum		Final product in vacuum annealed in vacuum at 550°C	
s	d	s	d	s	d	s	d	s	d
2.138	4.41	1.626	5.78	2.146	4.39	1.613	5.83	2.084	4.52
2.242	4.21	2.120	4.44	2.805	3.37	2.107	4.47	2.151	4.31
2.778	3.38	2.240	4.22	3.312	2.87	2.789	3.39	2.580	3.66
3.296	2.88	2.754	3.43	3.444	2.76	3.290	2.89	2.756	3.43
3.440	2.76	2.977	3.18	3.660	2.60	3.629	2.62	3.245	2.93
3.640	2.62	3.289	2.90	4.418	2.17	4.384	2.19	3.384	2.81
4.362	2.20	3.382	2.81	4.907	1.97	5.046	1.91	3.586	2.65
4.836	1.99	3.618	2.63	5.062	1.91	5.405	1.79	4.334	2.21
5.040	1.92	4.340	2.21	5.459	1.78	6.582	1.49	4.744	2.03
5.450	1.78	4.988	1.93	5.902	1.65			4.965	1.94
5.904	1.65	5.401	1.80	6.228	1.57			5.171	1.87
6.260	1.57	5.864	1.66	6.508	1.51			5.365	1.81
6.498	1.52	6.431	1.53	6.600	1.49			5.896	1.65
6.602	1.49	6.539	1.51					6.144	1.59
7.612	1.32							6.400	1.53
7.850	1.28							6.526	1.51

TABLE B5 Reflections of the Products of the Various Stages of the Decomposition in NH_3

Product of:	2nd stage of decomposition		3rd stage of decomposition		VO_2 (Alfa Inorganics)	
	s	d	s	d	s	d
	2.705	3.50	1.591	5.90	1.602	5.87
	2.960	3.20	2.669	3.53	2.684	3.52
	3.311	2.87	3.045	3.09	3.045	3.09
	3.632	2.62	3.172	2.99	3.251	2.92
	5.024	1.92	3.552	2.67	3.641	2.66
	5.288	1.83	4.760	2.02	4.842	1.99
			5.193	1.86	5.290	1.83
			6.236	1.57	6.301	1.56
					7.367	1.35

TABLE B6 Photographs Taken at Various α' Values During the Recombination of V_2O_5 to Form AMV

$\alpha' = 0.33$		$\alpha' = 0.76$		$V_2O_5+H_2O+NH_3$ to end of the rapid reaction	
s	d	s	d	s	d
1.620	5.80	1.602	5.87	1.135	7.14
1.891	4.98	1.907	4.93	1.611	5.84
2.116	4.45	2.268	4.16	1.854	5.07
2.292	4.11	2.480	3.81	2.270	4.15
2.777	3.41	2.987	3.17	2.721	3.48
2.993	3.16	3.237	2.93	2.956	3.20
3.265	2.91	3.568	2.67	3.214	2.95
3.422	2.78	3.870	2.47	3.550	2.68
3.628	2.62	4.485	2.14	3.865	2.47
4.805	2.00	4.945	1.95	5.355	1.81
5.002	1.93	5.345	1.81		
5.180	1.87				
5.437	1.78				
5.891	1.66				
6.245	1.57				
7.634	1.31				